CHEMOGENETIC G PROTEIN-LIGAND PAIRS FOR CAUSAL INVESTIGATION OF CELLULAR BIOLOGY *IN VITRO* AND *IN VIVO*

Dissertation

zur

Erlangung des Doktorgrades (Dr. rer. nat.)

der

Mathematisch-Naturwissenschaftlichen Fakultät

der

Rheinischen Friedrich-Wilhelms-Universität Bonn

vorgelegt von

Judith Alenfelder

aus

Siegburg

Bonn 2025

Angefertigt mit Genehmigung der Mathematisch-Naturwissenschaftlichen Fakultät
der Rheinischen Friedrich-Wilhelms-Universität Bonn

Gutachterin/Betreuerin: Prof. Dr. Eva Kostenis

Gutachter: Prof. Dr. Bernd K. Fleischmann

Gutachter: Prof. Dr. Christian Helker

Tag der Promotion: 18. Mai 2026

Erscheinungsjahr: 2026

Die vorliegende Arbeit wurde in der Zeit von Juni 2020 bis Oktober 2025 am Institut für Pharmazeutische Biologie der Rheinischen Friedrich-Wilhelms-Universität Bonn unter der Leitung von Frau Prof. Dr. Evi Kostenis angefertigt.

Abstract

The targeted pharmacological inhibition of signaling pathways is an appealing experimental approach for deconvoluting signal transduction downstream of G protein-coupled receptors (GPCRs). A powerful and broadly used molecule to pharmacologically inhibit Gq, G11, and G14 heterotrimers with remarkable specificity is the natural depsipeptide FR900359 (FR). FR prevents nucleotide exchange on the Gα subunit and, consequently, its activation, and can, therefore, be used as a tool to study the contribution of Gq family proteins to complex cellular processes. Similar specific inhibitors for other G protein families are urgently needed, as their availability would tremendously advance the field. Despite extensive efforts, developing such molecules has proven extremely challenging, and no suitable cell-permeable compounds have been identified to date.

To overcome this lack of specific inhibitors, we suggest harnessing the specificity of FR by placing the remaining G protein families under its direct pharmacological control. This strategy involves creating artificial FR binding sites to construct a modular “chemogenetics-like” toolkit, from which engineered FR-sensitive G protein subtypes can selectively be chosen. In this thesis, as a first step towards such a toolbox, we aimed to design and validate FR-resistant Gαq isoforms that remain fully functional and can be employed *in vivo*.

We selected the fruit fly, *Drosophila melanogaster*, as our experimental model due to its genetical tractability and potential for the detailed dissection of signaling circuits *in vivo*. We rationally designed *Drosophila* Gαq (DGq) variants that retain wildtype-like signaling properties and display markedly reduced FR sensitivity. These mutants were characterized in HEK293 cells using a suite of assays covering G protein dissociation, downstream signaling, and whole-cell activation. Several mutants were excluded from further studies due to poor expression, aberrant subcellular localization or residual FR sensitivity. Ultimately, we succeeded in developing DGq proteins combining wild type-like behavior with robust resistance to FR that qualified for proof-of-concept experiments *in vivo*.

FR exhibits dose-dependent oral lethality in insects, an effect that we exploited to investigate whether lethality is causally linked to Gq inhibition. By ubiquitously overexpressing our DGαq variants, we rescued the FR-induced lethality in *Drosophila* without any obvious adverse effects, providing direct experimental proof that FR lethality in this model is mediated by Gq inhibition. Encouraged by these results, we introduced analogous mutations to murine Gαq, generating functional mGαq variants refractory to FR inhibition and suited for future application in live mice.

We envision our engineered *Drosophila* and mouse Gq protein-ligand pairs to serve as versatile chemogenetics-like tools for noninvasive, cell type-specific manipulation of Gq-mediated and -modulated signaling, enabling causal exploration of these pathways *in vitro* and *in vivo*.

Kurzfassung

Die gezielte pharmakologische Signalweghemmung ist ein attraktiver experimenteller Ansatz zur Aufschlüsselung der Signalweiterleitung, die G-Protein-gekoppelten Rezeptoren (GPCRs) nachgeschaltet ist. Ein bedeutungsvolles und breit angewendetes Molekül, das Gq-, G11- und G14-Proteine mit bemerkenswerter Spezifität hemmt, ist das natürlich vorkommende Depsipeptid FR900359 (FR). FR verhindert den Nukleotidaustausch an der Gα-Untereinheit und folglich deren Aktivierung und kann daher als Werkzeug zur Untersuchung des Beitrags von Gq-Proteinen zu komplexen zellulären Prozessen eingesetzt werden. Ähnliche spezifische Inhibitoren für die anderen G-Protein-Familien werden dringend gebraucht und würden das Forschungsfeld stark voranbringen. Spezifische Inhibitoren für andere G-Protein-Familien fehlen bislang trotz intensiver Forschung.

Um den Mangel an spezifischen Inhibitoren zu umgehen, schlagen wir vor, die Spezifität von FR gezielt auszunutzen und andere G-Protein-Familien unter dessen pharmakologische Kontrolle zu bringen. Diese Strategie beinhaltet die Entwicklung artifizieller FR-Bindestellen, um eine modulare „Chemogenetik-ähnliche“ Werkzeugkiste zu schaffen, aus der die konstruierten, FR-sensitiven G-Protein-Subtypen selektiv ausgewählt werden können. In dieser Arbeit beabsichtigten wir, als ersten Teil einer solchen Werkzeugkiste FR-resistente Gαq-Isoformen zu entwickeln, die ihre volle Funktionsfähigkeit erhalten und daher *in vivo* eingesetzt werden können.

Wir wählten die Taufliege, *Drosophila melanogaster*, als experimentelles Modell aus, ob ihrer genetischen Manipulierbarkeit und ihres Potentials für die detaillierte Untersuchung von Signalabläufen *in vivo*. Basierend auf strukturellen Überlegungen, entwarfen wir *Drosophila* Gαq (DGq)-Varianten mit reduzierter FR-Empfindlichkeit bei Erhalt ihrer Wildtyp-Eigenschaften. Diese Mutanten wurden in HEK293-Zellen auf G-Protein-, Second Messenger- und Ganzzellebene charakterisiert. Mehrere Varianten schieden wegen geringer Expression oder Restempfindlichkeit aus. Schließlich entwickelten wir erfolgreich DGq-Proteine, die Wildtyp-artiges Verhalten mit robuster FR-Resistenz vereinten und sich für *proof-of-concept*-Experimente *in vivo* eigneten.

Für Insekten ist die orale Aufnahme von FR dosisabhängig letal, was wir ausnutzten, um zu untersuchen, ob diese Letalität kausal mit der Hemmung von Gq-Proteinen zusammenhängt. Indem wir unsere DGq-Varianten ubiquitär überexprimierten, konnten wir die FR-induzierte Letalität in *Drosophila* ohne offensichtliche Nebenwirkungen aufheben und damit einen direkten experimentellen Nachweis erbringen, dass die Letalität von FR in diesem Organismus durch die Inhibition von Gq vermittelt wird. Durch diese Ergebnisse ermutigt, brachten wir analoge

Mutationen in murines Gαq ein und generierten so funktionelle mGq-Varianten, die gegenüber FR resistent sind und sich für den zukünftigen Einsatz in Mäusen eignen.

Wir betrachten die von uns entwickelten *Drosophila*- und Maus-Gq-Protein/Liganden-Paare als vielseitige, Chemogenetik-ähnliche Werkzeuge für die nicht-invasive, zelltypspezifische Modulation Gq-vermittelter oder -beeinflusster Signalkaskaden, die die kausale Untersuchung dieser Signalwege *in vitro* und *in vivo* möglich machen.

Table of Contents

1. Introduction

1.1. The importance of target knowledge in drug discovery

Pharmaceutical drugs are high-value products and gain more and more importance the higher the average age of the human population rises. While many diseases can already be treated symptomatically or cured, the hunt for new therapeutic approaches and more efficient medicines continues.

The oldest approach for drug discovery is serendipity (Ban, 2006) – "the faculty or phenomenon of finding valuable or agreeable things not sought for"[1]. The cleverer and more advanced method of rational drug design is based on finding a target biomolecule that is involved in the disease to be treated and iterative improvement of a hit compound that favorably targets the desired molecule. While this approach is cheaper than other drug discovery methods such as screening of large compound databases or chemical modification of an already existing drug, the recognition of a potential target molecule and extensive knowledge about its behavior and involvement in physiological processes is equally essential (Doytchinova, 2022).

A highly exploited but far from exhausted group of target biomolecules are G protein-coupled receptors (GPCRs), which constitute the largest group of transmembrane receptors with more than 1,000 GPCR expression products encoded in over 800 genes (Bockaert & Pin, 1998, 1999; Fredriksson & Schiöth, 2005; Kolakowski, 1994; Pierce et al., 2002). GPCRs detect a variety of extracellular cues, including neurotransmitters, photons, and protons, with their extracellular region and relay them over the plasma membrane (Fredriksson et al., 2003). Intracellularly, a signal-induced conformational change in the receptor is recognized by guanine nucleotide-binding proteins (G proteins) and translated via several distinct but interconnected signaling cascades into integrated biological responses (Gilman, 1987; Neves et al., 2002), for example homing of immune cells and their migration to the site of inflammation (Goldman et al., 1985; Spangrude et al., 1984), contraction of endothelial smooth muscle cells to increase blood pressure (Wynne et al., 2009), or closure of sodium channels in photoreceptor cells to allow sight (Hargrave et al., 1993; Kwok-Keung Fung & Stryer, 1980) (Figure 1).

[1] ("Serendipity." *Merriam-Webster.com Dictionary*, Merriam-Webster, https://www.merriam-webster.com/dictionary/serendipity. Accessed 10 Sep. 2024.).

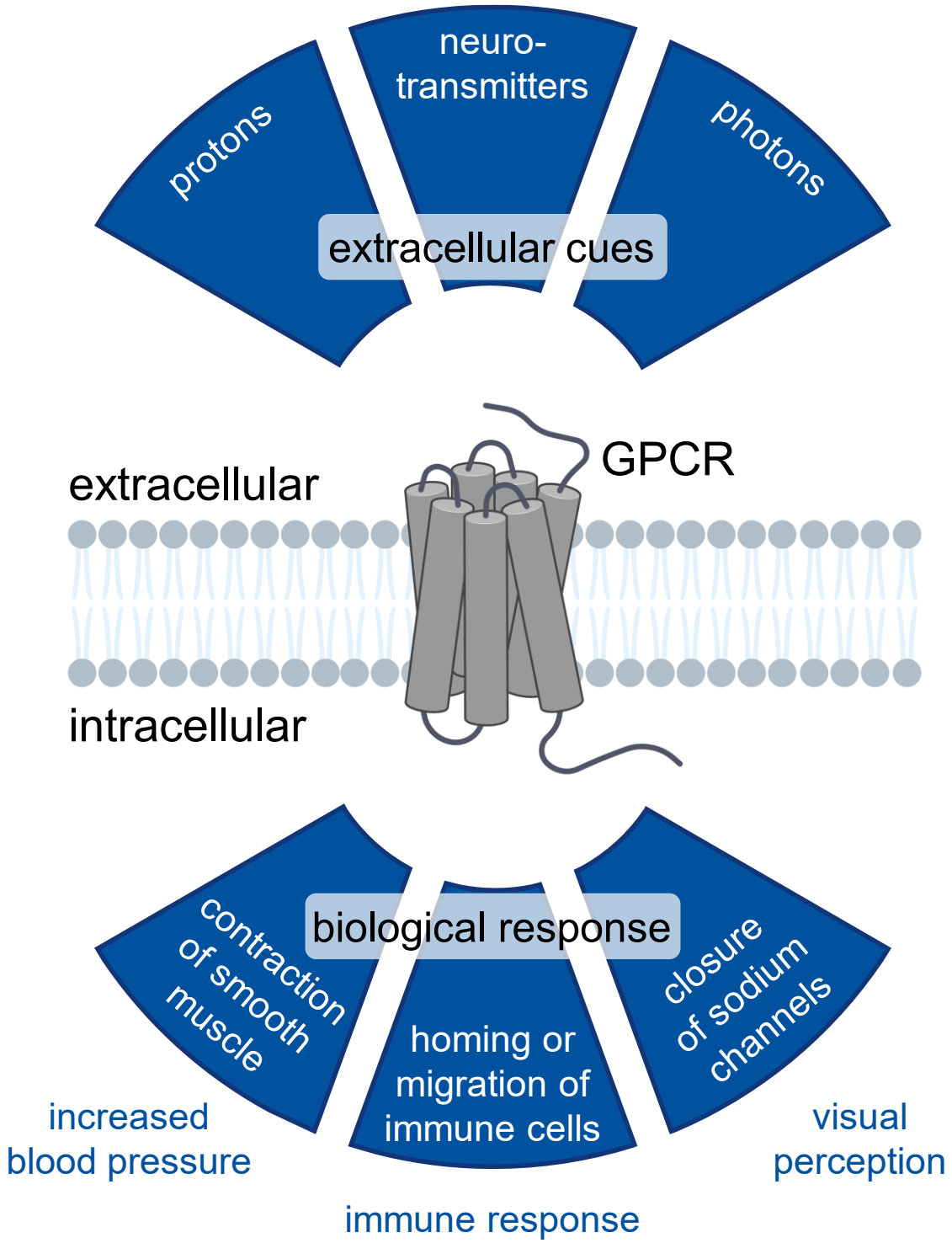

Figure 1: G protein-coupled receptors (GPCRs) relay a multitude of signals over the cell membrane to create various physiological responses.
GPCRs (grey) are seven-pass transmembrane receptors that detect stimuli with their extracellular face and relay them to the intracellular face of the plasma membrane (light grey). These extracellular cues include hormones and peptides but also protons, neurotransmitters, and photons. Intracellularly, GPCRs trigger downstream signaling culminating in biological responses such as increased blood pressure due to a contraction of smooth muscle cells, modulation of immune responses via the induction of homing or migration of immune cells, and even sight, a process that includes closure of sodium channels in photoreceptor cells downstream of the visual GPCR rhodopsin. The figure was partially created with BioRender.com.

1.2. Open questions in GPCR research

While GPCRs as a protein class and some receptors in particular have been extensively studied and exploited as drug targets, there are still plenty of open questions and challenges surrounding these receptors. Some GPCRs remain poorly investigated and understood, others are even considered orphan receptors signifying that their endogenous ligand has not been found, yet (Scharf et al., 2025). Similarly, the downstream signaling axes of some receptors, as well as the interaction of multiple downstream signaling pathways remains obscure. Both cases complicate drug discovery: an orphan GPCR's involvement in physiology and potential as drug target is hard to evaluate; the induction of specific downstream signaling pathways over others with a drug might be either beneficial or detrimental depending on the disease context. The understanding of signaling mechanisms downstream of receptors involved in pathophysiology, as well as GPCRs as receptor class, is crucial to the development of effective and potent therapies with low adverse effects and will ultimately facilitate production of new medicines.

1.3. Importance of universally applicable tools

To investigate GPCR signaling pathways, work must often be carried out under artificial conditions that only moderately reflect actual physiological conditions: immortalized cell lines, as well as labeling and overexpression of proteins are frequently used methods. Results obtained under these conditions cannot necessarily be transferred to actual physiology (Böhme & Beck-Sickinger, 2009; Eglen et al., 2008; Fogel, 2018; McNeely et al., 2012; Wright et al., 2024).

Inhibition is a classical and popular pharmacological technique to investigate the function and involvement of GPCRs and their downstream signaling that can be used without tagging or overexpression of proteins, in primary cells and even in animal models, and allows for dose-dependent modulation of the effect (Figure 2A). GPCR research heavily relies on the use of inhibitors that prevent the activation of receptors themselves, e.g. β-adrenoceptor blockers such as propranolol (Baker et al., 2011) (Figure 2B). In addition, the intracellular signaling downstream of G protein-coupled receptors can be blocked by inhibitors of signal transducers further downstream in the signaling cascade, such as inhibitors of the mitogen-activated protein (MAP) kinase pathway (Burkhard & Shapiro, 2010). However, for the most direct GPCR interaction partner, the G protein, pharmacological inhibition has not yet been fully realized and is not a common strategy for all G protein classes. The prominent exceptions are two potent and specific Gq/11 protein family inhibitors, FR900359 (FR) and YM-254890 (YM) (Fujioka et al., 1988; Nishimura et al., 2010) (Figure 2C). Isolated from their respective bacteria of origin (Carlier et al., 2016; Crüsemann et al., 2018; Hermes et al., 2021; Pistorius et al., 2022), they can easily be used in cells or *in vivo* for rapid and long-lasting inhibition of Gq/11 signaling, as

they combine high potency with cell permeability and lack of off-target effects (Nishimura et al., 2010; Patt et al., 2021; Schrage et al., 2015; Jan Hendrik Voss, 2023).

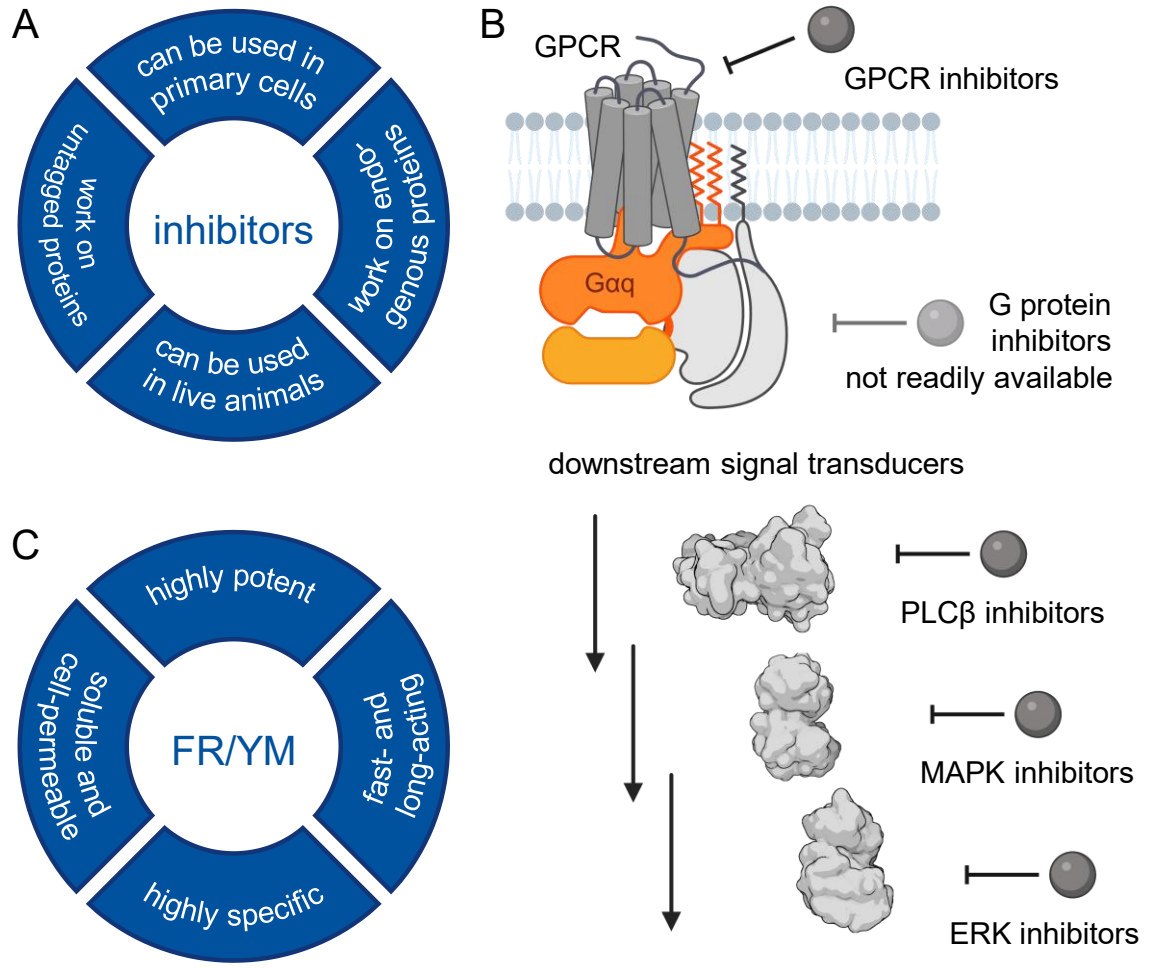

Figure 2: Inhibition is a classical technique in pharmacology, including research on G protein-coupled receptors (GPCRs).
A. *Inhibitors as pharmacological tools combine multiple advantages. They enable work on endogenous, untagged proteins and can be used in primary cells or live animals, thus circumventing limitations to the translation of research results.* ***B.*** *For the investigation of GPCR signaling, inhibitors which intervene at various points in the signal transduction cascade are available. Common examples act directly on the GPCR or, alternatively, on downstream transducers such as phospholipase Cβ (PLCβ), mitogen-activated protein kinases (MAPKs) or, specifically, extracellular signal-regulated kinase (ERK). In contrast, inhibitors for all G proteins families are not readily available. The panel was created with BioRender.com.* ***C.*** *Important exceptions are the Gq/11 protein inhibitors FR900359 (FR) and YM-254890 (YM). These molecules are tremendously important pharmacological tool compounds as they unite high potency and specificity, are soluble and cell-permeable, and cause immediate and prolonged effects.*

Development of similar inhibitors for the remaining G protein families –of which there are four (Gq/11, Gs/olf, Gi/o, G12/13) (Cabrera-Vera et al., 2003; Simon et al., 1991; Syrovatkina et al., 2016; Wilkie et al., 1992)– that combine selectivity with potency, ease of application in cells and *in vivo*, and a long duration of action would tremendously benefit GPCR research. Apart from more easily uncovering GPCR signaling profiles, pharmacological inhibition of selected G protein pathways could

be a helpful strategy in understanding (patho)physiological processes and, ultimately, facilitate the development of new therapeutics.

However, the development of such inhibitors has proven to be challenging. Several attempts to develop or uncover (natural product) G protein family-specific inhibitors have produced various compounds, all of them lacking one or the other necessary property to achieve potent inhibition of G protein signaling in living cells (Ayoub, 2018; Campbell & Smrcka, 2018; Dai et al., 2022; Freissmuth et al., 1996; Keen et al., 2022). Among the frequent limitations are toxicity, low cell permeability, and loss of efficacy in cells compared to *in vitro* applications. Endeavors derivatizing the FR and YM scaffolds to unlock specific inhibition of other G protein families have yielded a plethora of analogs. However, these retain their Gq/11 specificity, often with reduced potency (Reher, Kühl, et al., 2018; Xiong et al., 2019; Xiong et al., 2016; Zhang et al., 2018; Zhang et al., 2017).

We suggest a temporary alternative solution to the obvious lack of G protein inhibitors. Instead of modifying the inhibitory compound, we propose to alter the G proteins of interest to render them inhibitor-sensitive; we suggest the development of a toolbox consisting of genetically engineered G proteins that are sensitive to the already available and easy-to-use inhibitor FR (Figure 3A). In this study, we aim to demonstrate the feasibility of such a toolbox by investigating whether the establishment requirements can be met and to develop the first part of this toolbox.

The first objective of this study is to rationally engineer a wild type-like Gαq mutant refractory to inhibition by FR. This is necessary for the exclusive inhibition of the desired engineered G family protein and will be the first part of the suggested toolbox. Secondly, we plan to employ this engineered Gq variant in live animals to investigate the overall suitability of FR in combination with artificial Gα protein subunits as fundament for a chemogenetics-like toolbox (Figure 3B).

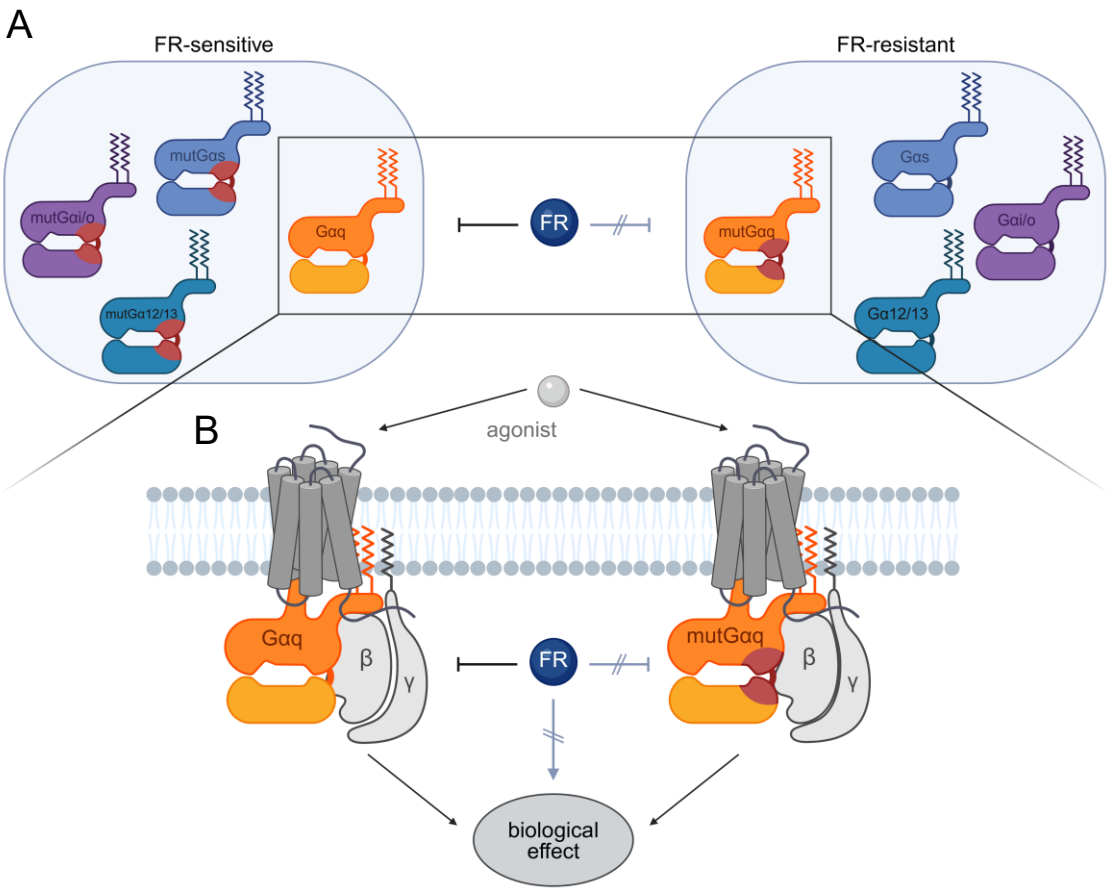

Figure 3: Principle of a chemogenetics-like toolbox for the causal investigation of G protein signaling. ***A.*** *The putative chemogenetic G protein toolbox comprises FR900359 (FR)-sensitive and -resistant variants of all Gα protein families, that is FR-sensitive mutant versions of naturally insensitive Gα proteins, as well as FR-resistant mutants of Gαq, Gα11, and Gα14. Selective combination of these Gα protein variants in vitro or in vivo allows for the unambiguous, causal investigation of any G protein-mediated or -modulated signaling pathway.* ***B.*** *The first step towards such a toolbox, which is the subject of this thesis, is the generation of an engineered Gαq protein that combines resistance to the inhibitor with wild type-like signaling behavior. This entails triggering a wild type-equivalent biological response after activation by agonist-bound GPCRs. Concurrently, FR should not elicit a biological response in the absence of wild-type Gq/11 proteins. The figure was created with BioRender.com.*

A chemogenetics-like toolbox like this would enable causal investigation of GPCR-mediated signaling events, deconvolution of G protein involvement in (patho)physiology, and, finally, the development of new drugs. In addition, the developed FR-insensitive Gq isoforms could be used in conjunction with FR as a standalone tool (Patt et al., 2021). One possible application allows for the investigation of Gq-mediated effects in a cell type- or tissue-specific manner *in vivo*. For this, wild-type Gq would be replaced by an FR-resistant but functionally wild type-like mutant in an entire animal apart from one cell type or tissue rendering Gq in this specific area only susceptible to inhibition by FR.

1.4. G protein activation cycle

The main goal of this thesis is the development of a mutant Gαq protein which is refractory to FR inhibition. Since the final purpose is the introduction of this mutant

in vivo, possibly by replacing the wild-type Gαq protein in live animals, it is paramount that the mutant Gαq protein retains wild-type functionality. Therefore, the wild-type G protein activation cycle needs to be addressed in this introduction.

G proteins are guanine nucleotide-binding proteins, specifically large heterotrimeric GTPases, comprising an α subunit and a constitutive βγ dimer (Gilman, 1987; Simon et al., 1991) (Figure 4). The Gα subunit consists of a GTPase or Ras-homology domain (RHD) and an α-helical domain (AHD) connected via two linkers whose flexibility is paramount to G protein activation (D. E. Coleman et al., 1994; D. E. Coleman & Sprang, 1998; Lambright et al., 1994; Lambright et al., 1996; Noel et al., 1993; Wall et al., 1995).

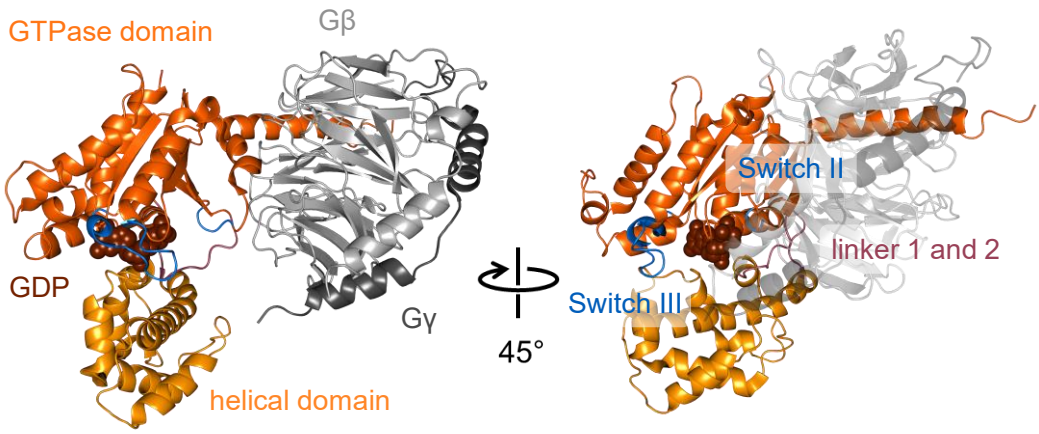

Figure 4: Cartoon representation illustrating the tertiary structure of the inactive chimeric Gq/i heterotrimer.
The Gα subunit consists of a GTPase (dark orange cartoon) and a helical domain (light orange cartoon) connected via two linkers (red cartoon). In the displayed inactive state, the Gα subunit is bound to GDP (dark red spheres) and in complex with the constitutive Gβγ heterodimer (light and dark grey cartoon, respectively; transparent in the right panel for better visibility of the Gα subunit). The three Switch regions (Switch II and III as blue cartoon, Switch I corresponds to linker 2) alter their conformation upon activation of the G protein. This structural representation shows the chimeric Gq/i heterotrimer, based on its X-ray structure in complex with YM-254890 published by Nishimura et al. (2010) (Proten Data Bank (PDB) ID: 3AH8), and was colored and oriented in PyMOL for clarity.

In the inactive state, the α subunit binds guanosine diphosphate (GDP) between its two domains, and the G protein exists in its heterotrimeric state. Upon activation by a ligand-activated GPCR or a non-receptor guanine nucleotide exchange factor (GEF) or during spontaneous activity, conformational changes in the G protein are induced (Oldham & Hamm, 2008) (Figure 5A). The helical domain moves into an open conformation and GDP is released. Due to the high excess of guanosine triphosphate (GTP) compared to GDP in the cytosol (Traut, 1994), binding of GTP to the nucleotide binding pocket of the α subunit is the most likely next event. Binding of GTP with its additional phosphate group triggers further conformational changes in the G protein inducing closure of the AHD. Concurrently, GEF- and Gβγ complex-interacting domains of Gα change conformation causing simultaneous dissociation or rearrangement of the G protein subunits and release from the receptor (Papasergi-Scott et al., 2024).

Both the Gα subunit and the Gβγ complex engage downstream signaling effectors. In the case of the α subunit, the conformational changes in three so-called Switch regions (Figure 4) induced by binding of GTP in lieu of GDP result in a reduction of affinity to the βγ complex and an increase in the affinity for effector proteins (Oldham & Hamm, 2008). Gβγ does not undergo any major conformational alterations. However, the effector interaction surface, which is obstructed by Gα in the inactive heterotrimeric state, is rendered accessible upon activation of the G protein (D. E. Clapham & Neer, 1997; Logothetis et al., 1987; Robishaw & Berlot, 2004; Smrcka, 2008) (Figure 5A). Which Gα effector proteins are bound and activated depends mainly on the family and subtype of the Gα subunit (Stefan Offermanns, 2003). Based on sequence similarity, the 21 different human Gα subunit isoforms are divided into four families (Gαq/11, Gαi/o, Gαs, and Gα12/13) (Simon et al., 1991; Wilkie et al., 1992), each interacting with a partially overlapping subset of effectors.

The Gq/11 family, which is of particular interest in this study, consists of Gαq, Gα11, Gα14, and Gα16, with the primary effector being phospholipase Cβ (PLCβ) (S. B. Lee et al., 1993) (Figure 5B). Upon activation by Gαq/11, PLCβ cleaves the membrane lipid phosphatidylinositol 4,5-bisphosphate (PIP_2) into soluble inositol 1,4,5-trisphosphate (IP_3) and diacylglycerol (DAG) which remains in the membrane (Smrcka & Sternweis, 1993; Sternweis & Smrcka, 1992). Both second messengers in turn potentiate their own signaling cascades. IP_3 diffuses through the cell and opens IP_3-gated calcium channels (IP_3 receptors, IP_3R) in the endoplasmic reticulum to increase the cytosolic calcium concentration (Schmitz et al., 2022; Smith et al., 2023). This causes physiological responses in the cell and consequently in tissues or organs, such as contraction of smooth muscle cells, secretion of hormones or action potentials in neurons (Berridge et al., 2003; Bootman & Bultynck, 2020; David E. Clapham, 2007).

What is the mechanism that allows the G protein to return to an inactive state? The GTPase domain of the Gα protein catalyzes the hydrolysis of the loaded GTP into GDP, which remains bound in the nucleotide binding pocket, and a phosphate molecule (D. E. Coleman et al., 1994; Sondek et al., 1994) (Figure 5A). The kinetic rate of this process is in part dependent upon the Gα subunit. For example, isolated Gαs proteins have been observed to cleave GTP at a faster rate than Gαq proteins (Elliott M. Ross, 2008). Furthermore, GTPase-accelerating proteins (GAPs), including regulator of G protein signaling (RGS) proteins and certain Gα effectors, can enhance the GTPase activity of Gα (Berman et al., 1996; Berstein et al., 1992; Hepler et al., 1997; E. M. Ross, 1995; E. M. Ross & Wilkie, 2000; O. Saitoh et al., 1997). The GTP-GDP turnover reverses the activating conformational changes in the Gα subunit, thereby allowing for the binding of Gβγ, which returns the G protein to its original heterotrimeric inactive state.

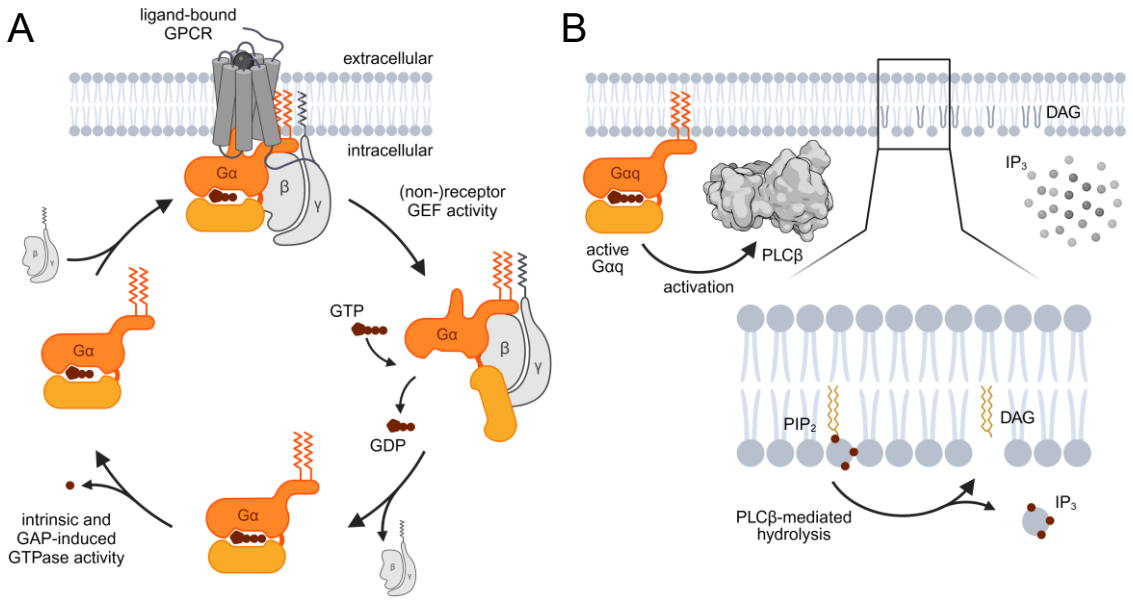

Figure 5: G protein activation cycle and first steps of the Gq signaling cascade.
A. *Cartoon depiction of the G protein activation cycle. Upon ligand binding to the extracellular face of a G protein-coupled receptor (GPCR), the activated receptor acts as guanine nucleotide exchange factor (GEF) on the G protein α subunit. Alternatively, non-receptor proteins can act as GEFs. Opening of the Gα subunit via the flexible hinge regions and GDP release from it are induced. This enables GTP to bind to the nucleotide binding pocket. Closing of Gα in the GTP-loaded state induces conformational changes in the Switch regions, culminating in dissociation from the receptor and release or rearrangement of Gβγ. Both Gα and Gβγ can now activate their respective effectors. Intrinsic or GTPase-activating protein (GAP)-induced GTPase activity of the Gα subunit terminates signaling via the hydrolysis of the bound GTP to GDP. The inactive Gα protein reassociates with the Gβγ complex and, thereby, inactivates it.* ***B.*** *Active GTP-bound Gαq will activate phospholipase C β (PLCβ) isozymes which catalyze the hydrolysis of phosphatidylinositol 4,5-bisphosphate (PIP_2) into soluble inositol 1,4,5-trisphosphate (IP_3) and diacylglycerol (DAG). Both second messengers induce further downstream signaling. The figure was created with BioRender.com.*

1.5. Mode of action and binding mode of FR

The central compound of this thesis, the cyclic depsipeptide FR900359 (FR) (Figure 6A), intervenes in this G protein activation cycle. FR is a natural product produced by the bacterium *Candidatus* Burkholderia crenata, an obligate endosymbiont residing in leaf nodules of the Asian ornamental plant *Ardisia crenata* (Carlier et al., 2016; Fujioka et al., 1988) and other *Ardisia* species (Reher, Kuschak, et al., 2018). Previously, FR was extracted primarily from *Ardisia crenata* leaves. Biotechnological production via heterologous expression of the FR nonribosomal peptide synthetase *frs* gene cluster in *Escherichia coli* (*E. coli)* was successful (Crüsemann et al., 2018), as was the development of a total synthesis protocol (Xiong et al., 2016). However, both methods only yielded small amounts of inhibitor. Meanwhile, a new FR producer, *Chromobacterium vaccinii* MWU205, has been identified. A knock-out mutant of this strain lacking a gene necessary for the production of its characteristic purple pigment violacein allows significantly enhanced yields in FR extractions (Hermes et al., 2021).

This increase in yield is necessary, as FR and the closely related compound YM-254890 (YM) have become universal and extensively used tools in GPCR research to inhibit Gq/11 family proteins. YM was initially discovered in a screen for platelet aggregation inhibitors (Taniguchi et al., 2003) and subsequently characterized as an inhibitor of Gαq/11 proteins (Takasaki et al., 2004). Both compounds act as specific and potent inhibitors of guanine nucleotide dissociation (GDIs) on the Gα subunits of Gq, G11, and G14 proteins, the fundamental first step of G protein activation (Nishimura et al., 2010; Patt et al., 2021; Schrage et al., 2015). FR and YM essentially stabilize the inactive GDP-bound form of the Gα subunit (Bonifer et al., 2024; Mühle et al., 2025; Nishimura et al., 2010; Todd et al., 2024; Trent et al., 2025).

In addition to biochemical methods, the clarification of the mechanism of action was advanced by elucidating the inhibitors' binding mode. YM's binding mode was resolved via X-ray crystallography of the inhibitor in complex with a heterotrimeric Gq/i protein chimera (Nishimura et al., 2010). Extensive mutagenesis studies, molecular modeling simulations, and subsequently resolved structures of FR and YM bound to heterotrimeric G11 demonstrated that FR shares YM's binding mode (Malfacini et al., 2019; Mühle et al., 2025; Patt et al., 2021; Schrage et al., 2015; Jan H. Voss et al., 2021). Both inhibitors form extensive contacts with residues of both Gα domains and the linkers connecting them (linker 1 and linker 2/Switch I), burying themselves in an intramolecular cleft between the GTPase and helical domains (Figure 6B).

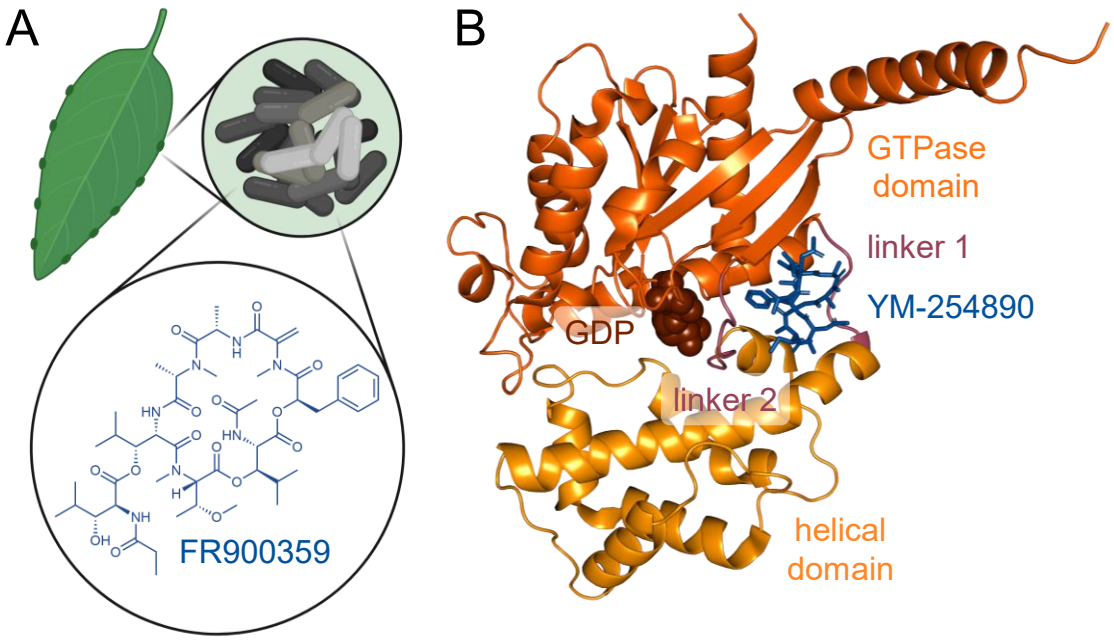

Figure 6: Origin, structure, and binding mode of FR900359 (FR).
A. *FR is as cyclic depsipeptide (structure in blue) produced, among others, by Candidatus Burkholderia crenata, an obligate bacterial endosymbiont living in leaf nodes of the ornamental plant Ardisia crenata. The panel was created with BioRender.com.* ***B.*** *Structure of FR's close relative, YM-254890 (YM, blue sticks), bound to the α subunit of a chimeric Gq/i heterotrimer. FR shares YM's binding mode, burrowing into the cleft between the GTPase (dark orange cartoon) and helical domain (light orange cartoon) in between linkers 1 and 2 (red*

cartoon), thereby stabilizing the GDP (dark red spheres)-bound form of Gα. This structural representation is based on the X-ray structure published by Nishimura et al. (2010) (PDB ID: 3AH8), and was colored and oriented in PyMOL for clarity.

The binding mode and the resulting mechanism of inhibition can roughly be broken down into four instances following an “interaction and stabilization” paradigm. The inhibitors contact and stabilize Switch I, linker 1, and the nucleotide binding pocket, as well as the interaction between Gα and the Gβ subunit which leads to stabilization of the entire heterotrimer.

Firstly, the inhibitors form extensive contacts with Switch I. This region consists of linker 2 and a few residues of the β2-sheet in the GTPase domain and undergoes conformational changes upon activation of the G protein. Inhibitor interactions include hydrogen bonds with the β2-sheet protein backbone, as well as hydrophobic interactions with a row of residues in Switch I and the extended β2-sheet. Most notably, a hydrophobic pocket formed by the side chains of valine-184$^{G.hfh2.3}$, threonine-187$^{G.hfh2.7}$, and isoleucine-190$^{G.S2.2}$ in Switch I and isoleucine-56$^{G.H1.5}$ and lysine-57$^{G.H1.6}$ in the α1αA-loop accommodates the inhibitors’ aromatic moiety[2]. Taken together, these interactions stabilize Switch I and prevent its movement towards the nucleotide binding pocket upon activation (Mühle et al., 2025; Nishimura et al., 2010).

In addition to the stabilizing effect on linker 2/Switch I, FR and YM form direct and indirect contacts with and stabilize linker 1, precluding the hinge motion of the interdomain linkers which facilitates domain opening prior to nucleotide exchange. The direct polar contact with tyrosine-67$^{G.h1ha.4}$ in linker 1 (Mühle et al., 2025) is completed by indirect contacts with the linker 1 backbone (Mühle et al., 2025; Nishimura et al., 2010). These indirect contacts are mediated by a salt bridge between arginine-60$^{G.H1.9}$ and asparagine-71$^{H.HA.3}$ in the α1- and the αA-helix, respectively. The inhibitors form hydrogen bonds with these two residues which then bridge to linker 1 through additional hydrogen bonds themselves.

In addition to the interactions with Gα regions that are responsible for domain separation prior to nucleotide release, FR and YM also interact with the nucleotide binding pocket directly. Hydrophobic interactions between the inhibitors and serine-53$^{G.H1.2}$ in the P-loop, which coordinates the GDP phosphates, stabilize the nucleotide-binding residues, contributing another aspect to the GDI action (Mühle et al., 2025).

Finally, hydrophobic interactions with additional residues in the αA-helix in the AHD, phenylalanine-75$^{H.HA.7}$ and leucine-78$^{H.HA.10}$, complete the picture. The inhibitors

[2] Position numbering is given in two manners in this thesis. In-line numbers connected with a hyphen are the murine or *Drosophila* Gαq residue number. Superscript position labeling is based on the CGN nomenclature by Flock et al. (2015). See Table 28 in Additional Material for a comparison of murine Gαq, *Drosophila* Gαq, and common Gαq numbering.

excel in forming contacts with all surrounding regions of the protein: the two linkers, the αA-helix of the helical domain, and the β2-sheet in the GTPase domain (Nishimura et al., 2010). This way, the inhibitors essentially freeze all regions undergoing the initial conformational changes during activation of the G protein and lock the Gα subunit in its GDP-bound, inactive state.

In the publication featuring the first available structure of YM in a chimeric Gq/i heterotrimer, the authors describe the binding of YM to occur “without contacting Gβγ” (Nishimura et al., 2010). However, in the higher-resolution G11/i structures that have recently been published, certain contacts between the inhibitors and the Gβ subunit have become apparent (Mühle et al., 2025). These direct contacts with the Gβ subunit do not affect the effectiveness of GDI action on Gα. However, FR and YM utilize this contact to effectively stabilize the entire Gq/11 heterotrimer, and thereby virtually obstruct their own path of dissociation. Consequently, the direct contacts with Gβ do not contribute to the potency of Gα inhibition; rather, they serve to facilitate the extraordinarily prolonged residence time of the inhibitors on the G protein (Mühle et al., 2025).

1.6. Altering FR sensitivity…

This comprehensive understanding of the FR binding site and mechanism allows for the rational alteration of a G protein’s FR sensitivity. Modifications of the FR binding site are necessary to either accommodate FR binding in natively non-sensitive Gα subunits or to prevent efficient inhibitor binding to the natively sensitive Gαq, Gα11 or Gα14 proteins.

Previously, attempts have been made to alter the (putative) FR binding region of multiple Gα proteins, among them Gαq. All studies followed one of two approaches: the substitution of residues in the (putative) FR binding site for the analogous amino acids of another Gα subunit, or the identification and rational substitution of key inhibitor binding residues for amino acids considered unfavorable for interaction (Figure 7).

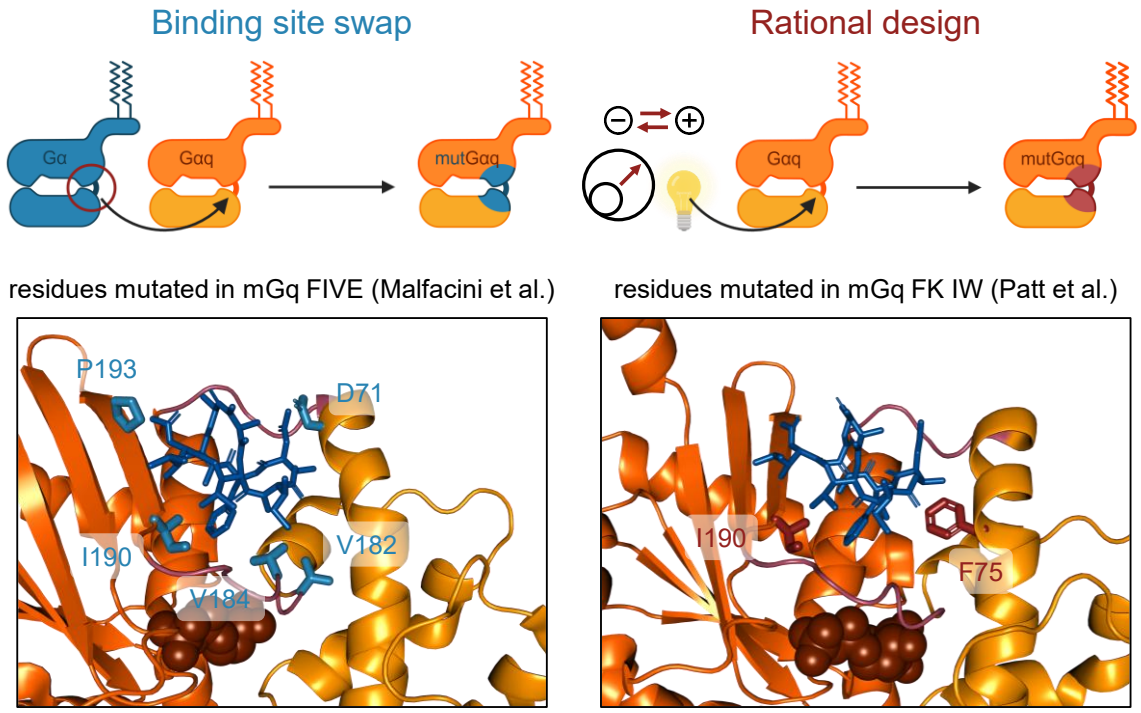

Figure 7: Approaches for the generation of inhibitor-resistant Gαq mutants.
Left. *The introduction of the putative FR binding site of naturally resistant Gα subunits renders Gαq inhibitor-insensitive, as has been done in the creation of mGq FIVE (Malfacini et al., 2019). The five residues mutated in mGq FIVE to match their Gα16 counterparts (D71, V182, V184, I190, P193) are depicted as turquoise sticks in the structure below.* ***Right.*** *Amino acids in the FR binding site can be swapped for residues with changed charge or larger side chain to create FR-resistant Gαq mutants by rational design. This has been done in the creation of mGq FK IW (Patt et al., 2021). The residues altered in this rationally designed mGαq mutant (F75, I190) are depicted as red sticks in the structure blow. The structural representations are based on the X-ray structure published by Nishimura et al. (2010) (PDB ID: 3AH8), and was colored (as in Figure 4 and Figure 6B) and oriented in PyMOL for clarity. The figure was partially created with BioRender.com.*

The generated Gα subunits with artificially introduced FR sensitivity include YM-sensitive Gαi1 (Onken et al., 2018), FR-sensitive Gαs (Boesgaard et al., 2020), FR-sensitive Gα13 (Todd et al., 2024), as well as FR- and YM-sensitive Gα16 mutants (Malfacini et al., 2019) with eight, eleven, eleven, and five residues transferred from Gαq, respectively. Similarly, transferring single or a combination of residues in the FR-binding site from natively insensitive Gα proteins to Gαq reduces the potency of the inhibitors. A combined substitution of three key inhibitor binding residues from Gαs to Gαq completely alleviates inhibition by FR (Boesgaard et al., 2020), while the transfer of five residues from Gα16 also transfers the FR and YM sensitivity profile (Malfacini et al., 2019) (Figure 7). These studies demonstrate that the transfer of the FR/YM binding region from a sensitive Gα to an insensitive protein and vice versa allows for the efficient transfer or disruption of inhibitor sensitivity.

The alternative structure-based approach to deliberately introduce mutations to weaken and preclude Gα/inhibitor interaction can only be used to diminish inhibitor sensitivity in natively sensitive Gα proteins with today's level of knowledge. Residues forming hydrophobic interactions can be exchanged for hydrophilic, charged amino acids creating electrostatic repulsion. Introducing bulky residues in

positions that are close to the inhibitor cause steric hinderance (Figure 7). This strategy has not only been used in the early characterization of the YM binding site (Nishimura et al., 2010), but also in the project directly preceding this study (Patt et al., 2021) (Figure 7). The knowledge of the inhibitor binding site and the most relevant interaction points was exploited to rationally design FR and YM-resistant mouse Gαq proteins with the aim to generate an *in vitro* tool for the delineation of Gq-mediated or -modulated signaling events (Patt et al., 2021). These experiments serve to further our understanding of the inhibitors' binding mode and inhibition mechanism but also showcase possible applications of Gα proteins with altered inhibitor sensitivity.

Even though many binding residues have successfully been replaced to influence inhibition, these studies also demonstrate that not all residues identified as contacting the inhibitors contribute equally to inhibitor binding. When replacing all differing FR binding residues of Gαq individually by the corresponding Gαs residues, three of the single mutants display superior reduction in FR sensitivity (Boesgaard et al. 2020). Similar results have been obtained by transferring Gα16 residues (Malfacini et al., 2019). Furthermore, combination of mutations regularly yields synergistic effects on inhibitor sensitivity (Malfacini et al., 2019; Patt et al., 2021).

While the data that we draw back on here to rationally select mutations to introduce is a mixture of studies using FR or YM or both, the overall picture that emerges is rather clear. Some residue substitutions are better suited to alter FR sensitivity than others, and synergistic effects come into play when combining two or more mutations. In general, the inhibitors need the hydrophobic pocket of the protein for proper binding. Consequently, introducing hydrophilic residues reduces binding and inhibition. The overall inhibitor binding site has been extensively characterized, and the literature fully maps the relevant inhibitor contact points.

1.7. … while retaining wild-type functionality

All efforts described above have primarily focused on either inducing or reducing the inhibition by FR, with minimal attention paid to the retention of the protein's wild-type functionality in downstream signaling. Most of the studies focus only on the general functionality of the generated mutants to enable the investigation of inhibition by FR. Beyond this, the signaling behavior of the mutants is only briefly discussed in two of the studies (Boesgaard et al., 2020; Patt et al., 2021).

The cleft to which FR and YM bind has been described as a novel binding site that is not targeted by other interaction partners of Gα (Nishimura et al., 2010). This is true for the binding site in total. However, some residues interacting with the inhibitors are in fact involved in the binding of other proteins, not only Gβγ (Lambright et al., 1996; Wall et al., 1995) but various effectors such as PLCβ (Lyon et al., 2013; Waldo et al., 2010), GPCR kinase 2 (Day et al., 2004), and RGS

proteins (Taylor et al., 2016; Tesmer et al., 1997). Moreover, linker 1 and 2 that sandwich FR in its binding pocket are crucial for interdomain opening and closure, a vital mechanical feature for the G protein activation cycle and for regulating activation kinetics (Papasergi-Scott et al., 2024). Changes in these residues can naturally affect both inhibitor binding but also any other functions that are encoded within this region.

Therefore and as demonstrated by earlier publications (Boesgaard et al., 2020; Patt et al., 2021), the challenge of this project is not primarily to rationally design FR-insensitive Gαq mutants but rather to do so while maintaining wild-type signaling behavior. This is the key requirement for the eventual use of the mutant proteins *in vivo*.

1.8. *Drosophila melanogaster* as model organism

Every mammal has G proteins with various degrees of conservation among species (Wettschureck & Offermanns, 2005; Wilkie et al., 1992). The use of a G protein chemogenetic toolbox as envisioned in this thesis depends on the selection of a model organism for which the toolbox is developed. For this thesis, we selected *Drosophila melanogaster* as model organism for multiple reasons.

Importantly, *Drosophila melanogaster* as model organism is characterized by good translational potential of physiological or pathological results to the human context. This stems from the similarity of some complex behaviors and in physiology (Spindler & Hartenstein, 2010; Ugur et al., 2016) and the high number of functional orthologs of human disease-related proteins in the fruit fly (Narayanan & Rothenfluh, 2016).

Drosophila melanogaster is a genetically easy to manipulate organism. This simplifies the second part of this project, the employment of a mutant Gαq protein *in vivo*. The introduction of a genetically engineered Gαq variant into the organism can be achieved easily and fast (Venken et al., 2016). The rather short lifespan and high fecundity of *Drosophila melanogaster* compared to other model organisms such as mice (Ziehm et al., 2013) shortens the timeframe of *in vivo* experiments and simplifies husbandry. Fruit flies are small in size which reduces equipment and maintenance space.

Apart from these practical reasons, *Drosophila melanogaster* is an ideal model organism for our study for biological reasons. The fruit fly provides us with an ideal endpoint for initial *in vivo* experiments. When *Drosophila* flies are kept on food containing FR, flies die in an FR dose-dependent manner (addressed in detail in Chapter 5.5.1. Lethality of FR). Survival of *Drosophila* flies ubiquitously expressing engineered inhibitor-resistant Gαq on FR-containing food is an ideal endpoint for this study, as it represents a conclusive black-and-white answer to our question of

the feasibility of a G protein and FR-based chemogenetic platform for *in vivo* application.

Finally and most importantly, *Drosophila melanogaster* does not express Gα11 or Gα14 variants (Katanayeva et al., 2010). This allows for the unambiguous interpretation of the planned *in vivo* experiment. If FR is in fact specific for Gq/11 family proteins *in vivo*, as we expect, all FR-induced effects are mediated via Gαq only. The introduction of an FR-insensitive *Drosophila* Gαq (DGαq) variant alone should, therefore, abolish FR effects without the need to consider effects mediated by FR-sensitive Gα11 and Gα14 wild-type proteins. However, *Drosophila* expresses seven splice variants of the same Gαq gene, resulting in the expression of three distinct Gαq isoforms (Alvarez et al., 1996; Y. J. Lee et al., 1990; Y. J. Lee et al., 1994; Scott et al., 1995; Talluri et al., 1995). One isoform, DGqC, is expressed only in the male gonads and suggested to function as part of an autonomous photosensory pacemaker for circadian functions in the testes (Alvarez et al., 1996). Due to its narrow expression and function, this isoform will be excluded from this thesis, narrowing down the isoforms to be considered to two, referred to here as isoform G (DGqG), also known as DGqB, DGαq-PG, dGqα-2 or DG_{q2}, and isoform D (DGqD), also called DGqA, DGαq-PA, dGqα-1 or DG_{q1}.

1.9. *Drosophila melanogaster* Gαq isoform G

Drosophila melanogaster Gαq isoform G can simply be expressed in human embryonal kidney cells (HEK293 cells) and yields functional protein which is able to signal via human effector proteins such as PLCβ when activated by a human receptor such as the muscarinic acetylcholine receptor type 3 (M3 receptor, M3R) which is endogenous to this cell system (Alenfelder, 2019) (Figure 8A and B). This enables the characterization of mutant Gαq proteins in the HEK293 cellular background. In contrast, *Drosophila melanogaster* Gαq isoform D does not respond to carbachol-induced activation of the M3 receptor in the same assay setup when expressed analogously to isoform G (Figure 8C). This is consistent with previously published results in which isoform D shows a much lower signal amplitude in G protein activation experiments in HEK293T/17 cells compared to isoform G (Himmelreich et al., 2017).This publication also confirmed the ability of isoform G to bind to the human Gβ1γ2 complex. Moreover, the expression of isoform D is limited to the flies' visual system (Y. J. Lee et al., 1990). Finally, DGqG is more closely related to other species' Gαq proteins, while DGqD is suggested to be evolved from DGqG through three exon duplications and to function more uniquely (Alvarez et al., 1996). For these three reasons, the focus of this work is on isoform G.

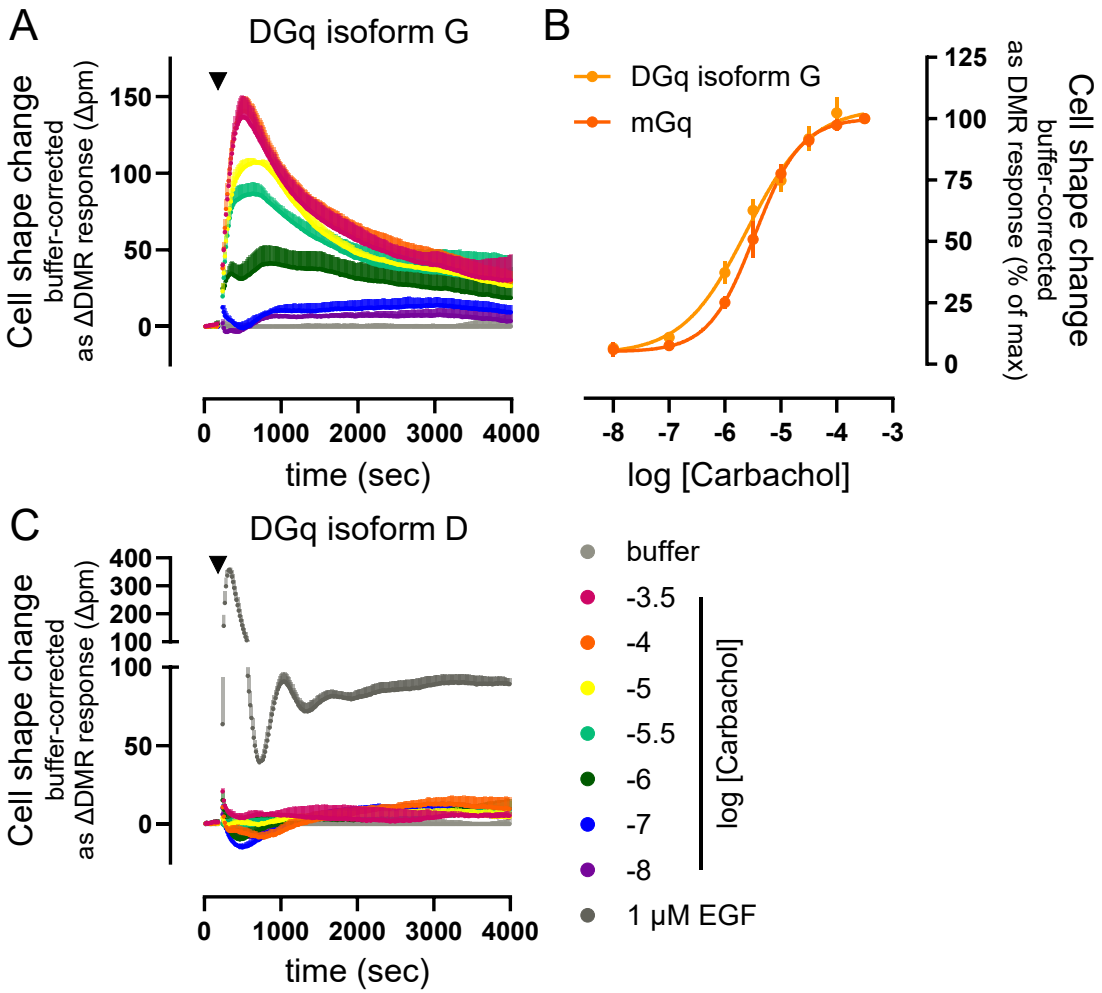

Figure 8: DGq isoform G but not isoform D can be functionally expressed in human cells as measured in dynamic mass redistribution (DMR) assays.
A. *Kinetic buffer-corrected DMR traces of HEK293 cells lacking Gαq and Gα11 proteins after CRISPR/Cas9 treatment (HEK293 Gq/11-KO) transiently transfected with a construct coding for DGq isoform G. Cells were activated with different concentrations of carbachol (CCh) or buffer after about 3 minutes of baseline measurement. Data are the means + SD of one experiment representative of four biologically independent experiments.* ***B.*** *CCh concentration-response curves measured as maximal buffer-corrected DMR response after stimulation with CCh or buffer normalized to the effect of 316 mM CCh in cells transfected as in A or with mGq. Data are the means ± SEM of three to four biologically independent experiments.* ***C.*** *Kinetic buffer-corrected DMR traces of HEK293 Gq/11-KO cells transiently transfected with a construct coding for DGq isoform D. Cells were activated with different concentrations of CCh, buffer or 1 µM of epidermal growth factor (EGF) as viability control after about 3 minutes of baseline measurement. Data are the means + SD of one experiment representative of at least three biologically independent experiments. Data presented in this figure have been adapted from Alenfelder (2019).*

The most important requirement for this entire project to even be feasible is the FR sensitivity of *Drosophila* Gαq which we assumed when initially planning the project. This is not a trivial supposition, as there are few differences between the (putative) FR binding site of *Drosophila* Gαq and murine Gαq, and numerous scientific findings published in literature hint at FR susceptibility of the protein.

Drosophila Gαq isoform G matches the murine Gαq to 85% in sequence (see Figure 66 in Additional Material). However, a sequence alignment of the (putative) FR

binding site of *Drosophila* and murine Gαq reveals an even higher degree of similarity: only two residues differ between the two proteins in this region (Figure 9A). In position H.HA.7 (numbering based on the Common Gα Numbering system (CGN) published in Flock et al. (2015)), there is a phenylalanine in murine Gαq but a tyrosine in *Drosophila* Gαq, while in position H.HA.8 the threonine in murine Gαq is swapped for an isoleucine in *Drosophila* Gαq. This essentially constitutes the shift of a hydroxy group by one amino acid and the addition of an ethyl moiety (Figure 9B). Phenylalanine-75$^{H.HA.7}$ and threonine-76$^{H.HA.8}$ in mGq are both positioned in linker 1. While F75$^{H.HA.7}$ forms hydrophobic contacts with the inhibitor (Nishimura et al., 2010), T76$^{H.HA.8}$ points away from the inhibitor and has not been implicated in inhibitor binding (Figure 9C). The additional bulk when an isoleucine is present in position H.HA.8 does not face the inhibitor and should not cause steric hinderance. While it is certainly not impossible that the more hydrophilic tyrosine in position H.HA.7 in DGq impacts FR binding and, therefore, inhibition by FR, it is rather unlikely.

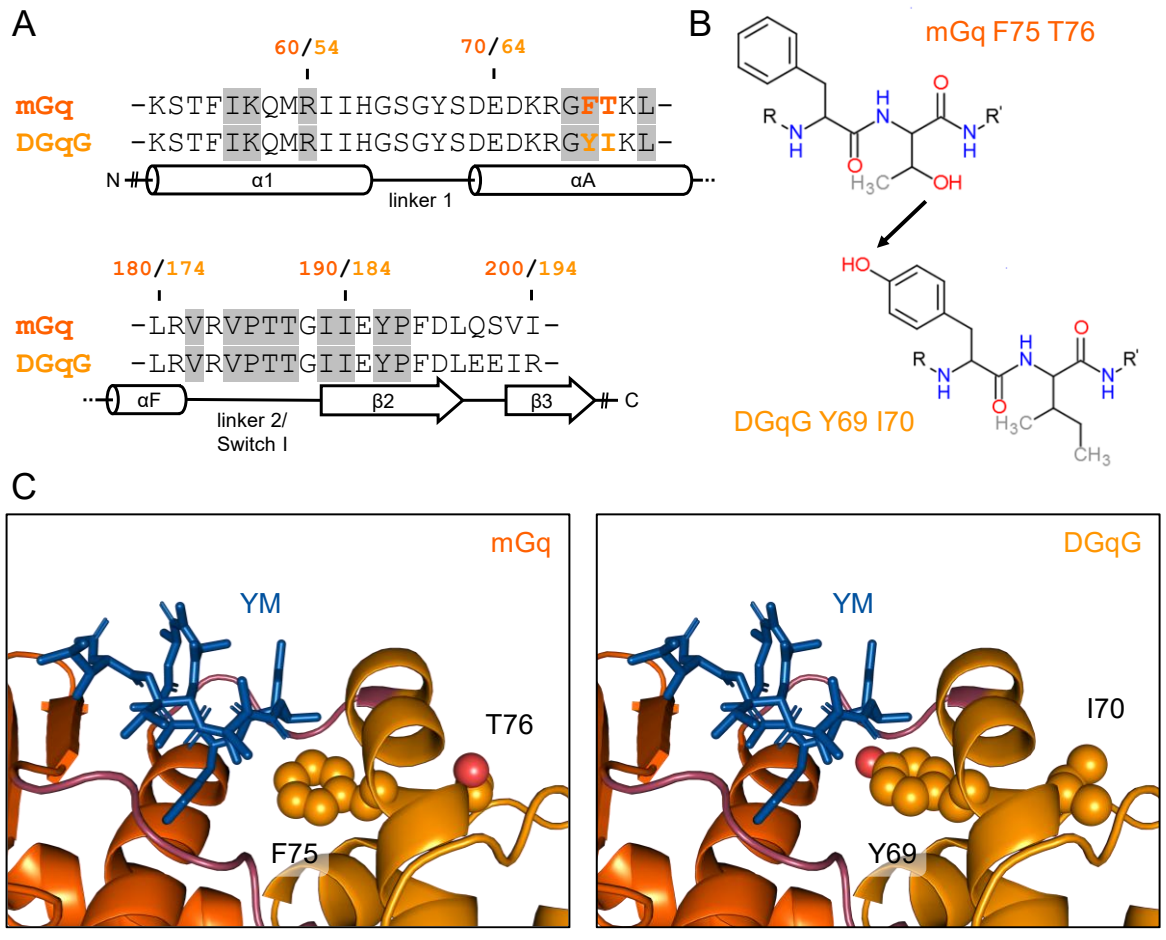

Figure 9: Comparison of the (putative) FR900359 (FR) binding sites in mGq and DGq isoform G.
A. *Alignment of the (putative) FR binding regions in murine and Drosophila Gq. Differing residues are marked in dark orange in the mGq sequence and in light orange in the DGqG sequence. Secondary structural elements are depicted below the sequence with cylinders (α-helices) and arrows (β-sheets). FR-interacting residues as taken from Nishimura et al. (2010) are highlighted in grey. The overall design of the alignment has been taken from Alenfelder (2019).* ***B.*** *Primary structure of the two differing residues in the (putative) FR binding site: F75 and T76 in mGq (top) and the corresponding Y69 and I70 in DGqG. The residue substitution constitutes the*

move of a hydroxyl group to the aromatic ring and the addition of an ethyl moiety to the second residue. This panel has been adapted from Alenfelder (2019). ***C.*** *Structural representation of the differing residues in the YM-254890 (YM)-bound structure of a chimeric Gq/i protein heterotrimer colored as in Figure 4 and Figure 6B. F75 and T76 in mGq and Y69 and I70 in DGqG are shown as spheres (carbons are orange or light orange in mGq and DGqG, respectively, oxygens are red). The addition of the hydroxyl group to the aromatic ring might influence inhibitor binding. The change of threonine to isoleucine is unlikely to change inhibitor binding, as the residue points away from the inhibitor.*

Strikingly, FR induces lethality of *Drosophila melanogaster* after oral ingestion (data shown in Chapter 5.5.1. Lethality of FR). Naturally, lethality alone does not necessarily translate to Gαq inhibition. However, multiple insect G proteins have been shown to bind (*Bemisia tabaci*, *Bombyx mori*, and Sf9 cell membrane preparations harboring *Spodoptera frugiperda* G proteins (Crüsemann et al., 2018)) or be susceptible to FR inhibition (*Caenorhabditis elegans* and *Heterodera schachtii* (Hanke et al., 2023)). In the case of *C. elegans* and *H. schachtii*, the putative FR binding site closely resembles the *Drosophila* Gαq sequence. Combined with the fact that stink bug nymphs (*Riptortus pedestris*) are similarly affected by FR ingestion (Crüsemann et al., 2018), *Drosophila* Gαq inhibition seems likely.

Taken together, all available evidence indicates that a) FR exhibits inhibitory potency on *Drosophila* Gαq and b) causes lethality via this mechanism. The first part of this assumption has been addressed in the master's thesis preceding this dissertation (Alenfelder, 2019), while the second part will be investigated in this study utilizing the rationally designed FR-insensitive *Drosophila* Gαq variants *in vivo*.

Signaling via *Drosophila* Gαq isoform G in HEK293 cells downstream of the M3 receptor is sensitive to pretreatment with FR (Alenfelder, 2019) (Figure 10A and B). The inhibitor is almost as potent on *Drosophila* Gαq as on murine Gαq with a 2 to 3-fold potency shift. Interestingly, this small shift in potency is faithfully recreated by transplanting the two residues differing in the FR binding site from *Drosophila* Gαq to murine Gαq (mGαq F75Y T76I) (Alenfelder, 2019) (Figure 10A and B). This loss-of-sensitivity experiment demonstrates that the two-residue difference in the binding site and not any differences in the rest of the protein cause this slight shift.

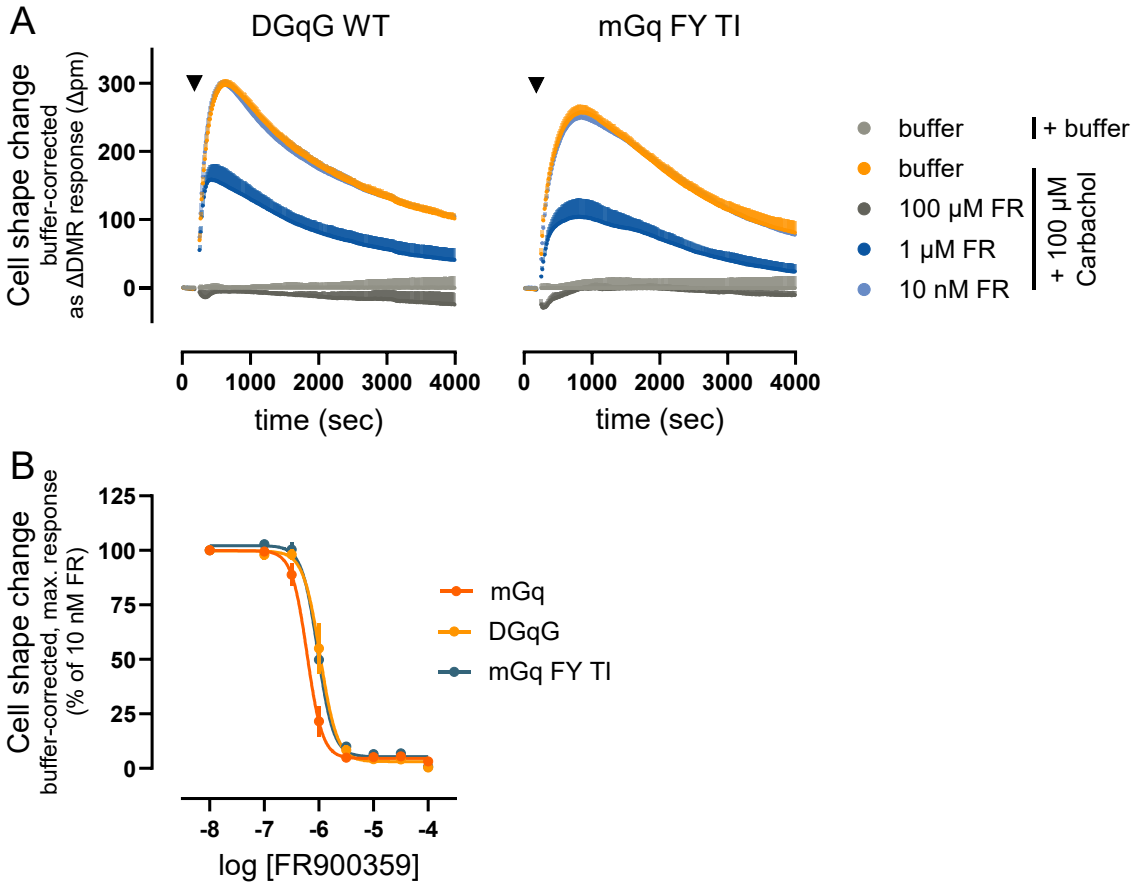

Figure 10: DGq isoform G is sensitive to FR900359 (FR), and its sensitivity is faithfully recapitulated by mGq F75Y T76I (FY TI) as measured in dynamic mass redistribution (DMR) assays.
A. *Kinetic buffer-corrected DMR traces of HEK293 cells lacking Gαq and Gα11 proteins after CRISPR/Cas9 treatment (HEK293 Gq/11-KO) transiently transfected with constructs coding for DGq isoform G or mGq FY TI. Cells were preincubated with different concentrations of FR or buffer and activated with 100 µM carbachol (CCh) or buffer after about 3 minutes of baseline measurement. Data are the means + SD of one experiment representative of four to five biologically independent experiments.* ***B.*** *FR concentration-response curves measured as maximal buffer-corrected DMR response after preincubation with FR and stimulation with 100 µM CCh normalized to the effect of 10 nM FR in cells transfected as in A or with mGq. Data are the means ± SEM of four to eight biologically independent experiments. Data presented in this figure have been adapted from Alenfelder (2019).*

In summary, these data show that the ultimate prerequisite for utilizing *Drosophila melanogaster* as *in vivo* model organism, the FR sensitivity of the predominant *Drosophila* Gαq protein, and thus all requirements for the project are met.

2. Aim of this Study

In an effort to bridge the lack of specific pharmacological inhibitors for the Gi, Gs, and G12/13 protein families, we suggest the temporary solution of a “chemogenetics-like” toolkit consisting of G protein subtypes with artificially introduced sensitivity to the known specific Gq/11 inhibitor FR. In this study, we aim to investigate the general feasibility of such a toolbox.

Firstly, we seek to generate FR-insensitive *Drosophila melanogaster* Gq/11 isoforms with wild type-like signaling behavior but robust resistance to FR. To this end, we will utilize our extensive knowledge of the FR binding site to rationally design FR-resistant DGq mutants. We will thoroughly characterize the developed mutants’ (signaling) behavior and sensitivity to the inhibitor FR. To this end, we will make use of a suite of (functional) readouts. Using western blotting and immunofluorescence microscopy, we will investigate the expression levels and subcellular distribution of the DGq variants, respectively. Activation and deactivation behavior will be investigated on the G protein dissociation level using a BRET-based Gβγ/masGRK3ct protein interaction assay. Moreover, we will evaluate signaling on the second messenger and whole-cell levels using an IP_1 accumulation assay and investigating dynamic mass redistribution following Gq stimuli. During this process, we will exclude DGq mutants displaying aberrant behavior from further testing and iteratively improve successful mutants to complete inhibitor resistance.

In a second step, we will employ the generated mutants for proof-of-concept experiments *in vivo* by expressing them ubiquitously using the GAL4/UAS system and an *actin5C-GAL4* driver in *Drosophila melanogaster*. To investigate the general compatibility of DGq variant overexpression, we will assay the transgenic fly strains in a negative geotaxis assay that measures a complex instinctual climbing response. We, then, intend to expose the probable causal link between inhibition of Gq and oral lethality induced by FR. This way, we aim to establish the general usability of the combination of the inhibitor FR and the chemogenetic Gq proteins developed in this project *in vivo*.

Finally, we aim to transfer the insight generated in the first part of the study to murine Gαq, generating a similar set of FR-resistant and fully functional mGq mutants to lay the groundwork for a similar undertaking in the murine background.

If successful, the engineered FR-resistant *Drosophila* and mouse Gq variants will constitute the fundament for a more extensive toolbox to put all G proteins under pharmacological control of FR, thus enabling causal investigation of cellular biology *in vitro* and *in vivo*.

3. Material

3.1. Bought materials

Table 1: Chemicals and Reagents.

Substance	Article Number	Company
0.05% Trypsin-EDTA (1X)	25300-054	Thermo Fisher Scientific Inc.
0.25% Trypsin-EDTA (1X)	25200-056	Thermo Fisher Scientific Inc.
1 kb Plus DNA Ladder	N3200S	New England Biolabs, Inc.
Acetic acid (glacial) 100%, anhydrous for analysis	1.00063.1000	Merck KGaA
Agar-Agar, BioScience	6494.3	Carl Roth GmbH + Co. KG
Ampicillin Natriumsalz	HP62.1	Carl Roth GmbH + Co. KG
Atropin sulfate salt monohydrate	A0257	Merck KGaA
Bovine serum albumin, fatty acid-free	A6003	Merck KGaA
Carbachol	C4382	Merck KGaA
Carbachol	108240050	Thermo Fisher Scientific
D-(+)-Glucose monohydrate	16301	Merck KGaA
Dimethyl sulfoxide (DMSO) for cell culture	A3572,0250	AppliChem GbmH
di-Natriumhydrogenphosphat Dodecahydrat	T106.2	Carl Roth GmbH + Co. KG
Distilled Water	15230-162	Thermo Fisher Scientific Inc.
DMEM (1X), Dulbecco's Modified Eagle Medium	41965-039	Thermo Fisher Scientific Inc.
dNTPs	U1515	Promega GmbH
Epidermal Groth Factor 500 µg	SRP3027	Merck KGaA
Ethanol 99% Petrolether	H1001057432000	JULI.O GmbH
Ethanol, absolute., >= 99.8%, Analytical reagent grade	E/0650DF/17	Thermo Fisher Scientific Inc.
Ethylenediamine tetraacetic acid	CN06.3	Carl Roth GmbH + Co. KG
FBS Good, EU approved regions, filtrated bovine serum	P40-37500	PAN Biotech GmbH
FR900359	produced in the lab of Gabriele König, Institute of Pharmaceutical Biology, University of Bonn	
Gel Loading Dye, Purple (6X)	B7024S	New England Biolabs, Inc.
Glycrin 85 %, GR for analysis	1.04094.1000	Merck KGaA
Goat Serum	S26	Merck KGaA
HBSS (1X), Hanks' Buffered Salt Solution	14025-050	Thermo Fisher Scientific Inc.
HEPES	HN77.4	Carl Roth GmbH + Co. KG
Hydrochloric acid	30721-1L-GL	Honeywell International Inc
Immobilon®-FL PVDF Membrane	IPFL00010	Merck KGaA
MIDORI Green Advance	MG04	NIPPON Genetics EUROPE GmbH
Nano-Glo® Luciferase Assay	N1130	Promega GmbH
NEBuffer™ 1.1	B7201	New England Biolabs, Inc.
NEBuffer™ r3.1	B6003S	New England Biolabs, Inc.
OPTI-MEM® I (1X)	31985-062	Thermo Fisher Scientific Inc.

Table 1 continued.

Substance	Article Number	Company
Paraformaldehyde	0335.2	Carl Roth GmbH + Co. KG
PBS Tablets, Phosphate-Buffered Saline	18912-014	Thermo Fisher Scientific Inc.
Penicillin-Streptomycin (10,000 U/ml; 10 mg/ml)	P06-07100	PAN Biotech GmbH
Poly-d-lysine (PDL)	P2636	Merck KGaA
Poly-ethylene imine, linear, M_W 2500 (PEI 2500)	24313-2	Polysciences, Inc.
Ponceau S Staining Solution	A40000279	Thermo Fisher Scientific Inc.
Powdered milk, Blotting Grade	T145.2	Carl Roth GmbH + Co. KG
Propan-2-ol	P/7507/17	Thermo Fisher Scientific Inc.
Protease inhibitor cocktail	S8830	Merck KGaA
Quick Start™ Bradford 1x Dye Reagent	5000205	Bio-Rad Laboratories, Inc.
S.O.C. Medium	15544034	Thermo Fisher Scientific Inc.
Sodium Chloride	BP358-212	Thermo Fisher Scientific Inc.
Sterile water for cell culture	P04-991500	PAN Biotech GmbH
Sulfuric acid 95-97%, GR for analysis	1.00731.2511	Merck KGaA
TMB One Solution	G7431	Promega GmbH
TRIS	4855.2	Carl Roth GmbH + Co. KG
Triton X-100	93420	Merck KGaA
Trypton/Pepton aus Casein, granuliert	6681.3	Carl Roth GmbH + Co. KG
UltraPure™ Agarose	16500500	Thermo Fisher Scientific Inc.
Yeast extract, micro-granulated	2904.3	Carl Roth GmbH + Co. KG

Table 2: Enzymes.

Enzyme	Article Number	Company
BamHI	R0136S	New England Biolabs, Inc.
DpnI	R6231	Promega GmbH
EcoRI	R0101S	New England Biolabs, Inc.
KpnI	R0142	New England Biolabs, Inc.
NheI-HF	R3131S	New England Biolabs, Inc.
Pfu DNA Polymerase	M7741	Promega GmbH
T4 DNA Ligase	M1801	Promega GmbH

Table 3: Antibodies (primary and secondary).

Anti-	Species	Clonality	Article Number	Company	RRID	Used for
HA, 12CA5	mouse	mono	11666606001	Roche Deutschland Holding GmbH	AB_514506	Microscopy, ELISA
Gαq/11/14, G-7	mouse	mono	sc-365906	Santa Cruz Biotechnology, Inc.	AB_10842057	Microscopy
Gαq, 10	mouse	mono	sc-136181	Santa Cruz Biotechnology, Inc.	AB_2232474	Microscopy
Gαq/11 CT	rabbit	poly	06-709	Merck KGaA	AB_310221	Microscopy
β-catenin, 14	mouse	mono	610153	Becton, Dickinson and Company	AB_397554	Microscopy
Gαq, NT, E-17	rabbit	poly	sc-393	Santa Cruz Biotechnology, Inc.	AB_631536	Western blot
HA, C29F4	rabbit	mono	3724	Cell Signaling Technology, Inc.	AB_1549585	Western blot (for RGS8)
RGS19 (GAIP)	rabbit	serum	-	kindly provided by Marilyn Farquhar, University of California, San Diego	-	Western blot
β-actin	mouse	mono	926-42212	LI-COR Biotech, LLC	AB_2756372	Western blot

Table 3 continued.

Anti-	Conjugation	Species	Clonality	Article Number	Company	RRID	Used for
mouse	FITC	goat	poly	F0257	Merck KGaA	AB_259378	Microscopy
rabbit	Cy3	goat	poly	AP132C	Merck KGaA	AB_92489	Microscopy
mouse	IRDye® 800CW	goat	poly	926-32210	LI-COR Biotech, LLC	AB_621842	Western Blot
rabbit	Alexa Fluor™ 680	goat	poly	A21077	Thermo Fisher Scientific Inc.	AB_2535737	Western Blot
mouse	horseradish peroxidase	goat	poly	4759.1	Carl Roth GmbH + Co. KG	AB_2857915	ELISA

Table 4: Commercial Kits.

Kit	Article Number	Company
NucleoBond Xtra Midi kit for transfection-grade plasmid DNA	740410.5	MACHEREY-NAGEL GmbH & Co. KG
NucleoSpin Plasmid, Mini kit for plasmid DNA	740588.25	MACHEREY-NAGEL GmbH & Co. KG
ReliaPrep™ DNA Clean-Up and Concentration System, 50 preps	A2892	Promega GmbH
HTRF IP-One Gq Detection Kit	62IPAPEB	Revvity Inc.

Table 5: Bacterial Strains.

Strain	Article Number	Company
E. coli DH5α (dam^+)	18265017	Thermo Fisher Scientific Inc.
E. coli XL1blue (dam^-)	200130	Merck KGaA

Table 6: Cell Lines.

Int. ID	Cell Line	Source	First described in
43	HEK293T	ATCC	DuBridge et al. (1987)
84	HEK293 Gq/11/12/13-KO	Asuka Inoue, Tohoku University	Devost et al. (2017)
86	HEK293 Gq/11-KO	Asuka Inoue, Tohoku University	Schrage et al. (2015)
88	HEK293 Gs/olf/q/11/12/13/z-KO (HEK293 Δ7)	Asuka Inoue, Tohoku University	Hisano et al. (2019)

Table 7: Equipment.

Equipment		Article Number	Company
Autoclave	Laboklav ECO Wastewater	-	SHP Steriltechnik AG
Balances	Talent Analytical Balance TE64	-	Sartorius AG
	Top Loading Balance A200S	-	Sartorius AG
	Analytical Balance MC210S	-	Sartorius AG
Cell Culture	Corning Cell Counter (CytoSMART™)	6749	Corning Inc.
	Fluid aspiration system	-	VacuuBrand GmbH & Co. KG
	Inverted microscope CKX31SF	6G01426	Olympus Europa SE & Co. KG
	Manifold, 8 Channel	1.170.058	Socorex Isba SA
	Neubauer Counting Chamber, 0.1 mm	640130	Paul Marienfeld-GmbH & Co. KG
Centrifuges	Eppendorf 5804R Centrifuge	5805000010	Eppendorf SE
	Eppendorf 5415D Centrifuge	-	Eppendorf SE
	Eppendorf 5810 Centrifuge	5810000420	Eppendorf SE
	VWR™ Galaxy Mini Microcentrifuge	37000-930	VWR International GmbH
	Sprout	HSA10825	Heathrow Scientific® LLC
Drying Cabinet	Heating Cabinet	-	JP SELECTA S.A.
Fluorescence microscope	Axio Observer.Z1	-	Carl Zeiss Microscopy GmbH
	Objektive Plan-Apochromat 63x/1,4 Oil DIC M27	420782-9900-799	Carl Zeiss Microscopy GmbH
	Axiocam 503 mono	426559-0000-000	Carl Zeiss Microscopy GmbH
	Axio Observer Anti vibration set	431007-9000-000	Carl Zeiss Microscopy GmbH
	Power Supply 232	-	Carl Zeiss Microscopy GmbH
	ApoTome.2	-	Carl Zeiss Microscopy GmbH
	Focus Controller.2	-	Carl Zeiss Microscopy GmbH
	HXP 120 V	-	Carl Zeiss Microscopy GmbH
Freezers	Upright Freezer	6483W	Gesellschaft für Labortechnik mbH
	Comfort NoFrost	-	Liebherr-Hausgeräte GmbH
	MVE High Efficiency 800 -190°C Series with TEC 3000	-	MVE Biological Solutions US, LLC
	FrosterLabo 330 PRO-ACTIVE	-	Philipp Kirsch GmbH
Fridges	SparkFree Laboratory Refrigerator	-	Thermo Fisher Scientific Inc.
Gel Electrophoresis	DeVision DBox	7110290	Decon Science Tec. GmbH
	ORCA-03G charge-coupled device camera	C11090-22B	Hamamatsu Photonics K.K.
	UV Transilluminator ECX-F20.M	-	VILBER LOURMAT Deutschland GmbH
	Mini-Sub® cell GT	1704406	Bio-Rad Laboratories, Inc.
	Wide Mini-Sub® cell GT	1704466	Bio-Rad Laboratories, Inc.
	PowerPac HC	1645052	Bio-Rad Laboratories, Inc.
Heating Unit	Thermomixer comfort	-	Eppendorf SE
Incubators	Heracell™ 240 CO_2 Incubator	-	Thermo Fisher Scientific Inc.
	Peltier-cooled incubator	IPP110	Memmert GmbH & Co. KG
	Incubator	IN160	Memmert GmbH & Co. KG
	Biotron Bacteriological Incubator	-	BINDER GmbH
	Minitron Incubator Shaker	-	Infors AG
Laminar Airflow	Herasafe™ Class II Biological Safety Cabinet, Type HS112	-	Thermo Fisher Scientific Inc.
	Safety Cabinet MRF-B-1300	-	STEAG Reinraumtechnik GmbH
LC/MS	micrOTOF-Q mass spectrometer	-	Bruker Corporation
	Dionex UltiMate 3000 HPLC System	-	Thermo Fisher Scientific Inc.
	NUCLEOSHELL RP 18, 2.7 µm, 100x2 mm, EC HPLC column (analytical)	763134.2	MACHEREY-NAGEL GmbH & Co. KG
Microwave	intellowave	-	LG Electronics Deutschland GmbH
Photometer	Eppendorf BioPhotometer™ D30	6133000001	Thermo Fisher Scientific Inc.

Table 7 continued.

Equipment		Article Number	Company
Pipettes	CyBio®-SELMA semi-automatic 384-channel Pipettor, 25 µL	OL7001-26-216	Analytik Jena AG
	E4™ XLS+ electronic single-channel pipette, 20-200 µL	17014486	Mettler-Toledo GmbH
	E4™ XLS+ electronic single-channel pipette, 2-20 µL	17014487	Mettler-Toledo GmbH
	Eppendorf Research, variable, 1-channel pipette, 0.5-10 µL	3111 000.122	Eppendorf SE
	Eppendorf Research, variable, 1-channel pipette, 10-100 µL	3111 000.149	Eppendorf SE
	Eppendorf Research® plus, variable, 1-channel pipette, 100-1000 µL	3123000063	Eppendorf SE
	Pipette controller, accu-jet® pro	26300	Brand GmbH & Co. KG
	Repetitive pipette, Multipette® plus	4891 000.019	Eppendorf SE
	Multi-channel micropipette Transferpette® -12 electronic	705454	Brand GmbH & Co. KG
Plate Readers	Epic® Whole cell biosensor	-	Corning Inc.
	Mithras LB 940	-	Berthold Technologies GmbH & Co. KG
	PHERAstar® FSX Microplate Reader	-	BMG Labtech GmbH
	SUNRISE Absorbance Reader	30041770	Tecan Group Ltd.
	POLARStar OMEGA Plate Reader	-	BMG Labtech GmbH
Scanner	Odyssey CLx Infrared Imaging System	-	LI-COR Biotech, LLC
Shaker	IKA KS 4000i Control	3510000	IKA-Werke GmbH & Co. KG
Thermocycler	GeneAmp PCR System 2720	272S6032784	Thermo Fisher Scientific Inc.
Vortex	VWR™ Vortex mixer	444-1372	VWR International GmbH
Water Bath	Precisdig 12 L 200 °C	6001237	JP SELECTA S.A.
Water Purification	Ultrapure water system OmniaPure series	-	stakpure GmbH

Table 8: Consumables.

Product	Article Number	Company
µ-Slide 8 Well, ibiTreat	80826	ibidi GmbH
250 µL TIPS, For use with Rainin	RC-250/10	Mettler-Toledo GmbH
50mL Centrifuge Tube, CentriStar™ Cap	430829	Corning Inc.
96 Well Cell Culture Cluster, Flat Bottom with Lid, TC Treated	3599	Corning Inc.
Assay Plate, 384 Well, White, Low Volume, Flat Bottom, TC Treated, With Lid	3826	Corning Inc.
Cap with volume limitation	65.71	SARSTEDT AG & Co. KG
Cell Scraper, sterile	3010	Corning Inc.
ClearLine® 50 mL Reservoirs Pre Sterile	63303328	BIOSIGMA S.p.A.
Combitips®advaned 0.1 ml	30089405	Eppendorf SE
Costar® Assay Plate, 96 Well, Clear, Flat Bottom, Medium Binding	9017	Corning Inc.
CryoPure Tube 1.8ml white	72.379	SARSTEDT AG & Co. KG
CyBi®-TipTray 384-25µl	OL3800-25-513-N	Analytik Jena AG
Epic® 384 Well Cell Assay Plate Fibronectin Coated	5042	Corning Inc.
Epic® 384 Well Cell Assay Plate Fibronectin Coated, Split Sensor	5442	Corning Inc.
Glass Pasteur Pipettes	7477 20	Brand GmbH & Co. KG

Table 8 continued.

Product	Article Number	Company
LABSOLUTE® PCR tubes 0.2 ml, domed cap, non-steri	6313402	Th. Geyer Ingredients GmbH & Co. KG
Micro tube 0,5ml PP	72.733.201	SARSTEDT AG & Co. KG
Micro tube 0.5ml, green	72.699.004	SARSTEDT AG & Co. KG
Microtest Plate 96 Well, R	92.1582	SARSTEDT AG & Co. KG
Microtubes 2.0ml CLEAR	MCT-200-C	Corning Inc.
Parafilm® M All-Purpose Laboratory Film	-	Amcor Limited
Petri dish 92x16mm with cams	82.1473.001	SARSTEDT AG & Co. KG
Pipette tip 10 µl	70.3010	SARSTEDT AG & Co. KG
Pipette tip 1000 µl, blue	70.3050.020	SARSTEDT AG & Co. KG
Pipette tip 200 µl, yellow	70.3030.020	SARSTEDT AG & Co. KG
ratiolab® tips Makro II 1 - 5 ml, bag of 300	2400650	Ratiolab GmbH
ritips evolution 0,1 ml	40077-0000	Ritter GmbH
ritips professional 2,5 ml	40007-0005	Ritter GmbH
SafeSeal tube 1.5ml	72.7060	SARSTEDT AG & Co. KG
SafeSeal tube 5ml	72.701.500	SARSTEDT AG & Co. KG
Serological pipette 10ml	86.1254.001	SARSTEDT AG & Co. KG
Serological pipette 25ml	86.1685.001	SARSTEDT AG & Co. KG
Serological pipette 2ml	86.1252.001	SARSTEDT AG & Co. KG
Serological pipette 5ml	86.1253.001	SARSTEDT AG & Co. KG
Storage Plate, 384 Well, Round Bottom, No Lid	3657	Corning Inc.
Storage Plate, No Lid, 96 Well Round Bottom, Non-Treated	3365	Corning Inc.
Surgical Disposable Scalpel	10567364	B. Braun SE
TC Dish 100, Standard	83.3902	SARSTEDT AG & Co. KG
TC Dish 60, Standard	83.3901.002	SARSTEDT AG & Co. KG
TC Plate 6 Well, Standard, F	83.3920.005	SARSTEDT AG & Co. KG
TC-Flask T175	83.3912.002	SARSTEDT AG & Co. KG
TC-Flask T25	83.3910.002	SARSTEDT AG & Co. KG
TC-Flask T75	83.3911.002	SARSTEDT AG & Co. KG
Tube 13 mL 100x16 mm PP	62.515.006	SARSTEDT AG & Co. KG
Tube 15 mL	62.554.502	SARSTEDT AG & Co. KG

Table 9: Plasmids.

Int. ID	Construct	Vector	Source
pEK228	pcDNA3.1(+)	vector only	
pEK728	mGαq (HA)	pcDNA3.1(+)	
pEK1071	hGα11 WT	pcDNA3.1(+)	bought from UMR
pEK1093	hGβ1	pcDNA3.1(+)	Michel Bouvier, Université de Montréal
pEK1106	hGγ2	pcDNA3.1(+)	Jean-Philippe Pin, Sanofi
pEK1262	M3 receptor	pcDNA3.1(+)	
pEK1307	mGαq "FIVE" D71E V182S V184M I190N P193C (HA)	pcDNA3.1(+)	mutated from pEK728 for Malfacini et al. (2019)
pEK1464	PTX A chain/S1 subunit	pCAGGS	Asuka Inoue, Tohoku University
pEK1503	Ric-8A	pcDNA3.1(+)	Asuka Inoue, Tohoku University
pEK1551	DGαqD	pCAGWBA	Kirill A. Martemyanov, The Herbert Wertheim UF Scripps Institute
pEK1552	DGαqG	pCAGWBA	Kirill A. Martemyanov, The Herbert Wertheim UF Scripps Institute
pEK1553	DGαqG	pcDNA3.1(+)	cloned from pEK1552
pEK1554	DGαqG (HA)	pcDNA3.1(+)	mutated from pEK1553
pEK1556	DGαqG I184W (HA)	pcDNA3.1(+)	mutated from pEK1554
pEK1591	mGαq F75K (HA)	pcDNA3.1(+)	mutated from pEK728 for Patt et al. (2021)
pEK1592	mGαq I190W (HA)	pcDNA3.1(+)	mutated from pEK728 for Patt et al. (2021)
pEK1593	mGαq F75K I190W (HA)	pcDNA3.1(+)	mutated from pEK728 for Patt et al. (2021)
pEK1599	masGRK3ct-Nluc	pcDNA3.1(+)	Kirill A. Martemyanov, The Herbert Wertheim UF Scripps Institute
pEK1601	Venus156-239-hGβ1	pcDNA3.1(+)	Kirill A. Martemyanov, The Herbert Wertheim UF Scripps Institute
pEK1602	Venus1-155-hGγ2	pcDNA3.1(+)	Kirill A. Martemyanov, The Herbert Wertheim UF Scripps Institute
pEK1649	NeonGreen(NG)-N-CAAX		Andy Chevigné, Luxembourg Institute of Health
pEK1726	DGαqG I184W	pcDNA3.1(+)	mutated from pEK1553
pEK1727	DGαqG V178S I184W	pcDNA3.1(+)	mutated from pEK1553
pEK1728	DGαqG Y69K	pcDNA3.1(+)	mutated from pEK1553
pEK1729	DGαqG "FIVE" D65E V176S V178M I184N P187C	pcDNA3.1(+)	bought from Genecust and mutated
pEK1731	DGαqG V178M I184W	pcDNA3.1(+)	mutated from pEK1553
pEK1734	DGαqG V178A I184W	pcDNA3.1(+)	mutated from pEK1553
pEK1751	3xHA-RGS8	pcDNA3.1(-)	Mikel Garcia-Marcos, Chobanian & Avedisian School of Medicine, Boston Univeristy
pEK1755	GAIP (RGS19)	pcDNA3	Mikel Garcia-Marcos, Chobanian & Avedisian School of Medicine, Boston Univeristy
pEK1779	DGαqG V178S I184W (HA)	pcDNA3.1(+)	mutated from pEK1554
pEK1780	DGαqG V178A I184W (HA)	pcDNA3.1(+)	mutated from pEK1554

Table 9 continued.

Int. ID	Construct	Vector	Source
pEK1791	mGαq V184S (HA)	pcDNA3.1(+)	mutated from pEK728
pEK1792	mGαq V184S I190W (HA)	pcDNA3.1(+)	mutated from pEK728
pEK1793	mGαq V184A (HA)	pcDNA3.1(+)	mutated from pEK728
pEK1794	mGαq V184A I190W (HA)	pcDNA3.1(+)	mutated from pEK728
pEK1795	mGαq V184M (HA)	pcDNA3.1(+)	mutated from pEK728
pEK1796	mGαq V184M I190W (HA)	pcDNA3.1(+)	mutated from pEK728
pEK1797	mGαq F75Y T76I (HA)	pcDNA3.1(+)	mutated from pEK728 for Alenfelder (2019)
pEK1805	mGαq F75K V182S I190W (HA)	pcDNA3.1(+)	mutated from pEK728

Table 10: Primers.

Int. ID	Primer	Sequence	Use
13	mGq_V182S_s	GTGCTTAGAAGTCGAGTCCCCACTACAGGGATC	mutagenesis
14	mGq_V182S_as	GATCCCTGTAGTGGGGACTCGACTTCTAAGCAC	mutagenesis
33	DGqG_Y69K_s	CAAGCGTGGGAAAATCAAGCTGG	mutagenesis
34	DGqG_Y69K_as	CCAGCTTGATTTTTCCCACGCTTG	mutagenesis
35	DGqG_I184W_s	CAACAGGGATATGGGAGTATCC	mutagenesis
36	DGqG_I184W_as	GGATACTCCCATATCCCTGTTG	mutagenesis
37	NheI_Kozak_DGqG_KpnI_s	CAACGGCTAGCGCCACCATGGAGTGCTGTTTATCGGAGGAG	generation of pEK1553
38	NheI_Kozak_DGqG_KpnI_as	CGTCAGGTACCTTAGACCAAATTATATTCCTTAAGGTTCG	generation of pEK1553
39	DGqG_HA_s	CGTTACCACGTTCGACGTTCCAGACTATGCTGCCATCAAAACG	mutagenesis
40	DGqG_HA_as	CGTTTTGATGGCAGCATAGTCTGGAACGTCGAACGTGGTAACG	mutagenesis
47	mGq_I190W_s	CAGGGATCTGGGAATACCCCTTTGACTTAC	mutagenesis
48	mGq_I190W_as	GTAAGTCAAAGGGGTATTCCCAGATCCCTG	mutagenesis
49	DGqG_I190W_s	CAGGGATATGGGAGTATCCCTTTGATTTAG	mutagenesis
50	DGqG_I190W_as	CTAAATCAAAGGGATACTCCCATATCCCTG	mutagenesis
59	DGqG_V178M_s	GAGTTCGTATGCCCACAACAGG	mutagenesis
60	DGqG_V178M_as	CCTGTTGTGGGCATACGAACTC	mutagenesis
61	DGqG_V178S_s	GAGTTCGTTCGCCCACAACAGG	mutagenesis
62	DGqG_V178S_as	CCTGTTGTGGGCGAACGAACTC	mutagenesis
63	DGqG_V178A_s	GAGTTCGTGCTCCCACAACAGG	mutagenesis
64	DGqG_V178A_as	CCTGTTGTGGGAGCACGAACTC	mutagenesis
92	DGqG_FIVE_HAweg_s	CGTGACCACCTTCGAGGATCCATACTTGAATGCCATTAAGACC	generation of pEK1729
93	DGqG_FIVE_HAweg_as	GGTCTTAATGGCATTCAAGTATGGATCCTCGAAGGTGGTCACG	generation of pEK1729
96	mGq_V184S_s	GCTTAGAGTTCGATCCCCCACTACAGGGATC	mutagenesis
97	mGq_V184S_as	GATCCCTGTAGTGGGGGATCGAACTCTAAGC	mutagenesis
98	mGq_V184A_s	GCTTAGAGTTCGAGCCCCCACTACAGGGATC	mutagenesis
99	mGq_V184A_as	GATCCCTGTAGTGGGGGCTCGAACTCTAAGC	mutagenesis

Table 10 continued.

Int. ID	Primer	Sequence	Use
100	mGq_V184M_s	GCTTAGAGTTCGAATGCCCACTACAGGGATC	mutagenesis
101	mGq_V184M_as	GATCCCTGTAGTGGGCATTCGAACTCTAAGC	mutagenesis
102	CMVfor	CGCAAATGGGCGGTAGGCGTGTACGG	mutagenesis
103	pcDNA3.1-RP_1	GAGGGGCAAACAACAGATGGCTGGC	mutagenesis

Table 11: Software.

Software	Developed by/Source	Version (latest used)
BioRender	Science Suite Inc.	-
Citavi	Lumivero LLC	7.1
DeVision G	Decon Science Tec. GmbH	1.0
Epic Autoalign/Imager Lab View 2009 Service Packet	PerkinElmer U.S. LLC	9.0.1f2
Fiji (“batteries-included” ImageJ2)	Schindelin et al. (2012)	20250514-1821
Image Studio™	LI-COR Biotech, LLC	6.1
MARS	BMG Labtech GmbH	3.32
Microsoft Excel 365	Microsoft Corporation	2509
Microsoft PowerPoint 365	Microsoft Corporation	2509
Microsoft Word 365	Microsoft Corporation	2509
MikroWin® 2000	Berthold Technologies GmbH & Co. KG	4.41
mzmine	mzio GmbH	4.7.29
PHERAstar	BMG Labtech GmbH	5.41
GraphPad Prism®	Dotmatics Limited	10.6.0
PyMOL 3.1	Schrodinger, LLC	3.1.6.1
SnapGene Viewer	Dotmatics Limited	8.1.1
ZEN (blue edition)	Carl Zeiss Microscopy GmbH	3.3.89.00000

3.2. Recipes

Table 12: Blotto.

Ingredient	Amount
Dry milk	3%

Suspend the required amount of dry milk in 50 mM Tris (pH 7.4) buffer. Use immediately.

Table 13: Cryo medium.

Ingredient	Amount
DMSO	1 mL
FBS	9 mL

Mix all ingredients and use immediately.

Table 14: Culture medium.

Ingredient	Amount
DMEM	500 mL
FBS	50 mL
Penicillin/Streptomycin (5 kU/mL, 5 mg/mL)	10 mL

Mix all ingredients and store at 4 °C.

Table 15: Goat serum blocking buffer (GSBB).

Ingredient	Amount
Goat serum	10%
BSA, fatty acid-free	1%

Mix the required quantities of all ingredients in PBS. Use immediately.

Table 16: 2-fold HEPES-buffered saline (HBS).

Ingredient	Amount
1 M HEPES	50 mL
5 M NaCl	28 mL
0.5 M Na_2HPO_4	1.5 mL

Add all ingredients to water. Adjust volume to 500 mL and pH to 7.05 to 7.10 using 1 M NaOH. Store aliquots at -20 °C.

Table 17: Lysis buffer for SDS-PAGE and western blotting.

Ingredient	Amount
HEPES	20 mM
$Mg(CH_3COO)_2$	5 mM
KCH_3COO	125 mM
Triton X-100	0.40%
Dithiothreitol (DTT)	1 mM
Protease inhibitor cocktail	1%

Mix the required quantities of all ingredients in water and store at -20 °C. Immediately before use, add protease inhibitor cocktail and store on ice.

Table 18: Lysogeny broth (LB).

Ingredient	Amount
Trypton/Pepton	10 g
Yeast extract	5 g
NaCl	5 g

Dissolve all ingredients in water. Adjust volume to 1 L and pH to 7.4 using 1 M NaOH. Sterilize by autoclaving and store at room temperature.

Table 19: LB agar.

Ingredient	Amount
Agar	15 g

Add agar to 1 L LB and sterilize by autoclaving. Store at room temperature. To pour plates, melt LB agar by heating. After cooling to 50 °C, add required antibiotics, pour plates, leave them to solidify at room temperature. Store at 4 °C.

Table 20: 50-fold Tris Acetate EDTA (TAE) buffer.

Ingredient	Amount
Tris base	242 g
Glacial acetic acid	57.1 mL
0.5 M EDTA solution (pH 8.0)	100 mL

Adjust volume to 1 L and store at room temperature.

4. Methods

4.1. Mutagenesis

To introduce the desired mutations into cDNA coding for *Drosophila melanogaster* or mouse Gαq, standard molecular biology techniques were used. The general workflow for mutagenesis is mapped out in Figure 11. For a list of all plasmids and their origin see Table 9. All constructs labeled as “mutated from…” or “cloned from…” were generated using the methods generally described below on the example of mutagenesis.

Mutants of mGq were generated together with Dr. Sophie Steinmüller (formerly Kostenis lab, University of Bonn).

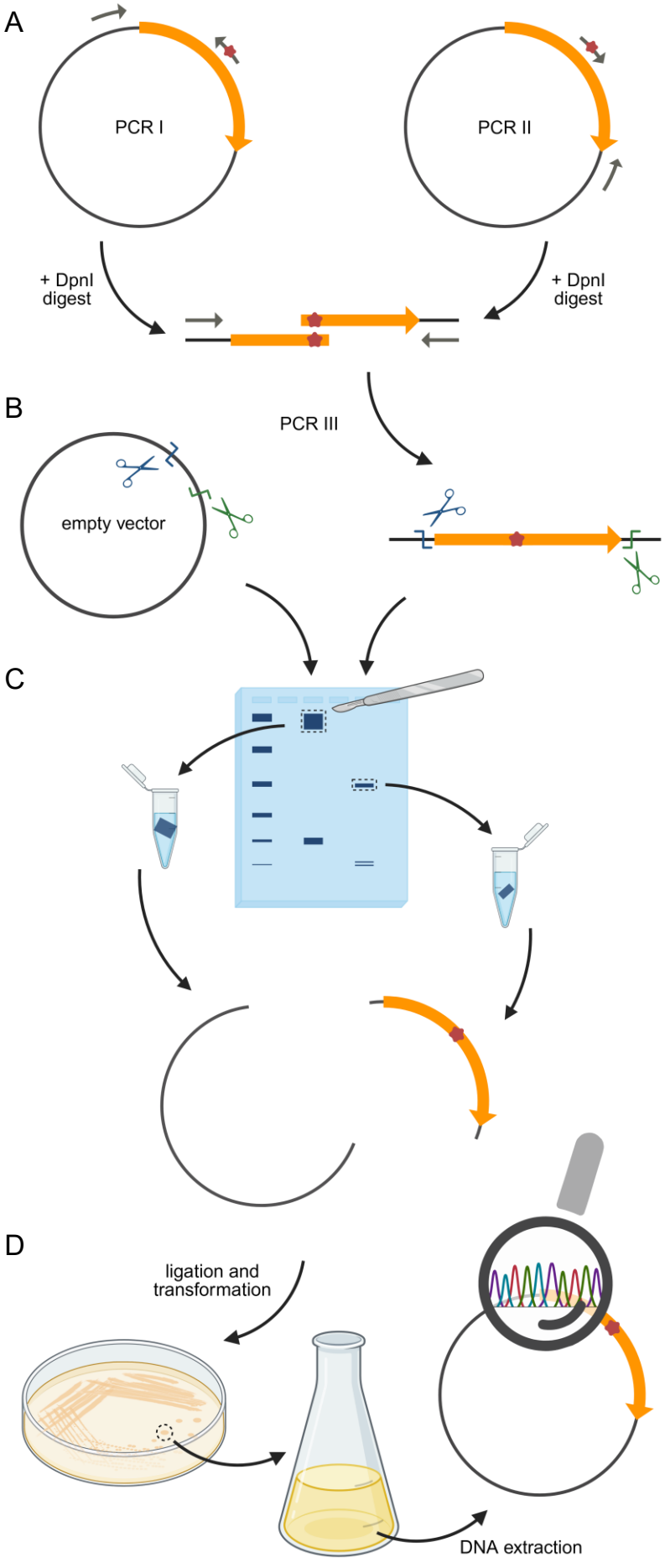
A
PCR I
PCR II
+ DpnI digest
+ DpnI digest
B
PCR III
empty vector
C
D
ligation and transformation
DNA extraction

Figure 11: General mutagenesis workflow.
A. *Two overlapping, mutated parts of the gene-of-interest (orange arrow) were amplified in separate polymerase chain reactions (PCRs) from plasmid containing the gene-of-interest. The mutation (red star) was introduced by using mutated primers. The methylated template DNA was digested with DpnI. In a third reaction, the PCR products were merged to yield a complete mutated gene-of-interest.* ***B.*** *The mutated final PCR product and empty vector DNA were digested with matching restriction enzymes (blue and green scissors) that cut close to the gene-of-interest to create matching ends.* ***C.*** *The restriction digest mixtures were purified using agarose gel electrophoresis. The bands of interest were cut from the gel and purified yielding cut vector backbone and insert containing the mutated gene-of-interest.* ***D.*** *The DNA pieces were ligated and introduced into E. coli using heat shock transformation. Successful transformants that contain ampicillin resistance-conferring plasmid were selected for by plating on ampicillin-containing agar plates. A single clone was picked and grown in liquid culture. Plasmid DNA was extracted and sequenced (magnifying glass). The figure was created with BioRender.com.*

4.1.1. Polymerase chain reaction (PCR)

Starting with a template plasmid coding for the wild-type Gαq gene in a pcDNA3.1(+) backbone, two polymerase chain reactions (PCRs) were performed to amplify two mutated overlapping fragments of the Gαq cDNA. For this, two standard primers binding to the pcDNA3.1(+) backbone flanking the gene-of-interest (CMVfor and pcDNA3.1-RP_1) were combined with primers that bind to the site to be mutated and contain the target sequence.

The mutated primers were designed to fully overlap, extend approximately 10 to 25 base pairs (bps) to either side of the desired mutation, and to end with one to three guanine or cytosine bases on either side. They were ordered desalted and without modifications on the 25-nanomolar scale from Invitrogen (Thermo Fisher Scientific Inc.) and are listen in Table 10. To minimize additional unwanted mutations in amplified DNA fragments, the high-fidelity Pfu polymerase that contains a 3’ -> 5’ exonuclease proofreading function was used. The composition of the PCR mixture and the thermocycling program used are listed in Table 21 and Table 22, respectively.

Methylated template DNA extracted from the dam methylase-positive *E. coli* DH5α strain was used to allow the specific degradation of the template DNA using the dam methylation-sensitive restriction enzyme DpnI. This way, a third PCR could be performed without prior DNA purification. By using the first two PCR mixtures as templates and CMVfor and pcDNA3.1-RP_1 as primers, the mutated DNA fragments were combined to obtain an insert that contains the complete mutated Gαq gene.

Table 21: Composition of PCR mixture.

Component	Amount
Pfu reaction buffer (10x)	5 µL
template DNA (30 ng/µL)	1 µL
fwd and rev primers, each	1 µL each
dNTPs	1 µL
DMSO	2.5 µL
Pfu polymerase (2-3 u/µL)	1 µL
water, DNAse- and RNAse-free	37.5 µL
Σ	50 µL

Table 22: Thermocycler program for mutagenesis PCRs.

Temp. (°C)	Time (min)	
94	3	
94	1	30 cycles
52	1	
68	8	
68	8	
8	∞	

Following the third polymerase chain reaction, the mutated insert was either immediately purified from the mixture using the ReliaPrep™ DNA Clean-Up and Concentration System or stored at -20 °C before purification.

4.1.2. Endonuclease restriction

To reincorporate the mutated gene back into the vector backbone, both empty vector and the insert were digested with the restriction enzymes NheI and KpnI that cut directly before and after the DGαq gene. This permitted the subsequent integration of the insert into the vector in the correct orientation. The composition of the double restriction mixture is detailed in Table 23. For the insert, all available DNA was used, while approximately 6 µg of empty vector DNA was digested. The reaction buffer was chosen to allow maximal combined efficiency of both restriction endonucleases as determined using the compatibility chart provided by the supplier of the restriction enzymes. The digestion mixture was incubated at 37 °C for one to four hours and either immediately processed further or stored at -20 °C.

Table 23: Composition of restriction digest mixture.

Component	Amount
DNA	x µL
selected buffer (10x)	2 µL
restriction enzyme, each	1 µL
BSA (1 mg/mL)	2 µL
water, DNAse- and RNAse-free	14 - x µL
∑	20 µL

The procedure was the same for the mGαq mutagenesis with slight modifications. The selected restriction enzymes were BamHI and EcoRI cutting directly before the mGαq gene and at the end of the gene in its sequence, respectively. Therefore, the vector backbone needed to contain the remaining sequence of the mGαq gene. Consequently, the mGαq wild type-containing plasmid instead of empty vector was cut with BamHI and EcoRI.

4.1.3. Gel electrophoresis and purification

The restricted DNA fragments were separated using agarose gel electrophoresis. 0.5 or 1 g of agarose was solved under heat in 50 or 100 mL of TAE buffer, respectively, to prepare 1% agarose gels. After the mixture had reached homogeneity, it was left to cool at room temperature for 15 min. Before pouring of the gel, the DNA stain MIDORI Green Advance was added at a ratio of 1:25,000. After complete solidification, the gel was transferred to the electrophoresis chamber. The restriction digests were mixed with 3 to 4 µL of 6x purple gel loading dye and transferred to the gel. Alongside, 6 µL of pre-diluted 1 kb Plus DNA Ladder was loaded. 50- and 100-mL gels were run at a voltage of 90 or 120 V, respectively, until the desired degree of band separation was achieved. The correct size of the cut fragments was confirmed by comparing the samples' migration distances with the DNA ladder after gel electrophoresis. Electrophoresis results were documented by photography with the DeVision G v1.0 software.

Correct fragments (vector backbone and cut insert) were excised with little excess and extracted from gel slices using the ReliaPrep™ DNA Clean-Up and Concentration System following the manufacturer's instructions. Concentration and purity were measured with an Eppendorf BioPhotometer™ D30.

4.1.4. Ligation

The extracted vector backbone and insert were combined into one plasmid using ligation. 27 fmol of vector DNA was combined with a 5-times excess of insert DNA, ligase buffer and T4 ligase (Table 24) and incubated for 1 to 1.5 hours at room temperature before transformation. A negative control without addition of insert DNA was performed in parallel.

Table 24: Composition of ligation mixture.

Component	Amount
vector DNA, 27 fmol	x µL
insert DNA, 135 fmol	y µL
T4 ligase buffer (10x)	2 µL
T4 ligase	1 µL
water, DNAse- and RNAse-free	17 - x - y µL
∑	20 µL

4.1.5. Transformation

5 µL of the ligation mix and the negative control was transformed into 50 µL chemically competent *E. coli* DH5α suspension using a heat shock protocol. The procedure is summarized in Table 25. After the final incubation on ice, 350 µL of S.O.C. medium was added, and the bacteria were incubated at 37 °C for approximately 1 hour in a shaking incubator at 220 rpm. Bacteria were plated onto LB agar plates containing 100 µg/mL ampicillin as selection antibiotic and grown overnight at 37 °C. The number of colonies grown when transformed with the ligation mixture was compared to the number of colonies grown when transformed with the negative control to estimate the number of colonies that needed to be picked to make picking a positive clone likely. Using an autoclaved pipette tip, single colonies were transferred to 5 mL of liquid LB media containing 100 µg/mL ampicillin and grown overnight at 37 °C in a shaking incubator at 220 rpm.

Table 25: Procedure of heat shock transformation.

Step	Time
Thawing of bacteria on ice	5 min
Incubation on ice after DNA addition	30 min
Heat shock	90 sec
Incubation on ice after heat schock	2 min

4.1.6. DNA preparation and sequencing

Plasmid DNA was extracted from 5-mL cultures of bacteria using the NucleoSpin Plasmid, Mini kit for plasmid DNA according to the manufacturer's instructions. Concentration and purity were measured with an Eppendorf BioPhotometer™ D30. Plasmid DNA was sent in for sequencing with the Sanger Sequencing TubeSeq Supreme services (Eurofins Genomics Europe Shared Services GmbH) to confirm successful mutation.

4.2. Other molecular biology techniques

For the larger-scale preparation of DNA for transfection, *E. coli* DH5α bacteria were transformed with 30 ng of plasmid DNA as described in Chapter 4.1.5. Transformation. A single colony was selected and transferred into a 150-mL liquid LB culture containing the suitable selection antibiotic, predominantly 100 µg/mL ampicillin. The liquid culture was incubated overnight at 37 °C in a shaking incubator at 220 rpm, and the plasmid DNA was extracted using the NucleoBond Xtra Midi kit for transfection-grade plasmid DNA following the manufacturer's instructions. Alternatively, a 150-mL liquid LB culture was inoculated with 80 µL of cryopreserved bacteria bypassing the need for repeated transformation. For cryopreservation, 850 µL of liquid bacterial culture was mixed with 150 µL sterilized glycerol (85 %), gradually frozen, and stored at -80 °C.

4.3. Cell culture

All cell lines used in this thesis were kept in Dulbecco's Modified Eagle's Medium (DMEM) supplemented with 10% FBS, 100 U/mL penicillin, and 0.1 mg/mL streptomycin (culture medium) and cultured at 37 °C in a humidified atmosphere at 5% CO_2.

For maintenance, cells were regularly passaged at about 90-95% confluence. To do so, cells were washed with phosphate-buffered saline (PBS) and gently detached using 0.05% or 0.25% trypsin-EDTA. Cells were split at ratios between 1:2 and 1:10 with exceptions and reseeded in fresh culture medium. All solutions used for cell passaging were pre-warmed to 37 °C on a water bath.

For some assays, as stated in the respective methods section, multi-well plates or µ-slides were coated with poly-D-lysine (PDL) to facilitate cell adhesion. For this, an appropriate amount of a 50 µg/mL PDL solution to cover the bottom of the plate or slide was added, and the plate or slide was incubated for 60 minutes at 37 °C. PDL was aspirated and collected for later use, and the plate or slide was washed three times with PBS and left to dry. Coated plates or slides were used immediately after drying or stored at 4 °C.

For calcium phosphate transfection, cells were seeded into gelatin-coated plates. For this, an appropriate amount of 0.1% gelatin solution to cover the bottom of the plate was added, and the plate was incubated at room temperature. The gelatin solution was aspirated, and the plate was used immediately.

For maintaining the cells over extended periods of time at lower passage numbers, the cells were taken out of culture and stored at -186 °C in a liquid nitrogen tank. For this, the cells were harvested as described above. The culture medium was substituted for cryo medium, and the cells were aliquoted in designated cryo tubes. The cells were slowly cooled in an insulated styrofoam box to -20 °C overnight. They

were then transferred to -80 °C while still in the box for one day. Finally, they were transferred to a liquid nitrogen tank without the box. To thaw cells, the cryo vial was placed on a 37 °C water bath for a few minutes. The cryo medium was replaced by pre-warmed culture medium, the cells were transferred to T-25 flasks and cultured at standard conditions.

4.4. Transient transfection

For most cell-based assays, cells were transiently transfected using polyethylenimine (PEI) either in suspension or adherently. Cell numbers, dish sizes, DNA amounts, and transfected constructs varied between applications and are detailed in the tables below. In general, cells were washed with PBS, gently detached using 0.05% or 0.25% trypsin-EDTA, counted and seeded at the desired density using fresh culture medium. Cells were incubated for 24 hours at 37 °C under maintenance conditions for adherent transfection or immediately transfected in suspension.

For transfection, the required amount of PEI was diluted in OptiMEM, vortexed, and incubated at room temperature for a few minutes. Meanwhile, the required amounts of the chosen DNA constructs were mixed in the same amount of OptiMEM and vortexed. For all transfections, a 3:1 PEI to DNA ratio was maintained. The PEI solution was added to the DNA mix in a dropwise manner. The DNA-PEI mixture was vortexed and incubated at room temperature for 15 to 20 minutes before dropwise addition to the cells. The plate was rocked gently to mix in the transfection mixture and incubated at standard culture conditions.

For Gβγ/masGRK3ct BRET measurements performed with DGq in the lab of Prof. Dr. Mikel Garcia-Marcos (Department of Biochemistry & Cell Biology, Chobanian & Avedisian School of Medicine, Boston University), cells were transfected using the calcium phosphate ($Ca_3(PO_4)_2$) transfection method on adherent cells. Cells were treated as described above but seeded into gelatin-coated 6-well plates. For transfection, the required amounts of the chosen DNA constructs were mixed in 120 µL 0.25 M calcium chloride solution and added dropwise under vortexing into 120 µL 2-fold concentrated HEPES-buffered saline (HBS). The DNA-$Ca_3(PO_4)_2$ mixture was incubated at room temperature for 25 minutes before dropwise addition to the cells. The plate was rocked gently to mix in the transfection mixture and incubated at standard culture conditions. The culture medium was changed 6 hours after transfection.

Table 26: Detailed transfection conditions.

Condition	BRET/WB	BRET/WB + RGS	DMR/IP	Microscopy	
Cell type	cEK43	cEK43	cEK86	cEK84	
Type of transfection	adherent	adherent	in suspension	in suspension	
Cell number	0.35 M	0.35 M	1.2 M	0.7 M	
Dish size	6 well-plate	6 well-plate	6 cm-dish	6 cm-dish	
Amount of culture medium	2 mL	2 mL	3 mL	3.5 mL	
Amount of OptiMEM for DNA/PEI solutions	100 µL	100 µL	150 µL	150 µL	
Total DNA amount	2.1 µg	3 µg	3 µg	2.5 µg	
Condition	**Fig. 19, left**	**Fig. 20**	**Fig. 29**	**Fig. 60**	**Fig. 68**
Cell type	cEK88	cEK43	cEK84	cEK86	cEK86
Type of transfection	adherent	adherent	adherent	in suspension	adherent
Cell number	0.35 M	0.35 M	0.7 M	2.8 M	1.8 M
Dish size	6 well-plate	6 well-plate	6 cm-dish	10 cm-dish	10 cm-dish
Amount of culture medium	2 mL	2 mL	3.5 mL	10 mL	10 mL
Amount of OptiMEM for DNA/PEI solutions	100 µL	100 µL	150 µL	250 µL	250 µL
Total DNA amount	2 µg	1 µg	2.5 µg	8 µg	8 µg

Table 27: Detailed DNA amounts for transient transfection.

BRET/WB				**BRET/WB + RGS**		
Int. ID	**Construct**	**Mass (µg)**		**Int. ID**	**Construct**	**Mass (µg)**
pEK1262	M3R	0.2		pEK1262	M3R	0.2
pEK1599	masGRK3ct-NLuc	0.025		pEK1599	masGRK3ct-NLuc	0.025
pEK1601	Venus156-239-hGβ1	0.2		pEK1601	Venus156-239-hGβ1	0.2
pEK1602	Venus1-155-hGγ2	0.2		pEK1602	Venus1-155-hGγ2	0.2
	indicated Gαq protein	1.0			indicated Gαq protein	1.0
pEK1503	Ric-8A	0.1			indicated RGS protein	1.0
pEK228	pcDNA3.1(+)	ad 2.1		pEK1503	Ric-8A	0.1
				pEK228	pcDNA3.1(+)	ad 3.0
Fig. 19, left				**Fig. 20**		
Int. ID	**Construct**	**Mass (µg)**		**Int. ID**	**Construct**	**Mass (µg)**
pEK1599	masGRK3ct-NLuc	0.025		pEK1262	M3R	0.2
pEK1601	Venus156-239-hGβ1	0.2		pEK1599	masGRK3ct-NLuc	0.1
pEK1602	Venus1-155-hGγ2	0.2		pEK1601	Venus156-239-hGβ1	0.1
pEK1071	Gα11 protein	1.0		pEK1602	Venus1-155-hGγ2	0.1
pEK1464	PTX A chain/S1 subunit	0.05			indicated Gαq protein	0.5
pEK228	pcDNA3.1(+)	ad 2.0		pEK228	pcDNA3.1(+)	ad 1.0
Fig. 21				**DMR**		
Int. ID	**Construct**	**Mass (µg)**		**Int. ID**	**Construct**	**Mass (µg)**
pEK1262	M3R	0.2			indicated Gαq protein	1.5
pEK1599	masGRK3ct-NLuc	0.025/0.05/0.1		pEK1503	Ric-8A	0.6
pEK1601	Venus156-239-hGβ1	0.1/0.2		pEK228	pcDNA3.1(+)	ad 3.0
pEK1602	Venus1-155-hGγ2	0.1/0.2				
	indicated Gαq protein	0.5/1.0		**IP**		
pEK1503	Ric-8A	0.1		**Int. ID**	**Construct**	**Mass (µg)**
pEK228	pcDNA3.1(+)	ad 1.0/2.1			indicated Gαq protein	1.2
				pEK228	pcDNA3.1(+)	ad 3.0
Microscopy				**Fig. 28**		
Int. ID	**Construct**	**Mass (µg)**		**Int. ID**	**Construct**	**Mass (µg)**
	indicated Gαq protein	0.75			indicated Gαq protein	0.5
pEK1649	NeonGreen-N-CAAX	0.25		pEK1093	hGβ1	0.5
pEK228	pcDNA3.1(+)	ad 2.5		pEK1106	hGγ2	0.5
				pEK228	pcDNA3.1(+)	ad 2.5

Table 27 continued.

Fig. 29 and 30				Fig. 31		
Int. ID	**Construct**	**Mass (µg)**		**Int. ID**	**Construct**	**Mass (µg)**
pEK1553	DGαq	0.5		pEK1553	DGαq	0.5/0.75/0.875/0.9375
pEK1649	NeonGreen-N-CAAX	0.5		pEK1649	NeonGreen-N-CAAX	0.5/0.25/0.125/0.0625
pEK228	pcDNA3.1(+)	ad 2.5		pEK228	pcDNA3.1(+)	ad 2.5
Fig. 60				**Fig. 68**		
Int. ID	**Construct**	**Mass (µg)**		**Int. ID**	**Construct**	**Mass (µg)**
pEK729	mGαq	0.05/0.1/1.0/4.0/8.0			indicated Gαq protein	8.0
pEK228	pcDNA3.1(+)	ad 8.0				

4.5. BRET-based biosensing

Theoretical background

To investigate Gαq mutant behavior as close to the site of activation as possible, we chose to monitor G protein dissociation using a bioluminescence resonance energy transfer (BRET)-based approach. However, as this technique requires labeling of interacting proteins, we decided to use a BRET sensor that monitors dissociation of the G protein indirectly by measuring the interaction of Gβγ with its effector mimic masGRK3ct after activation of the G protein. This way, the additional variable of labeling the Gαq variants was circumvented. The theoretical background of BRET-based biosensing in general and the Gβγ/masGRK3ct BRET sensor (Hollins et al., 2009; Masuho et al., 2015) in particular is described in Chapter 5.2.2. G protein level in the results section.

Practical procedure

HEK293T cells were transiently transfected with the DNA constructs and under the conditions listed in Chapter 4.4. Transient transfection. 28 hours post-transfection, cells were washed with PBS, gently detached in PBS using a cell scraper, and pelleted by centrifugation at 500 rcf for 5 minutes. The supernatant was discarded, and the cell pellet was resuspended in 750 µL Hanks' Balanced Salt Solution (HBSS) supplemented with 20 mM HEPES (assay buffer).

In general, luminescence and fluorescence emissions were measured to assess the signal. The BRET ratio was calculated by dividing the fluorescence intensity by the corresponding luminescence intensity. As the experiments with *Drosophila* Gαq isoforms were performed during a research stay in the lab of Prof. Dr. Mikel Garcia-Marcos (Department of Biochemistry & Cell Biology, Chobanian & Avedisian School of Medicine, Boston University), the assay conditions differ slightly from the experiments with mGαq mutants performed in the lab of Prof. Dr. Evi Kostenis. For all *Drosophila* Gq measurements, a POLARStar Omega plate reader was used measuring luminescence and fluorescence at 450 ± 40 and 535 ± 15 nm, respectively. 1 µL of Coelenterezine 400a per well was used as substrate for the NanoLuc® luciferase. For all murine Gq measurements, a PHERAStar FSX plate reader with a BRET1 optical module was used measuring luminescence and

fluorescence at 475 ± 15 and 535 ± 15 nm, respectively. The focal height was set to 12.5, the fluorescence gain (gain A) to 3115, and the luminescence gain (gain B) to 2526. 0.1 µL of NanoGlo® per well was used as substrate for the NanoLuc® luciferase. BRET assays for mGq mutants were performed together with Dr. Sophie Steinmüller (formerly Kostenis lab, University of Bonn).

For basal BRET measurements, cells were resuspended by gently pipetting them up and down, and 20 µL of cell suspension of each transfection condition was transferred into separate wells of a white flat-bottom 96-well plate. 80 µL of appropriately prediluted NanoLuc® luciferase substrate was added to each well. The contents of the plate were mixed by gently tapping the side of the plate. Luminescence and fluorescence counts were recorded three to six times at one-minute intervals with an integration time of 0.48 seconds. Raw luminescence and fluorescence counts were exported using the MARS data analysis software. The average of all three to six luminescence and fluorescence values of each condition was used for the calculation of the basal BRET ratio.

Kinetic traces were recorded analogously in single-well mode. Cells were resuspended by gently pipetting them up and down, and 20 µL of cell suspension was transferred into a single well of a white flat-bottom 96-well plate. 80 µL of appropriately prediluted substrate was added. The contents of the plate were mixed by gently tapping the side of the plate. Luminescence and fluorescence counts were measured after 30 seconds of incubation with integration and cycle times of 0.48 seconds. After 30 seconds of baseline read, 5 µL of 20-fold concentrated M3R agonist carbachol (CCh) was added using the injector to a final concentration of approximately 100 µM. After 90 additional seconds of measurement, 5 µL of 20-fold concentrated M3R antagonist atropine (Atrp) was added with the injector to a final concentration of approximately 100 µM. The measurement was continued for 300 seconds. Raw luminescence and fluorescence counts were exported using the MARS data analysis software. For kinetic activation traces, the BRET ratio was baseline-corrected by subtracting the average BRET ratio before the first compound addition (ΔBRET, baseline-corrected). For kinetic deactivation traces, the BRET ratio was normalized to the first time point after the Atrp addition with 0% set to the smallest value in each data set (BRET ratio, % of first point after add, smallest value = 0%). The procedure for the evaluation of kinetic traces is described in Chapter 4.14. Data analysis.

For CCh concentration-response measurements, a 5- or 6-fold concentrated CCh dilution series in assay buffer was prepared, and 20 µL of each concentration and buffer was transferred into a well of a white flat-bottom 96-well plate. 60 µL (for 5-fold concentrated CCh) or 80 µL (for 6-fold concentrated CCh) of appropriately prediluted substrate was added. Finally, cells were resuspended by gently pipetting them up and down, and 20 µL of cell suspension was added. The contents of the

plate were mixed by gently tapping the side of the plate. Luminescence and fluorescence counts were recorded six times at one-minute intervals with an integration time of 0.48 seconds. Raw luminescence and fluorescence counts were exported using the MARS data analysis software. The BRET ratio was buffer-corrected by subtracting the BRET ratio measured in cells treated with buffer only (ΔBRET ratio, buffer-corrected). The average of the four- and five-minute BRET ratio was plotted against the corresponding CCh concentration. The procedure for nonlinear regression of concentration-response curves is described in Chapter 4.14. Data analysis.

For FR concentration-response measurements, a 1.34- or 1.33-fold concentrated FR dilution series in assay buffer was prepared, and 67.6 µL (for 1.34-fold concentrated FR) or 60 µL (for 1.33-fold concentrated FR) of each concentration and dimethyl sulfoxide (DMSO)-corrected buffer was transferred into wells of a white flat-bottom 96-well plate. Cells were resuspended by gently pipetting them up and down.
22.4 µL (for 1.34-fold concentrated FR) or 20 µL (for 1.33-fold concentrated FR) of cell suspension was added and incubated for 15 minutes at room temperature. Finally, 10 µL of a 10-fold concentrated (for 1.34-fold concentrated FR) or 20 µL of a 5-fold (for 1.33-fold concentrated FR) 100 µM CCh dilution or buffer containing the appropriate amount of substrate was added. The contents of the plate were mixed by gently tapping the side of the plate. Luminescence and fluorescence counts were recorded six times at one-minute intervals with an integration time of 0.48 seconds. Raw luminescence and fluorescence counts were exported using the MARS data analysis software. The BRET ratio was buffer-corrected by subtracting the BRET ratio measured in cells treated with buffer only and normalized to the BRET ratio measured in cells treated with 100 µM CCh only (ΔBRET ratio, buffer-corrected, % of 100 µM CCh). The average of the four- and five-minute BRET ratio was plotted against the corresponding FR concentration. The procedure for nonlinear regression of concentration-response curves is described in Chapter 4.14. Data analysis.

Immediately after the experiment, left-over cells were pelleted at 11,000 rcf for 1 min. The supernatant was discarded, and the cell pellet was stored at -20 °C for potential future western blot analysis.

4.6. Western blot

To investigate and compare the expression levels of transiently expressed proteins, we combined sodium dodecyl sulfate-polyacrylamide gel electrophoresis (SDS-PAGE) to separate the proteins contained in cell lysates and western blotting (WB) to visualize and compare amounts of the proteins of interest.

After Gβγ/masGRK3ct BRET and IP_1 accumulation assays, remaining cells were pelleted by centrifugation at 11,000 rcf for 1 minute. The supernatant was discarded,

and the cell pellets were stored at -20 °C for future protein quantification. For SDS-PAGE and WB analysis, frozen cells were thawed and lysed using lysis buffer for SDS-PAGE and western blot. Lysates were centrifuged at 4 °C and 14,000 rcf for 10 minutes to clear them of cell debris, and the protein concentration in the supernatant was determined with Quick Start™ Bradford Dye Reagent following the manufacturer's instructions. Before gel electrophoresis, Laemmli buffer was added, and samples were boiled at 100 °C for 5 minutes. The appropriate volume of samples amounting to 15 µg of total protein was applied to the gel.

After SDS-PAGE, the separated proteins were transferred to a polyvinylidene difluoride (PVDF) membrane, stained with Ponceau S staining solution and scanned to evaluate transfer efficiency. The membrane was blocked with 5 g/100 mL non-fat dry milk in tris-buffered saline (TBS) for 30 to 60 minutes and incubated with primary antibody diluted at a 1:1000 ratio (1:500 for anti-Gq antibody and 1:2500 for anti-RGS19 serum) in 2.5 %/100 mL non-fat dry milk in TBS supplemented with 0.1% Tween20 (TBST) overnight at 4 °C (or in 5% BSA in TBST for the anti-HA antibody to detect RGS8). The membrane was washed with TBST and incubated with secondary antibody at a 1:10,000 ratio in 2.5 g/100 mL non-fat dry milk in TBST. For primary and secondary antibodies used, see Table 3.

After antibody staining, the western blot membrane was imaged using an Odyssey CLx Infrared Imaging System following the manufacturer's instructions. The images taken were edited using Image Studio and densiometrically quantified using Fiji.

4.7. Immunofluorescence microscopy

To investigate the subcellular localization of Gq proteins, we performed immunofluorescence microscopy. HEK293 Gq/11/12/13-KO cells were transiently transfected with the DNA constructs and under the conditions listed in Chapter 4.4. Transient transfection. 24 hours post-transfection, cells were washed with PBS, gently detached using 0.05% trypsin-EDTA, and collected in culture medium. Cells were pelleted by centrifugation at 500 rcf for 5 minutes. The supernatant was discarded, and the pellet was resuspended in 3 mL PBS. Using a Neubauer chamber, cells were either counted manually with a microscope or with the CytoSMART™ automated cell counter. Cells were pelleted again by centrifugation at 500 rcf for 5 minutes. The supernatant was discarded, and the cells were resuspended in the appropriate volume of culture medium to achieve a cell concentration of 100,000 cells/250 µL. 250 µL of cell suspension was seeded into PDL-coated 8-well µ-slides. Cells were grown at standard conditions for 24 hours.

The next day, the cells were gently washed using PBS and fixed with 4% paraformaldehyde (PFA) in PBS for 20 to 25 minutes at room temperature. The PFA solution was then aspirated, and the fixed cells were washed three times with PBS. Both the PFA solution and the PBS used for washing were disposed of in a separate

PFA waste bin. After fixing, the cells were either permeabilized and stained immediately or stored covered with PBS at 4 °C.

Before staining, the cells were permeabilized using a solution of 0.3% Triton X-100 in PBS for 20 minutes at room temperature. The cells were washed three times with PBS and blocked with goat serum blocking buffer (GSBB) for 1 hour at 37 °C. The cells were incubated with primary antibody diluted at a 1:500 ratio in GSBB for 1 hour at 37 °C. Before incubating with the secondary antibody, the cells were washed three times by incubating them with PBS for 15 minutes at 37 °C. Afterwards, the cells were incubated with secondary antibody at a 1:500 ratio in GSBB for 1 hour at 37 °C in the dark. For primary and secondary antibodies used, see Table 3. Finally, the cells were washed three times by incubating them with PBS for 15 minutes at 37 °C in the dark. If a 4´,6-diamidin-2-phenylindol (DAPI) staining was performed to visualize nuclei, the cells were incubated with DAPI staining solution for 15 minutes at room temperature between the first and second washing after the secondary antibody incubation. After antibody and DAPI staining, cells were either imaged immediately or stored covered with PBS at 4 °C.

The cells were imaged using a Zeiss AxioObserver Z with an ApoTome2.0 and plan-apochromat 63x/1.40 oil M27 magnification optics. The images were processed using ZEN (blue edition).

Immunofluorescence microscopy experiments were performed together with Aram Kamalizade (formerly Kostenis lab, University of Bonn).

4.8. Inositol monophosphate (IP_1) accumulation assays

Theoretical background

To investigate Gαq mutant behavior on the second messenger level, we chose to use a homogeneous time-resolved fluorescence (HTRF)-based approach to monitor the production of inositol monophosphate (IP_1). IP_1 is a metabolite of the second messenger inositol 1,4,5-trisphosphate (IP_3) that is produced downstream of Gq-coupled GPCRs simultaneously with diacylglycerol (DAG) upon cleavage of the membrane lipid phosphatidylinositol 4,5-bisphosphate (PIP_2) by Gαq-activated phospholipase C β (PLCβ) (Figure 5). IP_3 acts as an agonist on IP_3 receptor calcium channels (IP_3Rs) at the endoplasmic reticulum, causing the receptors to open and consequently results in an increase in cytosolic calcium levels. This makes IP_3 measurements the classical downstream signaling readouts for Gq-coupled GPCRs and the Gq heterotrimer in general.

In this thesis, instead of measuring IP_3 directly, the accumulation of its degradation product IP_1 is detected, as the further degradation of IP_1 by inositol monophosphatase can reliably be inhibited with lithium chloride (LiCl). Addition of LiCl to the assay buffer, consequently, causes accumulation of IP_1 following Gq

activity in the cell. Measuring the resulting IP_1 concentration in cell lysates as a proxy for Gq-mediated IP_3 production is, therefore, a suitable endpoint to compare DGq wild-type and mutant signaling behavior via PLCβ at the second messenger level.

The detection of IP_1 was performed with the HTRF IP-One Gq Detection Kit which is a competitive immunoassay utilizing Förster resonance energy transfer (FRET). FRET is, just like BRET, a radiation-free energy transfer, but from one fluorophore (the donor) to a second (the acceptor). Just like BRET, donor and acceptor molecules must be in proximity to each other for energy transfer to take place. In this assay, a Lumi4-Tb™ cryptate-labeled IP_1 antibody constitutes the FRET donor, while d2-labeled IP_1 molecules serve as FRET acceptors (Figure 12A). Native, unlabeled IP_1 produced in cells, in this case after Gαq stimulation, competes with d2-labeled IP_1 for antibody binding reducing the number of FRET events between the two fluorescent probes. Therefore, the measured FRET or HTRF ratio, i.e. the ratio of acceptor and donor fluorescence, is inversely proportional to the IP_1 concentration in the assayed cells which can be calculated using a standard curve prerecorded with dilutions of an IP_1 standard provided by the manufacturer (Figure 12B).

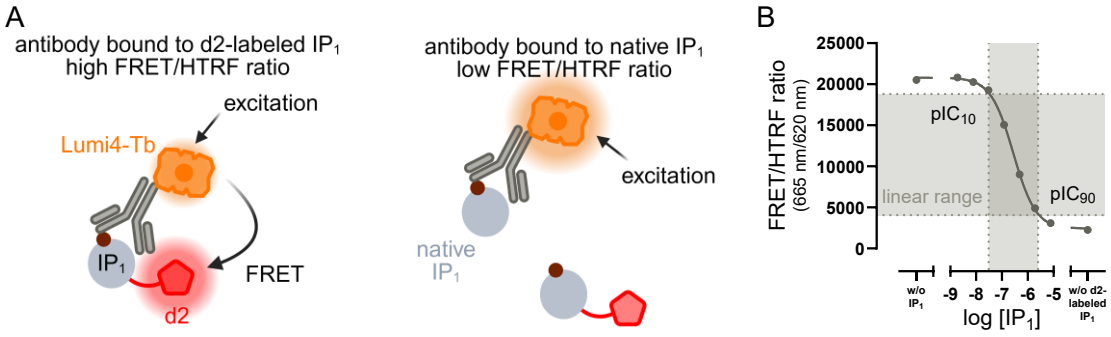

Figure 12: Principle of homogenous time resolved fluorescence (HTRF)-based inositol monophosphate (IP_1) detection.
A. *The Lumi4-Tb™ label which is fused to an anti-IP_1 antibody is excited. If the antibody is bound to d2-labeled IP_1 and the two fluorophores consequently are in spatial proximity, radiation-free energy transfer occurs and the FRET or HTRF ratio is high. When native IP_1 is present, e.g. produced in the cell after Gq activation, it displaces the labeled IP_1. This increases the spatial distance between the two tags, and the energy transfer is suspended. The FRET/HTRF ratio is low. The panel was created with BioRender.com.* ***B.*** *Exemplary standard curve for the calculation of IP_1 concentrations from the measured FRET/HTRF ratio. The higher the amount of IP_1 standard, the less resonance energy transfer occurs and the lower the FRET/HTRF ratio. A condition lacking the FRET acceptor, i.e. the d2-labeled IP_1, serves as negative control. Only FRET/HTRF ratio values in the linear range defined as range between the pIC_{10} and pIC_{90} values (dark grey area) can faithfully be converted to the corresponding IP_1 concentrations.*

Practical procedure

The HTRF IP-One Gq Detection Kit was used according to the manufacturer's instructions. HEK293 Gq/11-KO cells were transiently transfected with the DNA constructs and under the conditions listed in Chapter 4.4. Transient transfection. 48 hours post-transfection, cells were washed with PBS, gently detached using 0.05% trypsin-EDTA, and collected in culture medium. Cells were pelleted by

centrifugation at 500 rcf for 5 minutes. The supernatant was discarded, and the cell pellet was resuspended in 3 mL PBS. Using a Neubauer chamber, cells were either counted manually with a microscope or with the CytoSMART™ automated cell counter. Cells were pelleted again by centrifugation at 500 rcf for 5 minutes. The supernatant was discarded, and the cells were resuspended in the appropriate volume of Stim buffer supplied with the assay kit to achieve a cell concentration of 20,000 to 35,000 cells/7 µL. As soon as cells are resuspended in LiCl-containing Stim buffer and monophosphatase is inhibited, IP_1 starts to accumulate. Therefore, the time between resuspension of cells in Stim buffer and their addition to the assay plate was minimized.

For the measurement of basal IP_1 production and its FR sensitivity, 7 µL of DMSO-corrected Stim buffer or 2-fold 100 µM FR in Stim buffer per well were added into a 384-well, small-volume microplate. 7 µL of cell suspension in Stim buffer was added. Cells were incubated at 37 °C for 30 to 45 minutes prior to lysis and detection.

For CCh concentration-response measurements, a 2-fold concentrated CCh dilution series in Stim buffer was prepared, and 7 µL of each concentration and buffer was transferred into a well of a 384-well, small-volume microplate. 7 µL of cell suspension in Stim buffer was added. Cells were incubated at 37 °C for 30 to 45 minutes prior to lysis and detection.

For FR concentration-response measurements, a 3.5-fold concentrated FR dilution series in Stim buffer was prepared, and 4 µL of each concentration and DMSO-corrected buffer was transferred into wells of a 384-well, small-volume microplate. Additionally, 3 µL of 4.66-fold 100 µM CCh in Stim buffer or Stim buffer only was added. Afterwards, 7 µL of cell suspension in Stim buffer was added. Cells were incubated at 37 °C for 30 to 45 minutes prior to lysis and detection.

After the indicated incubation time, 3 µL of d2-labeled IP_1 in lysis buffer supplied with the assay kit and, subsequently, 3 µL of cryptate-labeled anti-IP_1 antibody in lysis buffer were added to each well. The addition of the detection reagents and simultaneous lysis of the cells stops the accumulation of IP_1. Cells were incubated for 60 additional minutes at room temperature in the dark, before measuring fluorescence values at 620 nm for the donor and 665 nm for the acceptor on a Mithras LB 940. The raw HTRF or FRET ratio was exported using the MikroWin® 2000 software and converted into the IP_1 concentrations using the prerecorded standard curve described above. The IP_1 concentration was buffer-corrected by subtracting the concentration measured in cells treated with buffer only and normalized to the IP_1 concentration measured in cells treated with 1 mM CCh only (ΔIP_1 concentration, buffer-corrected, % of 1 mM CCh). For the data in Figure 61, the IP_1 concentration was vector control-corrected by subtracting the corresponding concentrations measured in cells transfected with empty vector and normalized to

the IP_1 concentration measured in cells transfected with 4 µg of plasmid coding for mGαq and treated with 100 µM CCh (IP_1 concentration, % of 100 µM CCh on 4 µg Gq). The procedure for nonlinear regression of concentration-response curves is described in Chapter 4.14. Data analysis.

Immediately after the experiment, left-over cells were pelleted at 11,000 rcf for 1 min. The supernatant was discarded, and the cell pellet was stored at -20 °C for potential future western blot analysis.

IP_1 accumulation experiments were performed by Uli Rick (Kostenis lab, University of Bonn). Preliminary experiments were performed by Lars Jürgenliemke (Kostenis lab, University of Bonn).

4.9. Dynamic mass redistribution (DMR) assays

Theoretical Background

To investigate amplified downstream effects of Gαq activation, we decided to monitor dynamic mass redistribution (DMR) using the Epic® technique (Corning Inc.) that has been established in the lab (Schröder et al., 2010; Schröder et al., 2011). This assay is a label-free whole-cell response readout based on cell shape, cytoskeletal dynamics, and mass distribution changes, instead of relying on the measurement of a single second messenger alone. It does not require labeling or overexpression of (sensor) proteins or the lysis of cells.

Practically, cells are grown in a microtiter plate on a specifically designed optical biosensor. During the measurement, polarized broadband light is directed onto the biosensor, and the wavelength of reflected light is measured. This wavelength is dependent on the optical density of material right above the biosensor, in this case the bottom slice (about 150 nm) of the attached cell matter. Changes in biomass close to the sensor caused by redistribution of biomolecules in the cell, cell shape change or other cytoskeletal changes are recorded as increases (higher mass on the sensor) or decreases (lower mass on the sensor) of reflected wavelength (Figure 13).

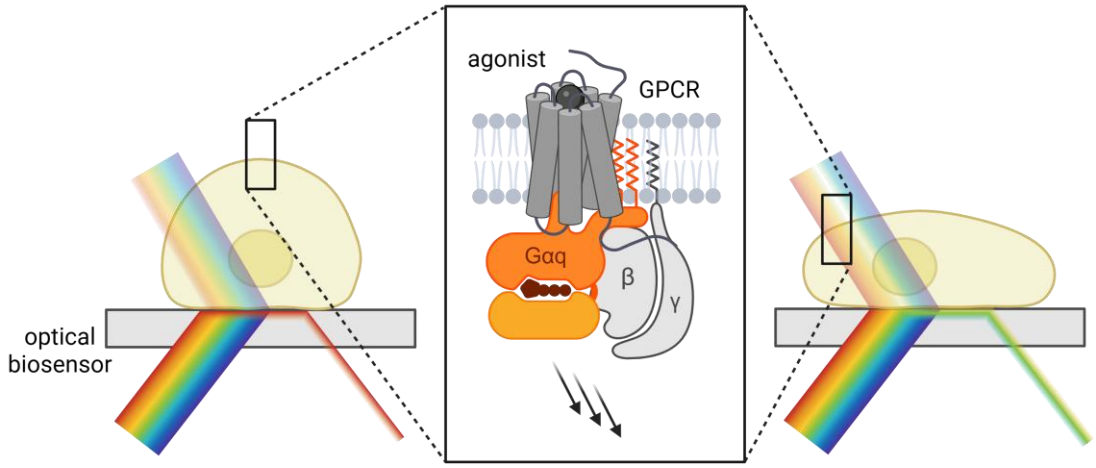

Figure 13: Principle of the dynamic mass redistribution (DMR) assay.
Cells are seeded on plates containing an optical biosensor. Polarized broadband light is directed onto the biosensor from below. Depending on the optical density of the biomass on the sensor, a single resonating wavelength is reflected and can be measured. When a GPCR is activated with an agonist, downstream signaling, in this case of Gq proteins, leads to changes in cell shape and, therefore, optical density. This is recorded as a change in resonant wavelength. The figure was created with BioRender.com.

Practical Procedure

HEK293 Gq/11-KO cells were transiently transfected with the DNA constructs and under the conditions listed in Chapter 4.4. Transient transfection. 24 hours post-transfection, cells were washed with PBS, gently detached using 0.05 % trypsin-EDTA, and collected in culture medium. Using a Neubauer chamber, cells were either counted manually with a microscope or with the CytoSMART™ automated cell counter. Cells were diluted with culture medium to a cell concentration of 18,000/30 µL. Alternatively, if the cell concentration was too low, cells were pelleted by centrifugation at 500 rcf for 5 minutes, the supernatant was discarded, and the pellet was resuspended in the appropriate volume of culture medium to achieve a cell concentration of 18,000/30 µL. 30 µL of cell suspension was seeded into an Epic® 384-well fibronectin-coated, biosensor microplate. Cells were grown at standard conditions for 26 hours.

On the day of the assay, the culture medium was aspirated to 10 µL using an 8-channel manifold attachment for the aspiration pump, and cells were washed with HBSS containing 20 mM HEPES and 1% DMSO (assay buffer). The first washing step was performed with 30 µL of assay buffer, followed by the second and third washing step with 20 µL of buffer. After each washing step, the assay plate was briefly centrifuged to ensure that the buffer reached the bottom of the wells, and the buffer was aspirated to 10 µL per well. After washing, 10 µL of 2-fold concentrated FR dilutions or DMSO-corrected buffer was added using the half-automated pipetting system SELMA. For economic reasons, concentrations above 10 µM FR were pipetted manually.

Cells were incubated at 37 °C in the EPIC® BT system while recording a pre-read until the traces were stable but at least for one hour. For the actual measurement, the difference in reflected wavelength was measured with 5 reads per data point. After approximately 3 minutes of initial baseline read, 10 µL of 3-fold concentrated CCh dilution or assay buffer was added using the SELMA pipettor and changes in wavelength were measured for a total of 300 data points resulting in a measurement time of approximately 4,500 seconds (75 minutes). Raw DMR data was exported from the txt file saved by the recording software using a macro-automated export sheet in Microsoft Excel which was provided by Corning Inc. The DMR traces were buffer-corrected by subtracting the data measured in cells treated with buffer only and normalized to the maximal value measured in each condition or to the value measured in cells treated with 100 µM CCh only (ΔDMR response, buffer-corrected, % of max or % of 100 µM CCh). The procedure for nonlinear regression of concentration-response curves is described in Chapter 4.14. Data analysis.

DMR experiments with DGq mutants were performed by Sergi Bravo (Kostenis lab, University of Bonn).

4.10. Enzyme-linked immunosorbent assays (ELISAs)

To investigate mGαq expression in the gene dosing experiments for Figure 61, we used enzyme-linked immunosorbent assays (ELISAs) on permeabilized cells. HEK293 Gq/11-KO cells were transiently transfected with the DNA constructs and under the conditions listed in Chapter 4.4. Transient transfection. 24 hours post-transfection, cells were washed with PBS, gently detached using 0.05% trypsin-EDTA, and collected in culture medium. Cells were pelleted by centrifugation at 500 rcf for 5 minutes. The supernatant was discarded, and the pellet was resuspended in 3 mL PBS. Using a Neubauer chamber, cells were either counted manually with a microscope or with the CytoSMART™ automated cell counter. Cells were pelleted again by centrifugation at 500 rcf for 5 minutes. The supernatant was discarded, and the cells were resuspended in the appropriate volume of culture medium to achieve a cell concentration of 60,000 cells/100 µL. 100 µL of cell suspension was seeded into PDL-coated transparent, flat-bottom, 96-well plates. Cells were grown at standard conditions for 24 hours.

The next day, the cells were gently washed using PBS and fixed with 4% PFA in PBS for 20 to 25 minutes at room temperature. The PFA solution was then aspirated, and the fixed cells were washed three times with PBS. Both the PFA solution and the PBS used for washing were disposed of in a separate PFA waste bin. After fixing, the cells were either permeabilized and stained immediately or stored covered with PBS at 4 °C.

For the ELISA, the cells were simultaneously blocked and permeabilized using a solution of 0.3% Triton X-100 in Blotto for 20 minutes at room temperature.

Afterwards, the cells were incubated with primary antibody diluted at a 1:400 ratio in Blotto with 0.3% Triton X-100 for 45 minutes at 37 °C. Before incubating with the secondary antibody, the cells were washed three times by incubating them with PBS for 15 minutes at 37 °C. Afterwards, the cells were incubated with horseradish peroxidase (HRP)-tagged secondary antibody at a 1:1000 ratio in Blotto with 0.3% Triton X-100 for 45 minutes at 37 °C. For primary and secondary antibodies used, see Table 3. Finally, the cells were washed three times by incubating them with PBS for 15 minutes at 37 °C.

100 µL of the ELISA substrate 3,3',5,5' tetramethylbenzidine (TMB) One Solution per well was added to start the color reaction, and the plate was gently tapped to fully cover the cells. After exactly 3.5 minutes, the reaction was stopped by adding 50 µL of 0.5 M sulfuric acid. 130 µL of the supernatant was transferred into unused wells of the same plate or, if unavailable, a new plate. The absorbance at 450 nm was measured with a reference wavelength of 620 nm using a SUNRISE Absorbance Reader. To evaluate the expression of mGαq, the absorbance was baseline-corrected by subtracting the absorbance measured in cells transfected with empty vector only and normalized to the absorbance measured in cells transfected with 4 µg of plasmid coding for mGαq (total expression, % of 4 µg Gq).

4.11. Structural and sequence analysis

To make informed assumptions regarding the behavior of DGαq isoform G and DGαq isoform D, as well as the Gq mutants generated in this thesis, we examined differences in amino acid sequence and structural features in alignments and extrapolated from the crystal structure of the chimeric Gq/i heterotrimer in complex with YM (PDB ID: 3AH8, Nishimura et al. (2010)) in PyMOL.

Sequence alignments were computed using the multiple sequence alignment program Clustal Omega (Sievers et al., 2011) via the European Molecular Biology Laboratory-European Bioinformatics Institute (EMBL-EBI) Job Dispatcher sequence analysis tool (Goujon et al., 2010; Madeira et al., 2024). Below the alignment, asterisks (*), colons (:), and periods (.) are used to label identical amino acids, or strongly and weakly similar properties of the compared amino acids with a scoring of >0.5 and ≤0.5 in the Gonnet PAM 250 matrix (Dayhoff, 1979; Gonnet et al., 1992; Polyanovsky et al., 2020), respectively. Secondary structural elements that are depicted below the sequence with cylinders (α-helices) and arrows (β-sheets) were estimated using the “human paralog reference” published in Flock et al. (2015).

The structures of PLCβ, mitogen-activated protein kinase (MAPK) representative p38, and extracellular signal-regulated kinase (ERK) in Figure 2 and Figure 5 were created with the PDB retrieval feature of BioRender.com using the PDB files 2ZKM, 5UOJ, and 2ERK, respectively.

All other structural depictions (Figure 4, Figure 6, Figure 7, and Figure 9) are based on the structure of chimeric Gq/i heterotrimer in complex with the inhibitor YM-254890 (PDB ID: 3AH8) published by Nishimura et al. (2010). The coloring, feature representation, and orientation were edited using PyMOL 3.1. In Figure 9, residues F75 and T76 were exchanged for Y75 and I76 using PyMOL 3.1's mutagenesis wizard. For orienting the "mutated" side chains, the rotamers with highest probability and fewest steric clashes were chosen, without considering the inhibitor in its binding pocket to prevent a bias in the results.

4.12. *In vivo* experiments

All *in vivo* experiments were performed by our collaborators Dr. Anne-Kristin Dahse and Dr. Nicole Scholz at the Rudolf Schönheimer Institute of Biochemistry, University of Leipzig. More detailed information on the methodology used for the *in vivo* experiments can be found in Dr. Anne-Kristin Dahse's PhD thesis (Dahse, 2024), on which this abbreviated methods section is based.

4.12.1. Fly culture

For maintenance, *Drosophila melanogaster* stocks were routinely kept at 15 °C on cornmeal food, composed as in Wagner et al. (2015) and prepared following the manufacturer's instructions.

4.12.2. Fly husbandry

Wild-type w^{1118} flies were bought from the Bloomington Drosophila Stock Center. Flies ubiquitously overexpressing DGαq variants were bought from BestGene Inc. (Chino Hills, CA, USA). Transgenic flies were generated from w^{1118} flies via phiC31 integrase-mediated transgenesis using sent-in plasmids coding for the DGq gene of choice (plasmids pEK1554, pEK1556, pEK1779, and pEK1780). Bought flies used for the *in vivo* experiments contain the chosen DGαq gene on one of its third chromosomes (integration on the second chromosome caused leaky expression (see Figure 69 in Additional Material)), while the other one is the balancer chromosome TM3 with the genetic marker mutation Stubble (*Tm3(sb)*). The bought heterozygous flies are shorter- and thicker-bristled. Therefore, stubble-negative F1 progeny are homozygous for the DGq gene of choice and can easily be selected. Consequently, only stubble-negative flies are used as "reporter" line and for mating with the GAL4 "driver" line. For further details on the phiC31 integrase and UAS/GAL4 systems see Chapter 5.5.2. Husbandry in the results section.

4.12.3. FR-feeding experiments

For FR-feeding experiments, *Drosophila melanogaster* flies were kept at 25 °C on cornmeal food laced with FR or corresponding amounts of DMSO and flipped every 24 hours. The populations of each genotype assayed were composed of 20 virgin

females and 10 males to ensure peaceful cohabitation. Dead flies were counted and removed during flipping, washed in PBS, and stored at -20 °C for later LC/MS analysis.

4.12.4. Negative geotaxis assay

The negative geotaxis assay was performed as previously detailed in Ali et al. (2011) with 50 virgin female flies of each genotype assayed using a customized apparatus for simultaneous tapping and video recording. The climbing pass rate was calculated by dividing the number of passing flies by the total number of flies.

4.13. HPLC/MS analysis

High performance liquid chromatography/mass spectrometry (HPLC/MS) analyses have been performed by our collaborators Prof. Dr. Max Crüsemann, Institute of Pharmaceutical Biology, Goethe University Frankfurt (formerly Institute of Pharmaceutical Biology, University of Bonn), and Dr. Wiebke Hanke (formerly Institute of Pharmaceutical Biology, University of Bonn).

In short, *Drosophila melanogaster* corpses were ground in methanol, vortexed for 20 seconds and ultrasound-treated for 30 to 60 minutes. The supernatant was separated by centrifugation and evaporated, and the residue was dissolved in solvent for HPLC/MS measurement.

HPLC was performed on a Dionex UltiMate 3000 HPLC system with an analytical stainless steel reversed-phase (RP) HPLC column (NUCLEOSHELL RP 18, 2.7 µm particle size, 100 mm in length, 2 mm inner diameter) at a column temperature of 25 °C. The HPLC was run for 20 minutes with an eluent gradient from 90% water/9.9% acetonitrile/0.1% acetic acid to 99.9% acetonitrile/0.1% acetic acid starting at 1 minute run time. 5 µL of sample was injected.

The micrOTOF-Q mass spectrometer used an electrospray ionization source. Positively charged ions with a mass-to-charge ratio (m/z) of 100 to 3000 were detected. MS/MS fragmentation was automatically applied to ions with intensities above 100 arbitrary units using a collision energy gradient (35 keV at 500 m/z to 50 keV at 2000 m/z) at a frequency of 4 Hz.

4.14. Data analysis

The data presented in this thesis were analyzed using GraphPad Prism. Figures were assembled using Microsoft PowerPoint 356. Structural representations were generated using PyMOL 3.1 as described in Chapter 4.11. Structural and sequence analysis. Some figures or parts thereof were created with BioRender.com, as indicated in the respective figure caption. The brightness of microscopy pictures was adjusted, and western blot scans were assembled during figure assembly in Microsoft PowerPoint 356.

Figure captions provide information on the chosen representation of the data presented, including the plotted error, the amount of technical replicates, and the number of biologically independent experiments, where applicable.

Concentration-response curves were generated as described in the axis titles and figure captions. Nonlinear regression was done in GraphPad Prism using the log(compound) vs. response model with a variable slope to fit concentration-response curves to a four-parameter logistic curve. The mathematical equation of this model is given below (Equation 1). The pEC_{50} and pIC_{50} values and errors for the summarized datasets are the means and standard errors of the mean (SEMs) calculated from the pEC_{50} and pIC_{50} values extracted from the four-parameter logistic fit for the individual biologically independent experiments contributing to the dataset. SEMs were calculated as shown in Equation 2.

Equation 1: Four-parameter logistic model for nonlinear regression of concentration-response curves.
Y: response; X: logarithm of the molar compound concentration; Bottom: Y value when X tends to negative infinity; Top: Y value when X tends to positive infinity; EC_{50}: concentration that gives the response halfway between Top and Bottom, for concentration-inhibition curves, this value is termed IC_{50}; Hill Slope: steepness of the curve.

$$Y = Bottom + \frac{Top - Bottom}{1 + 10^{(\log(EC_{50}) - X) * Hill\ Slope}}$$

Equation 2: Calculation of the standard error of the mean (SEM).
SEM: standard error of the mean; σ: standard deviation; n: total number of values.

$$SEM = \frac{\sigma}{\sqrt{n}}$$

Kinetic traces were mostly plotted without a nonlinear regression curve. For the nonlinear regression of the Gβγ/masGRK3ct BRET assay deactivation data depicted in Figure 33, GraphPad Prism's one-phase decay and a Weibull fit were used. The mathematical equations of these models are given below (Equation 3 and Equation 4).

Equation 3: One-phase decay model for nonlinear regression of kinetic data.
Y: normalized ΔBRET ratio, first timepoint = 100%, smallest value = 0% (in %); t: time after atropine addition (in sec); Y_0: normalized ΔBRET ratio at t=0 (in %); Plateau: Y value when t tends to positive infinity (in %); k: rate constant (in sec^{-1}).

$$Y = (Y_0 - Plateau) * e^{-kt} + Plateau$$

Equation 4: Weibull fit model for nonlinear regression of kinetic data.
Y: normalized ΔBRET ratio, first timepoint = 100%, smallest value = 0% (in %); t: time after atropine addition (in sec); Y_0: normalized ΔBRET ratio at t=0 (in %); T: scale parameter (in sec); b: shape parameter; Plateau: Y value when t tends to positive infinity (in %).

$$Y = Y_0 * e^{-\left(\frac{t}{T}\right)^b} + Plateau$$

To extract G protein activation rate constants in the Gβγ/masGRK3ct BRET assay, the baseline-corrected ΔBRET ratio traces were fitted using the plateau followed by one-phase association model for nonlinear regression in GraphPad Prism. The mathematical equation is given below (Equation 5).

Equation 5: Plateau followed by one-phase association model for nonlinear regression of kinetic data. *t: time (in sec); t_0: time at which association begins (in sec); Y: baseline-corrected ΔBRET ratio; Y_0: average Y value up to t_0; Plateau: Y value when t tends to positive infinity; k: rate constant in sec^{-1}.*

$$If\ t < t_0 : Y = Y_0$$

$$If\ t \geq t_0 : Y = (Plateau - Y_0) * (1 - e^{-k*(t-t_0)})$$

The rate constants of G protein deactivation in the Gβγ/masGRK3ct BRET assay were not determined, since both nonlinear regression models, one-phase decay and Weibull fit, were discarded. Instead, the time required for the signal to return to 50% ($t_{1/2}$) and 25% ($t_{1/4}$) of its peak value was determined manually. For this, the first five consecutive data points that fell below 50% and 25% of the signal were determined. The measurement time corresponding to the first of these was defined as $t_{1/2}$ and $t_{1/4}$, respectively.

To compare relative FR contents in survivor and victim *Drosophila melanogaster* corpses from different condition in the FR-feeding experiments (Figure 56), base peak intensities for m/z values of 1002.5400 ± 0.02 corresponding to unfragmented FR eluted between 13.5 and 16 minutes were summed up.

4.15. Data availability

The data presented in this thesis are available from the author, Judith Alenfelder, upon reasonable request.

5. Results

5.1. Design approaches of FR-insensitive *Drosophila* Gαq isoforms

For the design of *Drosophila* Gq mutants with reduced FR sensitivity but wild type-like signaling behavior, we leveraged our extensive experience in mutating the FR binding site of murine Gαq and applied it to *Drosophila* Gαq. We implemented both strategies outlined in Chapter 1.6. Altering FR sensitivity… in the introduction, namely the transfer of residues from an FR-insensitive Gα protein and the rational substitution of binding residues, pursuing two promising approaches in parallel.

The first approach entailed the replacement of residues in the putative FR binding site with analogous amino acids found in the FR-insensitive human Gα16 (Malfacini et al., 2019). In this study, an alignment of murine Gαq with Gα16 revealed a high sequence similarity of the putative inhibitor binding site with only five residues differing between the proteins. All five residues in Gαq were substituted with their Gα16 counterparts to obtain Gαq FIVE. The study demonstrated a complete loss of YM sensitivity and a reduction in FR sensitivity to the level of Gα16. All original residues that are changed in mGq FIVE are conserved in DGq (Figure 14), and the resulting *Drosophila* Gαq mutant is, therefore, DGq D65E V176S V178M I184N P187C (see also Figure 7).

Importantly, the primary objective of the original mGq study was not to generate a tool to be used *in vivo*. A thorough examination of the signaling data reveals remarkable differences in efficacy between Gαq wild type and Gαq FIVE. However, this does not necessarily imply that these defects will manifest in a *Drosophila* Gq mutant with analogous mutations. A more exhaustive investigation of the mutant's signaling behavior is imperative to determine whether fewer, additional or different mutations should be introduced.

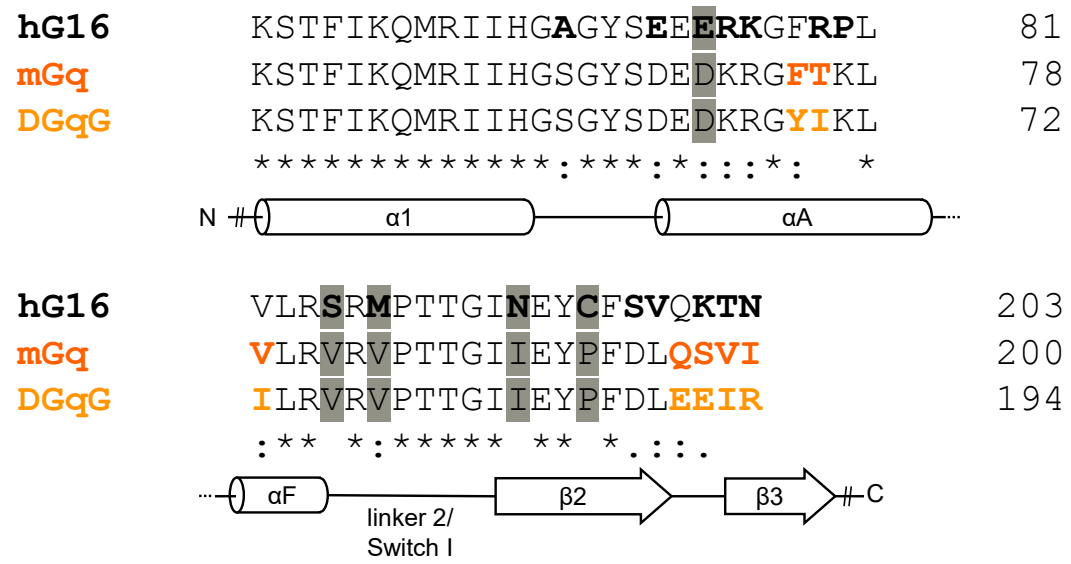

Figure 14: The residues substituted in mGαq to generate mGαq FIVE do not differ in Drosophila Gαq. *Alignment of the extended (putative) FR binding regions of human Gα16, murine Gαq, and Drosophila GαqG. Residues differing between mGαq and DGαqG are marked bold and dark orange in the sequence of mGαq and bold and light orange in the sequence of DGαqG. Residues differing between hGα16 and mGαq are marked bold and black in the sequence of hGα16. Residues substituted in mGαq to generate mGαq FIVE are highlighted in grey. Secondary structural elements are depicted below the sequence with cylinders (α-helices) and arrows (β-sheets). Asterisks (*) signify identical amino acids. Colons (:) and periods (.) signify strongly and weakly similar properties of the amino acids compared, with a scoring of >0.5 and ≤0.5 in the Gonnet PAM 250 matrix, respectively. For the full alignment see Figure 67 in Additional Material.*

The second approach, i.e. rational, structure-guided design of mutants, is based on another publication in which an FR-resistant mouse Gαq mutant was generated by replacing two key binding residues, phenylalanine-75$^{H.HA.7}$ and isoleucine-190$^{G.S2.2}$ (Patt et al., 2021) (Figure 7). F75$^{H.HA.7}$ is located at the beginning of the αA-helix, a part of the AHD directly following linker 1, that effectively closes the inhibitor binding pocket at the bottom. The replacement of this nonpolar side chain with lysine, a polar and charged amino acid lacking the aromatic ring present in phenylalanine, prevents nonpolar contacts between the Gα protein and the inhibitor and potentially even leads to electrostatic repulsion. In the analogous position in *Drosophila* Gq, there is a polar tyrosine instead of a phenylalanine moiety (Figure 9). By substituting this residue with lysine, the polarity of this residue is maintained but converted from an electron-dense hydroxy group to a positively charged primary amine (Figure 15).

The second residue that was replaced, I190$^{G.S2:2}$ which is also mutated in mGq FIVE, is part of the extensive hydrophobic pocket that accommodates nonpolar parts of the inhibitor (Figure 7). Substituting this rather small amino acid for tryptophan, a residue with a similarly nonpolar but bulky side chain, might prevent the inhibitor from burying into the hydrophobic binding pocket (Figure 15).

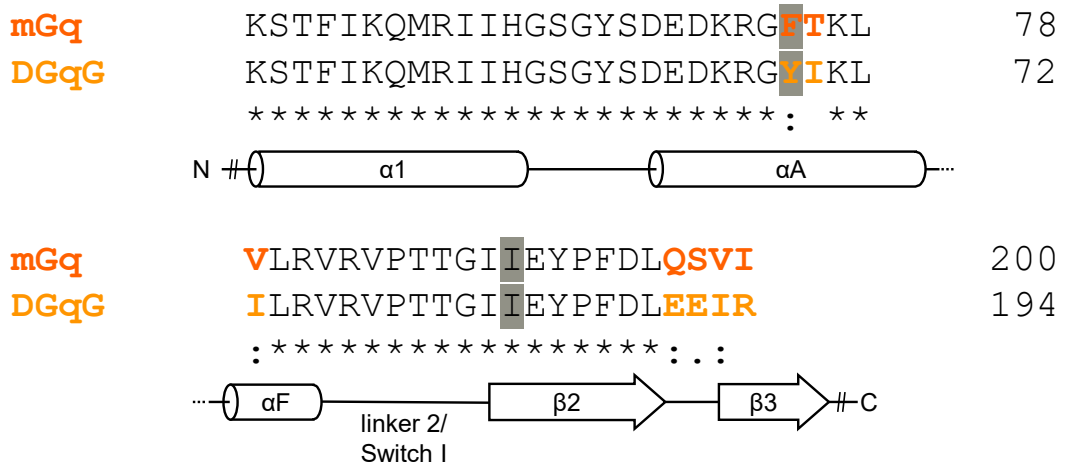

Figure 15: In Drosophila Gαq, the analogous mutations to mGαq F75K I190W are Y69K and I184W. *Alignment of the extended (putative) FR binding regions of murine Gαq and Drosophila GαqG. Residues differing between mGαq and DGαqG are marked bold and dark orange in the sequence of mGαq and bold and light orange in the sequence of DGαqG. Residues substituted to generate analogous single mutants to mGαq FK IW are highlighted in grey. Secondary structural elements are depicted below the sequence with cylinders (α-helices) and arrows (β-sheets). Asterisks (*) signify identical amino acids. Colons (:) and periods (.) signify strongly and weakly similar properties of the amino acids compared, with a scoring of >0.5 and ≤0.5 in the Gonnet PAM 250 matrix, respectively. For the full alignment see Figure 66 in Additional Material.*

The combination of both mutations, F75K and I190W, in murine Gq results in a complete loss of sensitivity to FR and YM. However, similar to mGq FIVE, this mutant does not display wild type-like properties. While this was not relevant in the original publication, it is of significant importance in the present project. mGq FK IW is not located at the plasma membrane as is wild-type mGq but is distributed throughout the cell except for the nucleus as determined with immunofluorescence microscopy. Furthermore, the expression level is reduced. Consequently, or in addition to this, mGq FK IW displays diminished amplitudes in signaling assays.

Investigations with the single mutants mGq FK and mGq IW reveal the substitution of phenylalanine with lysine to be the determining factor in this observed change of behavior (Patt et al., 2021). As previously mentioned, these changes in murine Gq behavior do not have to occur when engineering *Drosophila* Gq. However, to be able to trace possible changes directly back to one of the mutations, separate single mutants were created: *Drosophila* Gαq Y69K and I184W.

5.2. Functional characterization of Gαq mutants

Therefore, the initial set of generated *Drosophila* Gαq mutants consists of Y69K, I184W, and DGαq FIVE (D65E V176S V178M I184N P187C). Careful characterization of the mutants is necessary, as *Drosophila* Gαq, despite of its high sequence similarity to mGαq, is a distinct protein and may exhibit divergent responses to the introduction of these mutations.

5.2.1. General procedure

In order to determine whether mutations in the FR binding site affect the overall functionality of the Gαq protein, all generated mutants will be characterized in a series of functional assays and compared to wild-type DGq. The selected assays span the assembly, localization and expression of the G protein, activation and deactivation, second messenger production, as well as whole-cell response to G protein activation (Figure 16).

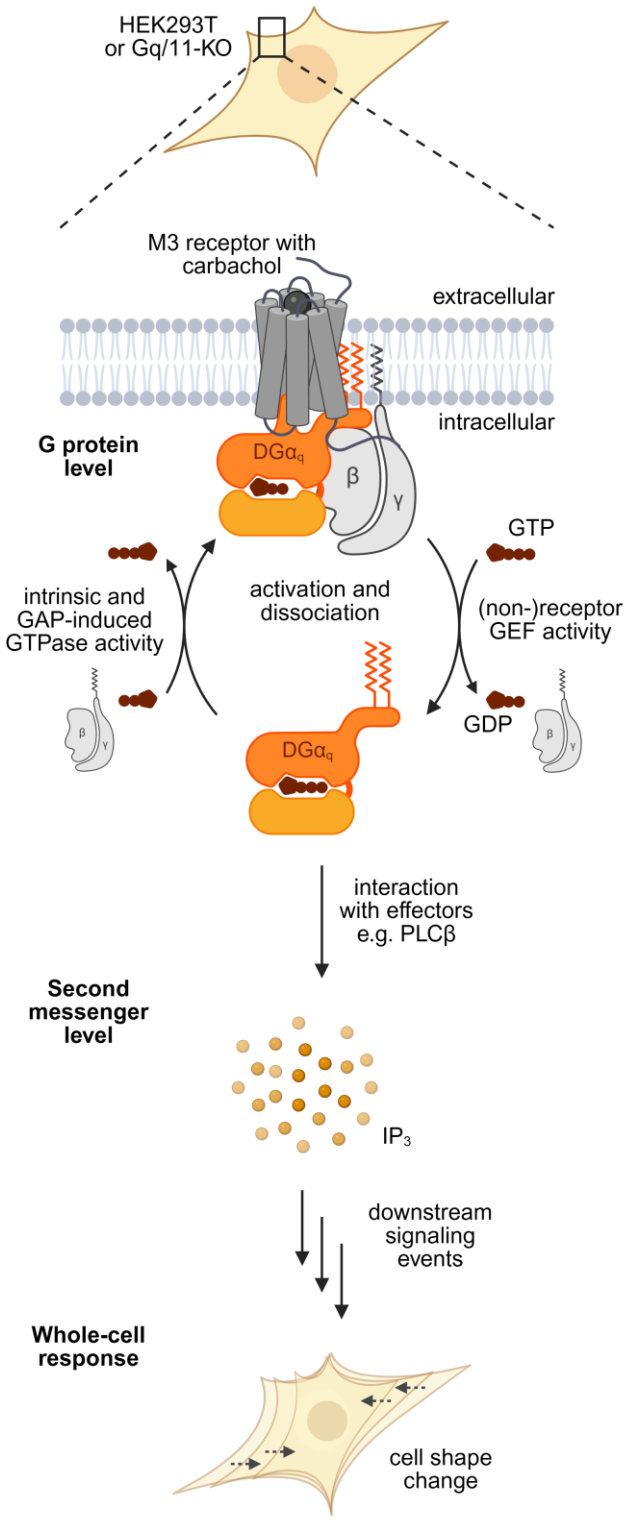

Assay
functional characteristics measured

Western Blot
- expression

Immunofluorescence Microscopy
- subcellular distribution/localization
- expression (qualitatively)

Gβγ/masGRK3ct BRET
- Gβγ interaction
- expression
- heterotrimer dissociation or rearrangement
- activation and deactivation kinetics
- GTPase activity
- indirectly: receptor and GAP interaction

IP_1 accumulation
- second messenger production
- indirectly: receptor and effector (PLCβ) interaction

DMR assay
- whole-cell response
- activation and deactivation kinetics
- indirectly: receptor and effector interaction

Figure 16: Assays employed and functional characteristics measured in relation to the Gq protein activation cascade.
Left. *G protein signaling cascade including activation and dissociation, second messenger production, and whole-cell response. The panel was created with BioRender.com.* ***Right.*** *Assays employed and functional characteristics measured in this thesis. The positions of grey boxes set the assays performed in relation to the signaling cascade on the left. HEK293 Gq/11-KO: HEK293 cells lacking Gαq and Gα11 proteins after CRISPR/Cas9 treatment, M3 receptor: M3 muscarinic acetylcholine receptor, GAP: GTPase-accelerating protein, GEF: guanine nucleotide exchange factor, PLCβ: phospholipase C β, IP_3: inositol 1,4,5-trisphosphate, IP_1: inositol monophosphate, DMR: dynamic mass redistribution.*

To obtain a comprehensive initial impression of the overall functionality and to be able to identify and exclude functionally altered DGq mutants as early as possible, one of these assays is particularly well-suited, as it provides a lot of information with little effort. We used a bioluminescence resonance energy transfer (BRET)-based approach that measures the interaction of Gβγ with a modified version of G protein-coupled receptor kinase 3 (GRK3) for the initial characterization of DGq mutants. Dissociation of the heterotrimer or rearrangement of the subunits after activation is necessary for the interaction of Gβγ with its effectors including GRK3. Thus, this readout can be used as a proxy for the activation of the G protein directly downstream of the receptor. In addition to the measurement of classical concentration-response curves, this versatile setup is suited to record kinetic traces of activation and inactivation processes. Furthermore, it can be used to quantify the interaction of DGαq wild-type and mutant subunits with the Gβγ complex. Overall, this assay allows us to draw multiple conclusions about the behavior of engineered DGαq constructs at the G protein level with little effort.

5.2.2. G protein level

BRET is a process combining bioluminescence of a protein with the principle of resonance energy transfer (RET) and is routinely used as a biophysical technique to monitor protein-protein interaction or conformational changes. If in proximity, typically below 10 nm, a radiation-free transfer of energy between a bioluminescent protein and a separate fluorescent moiety occurs. The energy usually emitted as bioluminescent light excites the fluorescent protein resulting in a drop in bioluminescence and an increase in fluorescence. The BRET ratio, defined as quotient of fluorescence and luminescence, therefore, increases with the average proximity between luminescent donor and fluorescent acceptor protein (Figure 17).

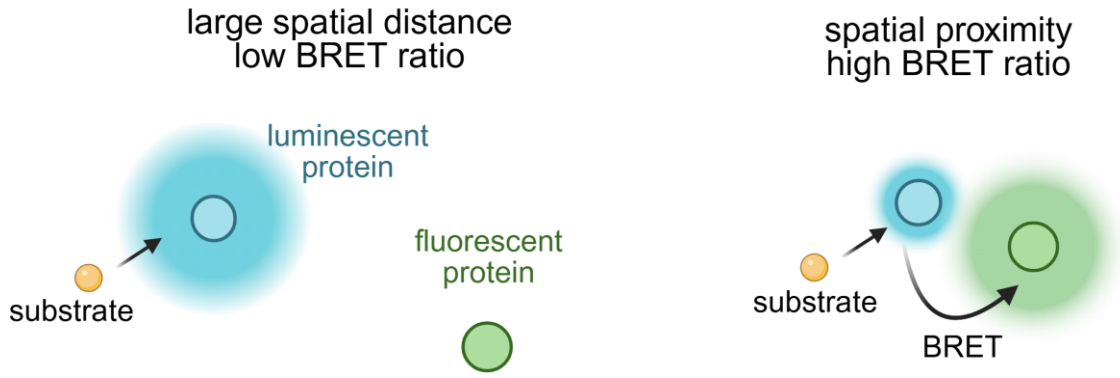

Figure 17: Principle of bioluminescence resonance energy transfer (BRET).
Left. *A luminescent protein converts a substrate producing bioluminescence. Due to the large spatial distance to the fluorescent protein, there is no energy transfer, and the BRET ratio is low.* ***Right.*** *If the fluorescent protein is in spatial proximity to the luminescent protein, radiation-free energy transfer occurs. The fluorescent protein is directly excited and produces fluorescence. The BRET ratio is high. The figure was created with BioRender.com.*

In the case of the Gβγ/masGRK3ct BRET sensor that we are using to indirectly monitor G protein activation, the bioluminescent donor NanoLuc® luciferase (NLuc) is fused to the c-terminus of GRK3 (GRK3ct-NLuc) which is membrane-associated through a myristic acid attachment peptide (mas), while the fluorescent protein Venus is split into two parts, with its N-terminal and C-terminal fragments fused to Gγ2 and Gβ1, respectively. Upon assembly of the constitutive Gβγ dimer, a functional Venus protein is formed. When the G protein is activated, the Gβγ effector mimic masGRK3ct-NLuc will interact with the released Gβγ-Venus subunit. The spatial proximity allows BRET to happen, and the BRET ratio increases (Figure 18). This assay setup conveniently monitors G protein activation without requiring the Gα subunit to be labeled. Apart from the practical advantage of a reduced cloning workload, this also elegantly permits assessment of the mutations' impact without the additional variable of a protein tag.

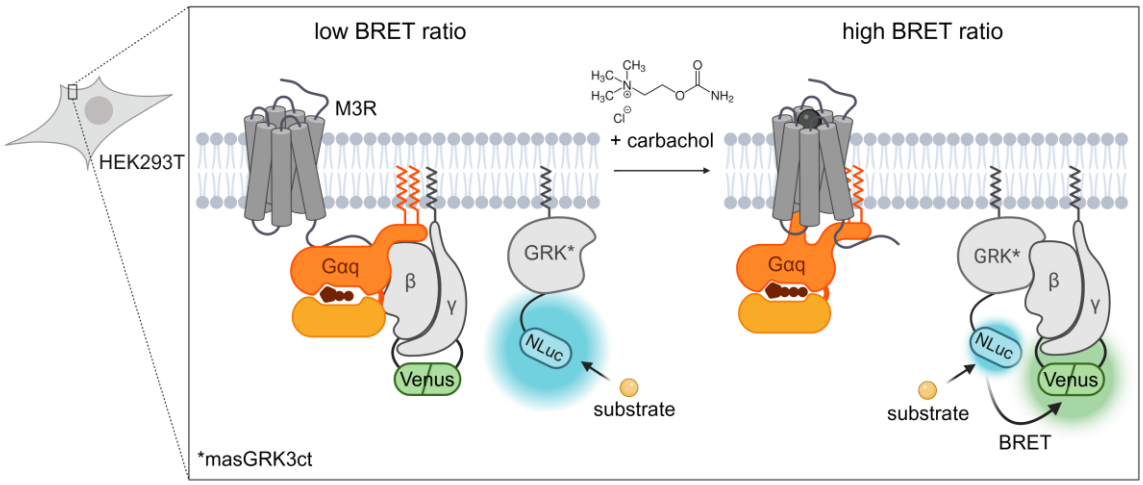

Figure 18: Gβγ/masGRK3ct BRET assay principle.
In the basal state, split Venus-tagged Gβγ interacts with Gαq and not with masGRK3ct-NLuc. The spatial distance of BRET donor and acceptor is high. Efficient BRET does not occur, and the BRET ratio is low. Upon activation of the M3 muscarinic acetylcholine receptor (M3R) with carbachol, the G protein is activated. Gβγ-Venus is released from the α subunit and free to interact with its effector mimic masGRK3ct-NLuc. BRET donor and acceptor are in proximity. BRET occurs and the BRET ratio is high. The figure was created with BioRender.com.

This particular BRET assay setup has successfully been performed with *Drosophila* DGαq isoform G in Chinese hamster ovary (CHO) cells (Himmelreich et al., 2017). Based on earlier results, we know that DGαq can also be functionally expressed in HEK293 cells and is able to interact with human receptor and effector proteins to finally initiate cell shape change as integrated whole-cell response (Alenfelder, 2019). However, the BRET assay still needs to be optimized for the investigation of DGαq in HEK293T cells.

We transiently transfected HEK293T cells with plasmid DNA coding for the M3 muscarinic acetylcholine receptor (M3 receptor, M3R), as a means to activate the G protein with carbachol, either murine or *Drosophila* Gαq wild type, and equal

amounts of all three sensor constructs. Murine Gq was included as a positive control for the interaction with the receptor and Gβγ.

We selected the M3 receptor in combination with its agonist carbachol to act as GEF on the G proteins in all assays in this thesis. This decision is based on the receptor's well-characterized Gq-activating properties (Ashkenazi et al., 1989; Conklin et al., 1988; Fukuda et al., 1988; Hulme et al., 1990), its endogenous presence in HEK293 cells (Atwood et al., 2011), and its demonstrated compatibility with *Drosophila* Gq (Alenfelder, 2019). Even though the receptor will be used at endogenous levels in some of the following assays, overexpression is necessary to obtain a signal in response to carbachol in the Gβγ/masGRK3ct BRET assay (data from different project, Figure 19). Therefore, for BRET measurements, cells have been transfected with plasmid DNA coding for the M3R.

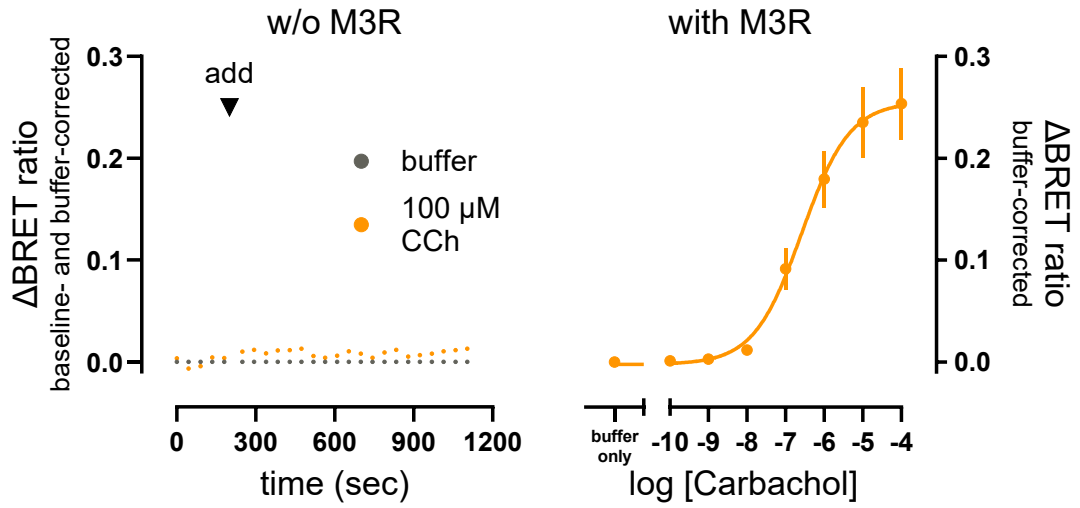

Figure 19: Introduction of exogenous M3R is necessary to obtain a CCh-induced signal in the Gβγ/masGRK3ct BRET assay.
HEK293 cells lacking Gαq, Gα11, Gα12, Gα13, Gαs, Gαolf, and Gαz proteins after CRISPR/Cas9 treatment (HEK293 Gq/11/12/13/s/olf/z-KO or Δ7) were transiently transfected with constructs coding for split Venus-tagged Gβγ, masGRK3ct-NLuc, Gα11, and PTX-S1, as well as M3R as indicated. Kinetic traces of cells without M3R show baseline- and buffer-corrected BRET ratios. Cells were activated with 100 µM carbachol (CCh) or buffer after 30 seconds of baseline measurement. Data are representative of two biologically independent experiments. The CCh concentration-response curve was measured as buffer-corrected BRET ratio after stimulation with CCh or buffer. Data are the means ± SEM of three biologically independent experiments performed by Dr. Lukas Grätz (Kostenis lab, University of Bonn), modified from Mühle et al. (2025). M3R: M3 muscarinic acetylcholine receptor.

The transfection ratio of 1:1:1 for the sensor constructs was taken from previous experience with the sensor (Maziarz et al., 2020). To assess the suitability of the chosen transfection conditions, we measured the BRET ratio without agonist stimulation (basal BRET ratio).

When transfecting the donor masGRK3ct-NLuc without Gβγ-Venus or Gα ("GRK only"), no BRET can occur, and the measured BRET ratio is a technical artifact resulting from the spill-over effect of bioluminescence emission into the fluorescence

optical sensor. Transfecting all sensor constructs without Gα (“GRK + Gβγ”), yields the maximal possible BRET ratio, as all available Gβγ-Venus acceptor proteins can interact with masGRK3ct-NLuc unhindered by the competing effects of Gα protein. Additionally coexpressed Gα will compete with masGRK3ct-NLuc and displace Gβγ-Venus from the donor protein, quenching the BRET ratio to levels close to the “GRK only” control.

Basal BRET ratios of the first experiment showed a lower maximal BRET ratio (“GRK + Gβγ”) compared to values from experience with this sensor in previous experiments (Figure 20A). However, the spill-over of the NLuc luminescence into the fluorescence channel (“GRK only”) was in the expected range based on the plate reader configuration. The quenching, i.e. the lowering of the BRET ratio through additional transfection of Gα subunits, under the chosen transfection conditions was lower the expected from previous experiments performed by others in the lab. This indicated insufficient competition of Gα with masGRK3ct-NLuc for Gβγ-Venus binding and could be due to low expression of the Gα isoforms and too low a ratio of Gα to Gβγ-Venus and GRK-NLuc.

Such low quenching also leads to slopes in the baseline of kinetic measurements which could clearly be seen in this experiment (Figure 20B). Although both Gq proteins properly responded to the activation of the M3R with carbachol, the signal amplitude was rather low. However, DGq is generally functional in this assay, as it responded to carbachol-activated receptor and returned to the heterotrimeric state when the receptor was inactivated with atropine.

When baseline and plateau of kinetic measurements are sloping as they were in this experiment, analysis of endpoint measurements such as concentration-response curves has to be done with care. Murine and *Drosophila* Gq responded concentration-dependently to activation with carbachol (Figure 20C) with similar potencies (Figure 20D). The greater amplitude of DGq compared to mGq corresponded well with the signal height differences in the kinetic measurements and with the superior quenching in the basal BRET measurements.

In conclusion, this experiment clearly showed that the Gβγ/masGRK3ct BRET assay is suited to investigate *Drosophila* Gαq mutants. However, the results differed in quality from our expectations. Although the lack of a signal plateau after activation and low quenching could be inherent characteristics of *Drosophila* Gq, the similar quality of results for murine Gq suggested otherwise. The transfection conditions for the sensor constructs needed to be optimized and the expression of DGq needed to be enhanced.

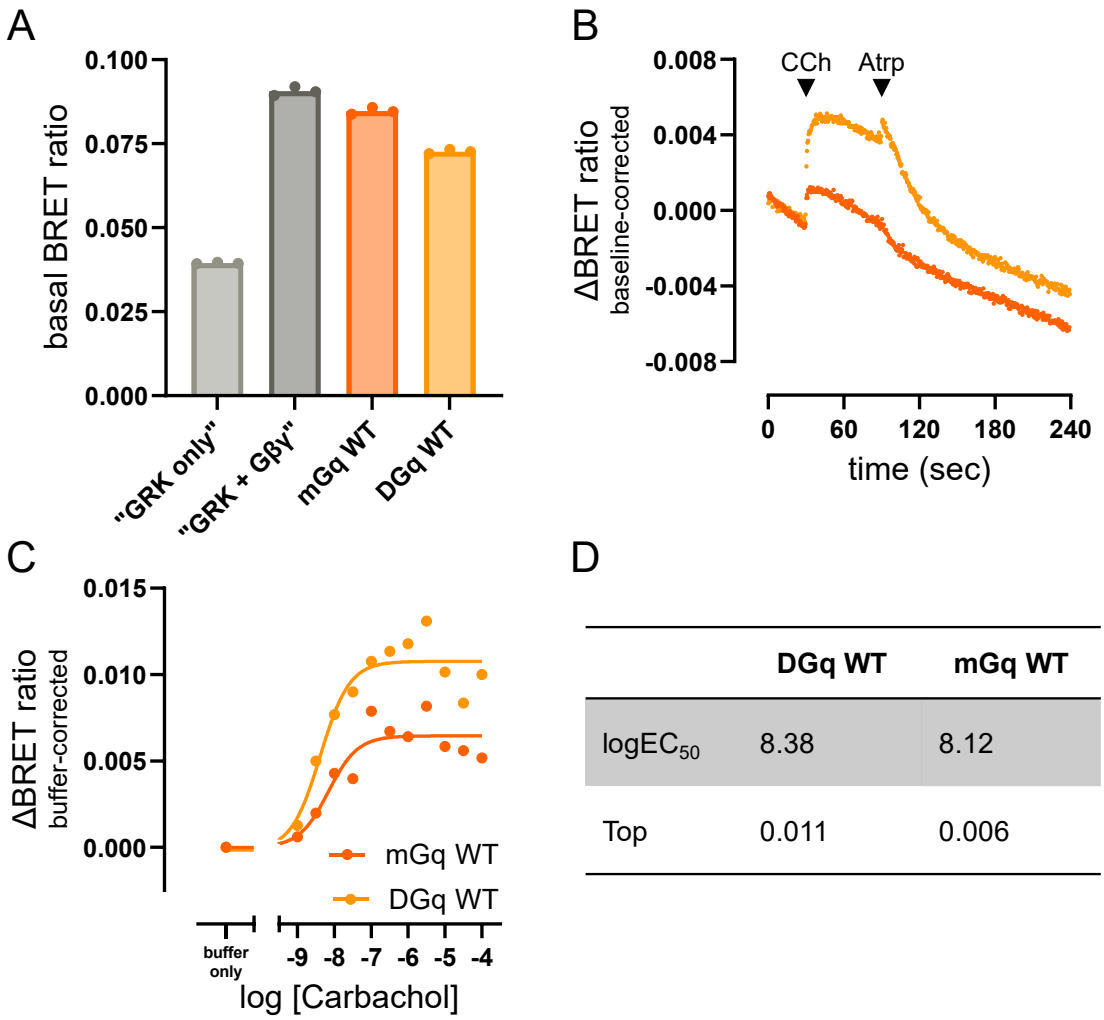

	DGq WT	mGq WT
$logEC_{50}$	8.38	8.12
Top	0.011	0.006

Figure 20: The first set of transfection conditions for the Gβγ/masGRK3ct BRET assay is not optimal. ***A.*** *Basal BRET ratio measured in HEK293T cells transiently transfected with constructs coding for M3R, split Venus-tagged Gβγ, masGRK3ct-NLuc, and either mGq or DGq wild type as indicated. Bar graphs represent the mean ± SD of one individual experiment. Data points represent technical replicates.* ***B.*** *Kinetic baseline-corrected BRET traces of cells transfected as in A. Cells were activated with 100 µM carbachol (CCh) after 30 seconds of baseline measurement. Deactivation with 100 µM atropine (Atrp) followed after 60 additional seconds. Data are the values of one individual experiment.* ***C.*** *CCh concentration-response curves measured as buffer-corrected BRET ratio after stimulation with CCh or buffer in cells transfected as in A. Data are the values of one individual experiment.* ***D.*** *Table summarizing pEC_{50} and top values of the CCh concentration-response curves shown in C.*

The transfection ratio between the BRET donor and acceptor directly influences the maximal BRET window (“GRK only” to “GRK + Gβγ”) but also impacts the quality of the signal obtained. The stability of the baseline and the amplitude and stability of the signal after activation can usually be improved by increasing the ratio of acceptor to donor amounts. Thus, we investigated if a decrease in the masGRK3ct-NLuc amounts and, therefore, an increase in ratio to 4:1 (“medium ratio”) or 8:1 (“high ratio”) improves maximal BRET window, signal stability, and amplitudes (Figure 21A).

On the other hand, the ratio between the Gα tested and the Gβγ-Venus sensor component needs to be optimized for the individual Gα subunit of interest. For Gαq,

a higher Gα/Gβγ ratio generally improves quenching and signal amplitudes (Masuho et al., 2015) probably due to increased Gβγ binding. We, therefore, increased the DGαq DNA amounts transfected with the Gβγ amount to maintain a 5:1 ratio (Figure 21A). Additionally, we investigated whether expression of Ric-8A, a chaperone for Gαq proteins which assists with expression and shuttling to the plasma membrane (Chan et al., 2013; Gabay et al., 2011), improves quenching and signaling as it did in the previous publication investigating DGαq using this BRET assay (Himmelreich et al., 2017).

As a reference, we tested the 1:1:1:5 ratio (GRK-NLuc/Gβ-splitVenus/Gγ-splitVenus/DGαq) used in the first assay (”low (old) ratio”) in parallel.

Basal BRET ratios revealed an improvement of the maximal BRET window from the previously used 1:1 ratio of sensor compounds (“low (old) ratio”) to higher ratios of 4:1 and 8:1 (Figure 21B). Interestingly, quenching of DGαq improved drastically when co-transfecting Ric-8A, suggesting that the chaperone facilitates Gβγ binding by supporting expression and proper folding of the α subunit. When examining the kinetic traces, it becomes obvious that the change in sensor ratio and presence of Ric-8A also improved the stability of both baseline and signal plateau (Figure 21C), more so for the higher ratio of 8:1 (“high ratio”). Additionally, the addition effect observable after atropine addition at 90 seconds was reduced in this condition. This effect might stem from substrate dilution when extra liquid was added, which might have less impact on lower amounts of masGRK3ct-NLuc and the associated lower rate of substrate turnover. Furthermore, the amplitude of carbachol-induced BRET responses was increased compared to the first assay (0.008 vs 0.005), even more so when Ric-8A was expressed (0.024).

All in all, the results of this optimization assay clearly showed that the higher 8:1 acceptor to donor ratio, the associated lower donor amount, and expression of the Gαq chaperone Ric-8A combined improve all quality parameters recorded. These conditions allowed a sufficiently high BRET window, stabilized the baseline and plateau of the kinetic BRET traces, increased agonist-induced signaling amplitudes, and markedly reduced addition effects.

For an accurate comparison of DGαq mutants to wild-type protein, it is beneficial if the agonist-induced signal originates solely from DGq without any interference from endogenous G proteins in HEK293T cells. The "GRK + Gβγ" condition allowed for the investigation of this requirement, as these cells are transfected similarly to the measurement condition but without DGαq. Cells of this condition showed no response to the addition of carbachol or atropine (Figure 21D), demonstrating that endogenous G proteins in HEK293T cells do not contribute to the BRET signals observed under these experimental conditions, and that HEK293T cells are, thus, suited for the comparison of DGq mutants and wild type.

A

DNA (µg/well)	high ratio	medium ratio	low (old) ratio
masGRK3 ct-NLuc	0.025	0.05	0.1
Gβ-Venus	0.2	0.2	0.1
Gγ-Venus	0.2	0.2	0.1
DGαq	1.0	1.0	0.5

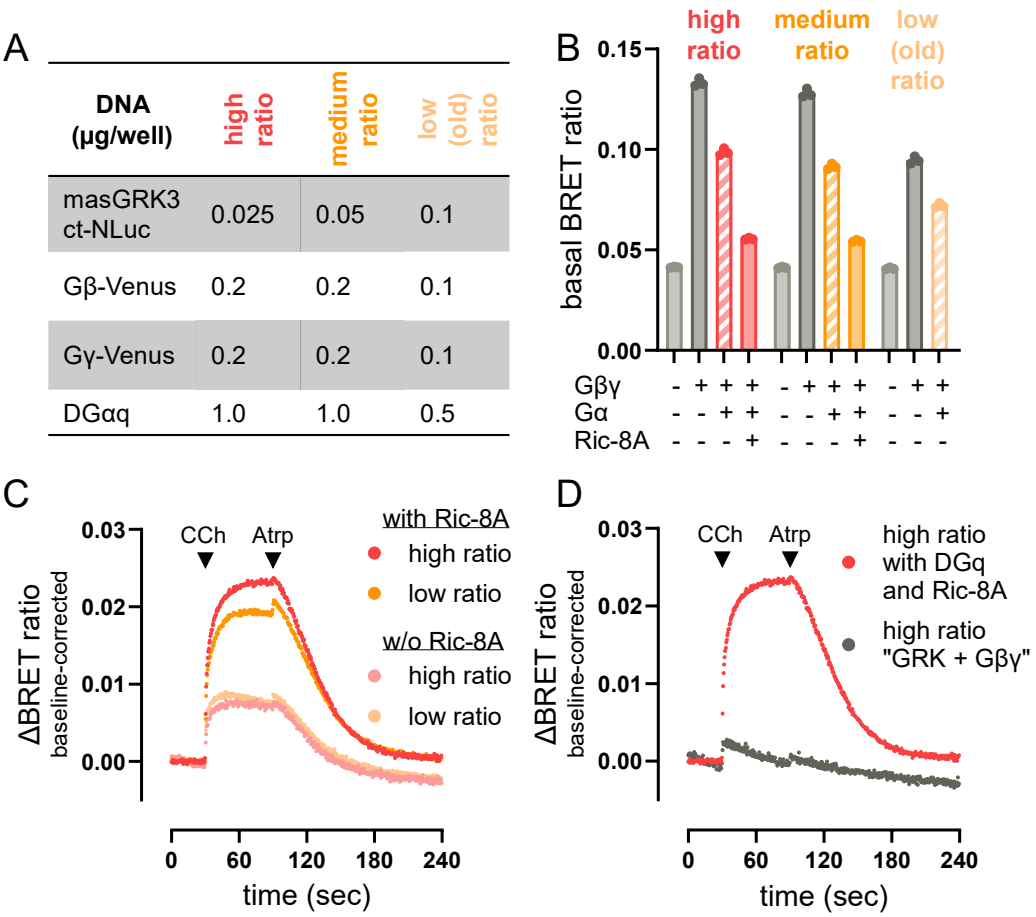

Figure 21: Optimization of transfection conditions improves quenching, addition effects, and amplitudes of Gβγ/masGRK3ct BRET signals.
A. *DNA amounts used for transfection in the optimization BRET assay. For a complete protocol see Chapter 4.5. BRET-based biosensing in the methods section.* ***B.*** *Basal BRET ratio measured in HEK293T cells transiently transfected with constructs coding for M3R, masGRK3ct-NLuc, and split Venus-tagged Gβγ, DGq wild type, and Ric-8A as indicated. Transfection amounts are listed in A. Bar graphs represent the means ± SD of one individual experiment. Data points represent technical replicates.* ***C and D.*** *Kinetic baseline-corrected BRET traces of cells transfected as in B. Cells were activated with 100 µM carbachol (CCh) after 30 seconds of baseline measurement. Deactivation with 100 µM atropine (Atrp) followed after 60 additional seconds. Legends indicate the transfection conditions measured. Data are the values of one individual experiment.*

Two further prerequisites for the later studies are concentration-response curves of carbachol and FR with sufficient quality to enable the comparison of DGαq mutants and wild type regarding their signaling behavior and FR sensitivity. To record carbachol concentration-response curves, cells transiently transfected with the optimized conditions (1:8:8:40 masGRK3ct:Gβ:Gγ:Gα) were treated with a carbachol dilution series or buffer. The BRET ratio for each condition and the difference in BRET ratio between carbachol and buffer treatment (ΔBRET ratio, buffer-corrected) was calculated. The resulting concentration-response curve displayed the expected sigmoidal shape with a pEC_{50} value of 6.90 with a recognizable top at the highest concentrations (Figure 22A). Similarly, FR inhibition was tested by pre-treatment with differing inhibitor concentrations and subsequent activation with a saturating concentration of carbachol (100 µM). FR fully inhibited agonist-induced BRET elevation with a pIC_{50} value of 5.74 (Figure 22B). This stable

and reproducible activation and inhibition of DGq wild type enables the investigation of DGαq mutants' signaling behavior and FR sensitivity in comparison to wild type in this Gβγ/masGRK3ct BRET assay setup.

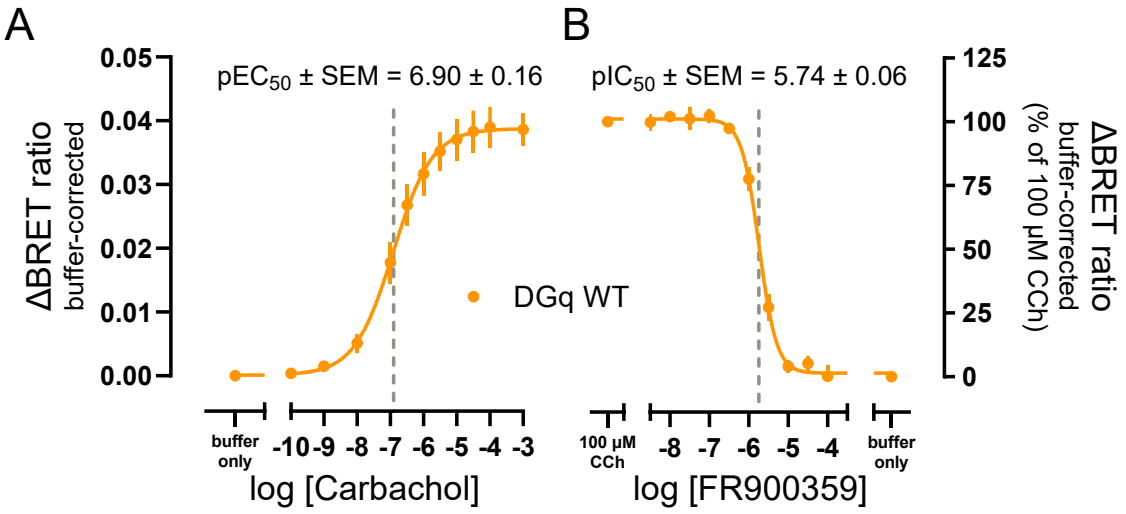

Figure 22: The Gβγ/masGRK3ct BRET assay is suited to investigate signaling behavior and FR900359 (FR) sensitivity of engineered DGαq mutants.
A. *Carbachol (CCh) concentration-response curve measured as buffer-corrected BRET ratio after stimulation with CCh or buffer in HEK293T cells transiently transfected with constructs coding for M3R, split Venus-tagged Gβγ, masGRK3ct-NLuc, DGq wild type, and Ric-8A. The resulting pEC_{50} value is indicated with a grey, dashed line. Data are the means ± SEM of four to five biologically independent experiments.* ***B.*** *FR concentration-response curve measured as buffer-corrected BRET ratio after preincubation with FR or buffer and stimulation with CCh or buffer in cells transfected as in A, normalized to the effect of 100 µM CCh. The resulting pIC_{50} value is indicated with a grey, dashed line. Data are the means ± SEM of four to five biologically independent experiments.*

With these initial experiments, we demonstrated that the Gβγ/masGRK3ct BRET assay utilizing HEK293T cells transfected with the optimized conditions is suited for the investigation of multiple DGαq mutant properties including Gβγ binding, activation and deactivation kinetics, potency and efficacy of activation, and sensitivity to FR. We, therefore, set out to investigate these parameters for the initial three DGαq mutants YK, IW, and FIVE.

5.2.2.1. Gβγ binding

Analysis of the quenching behavior of all three mutants in comparison to DGαq wild type revealed a striking difference between YK on the one hand and IW and FIVE on the other hand (Figure 23). DGq IW and FIVE quenched the basal BRET ratio to the same extent as wild type. Since quenching is a composite result of Gα expression and binding to Gβγ this could indicate that IW and FIVE retain their Gβγ binding capabilities despite the mutations assuming similar expression levels to wild-type DGαq. In contrast, YK showed reduced quenching. This could result from defective Gβγ binding, mislocalization, reduced expression or a combination of these factors.

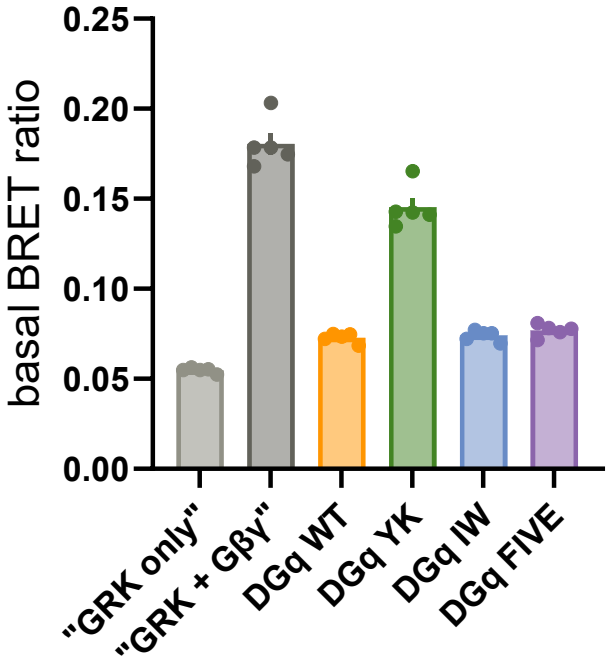

Figure 23: DGαq IW and FIVE exhibit wild type-like Gβγ binding capabilities, while Gβγ binding or expression of YK is reduced.
Basal BRET ratio measured in HEK293T cells transiently transfected with constructs coding for M3R, masGRK3ct-NLuc, split Venus-tagged Gβγ, Ric-8A, and DGq wild type or mutants as indicated. Bar graphs represent the means ± SEM of five biologically independent experiments. Data points represent individual replicates.

There are two Gβγ binding interfaces on Gα: the N-terminal helix and a region around Switch II, including the β2- and β3-sheets as well as the α2-helix (Lambright et al., 1996; Neuwald, 2007; Wall et al., 1995). Of the six mutated residues in the DGαq mutants, four (valine-176$^{G.hfs2.1}$, valine-178$^{G.hfs2.3}$, isoleucine-184$^{G.S2.2}$, and proline-187$^{G.S2.5}$) are part of or located directly before the β2-sheet. However, none of these residues contribute to the hydrophobic pocket interacting with Gβγ (Lambright et al., 1996). The mutated residue in DGαq YK (tyrosine-69$^{H.HA.7}$) is located remotely and does not participate in the formation of Gβγ contacts.

Therefore, it is unlikely though not impossible that a mutation of these residues impacts the Gα protein's interaction with the Gβγ complex. To draw certain conclusions on the behavior of DGαq IW and FIVE, but more so of DGαq YK, examination of DGαq mutants' expression levels is essential.

5.2.2.2. Expression

To investigate DGαq wild-type and mutant expression levels in HEK293T cells used for the Gβγ/masGRK3ct BRET assay, we used a combination of sodium dodecyl sulfate polyacrylamide gel electrophoresis (SDS-PAGE) and western blotting (WB). DGαq isoforms were stained with a primary polyclonal rabbit anti-Gαq IgG antibody that targets the N-terminus of murine Gαq and a secondary AlexaFluor680-tagged anti-mouse antibody.

“GRK + Gβγ” control cell lysates presented one faint band only at approximately 38 kDa, the height expected for endogenous Gαq (Patt et al., 2021) (Figure 24). Cell lysates transfected with mGαq DNA showed a more intense band at the same height, indicating that the faint band in all other conditions indeed stems from HEK293T-endogenous human Gαq. Lysates of cells transfected with DGαq wild type DNA exhibit a second more intense band migrating slightly above human/murine Gαq, even though the predicted molecular weight of DGαq isoform G is roughly similar with 41.65 kDa as compared to 42.16 kDa (Stothard, 2000). Mutant DGαq proteins displayed electrophoretic mobility indistinguishable from the wild type.

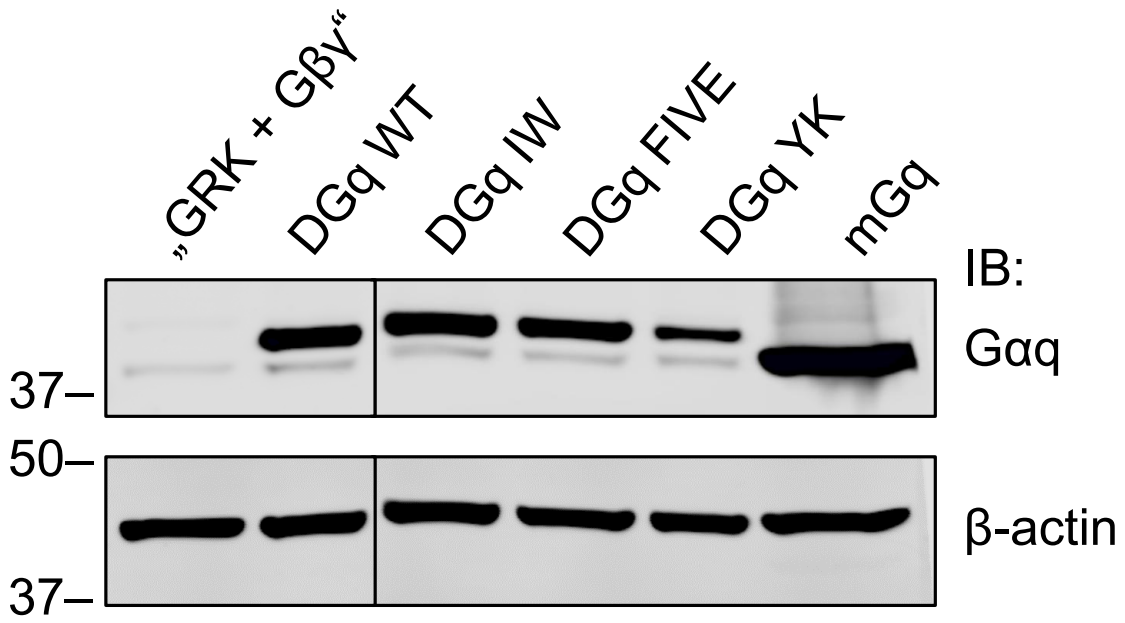

Figure 24: All transfected DGαq variants can be detected by western blotting, migrating slightly above murine Gαq.
Western blot of SDS-PAGE performed with lysates of HEK293T cells used for Gβγ/masGRK3ct BRET experiments shown in Figure 23, Figure 26, and Figure 27, and cells similarly transiently transfected with a construct coding for mGαq instead of DGαq. β-actin was used as protein loading control. Depicted are results representative of three individual western blots with cells from biologically independent BRET assays. The image originated from one blot but is cropped to remove irrelevant samples. IB: immunoblotted.

DGαq IW and FIVE were expressed at similar levels to the wild-type DGαq protein (Figure 25). In contrast, DGαq YK was expressed at approximately a third of the level of the wild type, despite the concurrent expression of the chaperone Ric-8A.

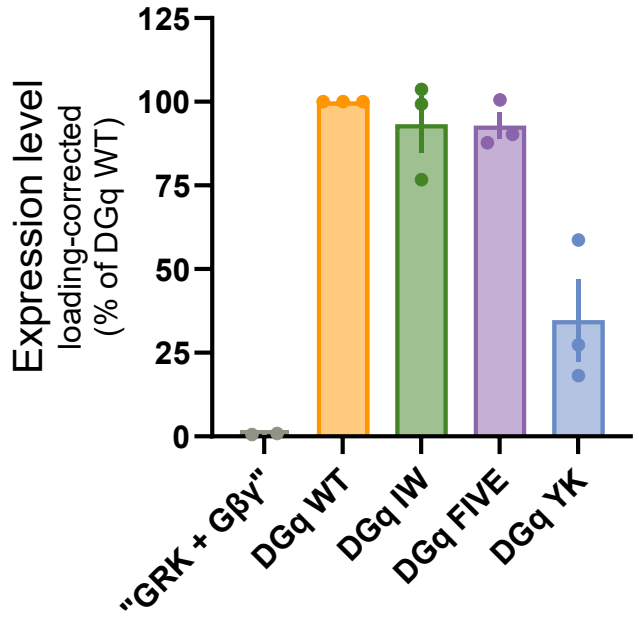

Figure 25: DGαq IW and FIVE are expressed at wild type-like levels, while expression of YK is reduced. *Quantitative analysis of the western blot expression data shown in Figure 24. Western blots of SDS-PAGE were performed with lysates of HEK293T cells used for Gβγ/masGRK3ct BRET experiments shown in Figure 23, Figure 26, and Figure 27. β-actin was used as protein loading control. Bar graphs represent the means ± SEM of two to three independent western blots corrected for loading and normalized to DGαq WT intensities. Data points represent individual replicates.*

In conjunction with the quenching data from the Gβγ/masGRK3ct BRET assay, these results revealed wild type-like Gβγ binding capabilities of DGαq IW and FIVE. Based on the lower expression of DGαq YK, it is plausible that its interaction with Gβγ remains similar to that of DGαq wild type. Nonetheless, the observed decrease in expression does not necessarily translate to altered signaling activity, warranting further investigation.

5.2.2.3. Activation with Carbachol

The Gβγ/masGRK3ct BRET assay is also suited to investigate the dissociation or rearrangement of the heterotrimer after GEF-mediated activation. Dissociation or rearrangement is the first step of G protein activation that precedes any other consequences in the cell. Release of Gβγ from the Gα subunit allows its association with the effector mimic masGRK3ct which translates to an increase in BRET and, therefore, the BRET ratio measured. This can be recorded in either endpoint or kinetic mode, allowing easy recording of concentration-response curves or activation and inactivation kinetics, respectively.

All three tested mutants reacted to activation by carbachol-stimulated M3R in a concentration-dependent manner (Figure 26A). Most strikingly, DGq YK yielded a decreased response apparent from the reduced efficacy compared to wild type (Figure 26B). While these results did not exclude other influences unfavorable to activation such as reduced interaction with the receptor or non-wild type-like

localization, they suggest that the reduction in expression of DGαq YK indeed translated to a reduction in signaling. Interestingly, though the potency of carbachol activation was unchanged compared to DGαq wild type when treating the concentration-response curve as a monophasic sigmoidal curve, the hill slope was reduced to about half of wild type and the curve showed hints of being biphasic. This suggests that the activation of YK is indeed hampered by more than reduced expression. In contrast, the efficacies of DGq IW and FIVE were virtually identical to that of wild type, and the potency of both mutants was slightly increased (Figure 26B). These results should be kept in mind during further analysis. The thorough characterization planned for candidate mutants should reveal probable causes that could be investigated further.

A

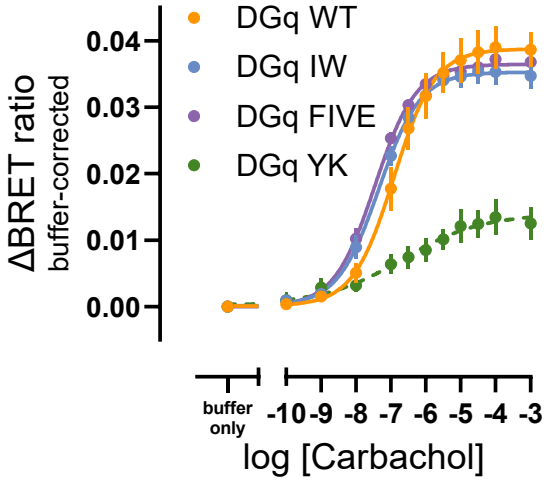

B

	pEC_{50} ± SEM	Top ± SEM
DGq WT	6.90 ± 0.16	0.039 ± 0.003
DGq IW	7.37 ± 0.15	0.035 ± 0.002
DGq FIVE	7.47 ± 0.12	0.036 ± 0.001
DGq YK	6.83 ± 0.26	0.014 ± 0.003

Figure 26: DGq IW and FIVE mimic wild type in the efficacy and potency of activation, while DGq YK signaling is impaired.
A. *Carbachol (CCh) concentration-response curves measured as buffer-corrected BRET ratio after stimulation with CCh or buffer in HEK293T cells transiently transfected with constructs coding for M3R, split Venus-tagged Gβγ, masGRK3ct-NLuc, DGq wild type or mutants, and Ric-8A. Data are the means ± SEM of four to six biologically independent experiments. Data for DGq WT were copied from Figure 22 for clarity.* ***B.*** *Table summarizing pEC_{50} values ± SEM and Tops ± SEM of the CCh concentration-response curves shown in A.*

Concentration-response curves provided us with key pharmacological parameters such as efficacy and potency but did not provide information regarding the kinetics of activation. Kinetic measurements of DGq wild-type and mutant activation with saturating concentrations of carbachol confirmed comparable efficacies of DGq WT, IW, and FIVE with similar amplitudes of the traces (Figure 27A). Furthermore, DGq YK displayed the expected reduction in amplitude.

The kinetics of activation for DGq YK were difficult to evaluate due to the sloping baseline and plateau of the corresponding curve (Figure 27A), likely resulting from low Gα expression and elevated initial BRET ratio in this condition. The activation kinetics of DGq IW and FIVE, however, are comparable to those of the wild-type protein (Figure 27A and B).

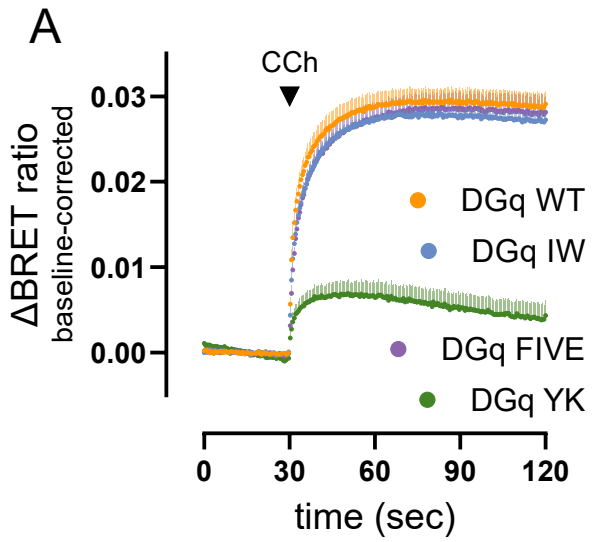

B

	k ± SEM (sec^{-1})
DGq WT	0.28 ± 0.04
DGq IW	0.25 ± 0.07
DGq FIVE	0.20 ± 0.01

Figure 27: DGq IW and FIVE mimic wild type in their kinetics of activation, while DGq YK is impaired. ***A.*** *Kinetic baseline-corrected BRET traces of HEK293T cells transiently transfected with constructs coding for M3R, split Venus-tagged Gβγ, masGRK3ct-NLuc, DGq wild type or mutants, and Ric-8A. Cells were activated with 100 µM carbachol (CCh) after 30 seconds of baseline measurement. Data are the means + SEM of three to five biologically independent experiments.* ***B.*** *Table summarizing activation rate constant values k ± SEM of the kinetic CCh activation curves shown in A extracted using the plateau followed by one-phase association model in GraphPad Prism.*

In summary, the reduced expression and possibly additionally compromised function or altered localization caused by the mutation of tyrosine-$69^{H.HA.7}$ to lysine reduce the efficacy of activation and decreased the steepness of the concentration-response curve compared to wild-type DGq. In contrast, the introduction of the single and five-fold mutations in DGαq IW and FIVE, respectively, largely upheld wild type-like activation behavior regarding efficacy, potency, and kinetics on the G protein activation and dissociation level.

5.2.2.4. Localization

All results obtained for DGαq YK are reminiscent of the corresponding mutant in murine Gq, mGαq F75K (Patt et al., 2021). Published data shows reduced expression levels and corresponding reduction in signaling amplitude for all murine FK-containing mutants. In addition to the reduction in cellular abundance, the distribution throughout the cell is altered. While wild-type mGαq is mainly located at the plasma membrane due to its two palmitate membrane anchors (Wedegaertner et al., 1993; Wedegaertner et al., 1995), mGαq FK is localized mainly in the cytosol. This behavior cannot be rescued by overexpression of Gβγ indicating that it is not a result of diminished Gβγ binding (Figure 28). Considering the overall similarity of the results for DGαq YK and mGαq FK, it seems reasonable to assume that DGαq YK also mimics the FK mutant's behavior regarding localization in the cell. Altered subcellular distribution in addition to the reduced expression levels would provide a comprehensive explanation for the data obtained so far.

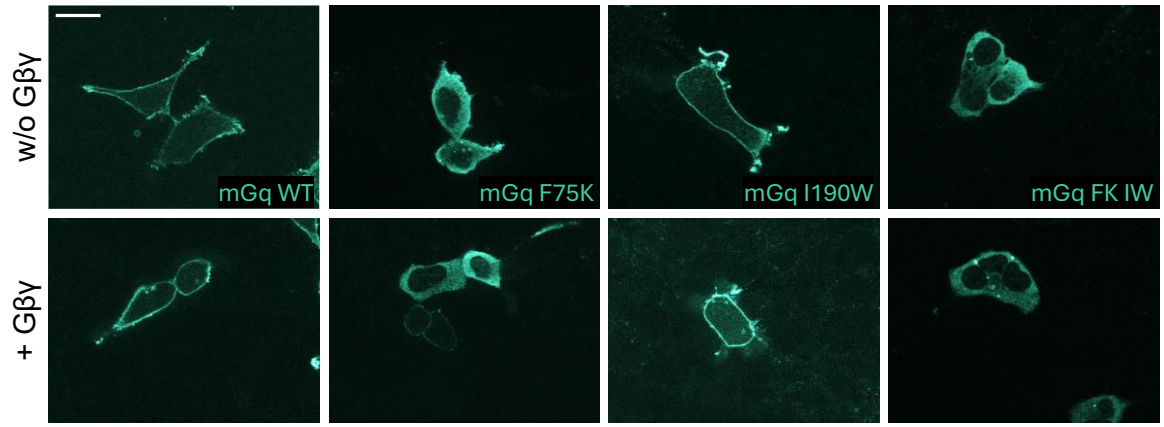

Figure 28: Presence of exogenous Gβγ does not rescue the intracellular localization of F75K-containing mGαq mutants.
HEK293 cells lacking Gαq, Gα11, Gα12, and Gα13 proteins after CRISPR/Cas9 treatment (HEK293 Gq/11/12/13-KO) were transiently transfected with constructs coding for HA-tagged mGαq wild-type or mutant proteins and either $Gβ_1γ_2$ or empty vector as indicated. Cells were stained with a primary mouse anti-HA and secondary FITC-tagged anti-mouse antibody. Depicted are representative pictures of two to four experiments. The scale bar in the top left corner represents 20 µm. The brightness of the pictures was increased by 50% (FK and FK IW) or 70% (WT and IW).

We, therefore, decided to investigate the mutants' subcellular localization in comparison to wild type using immunofluorescence microscopy. Transfection of HEK293 cells devoid of Gαq, Gα11, Gα12, and Gα13 proteins after CRISPR/Cas9 treatment (HEK293 Gq/11/12/13-KO) (Devost et al., 2017) allows for the unambiguous detection of exogenous DGαq proteins circumventing signals from endogenous protein.

In contrast to murine Gαq, for which an epitope-tag using a shortened human influenza hemagglutinin-derived (HA) tag has been developed and characterized (Wilson & Bourne, 1995) and has been in use for the last three decades, no such tagged protein exists for *Drosophila* Gαq. Therefore, the use of a primary antibody that recognizes an epitope on DGαq in combination with a fluorescent secondary antibody is necessary for detection. We screened three different commercially available antibodies raised against murine Gαq or parts of it for their suitability to detect DGαq in immunofluorescence microscopy.

To confirm the presence of exogenous protein, we transfected plasmid DNA coding for HA-tagged mGαq and stained the protein with a primary monoclonal mouse anti-HA antibody as a positive control for all screening experiments. However, even though the protein was present, the first primary antibody tested, a monoclonal mouse antibody raised against residues 60 to 359 of murine and human Gα11 (AB_10842057), which is marketed for the use in immunofluorescence staining for mouse, rat, and human Gαq, failed to stain both HA-tagged murine and untagged *Drosophila* Gαq. A second monoclonal mouse antibody raised against residues 22 to 31 of the human Gαq protein (AB_2232474), which is also marketed for immunofluorescence applications of various species' Gαq proteins, allowed the

detection of HA-tagged mGαq but with lower intensity compared to the anti-HA antibody. A detection of *Drosophila* Gαq was not successful.

These results can be rationalized by sequence differences between the Gαq proteins of mouse and *Drosophila* origin, more easily for the first compared to the second antibody. We, therefore, specifically looked for an antibody raised against a protein part with higher similarity. We found that a polyclonal rabbit IgG antibody raised against the final ten C-terminal residues of murine Gαq and Gα11 (AB_310221) effectively stained both murine and *Drosophila* Gαq proving our strategy successful. This primary antibody was used in all subsequent immunofluorescence experiments. For all microscopy experiments with mouse or rabbit primary antibodies, we used a green-fluorescent FITC-tagged or orange-fluorescent Cy3-tagged secondary anti-mouse antibody, respectively.

To better evaluate the subcellular localization of the *Drosophila* Gαq mutants, two structural features of the cell, the membrane and the nucleus, were stained. We evaluated the quality of membrane staining using two different approaches. Staining of the membrane with a mouse antibody against β-catenin, a membrane-bound protein (Bernard et al., 2008; Orsulic et al., 1999), resulted in lower intensity than transfection of a membrane-anchored fluorescent protein (NeonGreen-CAAX) (Figure 29). Furthermore, the transfection approach yielded a more uniform and less spotty staining of the membrane. In addition, we visualized the nucleus using the DNA-specific fluorochrome 4'-6-diamidino-2-phenylindole (DAPI) (A. W. Coleman et al., 1981).

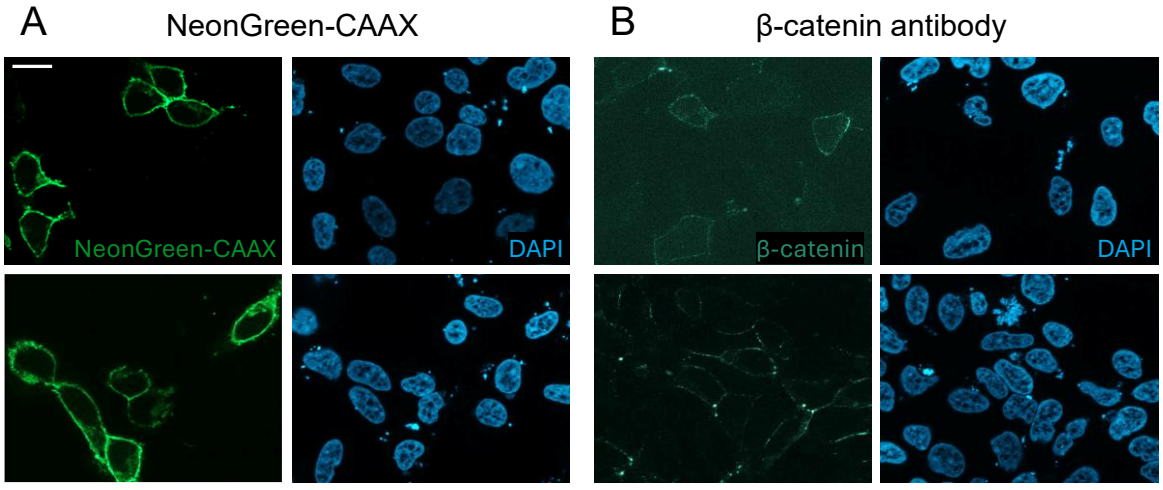

Figure 29: Transfection of NeonGreen-CAAX is better suited to mark the plasma membrane than staining with an anti-β-catenin antibody.
*HEK293 cells lacking Gαq, Gα11, Gα12, and Gα13 proteins after CRISPR/Cas9 treatment (HEK293 Gq/11/12/13-KO) were transiently transfected with a construct coding for the membrane-targeted green-fluorescent protein NeonGreen-CAAX (**A**) or empty vector (**B**) and stained with DAPI to visualize the nucleus (blue). Cells transfected with empty vector only were additionally stained with a primary mouse anti-β-catenin and secondary green-fluorescent FITC-tagged anti-mouse antibody to visualize the membrane. Depicted are representative pictures of a single experiment. The scale bar in the top left corner represents 20 µm. The brightness of the pictures was increased by 50% (DAPI, upper β-catenin image due to background signals) or 70% (others).*

To investigate the subcellular localization of DGαq wild type, we transiently co-transfected equal amounts of plasmid DNA coding for DGαq wild type or empty vector and the membrane marker NeonGreen-CAAX. We expected *Drosophila* Gαq to be localized at the plasma membrane, even though the protein is foreign to the human cell background. Not only does DGαq contain the necessary CC motif for double palmitoylation that is present in mGαq (see Figure 66 in Additional Material), but the protein also interacts with human Gβγ complex (see Chapter 5.2.2.1. Gβγ binding). Both of these are requirements for proper membrane localization (Evanko et al., 2000; Parenti et al., 1993; Wedegaertner et al., 1995) and are fulfilled for *Drosophila* Gαq. Indeed, the colocalization of anti-Gαq antibody fluorescence with that of the membrane marker revealed the expected membrane localization of the protein (Figure 30).

Furthermore, the lack of fluorescence in antibody-stained cells mock-transfected with empty vector instead of DGq confirmed the specificity of the selected antibody and the lack of interference with other membrane proteins (Figure 30). However, fluorescence intensities of the two transfected constructs DGαq and the membrane-targeted fluorescent protein differed extensively, with the NG-CAAX fluorescence overpowering that of the Gα protein.

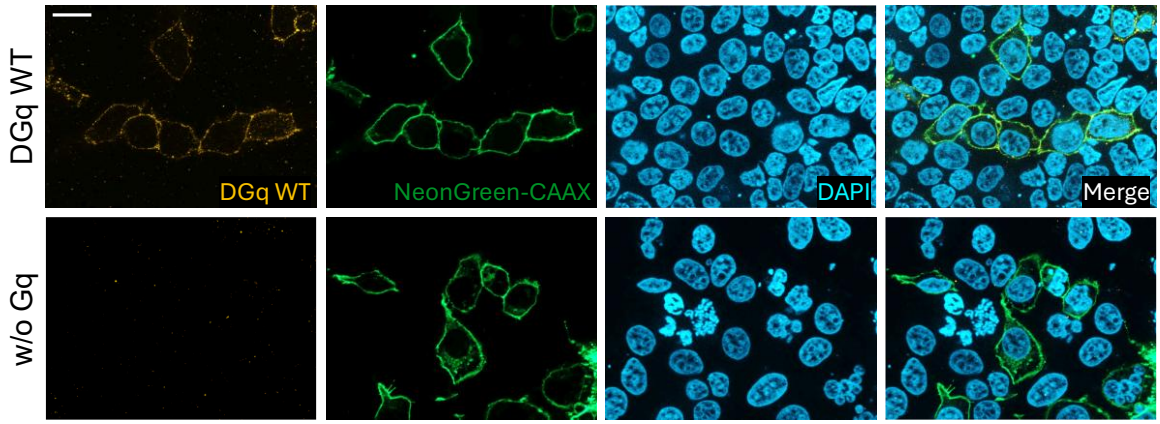

Figure 30: DGαq wild type is located at the plasma membrane and the antibody used is specific for DGαq staining.
HEK293 cells lacking Gαq, Gα11, Gα12, and Gα13 proteins after CRISPR/Cas9 treatment (HEK293 Gq/11/12/13-KO) were transiently transfected with constructs coding for the membrane-targeted green-fluorescent protein NeonGreen-CAAX, and with (upper row) or without (lower row) DGαq wild type. Cells were stained with a primary rabbit anti-Gq and secondary orange-fluorescent Cy3-tagged anti-rabbit antibody to visualize DGαq, as well as DAPI to visualize the nucleus (blue). Depicted are representative pictures of a single experiment performed by Aram Kamalizade (formerly Kostenis lab, University of Bonn). The scale bar in the top left corner represents 20 µm. The brightness of all pictures was increased by 70%.

To improve the quality of microscopy pictures, we titrated the transfected DNA amounts of DGαq wild type and NeonGreen-CAAX against each other. As intended, an increase in transfected plasmid coding for DGαq wild type enhanced both fluorescence intensity and transfection efficiency (Figure 31A). However, the localization of DGαq wild type concurrently shifted from confinement to the plasma membrane towards additional distribution throughout the cytosol possibly due to

increased expression levels and resultant overloading of the cell membranes. Similarly, decreasing the transfected amounts DNA coding for NeonGreen-CAAX reduced the number of stained cells and the fluorescence intensity of the membrane but simultaneously reduced unwanted, nonspecific staining of membranes inside the cell. We chose a DGαq wild type/NeonGreen-CAAX DNA ratio of 3:1 for subsequent assays, as these conditions allow for the optimal investigation of DGαq mutant localization. Both DGαq wild type and NeonGreen-CAAX also localized to the membrane when expressed solitarily without co-transfection of the other construct demonstrating that the membrane marker does not interfere with the localization of the protein and vice versa (Figure 31B).

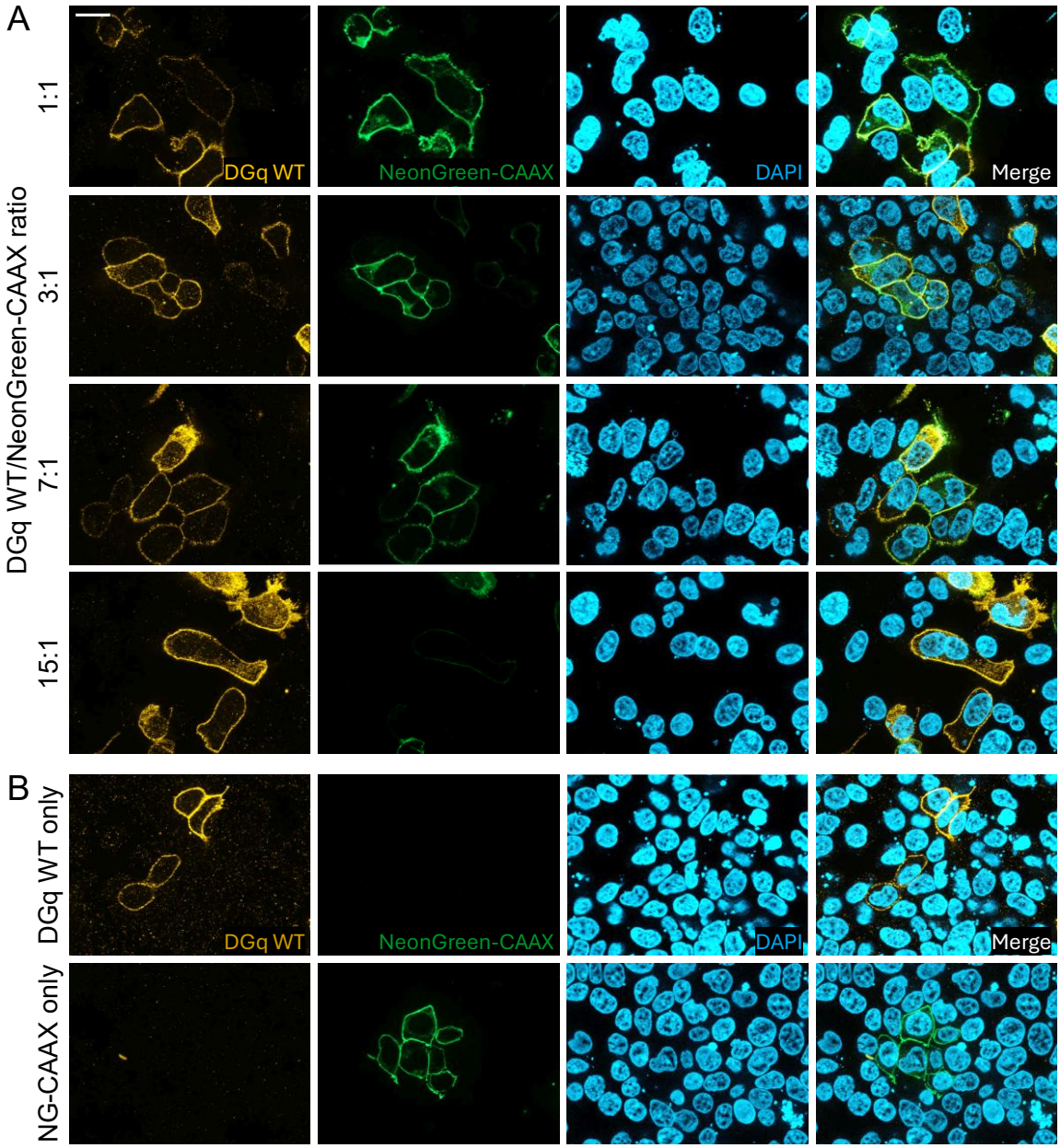

Figure 31: Transfecting three times as much plasmid coding for DGαq wild type than NeonGreen-CAAX results in optimal conditions for the evaluation of subcellular localization of DGαq wild type and mutants. Transfection of the constructs is mutually compatible.
A. *HEK293 cells lacking Gαq, Gα11, Gα12, and Gα13 proteins after CRISPR/Cas9 treatment (HEK293 Gq/11/12/13-KO) were transiently transfected with different ratios of constructs coding for DGαq wild type and the membrane-targeted green-fluorescent protein NeonGreen-CAAX. Cells were stained with a primary rabbit anti-Gq and secondary orange-fluorescent Cy3-tagged anti-rabbit antibody to visualize DGq, as well as DAPI to visualize the nucleus (blue). Depicted are representative pictures of a single experiment performed by Aram Kamalizade (formerly Kostenis lab, University of Bonn).* ***B.*** *HEK293 Gq/11/12/13-KO cells were transiently transfected with constructs coding for either DGαq wild type or the membrane-targeted green-fluorescent protein NeonGreen-CAAX (NG-CAAX) in amounts corresponding to the 3:1 ratio and stained as in A. Depicted are representative pictures of at least two experiments performed by Aram Kamalizade (formerly Kostenis lab, University of Bonn). The scale bar in the top left corner represents 20 µm. The brightness of all pictures was increased by 70%.*

The visually obvious membrane localization of DGαq wild type was confirmed with a more objective line scan. The peaks of membrane marker fluorescence intensity and DGαq secondary antibody fluorescence intensity in the line scan clearly

coincided suggesting a colocalization of DGαq wild type and the membrane marker (Figure 32). Similarly, DGαq IW localization overlaps with the membrane marker indicating that the mutant mimics the subcellular distribution of the wild type α (Figure 32).

The second single mutant YK did not localize to the membrane but was instead distributed throughout the entire cell apart from the nucleus (Figure 32). Moreover, this cytosolic distribution was not additional to the presence at the cell membrane as was the case for cells overloaded with DGαq wild type in earlier experiments (compare Figure 31). Instead, the orange fluorescence visualizing DGαq YK was low at the membrane compared to the cytosol. This suggests that the protein is not properly shuttled to the membrane but is targeted to the wrong compartment instead. Additionally, the overall intensity of fluorescence in the DGαq YK condition seemed to be increased over wild type and IW, indicating that the protein is not only expressed less (see Figure 25) but expression is also limited to a smaller subset of cells.

All of these observations fit with the phenotype expected based on the experience with murine Gαq FK. The localization of the G protein is crucial for its activation. Therefore, cytosolic distribution might be an additional factor next to reduced expression which explains the reduced quenching and activation amplitudes in the previously performed Gβγ/masGRK3ct BRET experiments. The altered localization might also explain the reduced steepness of DGq YK's carbachol concentration-response curves and the apparent biphasicity. Activation of the cytosolic subset of DGq YK proteins might require a higher number of activated M3 receptors than G protein located closer to the membrane resulting in the drastically reduced steepness of the curve or even a second distinct jump.

Finally, a roughly equal number of cells expressed DGαq FIVE in a membrane-restricted pattern or a broader distribution throughout the cytosol. The cells in which DGαq FIVE was present cytosolically resemble the phenotype of overloaded DGαq WT-expressing cells more closely than the YK phenotype.

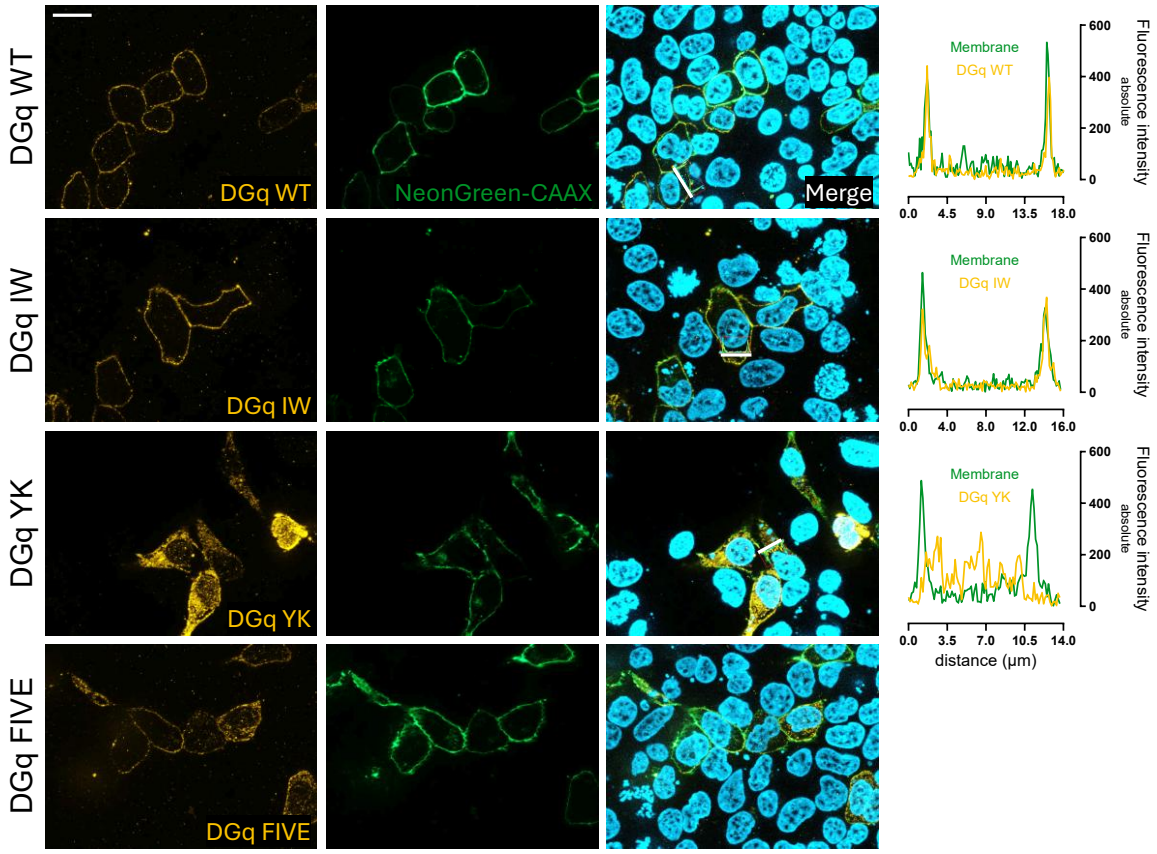

Figure 32: DGαq YK and FIVE differ from wild type in their subcellular distribution, while DGαq IW is located at the plasma membrane mimicking wild-type behavior.
HEK293 cells lacking Gαq, Gα11, Gα12, and Gα13 proteins after CRISPR/Cas9 treatment (HEK293 Gq/11/12/13-KO) were transiently transfected with constructs coding for DGαq wild type or mutants and the membrane-targeted green-fluorescent protein NeonGreen-CAAX. Cells were stained with a primary rabbit anti-Gαq and secondary orange-fluorescent Cy3-tagged anti-rabbit antibody to visualize DGαq variants, as well as DAPI to visualize the nucleus (blue). For the line scan, absolute green and orange fluorescence intensities representing membrane and DGαq wild type and mutants, respectively, were measured along the white lines indicated in the merge panel and plotted against the distance from the starting point. For DGαq FIVE, no representative line scan could be selected due to the variance in distribution between cells. Depicted are representative pictures and line scans of three (mutants) or six (wild type) experiments performed by Aram Kamalizade (formerly Kostenis lab, University of Bonn). The scale bar in the top left corner represents 20 µm. The brightness of all pictures was increased by 70%.

Based on all collected obvious differences of *Drosophila* Gαq YK in comparison to wild type, this mutant is excluded from further analysis. The slightly deviating behavior of DGαq FIVE does not have an obvious influence on the signaling behavior tested so far and will be analyzed further. However, up to this point, the mutation of isoleucine-184$^{G.S2.2}$ to tryptophan is the most promising mutant due to the wild type-like behavior in all assays run so far.

5.2.2.5. Deactivation

Apart from expression, localization, and activation, the deactivation of a G protein is crucial for proper functioning in cells and in the entire organism. For instance, Gαq proteins with strong deficiency in their GTPase activity are oncogenic (Onken et al., 2008; van Raamsdonk et al., 2009), as are Gα11 and Gα14 (Chua et al., 2017; Lim et al., 2016), as well as other Gα family proteins (Landis et al., 1989; Vallar et al.,

1987; Xu et al., 1993). Therefore, to test deactivation of the DGq mutant proteins in comparison to wild type, we performed kinetic measurements in the Gβγ/masGRK3ct BRET assay. After addition of the M3R agonist carbachol and the development of a stable plateau (see Figure 27), we added an excess of the M3R antagonist atropine to remove active receptor from the signaling equation. With this experimental setup, the subsequent reduction in BRET signal is solely dependent on the hydrolysis of GTP and the reassembly of the G protein in question (Masuho et al., 2020).

Our data revealed a fast return of DGq wild type into the inactive heterotrimeric state, a slightly slower decrease for the DGq IW protein, and an even slower decrease for the FIVE mutant (Figure 33A, left). The shape of the kinetic curve, which corresponds well to the shape of recovery kinetics measured previously in this assay (DiGiacomo et al., 2020; Lambert et al., 2010), did visually not correspond to a one-phase decay (Figure 33A, middle) but was noticeably slower at the beginning and faster after returning to approximately 33% of the signal. Instead, a Weibull fit nicely recapitulated the curve shape (Figure 33A, right) (for equations of both fits see Chapter 4.14. Data analysis in the methods section). However, there is no biological reasoning to use this more complex model. Therefore, we analyzed the original kinetic traces, rather than the fitted data. To quantitatively assess the apparent differences in deactivation kinetics, we calculated the time required for the signal to return to 50% ($t_{1/2}$) and 25% ($t_{1/4}$) of its peak value. The analysis confirmed the optically obvious reduction in deactivation kinetics of DGq IW and FIVE compared to the wild type (Figure 33B).

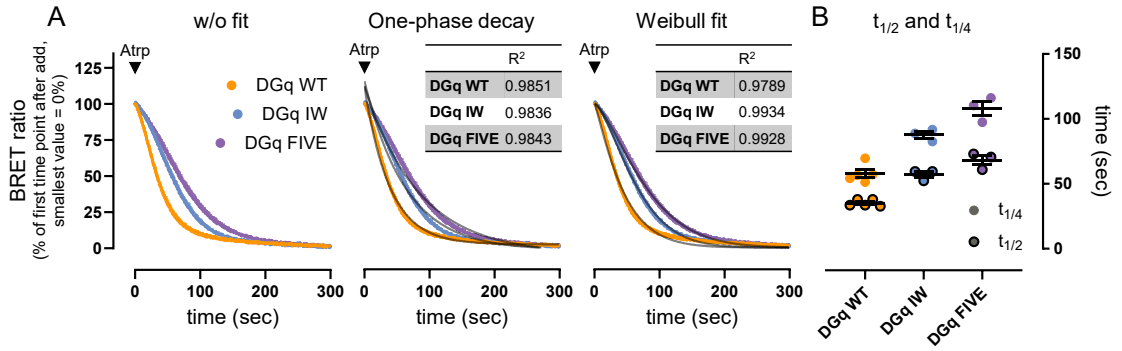

Figure 33: DGq IW and FIVE show decelerated kinetics of deactivation.
A. *Normalized kinetic BRET traces of HEK293T cells transiently transfected with constructs coding for M3R, split Venus-tagged Gβγ, masGRK3ct-NLuc, DGαq wild type or mutants, and Ric-8A. After activation with 100 µM carbachol (CCh), 100 µM atropine are added at t = 0. Data are shown without fit (left), with a one-phase decay fit (middle), and with a Weibull fit (right). Equations of the fits are in the methods section. Inset tables show coefficients of determination (R^2) for all fits. Data were normalized to the first timepoint, with the smallest value = 0%. Data are the means + SEM of three to five biologically independent experiments.* ***B.*** *Time required for a decay to 50% ($t_{1/2}$, outlined circles) or 25% ($t_{1/4}$, plain circles) of the initial value for each condition shown in A.*

The deactivation kinetics, i.e. the speed of nucleotide hydrolysis, are dependent on the intrinsic activity of the G protein GTPase but also on the activity of GTPase-

accelerating proteins (GAPs) in the cell. These can be effectors with GAP activity such as PLCβ (Berstein et al., 1992; Biddlecome et al., 1996), or regulators of G protein signaling (RGS) proteins (reviewed in E. M. Ross & Wilkie, 2000; Vries et al., 2000). Therefore, the reasons for the observed, slightly slower deactivation can be manyfold.

To narrow down the possible causes and define the next experiment as sensibly as possible, we examined the mutated residues regarding their involvement in GTPase activity and GAP binding. The catalytic residues in the Gα subunit responsible for intrinsic GTPase activity are arginine$^{G.hfs2.2}$ in linker 2/Switch I and glutamine$^{G.s3h2.3}$ in Switch II, stabilizing the leaving γ-phosphate and the attacking water molecule, respectively (Sprang, 2016). These residues (R177 and Q203 in DGq) have not been altered in the engineered proteins in question. Serin$^{G.H1.2}$ (S47 in DGq) stabilizes the Mg^{2+} ion necessary for GTP hydrolysis (D. E. Coleman et al., 1994; Sondek et al., 1994) and also remains intact in all mutants. Another unaltered residue, threonine$^{G.hfs2.5}$ (T180 in DGq), is involved in positioning the water nucleophile for GTP hydrolysis via its main chain only (Sprang, 2016). Even though all residues implicated in nucleotide hydrolysis are unaltered in the mutants, it is conceivable that mutations in the vicinity, e.g. V176S and V178M in DGq FIVE, exert an influence on the conformation required for GTP hydrolysis.

The binding interfaces of PLCβ and RGS proteins, all of which possess GAP activity on Gαq, somewhat overlap (Waldo et al., 2010). The PLCβ binding site consists mainly of Switch II and the α3-helix, while contacts with Switch I are mediated via threonine-187$^{G.hfs2.7}$ and amino acid backbone atoms (Waldo et al., 2010). Two of the residues altered in the DGαq mutants are implicated in PLCβ binding, namely isoleucine-184$^{G.S2.2}$ and proline-187$^{G.S2.5}$ which are suggested to form nonpolar contacts with PLCβ (Navot & Kosloff, 2019).

Based on the available structures of Gαq (Nance et al., 2013; Taylor et al., 2016) and Gαi (Soundararajan et al., 2008; Tesmer et al., 1997) in complex with RGS proteins, a few regions of Gαq are implicated in RGS binding. These include all three Switch regions. We did not mutate any residues in Switch III which has been proposed to be a key determinant for RGS selectivity (Taylor et al., 2016). Of the residues mutated in the first three engineered DGαq isoforms, valine-178$^{G.hfs2.3}$ and isoleucine-184$^{G.S2.2}$ participate in RGS protein binding via nonpolar contacts (Navot & Kosloff, 2019). However, as these residues contact RGS2/8 with their main chain only, an influence of the mutations on RGS binding is possible but cannot be predicted with certainty. Interestingly, basal quenching and signaling amplitudes of the mutants are unchanged possibly due to the high ratio of exogenous G protein and endogenous RGS protein levels.

Based on this combined evidence, we deem a diminished sensitivity of DGαq IW and FIVE towards proteins with GAP activity, specifically RGS proteins, possible. This would cause a reduction in overall GTPase activity, as the Gα subunit would be assisted by these accessory proteins to a lesser extent. Diminished RGS sensitivity is, therefore, a likely explanation for the mutants' reduced speed of deactivation.

5.2.2.6. RGS Sensitivity

In the previously performed experiments, the inactivation kinetics can have only been influenced by human RGS proteins endogenously expressed in HEK293T cells. As multiple RGS proteins are expressed in HEK293 cells (Atwood et al., 2011), expression of a similar set can be expected for the closely related HEK293T cells. However, an influence is only possible provided the sensitivity of DGq wild type to the GAP activity of human RGS and PLCβ proteins. *Drosophila* Gαq is perfectly able to interact with various human proteins, such as the M3R, Gβγ, and at least some effectors as demonstrated in previous DMR and BRET assays. However, considering the fact that DGq wild type shows decelerated deactivation kinetics in the Gβγ/masGRK3ct BRET assay in HEK293T cells as compared to murine Gq (Figure 34), it is reasonable to posit that the wild-type DGq protein may exhibit limited or ineffective interaction with human RGS proteins. The response of DGq wild type to human RGS proteins can easily be qualitatively investigated in the Gβγ/masGRK3ct BRET assay setup. The deactivation kinetics of the Gαq protein in question should be accelerated in the presence of RGS protein.

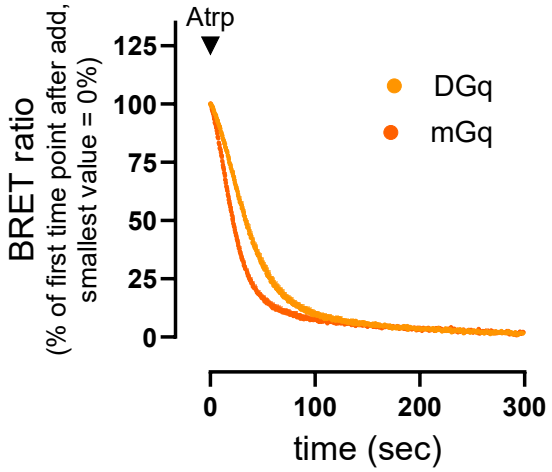

Figure 34: DGq WT shows decelerated kinetics of deactivation compared to mGq.
Normalized kinetic BRET traces of HEK293T cells transiently transfected with constructs coding for M3R, split Venus-tagged Gβγ, masGRK3ct-NLuc, DGαq or mGαq, and Ric-8A. After activation with 100 µM carbachol (CCh), 100 µM atropine are added at t = 0. Data were normalized to the first timepoint, with the smallest value = 0%. Data are the means + SEM of four to five biologically independent experiments. Data for DGαq WT were copied from Figure 33 for clarity.

To validate the experimental setup, we transiently transfected HEK293T cells with plasmid DNA coding for mGαq in the absence and presence of exogenous RGS proteins, specifically RGS8 and RGS19 (GAIP), and measured the deactivation kinetics. RGS8 and RGS19 were selected as representative RGS proteins based on their effect on Gαq proteins and the availability of DNA in the laboratory. When RGS8 was discovered, it was classified as Gαo- and Gαi3-specific RGS protein (O. Saitoh et al., 1997). Later, its GAP activity on Gαq was discovered to depend on the receptor subtype responsible for signal initiation with a weak impact on M3R signaling (Osamu Saitoh et al., 2002). RGS19 has first been described to act exclusively on Gαi family members (Berman et al., 1996; Vries et al., 1995). Later observations, however, detected an RGS19-mediated GAP activity on Gαq (Masuho et al., 2020). We will simultaneously use these experiments to investigate these seeming discrepancies in the literature.

The deactivation of mGq was influenced by both RGS proteins (Figure 35A), demonstrating sensitivity to their GTPase-accelerating effect regardless of its activation by M3R. Furthermore, RGS8 modestly increased the maximal amplitude. In contrast, the amplitude was maintained in the presence of exogenous RGS19. This differential effect on the signal amplitude in combination with the seemingly similar effect on the deactivation kinetics suggests that both RGS proteins increase the GTPase activity maximally and, therefore, show the same effect on the deactivation kinetics. Alternatively, the differential effect could indicate that the parameters are uncoupled and affected differentially by RGS proteins as previously described (Lambert et al., 2010). Moreover, the plateau that was stable in the absence of exogenous RGS proteins was markedly destabilized in the presence of exogenous RGS8 and RGS19. The accelerated deactivation rate induced by these RGS proteins precluded the maintenance of a stable plateau.

To investigate whether DGq wild type is similarly affected by coexpression of RGS proteins, we performed an analogous experiment. The foreign *Drosophila* protein exhibited comparable sensitivity to the modulatory effect of the chosen RGS proteins on deactivation kinetics (Figure 35B). The response to RGS8 is virtually identical to that of mGq, including the slightly elevated maximal signal amplitude and the instability of the plateau. Interestingly, addition of exogenous RGS19 reduced the maximal BRET ratio after activation suggesting some differential effect on DGq and mGq. However, these data clearly indicate that DGq wild type is sensitive to human RGS proteins and that the behavior of the mutants in HEK293T cells may be attributable to modifications in their sensitivity to RGS-mediated regulation.

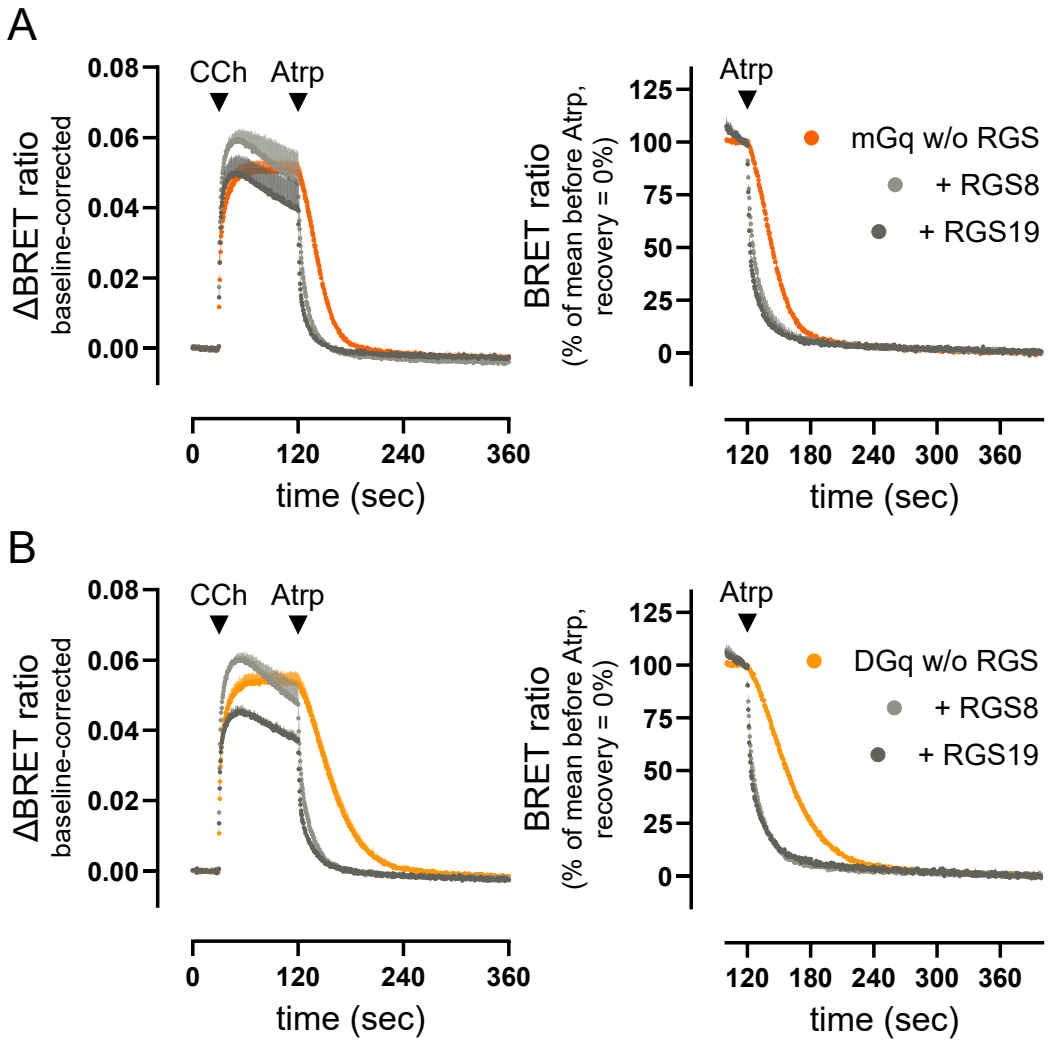

Figure 35: mGq and DGq WT are sensitive to RGS8 and RGS19's GAP activity.
Left. *Kinetic baseline-corrected BRET traces of HEK293T cells transiently transfected with constructs coding for M3R, split Venus-tagged Gβγ, masGRK3ct-NLuc, mGαq (A) or DGαq wild type (B), Ric-8A, and either RGS8, RGS19 or without RGS protein. Cells were activated with 100 µM carbachol (CCh) after 30 seconds of baseline measurement. Deactivation with 100 µM atropine (Atrp) followed after 90 additional seconds. Data are the means + SEM of three biologically independent experiments.* ***Right.*** *Normalized kinetic BRET traces of the left panels from 100 to 400 sec. Data were normalized to the mean of the last 10 timepoints before Atrp addition, with the mean of the last 10 timepoints (recovery) = 0%. Data are the means + SEM of three biologically independent experiments.*

An analogous experiment conducted with DGq IW demonstrated that the mutant retains sensitivity to both RGS proteins (Figure 36B). Although the presence of RGS19 exerted a less pronounced effect on plateau stability in the DGq IW mutant compared to wild type (Figure 36A), the acceleration of deactivation was clearly visible. The impact of RGS8 on the signaling of the FIVE mutant was virtually identical to that on the wild type (Figure 36C). However, DGq FIVE did not respond to RGS19 at all, suggesting insensitivity to this regulator.

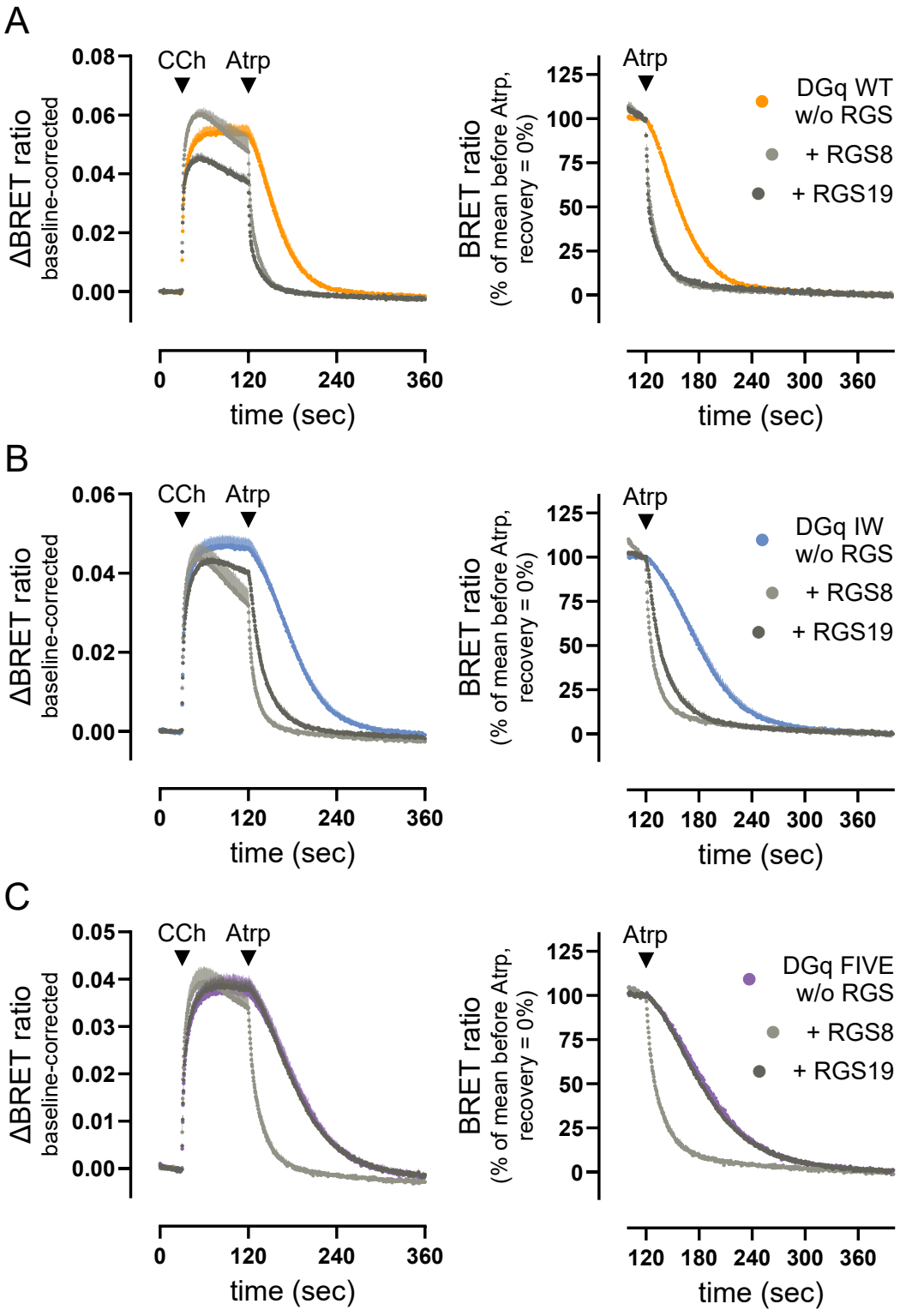

Figure 36: DGq IW is sensitive to RGS8 and RGS19's GAP activity, while DGq FIVE is insensitive to RGS19.
Left. *Kinetic baseline-corrected BRET traces of HEK293T cells transiently transfected with constructs coding for M3R, split Venus-tagged Gβγ, masGRK3ct-NLuc, DGαq wild type (A), IW (B) or FIVE (C), Ric-8A, and either RGS8, RGS19 or without RGS protein. Cells were activated with 100 µM carbachol (CCh) after 30 seconds of baseline measurement. Deactivation with 100 µM atropine (Atrp) followed after 90 additional seconds. Data are the means + SEM of three biologically independent experiments.* ***Right.*** *Normalized kinetic BRET traces of the left panels from 100 to 400 sec. Data were normalized to the mean of the last 10 timepoints before Atrp addition,*

with the mean of the last 10 timepoints (recovery) = 0%. Data are the means + SEM of three biologically independent experiments. Data for DGq WT were copied from Figure 35 for clarity.

To investigate RGS protein expression across the different conditions and to possibly exclude an effect of differential protein levels, we performed SDS-PAGE and western blots with cell lysates obtained from RGS sensitivity BRET experiments. We succeeded in detecting both RGS proteins using an RGS8-specific primary antibody and an RGS19-specific serum, albeit with slightly lower electrophoretic mobility than expected for the calculated molecular weights of 24.3 kDA for 3xHA-RGS8 and 24.7 kDa for RGS19 (Stothard, 2000) (Figure 37). Most strikingly, the expression level of RGS8 was reduced in the DGq FIVE condition (Figure 37). Despite this reduction, the comparable effect of RGS8 on the deactivation kinetics of both the FIVE mutant and the wild-type protein suggests that its modulatory influence is already saturated at these expression levels. In contrast, the expression of RGS19 remained unaltered, thus excluding differential expression as an explanation for its lack of effect on the DGq FIVE mutant.

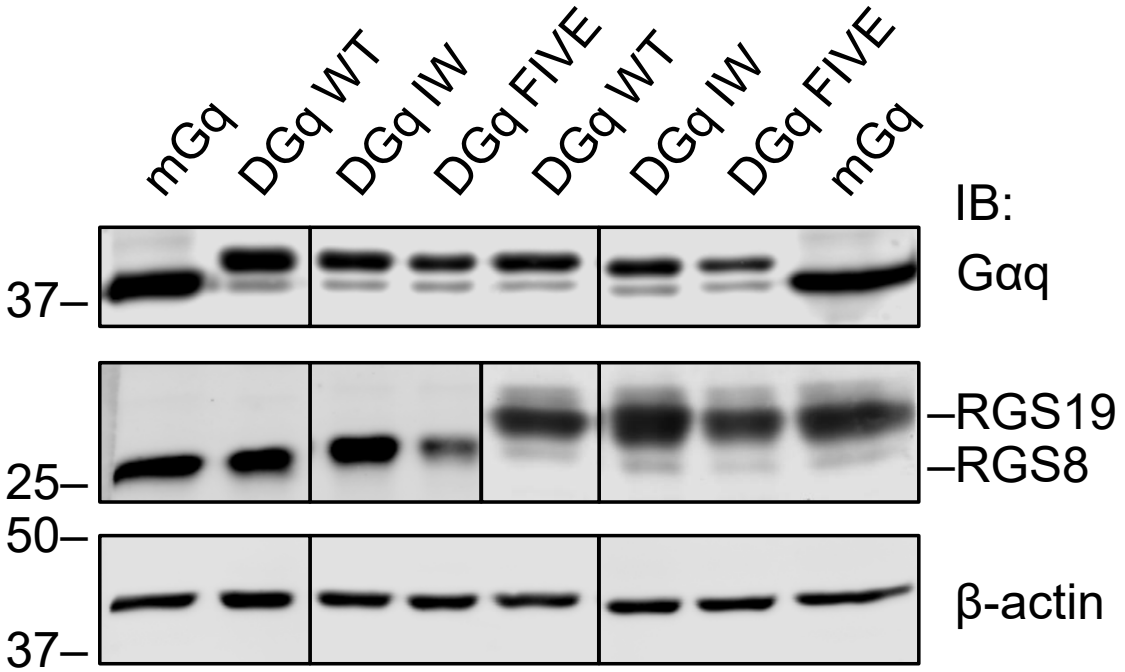

Figure 37: The RGS8 and RGS19 proteins are coexpressed with the different Gαq variants in equal amounts except for the DGq FIVE condition in which RGS8 expression is slightly lower.
Western blot of SDS-PAGE performed with lysates of HEK293T cells used for Gβγ/masGRK3ct BRET experiments shown in Figure 35 and Figure 36. β-actin was used as protein loading control. Depicted are results of an individual western blot with cells used for a representative BRET assay. The image originated from one blot but is assembled to remove irrelevant samples. The image parts for RGS19 and RGS8 originate from the same stained membrane strip with different exposure times. IB: immunoblotted.

As demonstrated in these experiments, RGS19 exerts GAP activity on murine and *Drosophila* Gαq proteins, but has no significant effect on Gα15 (Masuho et al., 2020) which is sequence-identical to Gα16. The transfer of five residues in the extended FR binding site – which extensively overlaps with the canonical RGS binding site –

from murine Gα16 to *Drosophila* Gαq may have partially conferred RGS insensitivity to the DGαq FIVE variant. Interestingly, while RGS8 also displays reduced activity on Gα15 compared to Gαq (Masuho et al., 2020), this is not reflected as diminished RGS8 function on DGαq FIVE in Gβγ/masGRK3ct BRET deactivation assays. This may be due to the inherently greater effect of RGS8 or indicate differential contribution of the mutated residues to RGS8 and RGS19 binding.

To conclude, the apparent partial RGS resistance of DGαq FIVE is consistent with the slower deactivation kinetics of this protein. The resistance may also account for the slight shift in the carbachol potency of FIVE compared to the wild-type protein, a phenomenon previously reported for other RGS-insensitive Gα protein mutants (Lambert et al., 2010). However, the minimal differences in RGS sensitivity between IW and wild type do not explain the comparable shift in potency observed for DGαq IW.

Importantly, these considerations pertain solely to DGq wild type and mutant signaling in human systems such as the HEK293 cells used in the previous experiments. For the intended application of the engineered mutants in the host *Drosophila melanogaster*, their sensitivity to *Drosophila* RGS proteins will be relevant.

Furthermore, the impact of RGS protein sensitivity on downstream signaling such as second messenger production or whole-cell responses cannot be estimated and requires further investigation. Even though findings in HEK293T cells may not be directly transferrable to Gq signaling in *Drosophila melanogaster*, they do serve as a preliminary approximation. The planned *in vivo* experiments, as well as more extensive subsequent investigations into the behavior of DGαq mutants *in vivo* will shed light on the physiological relevance of these findings.

However, as the effects cannot be conclusively determined, the DGαq FIVE mutant, which displayed insensitivity towards one of the RGS proteins tested, will be excluded from further experiments. Instead, investigations are continued with the most promising variant engineered so far, DGαq IW.

5.2.3. Second messenger level

All information collected about DGαq IW so far suggests wild type-like behavior of the mutant. However, these data only stem from a protein-protein interaction assay on the level of G protein activation. This does not provide any reliable information about functional consequences in the cell. We, therefore, decided to confirm the results obtained so far using a readout that measures Gq-mediated second messenger production as the first functional consequence of heterotrimer activation.

The main Gq signaling pathway is induction of IP_3 production via PLCβ. The production of IP_3 is transient due to the enzymatic degradation to inositol. We

decided on an experimental procedure that also allows for the investigation of intrinsic activity. For this, we measured IP_1 accumulation over a defined amount of time as a proxy for IP_3 production following Gq activation making use of lithium chloride (LiCl) to inhibit further enzymatic degradation by inositol monophosphatase (Figure 38A). While this is an endpoint approach and does not yield kinetic information about second messenger production, accumulation of IP_1 in the cell can be measured under unstimulated conditions to estimate the intrinsic activity of Gq proteins. Furthermore, measurement of IP_1 accumulation in the presence of a ligand allows an estimation of receptor-stimulated Gq signaling. To reduce background IP_1 production and to limit the assessment to transiently transfected *Drosophila* Gαq isoforms only, independent of any endogenous Gq/11 family proteins, we performed the experiments in HEK293 cells devoid of Gαq and Gα11 proteins after CRISPR/Cas9 treatment (HEK293 Gq/11-KO) (Schrage et al., 2015). To measure IP_1 concentrations in the cell, we used the commercially available HTRF IP-One Gq Detection Kit employing homogeneous time-resolved fluorescence (HTRF) technology which is explained in detail in the methods section (see Chapter 4.8. Inositol monophosphate (IP_1) accumulation assays).

Even though mock-transfected HEK293 Gq/11-KO cells do not express Gαq or Gα11 proteins, incubation in LiCl-containing buffer still yielded basal IP_1 levels of about 170 nM under the selected assay conditions (Figure 38B) stemming from other IP_3-producing pathways. Transient transfection of DGq wild type elevated basal IP_1 levels. These results demonstrate the ability of DGαq to productively interact with human PLCβ enzymes leading to IP_3 and subsequent IP_1 production, as well as slight intrinsic activity of DGq wild type compounding over time. The intrinsic activity of DGq IW does not differ from wild type, since similar levels of IP_1 were produced (Figure 38B).

To investigate the GEF-mediated activation of DGq wild type and IW via the endogenous M3 receptor, cells were incubated with different concentrations of carbachol for a defined period of time generating concentration-response curves. For this, the data were buffer-corrected, as the buffer values differed between individual replicates of the assay. Data were then normalized to the effect of the highest concentration of carbachol (1 mM) on wild-type *Drosophila* Gq for each individual experiment to compensate for different amplitudes in response between replicates.

IP_1 accumulation in mock-transfected cells was stable and carbachol-independent (Figure 38C), demonstrating the lack of any Gα protein coupling carbachol-activated receptors to IP_3 and consequently IP_1 production. Cells expressing DGαq wild type responded to carbachol in a concentration-dependent manner. The potency of carbachol (pEC_{50} of about 5) differs from that measured in the Gβγ/masGRK3ct BRET assays (pEC_{50} of about 7). This is not surprising as signals in different assays

are differentially amplified and characterized by shifts in potency values. DGq IW is similarly activated by carbachol-bound M3R in a concentration-dependent manner. The concentration-response curve mimics the wild-type behavior in potency and efficacy (Figure 38C).

Interestingly, the potency shift compared to wild type recorded on the G protein activation level was not reproduced in the second messenger assays. This might just not be resolvable due to the high variations between replicates of the assay. Moreover, IP_1 accumulation assays were performed in cells transfected with plasmid DNA coding for Gαq isoforms only, lacking co-transfection of Ric-8A DNA. This or the level of amplification could possibly explain the variation between individual experiments and also the absence of a detectable potency shift for DGq IW. Though the IP_1 accumulation experiments confirmed wild type-like behavior both intrinsically and upon stimulation, the question whether RGS sensitivity and potency shifts in concentration-response curves in the Gβγ/masGRK3ct BRET translate to the signaling level requires additional experimentation.

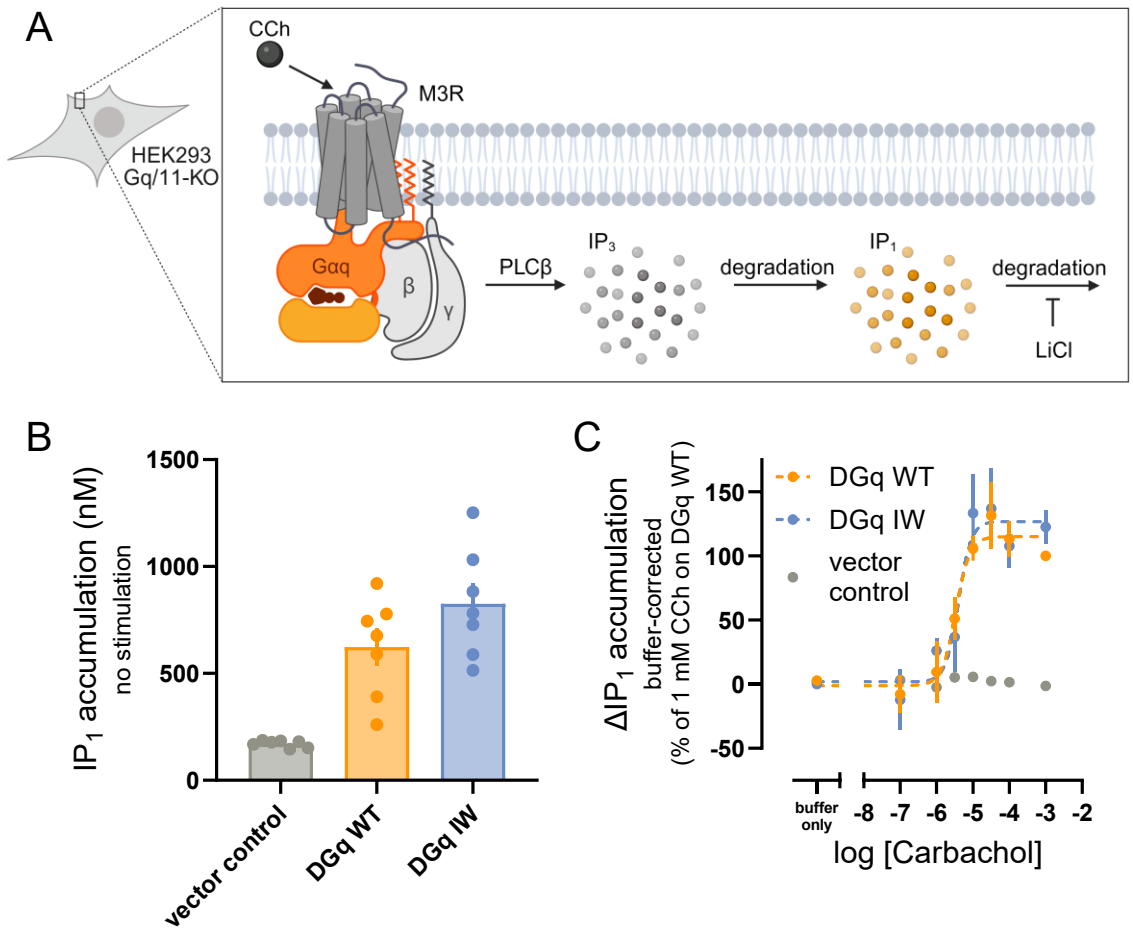

Figure 38: DGq IW behaves wild type-like regarding second messenger production as determined in IP_1 accumulation assays.
A. *IP_1 accumulation assay principle. After activation by CCh-bound M3R, Gαq activates PLCβ resulting in the production of IP_3 which is transient due to its degradation to IP_1. Inhibition of further degradation using LiCl causes the measurable accumulation of IP_1. The figure was created with BioRender.com.* ***B.*** *Intrinsic IP_1*

accumulation in HEK293 cells lacking Gαq and Gα11 proteins after CRISPR/Cas9 treatment (HEK293 Gq/11-KO) transiently transfected with constructs coding for DGαq wild type, IW or empty vector. Bar graphs represent the means ± SEM of seven biologically independent experiments performed by Uli Rick (Kostenis lab, University of Bonn). Data points represent the means of individual experiments. ***C.*** *CCh concentration-response curves measured as buffer-corrected IP_1 accumulation after stimulation with CCh or buffer in cells transfected as in B normalized to the effect of 1 mM CCh on DGq wild type. Data are the means ± SEM of three to seven biologically independent experiments performed by Uli Rick (Kostenis lab, University of Bonn). CCh: carbachol, M3R: M3 muscarinic acetylcholine receptor, PLCβ: phospholipase Cβ, IP_3: inositol 1,4,5-trisphosphate, IP_1: inositol monophosphate.*

5.2.4. Whole-cell response

IP_3 production in response to activated Gq elicits diverse cellular responses including changes in cell morphology mediated by cytoskeletal reorganization. Monitoring these morphological changes with a label-free optical biosensor, based on the detection of dynamic mass redistribution (DMR), offers several advantages: The measurement can be performed in a time-resolved manner and, therefore, allows a second look at G protein activation and deactivation dynamics in an integrated functional assay. Moreover, for this assay, proteins do not have to be tagged, lysis is not necessary, and the investigation is performed in real time in living cells. For these reasons, we selected DMR measurements to serve as readout for the investigation of *Drosophila* Gq-induced downstream response on the whole-cell level.

Similar to the IP_1 accumulation assays, we used HEK293 Gq/11-KO cells to eliminate background signaling from endogenous Gαq proteins and made use of the endogenously expressed M3 receptor, functionality of which is readily detectable in this assay (Schrage et al., 2015; Schröder et al., 2010; Schröder et al., 2011). Mock-transfected cells did not react to carbachol (Figure 39), but exhibited a robust composite DMR response to epidermal growth factor (EGF), confirming cell viability. Furthermore, treatment with FR alone did not elicit a response. This demonstrates that there is no G protein present in the cell to couple carbachol-activated receptor to cell shape dynamics or that is sensitive to FR. The following experiments can be interpreted without confounding background signals.

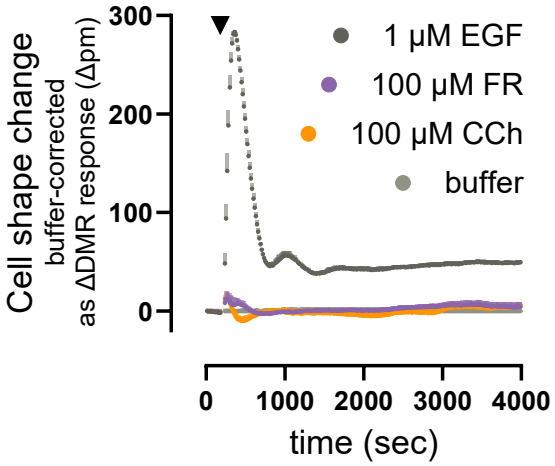

Figure 39: HEK293 Gq/11-KO cells are suited for the investigation of DGq mutant behavior in the DMR assay.
Kinetic buffer-corrected DMR traces of HEK293 cells lacking Gαq and Gα11 proteins after CRISPR/Cas9 treatment (HEK293 Gq/11-KO) transiently transfected with empty vector. Cells were activated with 1 µM of epidermal growth factor (EGF), 100 µM FR900359 (FR), 100 µM carbachol (CCh) or buffer after about 3 minutes of baseline measurement. Data are the means + SD of one experiment representative of at least three biologically independent experiments. Data presented in this figure have been adapted from Alenfelder (2019).

Drosophila Gq wild type reacted to carbachol in a concentration-dependent manner with a similar kinetic curve shape compared to known data using mouse Gq (Malfacini et al., 2019; Patt et al., 2021) and to earlier experiments during the Master's thesis (Alenfelder, 2019) (Figure 40A). Maximum signaling amplitudes fluctuate in the DMR assay from experiment to experiment due to the assay's sensitivity to subtle changes in cell density, growth phase or transfection efficiency, often necessitating the normalization of the data for the generation of an interpretable concentration-response curve. However, data quality in the experiments performed here was high, and a comparison was possible without the need for data normalization.

The resulting concentration-response curve displayed the usual sigmoidal shape (Figure 40B) and yielded a pEC_{50} value of 5.65 (Figure 40C). DGq IW showed very similar traces. Efficacy and potency of the carbachol-induced response were comparable to wild type. The downstream, integrated whole-cell response does not seem to portray the small change in activation potency observed in the previous BRET-based protein-protein interaction assays.

A normalization of the kinetic traces to the maximal wavelength shift in each condition also allows for the comparison of signal kinetics. DGq IW mimicked the wild type's curve shape indicating that signaling kinetics are comparable between wild type and mutant DGq on the whole-cell level. The deactivation kinetics in DMR measurements are influenced by various factors. The receptor has not been inactivated with inhibitor after activation as it was in BRET assays, and the agonist

was continuously present. Therefore, receptor deactivation, phosphorylation, and desensitization influence the return of the cell shape to baseline. Nonetheless, differences in deactivation kinetics of the G protein heterotrimer which have been observed in the previous Gβγ/masGRK3ct BRET assays did not translate to differences in the kinetics of cell shape change. The whole-cell signaling response of DGq IW appears wild type-like.

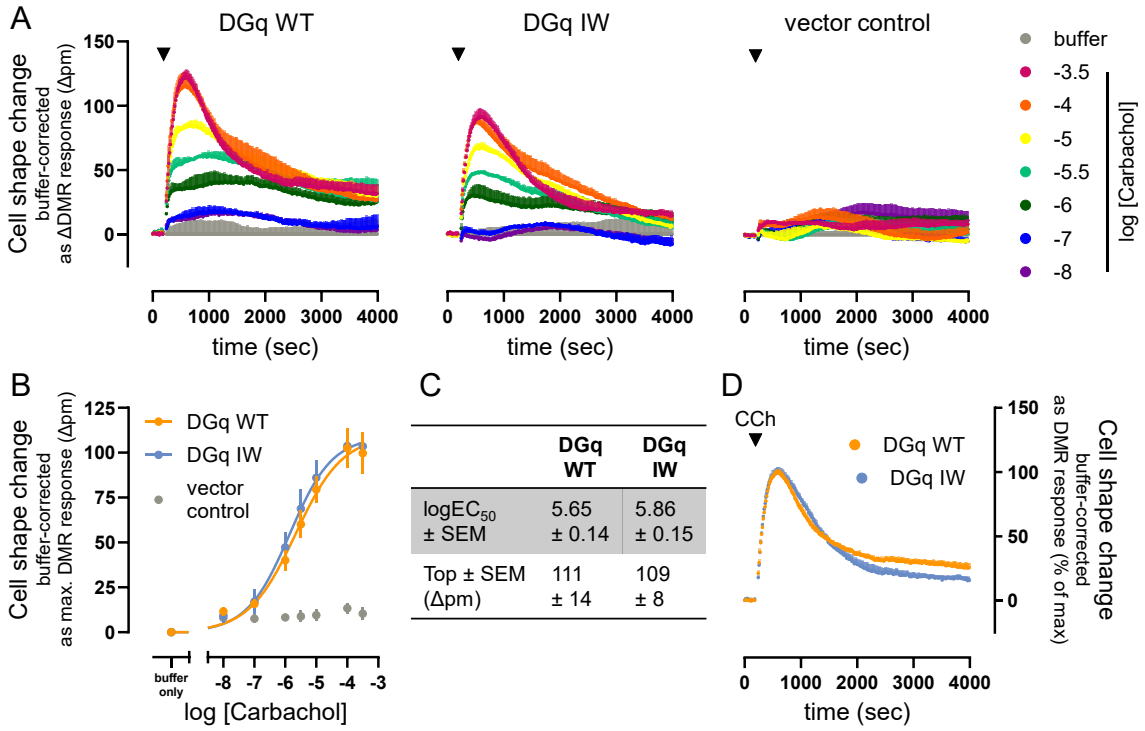

	DGq WT	DGq IW
$logEC_{50}$ ± SEM	5.65 ± 0.14	5.86 ± 0.15
Top ± SEM (Δpm)	111 ± 14	109 ± 8

Figure 40: DGq IW behaves wild type-like regarding integrated whole-cell response as measured in dynamic mass redistribution (DMR) assays.
A. *Kinetic buffer-corrected DMR traces of HEK293 cells lacking Gαq and Gα11 proteins after CRISPR/Cas9 treatment (HEK293 Gq/11-KO) transiently transfected with constructs coding for Ric-8A and DGαq wild type, mutant or empty vector as indicated. Cells were activated with different concentrations of carbachol (CCh) or buffer after about 3 minutes of baseline measurement. Data are the means + SD of one experiment representative of three to five biologically independent experiments performed by Sergi Bravo (Kostenis lab, University of Bonn).* ***B.*** *CCh concentration-response curves measured as maximal buffer-corrected DMR response after stimulation with CCh of buffer in cells transfected as in A. Data are the means ± SEM of three to five biologically independent experiments performed by Sergi Bravo (Kostenis lab, University of Bonn). The bottom of the nonlinear fit was constrained to 0.* ***C.*** *Table summarizing pEC_{50} values ± SEM and Tops ± SEM of the CCh concentration-response curves shown in B.* ***D.*** *Kinetic buffer-corrected DMR traces of cells transfected as in A normalized to the top of each individual trace. Cells were activated with 100 µM CCh after about 3 minutes of baseline measurement. Data are the means + SD of one experiment representative of three to five biologically independent experiments performed by Sergi Bravo (Kostenis lab, University of Bonn).*

The results obtained in the DMR assay are especially promising, as the assay records a highly amplified output that cannot be attributed to the specific underlying molecular processes. Therefore, the assay detects a plethora of G protein-initiated or -influenced processes signaling events, which in turn increases the significance of these results.

5.2.5. Conclusions

In conclusion, we generated three different DGαq mutants based on a rational design and transfer of the putative FR binding site of a closely related and naturally insensitive Gα protein. Two of these mutants, DGq YK and FIVE, have been excluded due to behavior that differed from that of the wild-type protein to varying degrees.

DGαq YK was excluded due to reduced expression, possibly due to folding and/or shuttling issues. Together, this massively influenced signaling properties of the protein, reducing basal quenching and signaling amplitudes in the Gβγ/masGRK3ct BRET assay.

Secondly, *Drosophila* Gαq FIVE showed less impairment compared to wild type, with only subtle changes in behavior. Its sensitivity to mammalian RGS proteins is reduced resulting in decelerated deactivation kinetics in the protein-protein interaction assay and shifting the concentration-response curve in this assay to slightly higher potencies. Furthermore, DGαq FIVE's localization is slightly changed to more cytosolic distributions, although this was less pronounced than for DGαq YK.

Importantly, even though these differences might be negligible, five mutations have been introduced in the FR binding site to generate this mutant. Using a mutant with more wild type-like properties which only harbors one mutation such as DGq IW seems advantageous at this point in the project. A thorough characterization of expression, localization, and activation and deactivation behavior in a set of assays ranging from protein-protein interaction far upstream directly succeeding GPCR activation, over second messenger assays, to downstream physiological signaling consequences revealed that the introduced IW mutation retained all major properties of the protein.

5.3. FR sensitivity

The overarching aim of this thesis is the development of FR-resistant DGαq isoforms for the application *in vivo*. After having established wild type-like behavior for DGαq IW, the mutant's sensitivity to the inhibitor FR needs to be investigated next. We chose to investigate FR sensitivity in all assays described above: on the G protein level in the Gβγ/masGRK3ct BRET assay, on the level of second messenger production in the IP_1 accumulation assay, and on the level of the integrated whole-cell responses in the DMR assay.

For all these assays transiently transfected HEK293T or Gq/11-KO cells were incubated with a dilution series of FR before M3R activation. This way, we recorded concentration-inhibition curves to estimate the FR potency on DGαq IW and to

compare it to DGαq wild type. We stimulated the receptor with a selected carbachol concentration in the plateau to ensure complete activation of the G protein.

In cellular Gβγ/masGRK3ct BRET assays, FR completely abolished activation of *Drosophila* Gq with low micromolar potency (Figure 41A and B, see also Figure 22). In contrast, the potency on IW was reduced approximately 75-fold (Figure 41B). While the highest concentration of FR used in this experiment only inhibited the signal partially to about 60%, it cannot be excluded that even higher concentrations might still inhibit DGq IW fully in this assay. Even though such high concentrations are rarely used in experiments, DGq IW displays slight residual sensitivity to FR.

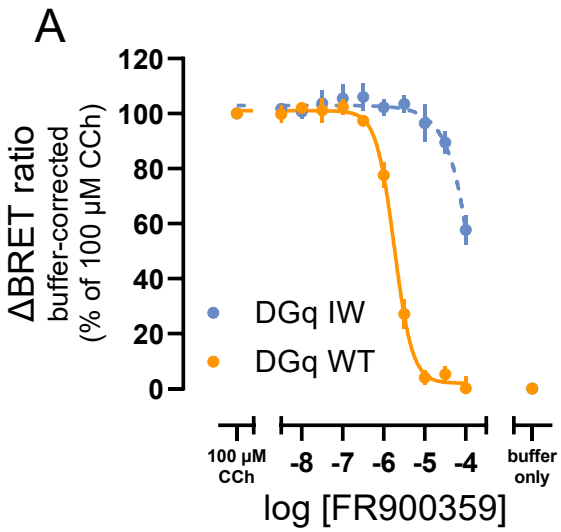

B

	pIC_{50} ± SEM	fold change
DGq WT	5.74 ± 0.06	
DGq IW	3.87 ± 0.05	~75

Figure 41: DGq IW is approximately 75-fold less sensitive to FR than DGq wild type in the Gβγ/masGRK3ct BRET assay.
A. *FR900359 (FR) concentration-response curves measured as buffer-corrected BRET ratio after preincubation with FR or buffer and stimulation with carbachol (CCh) or buffer in HEK293T cells transiently transfected with constructs coding for M3R, split Venus-tagged Gβγ, masGRK3ct-NLuc, DGαq wild type or IW, and Ric-8A normalized to the effect of 100 µM CCh. Data are the means ± SEM of four to five biologically independent experiments. Data for DGq WT were copied from Figure 22 for clarity.* ***B.*** *Table summarizing pIC_{50} values ± SEM and the potency fold change of DGq IW compared to wild type of the FR concentration-response curves shown in A.*

In accordance with the BRET data, *Drosophila* Gq wild type was completely inhibited by FR in IP_1 accumulation assays (Figure 42), while mock-transfected cells lacking any Gαq and Gα11 proteins expectedly responded to neither CCh nor FR treatment. For DGq WT, pretreatment with high concentrations of FR lowered the IP_1 accumulation to the level of mock-transfected cells, while there was negligible residual IP_1 accumulation when IW was expressed. DGq IW displayed full FR sensitivity in this assay, albeit with strongly reduced potency. Due to concerns regarding the substandard quality of the data, we did not calculate pIC_{50} values or determine a fold potency shift in this assay.

As this accumulation assay also allows for the investigation of intrinsic signaling, we investigated the effect of a high FR concentration (100 µM) on unstimulated cells.

The IP_1 accumulation of mock-transfected, unstimulated cells was not affected by the presence of the inhibitor. However, when cells expressing either wild-type DGαq or its IW mutant were pretreated with FR, the IP_1 concentration was reduced to a level corresponding to that of cells lacking Gαq and Gα11. This suggests that FR is able to fully suppress both GEF-induced and intrinsic signaling.

In conclusion, DGq IW showed reduced FR sensitivity in second messenger assays, similar to its behavior in the Gβγ/masGRK3ct BRET assay.

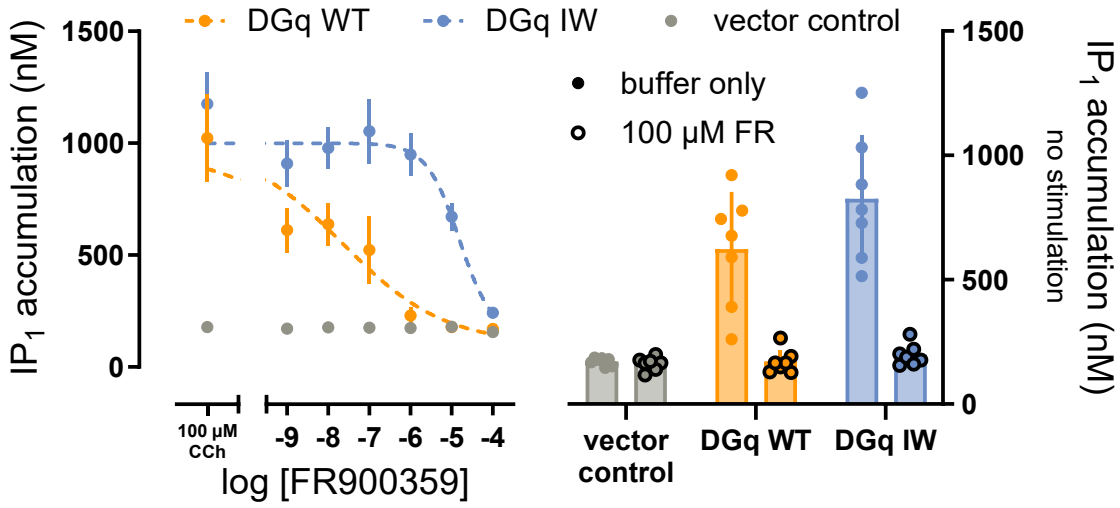

Figure 42: The FR sensitivity of DGq IW is reduced compared to DGq WT on the second messenger level.
Left. *FR900359 (FR) concentration-response curves measured as IP_1 accumulation after preincubation with FR or buffer and stimulation with 100 µM carbachol (CCh) in HEK293 cells lacking Gαq and Gα11 proteins after CRISPR/Cas9 treatment (HEK293 Gq/11-KO) transiently transfected with constructs coding for DGαq wild type, IW or empty vector. Data are the means ± SEM of three to seven biologically independent experiments performed by Uli Rick (Kostenis lab, University of Bonn).* ***Right.*** *Influence of 100 µM FR on intrinsic IP_1 accumulation in cells transfected as in the left panel. Bar graphs represent the means ± SEM of seven biologically independent experiments performed by Uli Rick (Kostenis lab, University of Bonn). Data points represent the means of individual experiments.*

On the whole-cell level, M3R-mediated activation of *Drosophila* Gq was completely abolished by FR in a concentration-dependent manner with high nanomolar potency (Figure 43, see also Figure 10), while pretreatment did not change the response to DMSO-controlled buffer.

DGq IW activation was only slightly affected by the inhibitor. Only the highest inhibitor concentration used affected the signal partially, reducing it to about 45%. This constitutes an approximate 320-fold shift in inhibitor potency for DGq IW compared to wild type. Interesting, the introduction of a single residue mutation has a tremendous impact on FR sensitivity in the *Drosophila* Gαq background. The analogous mutation in murine Gαq shifts signaling responses by only 16-fold in the DMR assay (Patt et al., 2021).

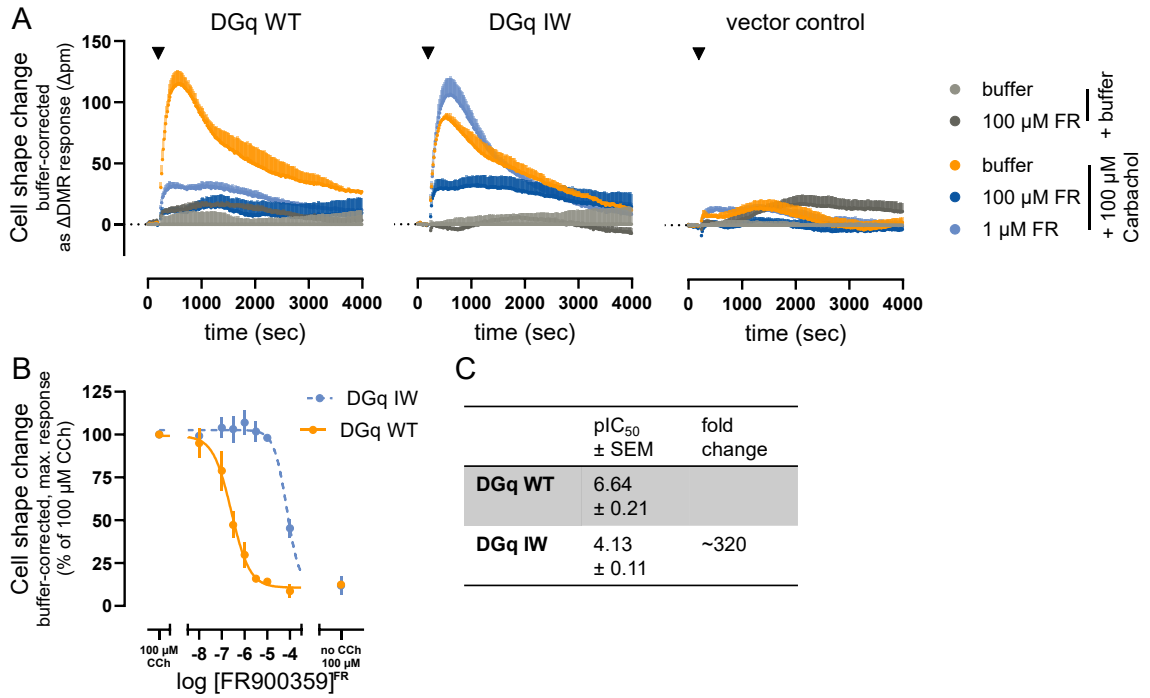

Figure 43: DGq IW is more than 300-fold less sensitive to FR than wild type in dynamic mass redistribution (DMR) assays.
A. *Kinetic buffer-corrected DMR traces of HEK293 cells lacking Gαq and Gα11 proteins after CRISPR/Cas9 treatment (HEK293 Gq/11-KO) transiently transfected with constructs coding for Ric-8A and DGαq wild type, mutant or empty vector as indicated. Cells were preincubated with 1 or 100 µM FR900359 (FR) or buffer and activated with 100 µM carbachol (CCh) or buffer after about 3 minutes of baseline measurement. Data are the means + SD of one experiment representative of three biologically independent experiments performed by Sergi Bravo (Kostenis lab, University of Bonn).* ***B.*** *FR concentration-response curves measured as maximal buffer-corrected DMR response after preincubation with FR or buffer and stimulation with CCh or buffer normalized to the effect of 100 µM CCh without FR in cells transfected as in A. Data are the means ± SEM of three biologically independent experiments performed by Sergi Bravo (Kostenis lab, University of Bonn). The bottom of the nonlinear fit was constrained to be the same for all data sets.* ***C.*** *Table summarizing pIC_{50} values ± SEM and the potency fold change of DGq IW compared to wild type of the FR concentration-response curves shown in B.*

In summary, DGq IW displayed strongly reduced FR sensitivity with potency shifts of 75- and 320-fold in Gβγ/masGRK3ct BRET and DMR assays, respectively. Depending on the assay used, we detected different extents of residual inhibitor activity at high concentrations. The data did not imply reduced efficacy of FR on *Drosophila* Gq IW, but a shift in the concentration-response curves.

Taking all results together, DGαq IW constitutes an ideal basis for further engineering. As the final concentration of inhibitor in the fly in the *in vivo* FR feeding experiments cannot be estimated, we will expand on the IW mutant and introduce a second mutation into this background to increase FR resistance.

5.4. Second generation of DGq mutants

5.4.1. Design

We, therefore, selected a second position in the DGαq FR binding site and introduced three different residue mutations in addition to the IW mutation.

Valine$^{G.hfs2.3}$ is heavily implicated in FR binding, as it is part of the hydrophobic network of amino acids that accommodate the inhibitor (Nishimura et al., 2010), and has been successfully mutated to achieve FR insensitivity in mGαq before without an influence on the signaling amplitude in the DMR assay (Malfacini et al., 2019).

Based on these considerations, we introduced either alanine, serine or methionine in the analogous position to swap out V178 in DGαq. Alanine was chosen as the smallest residue to simply remove interaction of the side chain with the inhibitor. We decided against the introduction of glycine due to this residue's flexibility and the possible negative influence on the conformational stability of the Gα protein (Richardson, 1981). Serine was chosen to introduce a hydrophilic side chain to disturb the hydrophobic inhibitor binding pocket. Methionine was selected as it contains a larger sulfur atom which might result in steric hindrance with the inhibitor. Secondly, methionine is the analogous residue in Gα16 and combination with a different isoleucine$^{G.S2.2}$ mutation (I190N) shows synergistic effects in mGαq (Malfacini et al., 2019). The resulting second generation of DGαq mutants encompassed DGαq V178A I184W (VA IW), DGαq V178S I184W (VS IW), and DGαq V178M I184W (VM IW).

5.4.2. Functional characterization

To thoroughly characterize the functionality and FR sensitivity of the newly generated DGαq mutants, as well as the impact of introducing the second-site mutations, we employed the same set of assays previously used for the DGαq IW mutant characterization, albeit in a different order to exclude unsuited mutants as early as possible. Western blot analysis revealed a similar pattern of protein expression in cells transfected with DGαq double mutants and wild type, with a distinct intense band migrating slightly above the endogenous Gαq protein (Figure 44).

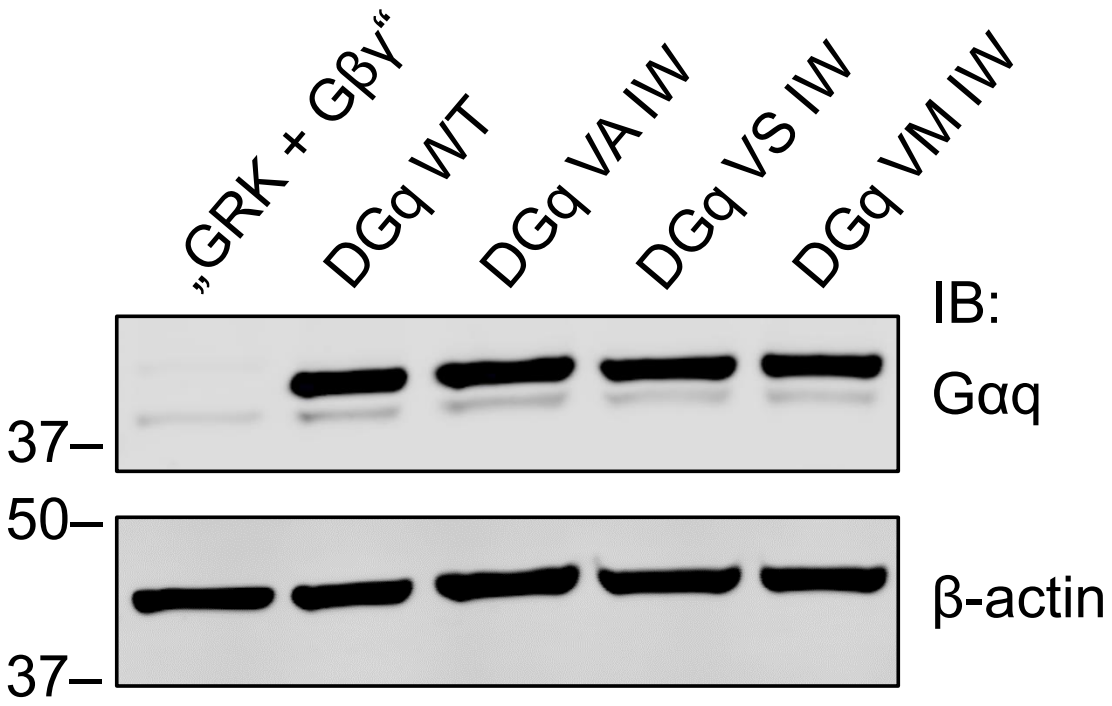

Figure 44: DGαq VA IW, VS IW, and VM IW display the same electrophoretic mobility as DGαq wild type. *Western blot of SDS-PAGE performed with lysates of HEK293T cells used for Gβγ/masGRK3ct BRET experiments shown in Figure 47, Figure 48, and Figure 51A. β-actin was used as protein loading control. Depicted are results representative of three individual western blots with cells from biologically independent BRET assays. The image originated from one blot. Lanes of "GRK + Gβγ" and DGq WT were already shown in Figure 24 and are shown again for clarity.*

Furthermore, all three double mutants were expressed at similar levels to that of wild-type *Drosophila* Gαq (Figure 45).

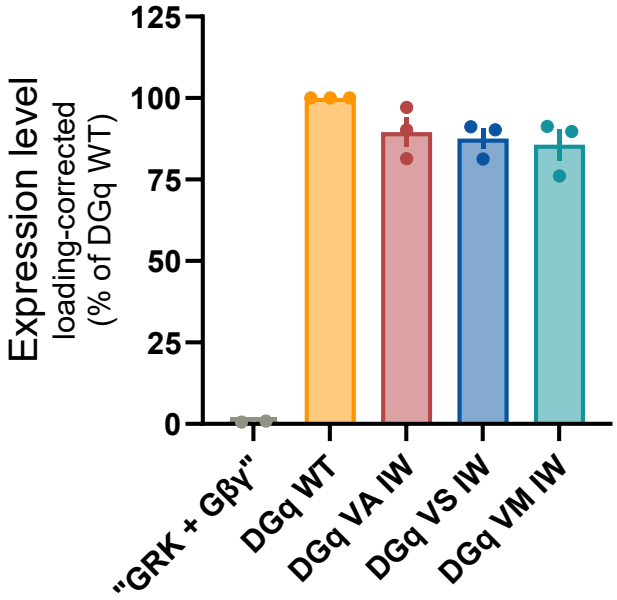

Figure 45: The DGαq double mutants VA IW, VS IW, and VM IW are expressed at wild type-like levels. *Quantitative analysis of the western blot expression data shown in Figure 44. Western blots were performed with lysates of HEK293T cells used for Gβγ/masGRK3ct BRET experiments shown in Figure 47, Figure 48, and Figure 51A. β-actin was used as protein loading control. Bar graphs represent the means ± SEM of three independent western blots corrected for loading and normalized to DGαq WT intensities. Data points represent individual replicates. Data for DGαq WT were copied from Figure 25 for clarity.*

The localization of the mutants is also wild type-like (Figure 46). The visually obvious colocalization with the membrane-marking fluorescent NeonGreen-CAAX protein in immunofluorescence microscopy experiments was confirmed with line scans. There was no detectable accumulation of the DGαq protein variants in intracellular organelles and no retention in the endoplasmic reticulum, demonstrating that shuttling to the membrane happened properly. This indicates proper folding of all mutant proteins. Neither expression nor localization of DGαq mutants yielded any reason to exclude them, as they displayed wild type-like characteristics.

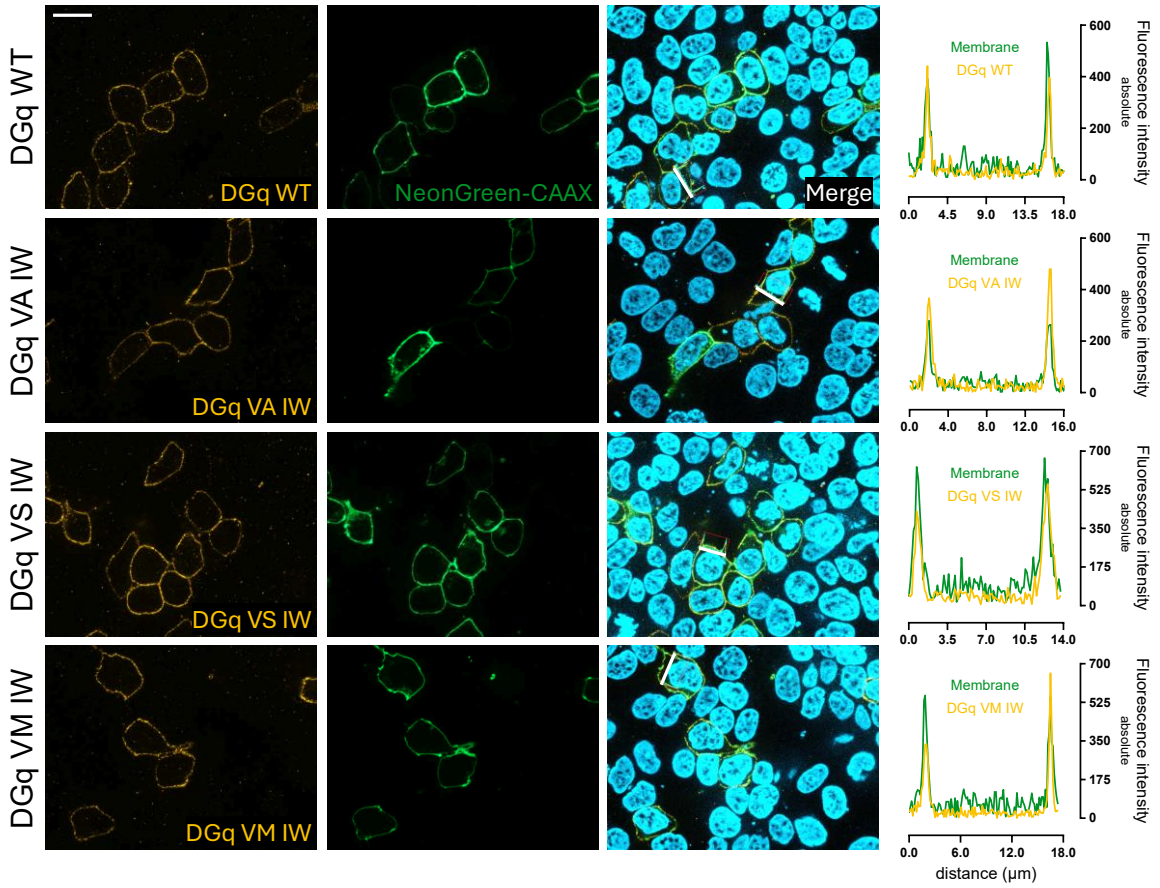

Figure 46: DGαq VA IW, VS IW, and VM IW are located at the plasma membrane mimicking wild-type behavior.
HEK293 cells lacking endogenous Gαq, Gα11, Gα12, and Gα13 proteins after CRISPR/Cas9 treatment (HEK293 Gq/11/12/13-KO) were transiently transfected with constructs coding for DGαq wild type or mutants and the membrane-targeted green-fluorescent protein NeonGreen-CAAX. Cells were stained with a primary rabbit anti-Gq and secondary orange-fluorescent Cy3-tagged anti-rabbit antibody to visualize DGαq variants, as well as DAPI to visualize the nucleus (blue). For the line scan, absolute green and orange fluorescence intensities representing membrane and DGαq wild type and mutants, respectively, were measured along the white lines indicated in the merge panel and plotted against the distance from the starting point. Depicted are representative pictures and line scans of three (mutants) or six (wild type) experiments performed by Aram Kamalizade (formerly Kostenis lab, University of Bonn). The scale bar in the top left corner represents 20 µm. The brightness of all pictures was increased by 70%. Pictures of and the line scan for DGαq WT were copied from Figure 32 for clarity.

After confirmation of the basis for functionality, we proceeded to investigate the mutants in the Gβγ/masGRK3ct BRET assay. We utilized the same assay setup as before. All three DGαq mutants quenched the basal BRET ratio to comparable levels as wild type (Figure 47). In combination with the verified similar levels of expression, this demonstrated similar binding to Gβγ. This is congruent with our expectations, as valine$^{G.hfs2.3}$ is close to but does not interact with the Gβγ complex (Lambright et al., 1996; Wall et al., 1995).

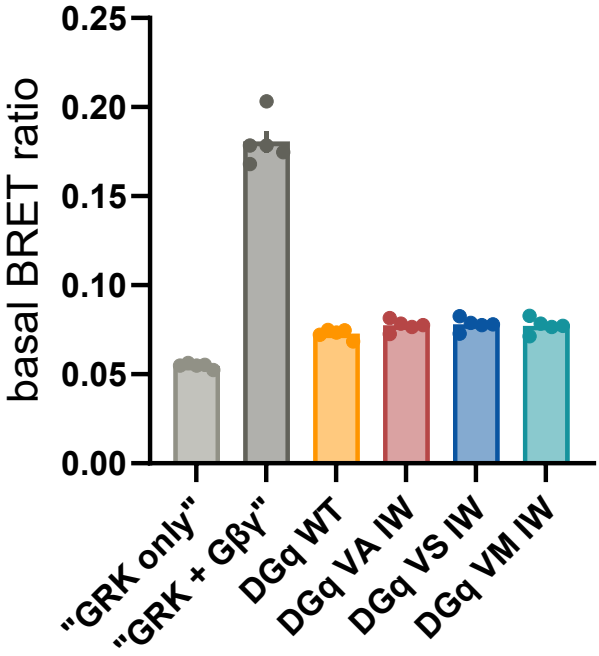

Figure 47: DGαq VA IW, VS IW, and VM IW exhibit wild type-like Gβγ binding capabilities.
Basal BRET ratio measured in HEK293T cells transiently transfected with constructs coding for M3R, masGRK3ct-NLuc, split Venus-tagged Gβγ, Ric-8A, and DGαq wild type or mutants as indicated. Bar graphs represent the means ± SEM of five biologically independent experiments. Data points represent individual replicates. Data for "GRK only", "GRK + Gβγ", and DGαq WT were copied from Figure 23 for clarity.

Furthermore, the activation kinetics in response to carbachol-activated M3R closely resembled those of the wild-type protein (Figure 48A and B). There seemed to be a slight reduction in signaling amplitude for VS IW and VM IW, but not for VA IW. These results need to be reevaluated after the recording of a full carbachol concentration-response curve.

The deactivation kinetics of all mutants were slower than wild type (Figure 48C), which was somewhat expected based on the behavior of the IW mutant in this assay. Interestingly, VM IW's speed of inactivation closely resembled DGq FIVE which shares the V178M mutation. A similar reduction in RGS sensitivity for the second generation of DGαq mutants needs to be evaluated. However, the fold-changes in deactivation kinetics were low (<3-fold) (Figure 48D) and an influence on downstream signaling seems improbable based on earlier results.

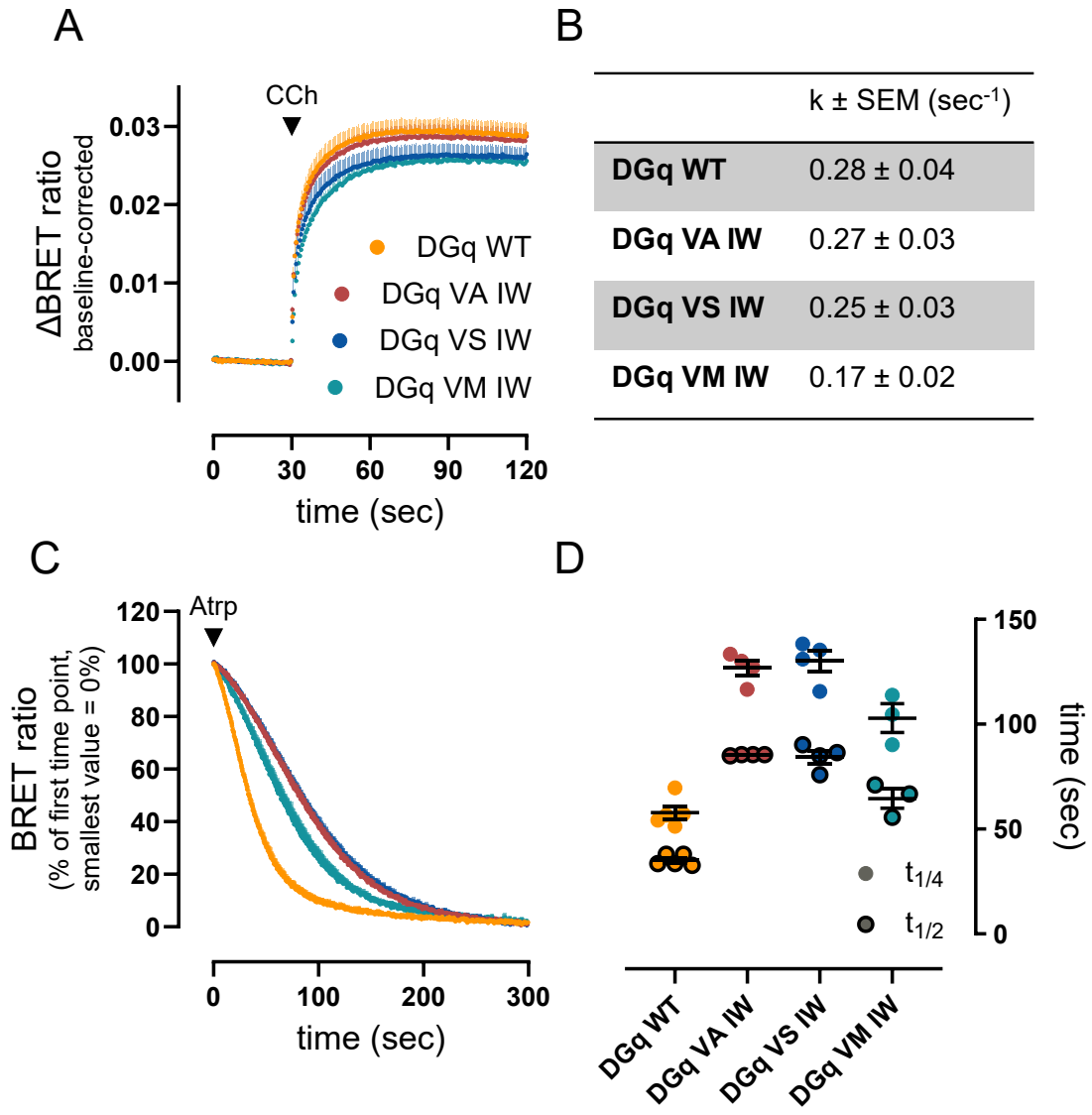

Figure 48: DGq VA IW, VS IW, and VM IW mimic wild-type DGq in their kinetics of activation, whereas their deactivation kinetics are decelerated.
A. *Kinetic baseline-corrected BRET traces of HEK293T cells transiently transfected with constructs coding for M3R, split Venus-tagged Gβγ, masGRK3ct-NLuc, DGαq wild type or mutants, and Ric-8A. Cells were activated with 100 µM carbachol (CCh) after 30 seconds of baseline measurement. Data are the means + SEM of three to five biologically independent experiments.* ***B.*** *Table summarizing activation rate constant values k ± SEM of the kinetic CCh activation curves shown in A extracted using the plateau followed by one-phase association model in GraphPad Prism.* ***C.*** *Normalized kinetic BRET traces of cells transfected as in A. After activation with 100 µM CCh, 100 µM atropine are added at t = 0. Data were normalized to the first timepoint, with the smallest value = 0%. Data are the means + SEM of three to five biologically independent experiments.* ***D.*** *Time required for a decay to 50% ($t_{1/2}$, outlined circles) or 25% ($t_{1/4}$, plain circles) of the initial value for each condition shown in B. Data for DGαq WT were copied from Figure 27 and Figure 33 for clarity.*

However, we still investigated our hypothesis regarding reduced sensitivity of DGαq VM IW and the behavior of VA IW and VS IW toward RGS proteins exploiting the same experimental setup as before.

All mutants still reacted to overexpression of two different RGS proteins with faster deactivation kinetics, demonstrating general sensitivity to the GAP activity of RGS proteins (Figure 49). The only exception was DGq VM IW which did not readily

respond to the presence of RGS19 and, thereby, mimicked the behavior of DGq FIVE.

Interestingly, RGS19 hardly influenced the amplitude and stability of the VA IW and VS IW signals, while still accelerating deactivation kinetics. This combination of effects might seem controversial but has extensively been discussed and resolved in literature (Elliott M. Ross, 2008).

The quantitative extent of sensitivity can hardly be estimated, as the kinetics without RGS overexpression are different between wild-type and mutant DGq variants. An assumed slightly lower sensitivity to RGS proteins for VA IW and VS IW compared to wild type could account for the changes in deactivation kinetics.

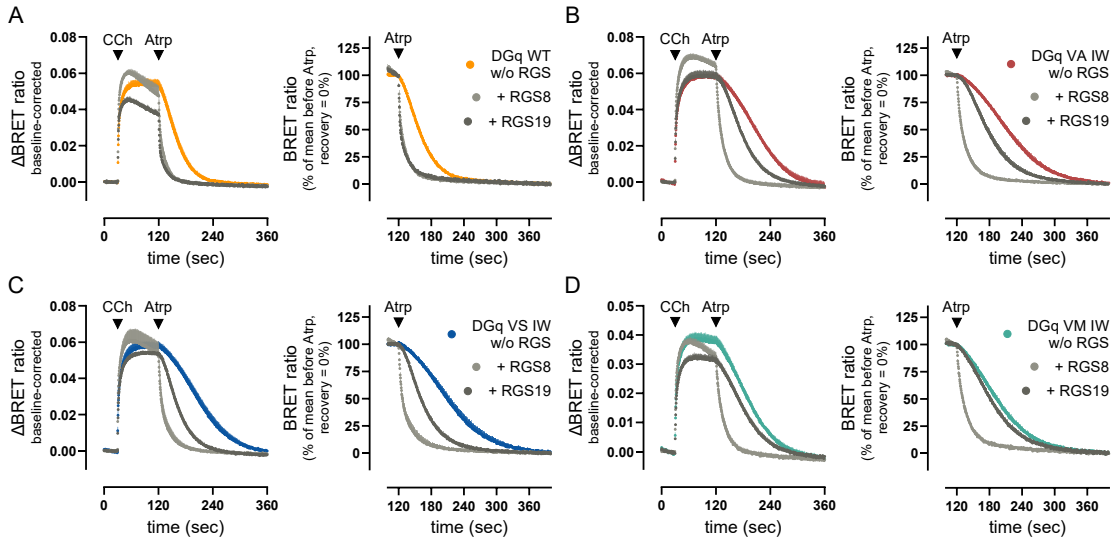

Figure 49: DGq VA IW and VS IW are sensitive to RGS8 and RGS19's GAP activity, while DGq VM IW is mostly insensitive to RGS19.
Left of A-D. *Kinetic baseline-corrected BRET traces of HEK293T cells transiently transfected with constructs coding for M3R, split Venus-tagged Gβγ, masGRK3ct-NLuc, DGαq wild type (A), VA IW (B), VS IW (C) or VM IW (D), Ric-8A, and either RGS8, RGS19 or without RGS protein. Cells were activated with 100 µM carbachol (CCh) after 30 seconds of baseline measurement. Deactivation with 100 µM atropine (Atrp) followed after 90 additional seconds. Data are the means + SEM of three biologically independent experiments.* ***Right of A-D.*** *Normalized kinetic BRET traces of the left panels from 100 to 400 sec. Data were normalized to the mean of the last 10 timepoints before Atrp addition, with the mean of the last 10 timepoints (recovery) = 0%. Data are the means + SEM of three biologically independent experiments. Data for DGαq WT were copied from Figure 35 for clarity.*

There were no differences in expression of RGS proteins between the conditions as seen in western blots of SDS-PAGE gels prepared with lysates of the cells used in these assays (Figure 50). Therefore, an influence of expression on the RGS sensitivity measurements could be excluded.

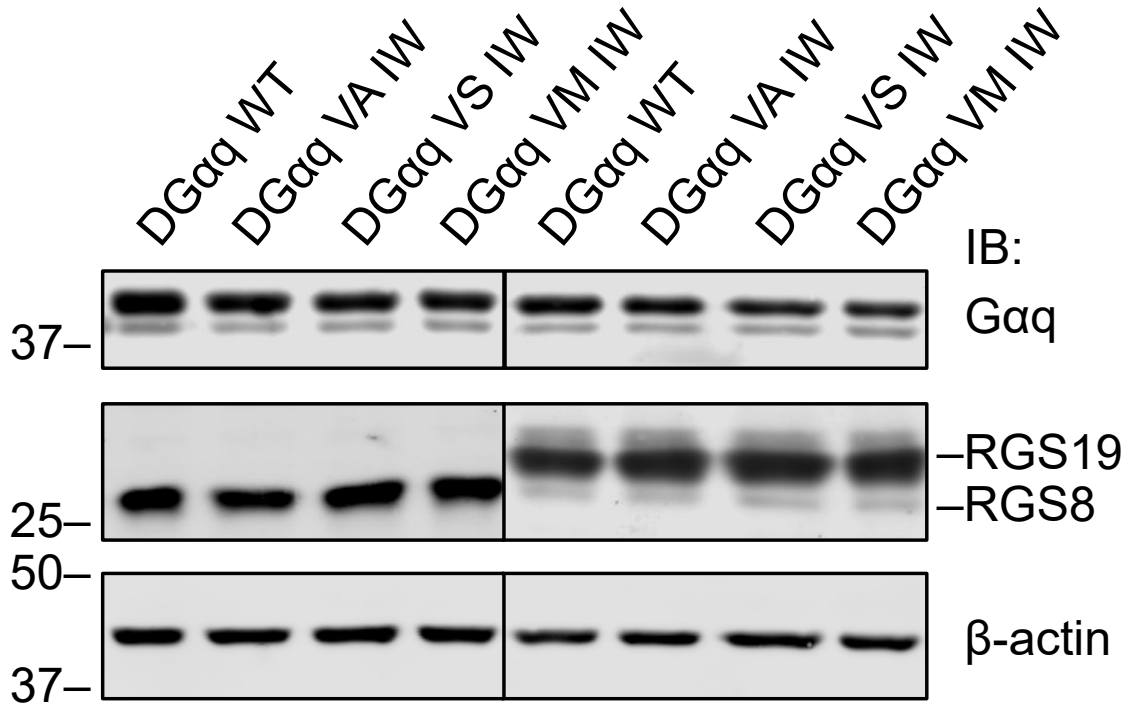

Figure 50: The RGS8 and RGS19 proteins are coexpressed with the different DGαq double mutants in equal amounts.
Western blot performed with lysates of HEK293T cells used for Gβγ/masGRK3ct BRET experiments shown in Figure 49. β-actin was used as protein loading control. Depicted are results of an individual western blot with cells used for a representative BRET assay. The image originated from one blot but is assembled to remove irrelevant samples. The image parts for RGS19 and RGS8 originate from the same stained membrane strip with different exposure times. Lanes of "GRK + Gβγ" and DGαq WT were already shown in Figure 37 and are shown again for clarity. IB: immunoblotted.

Upon the addition of carbachol to activate exogenous M3 receptors in the Gβγ/masGRK3ct BRET assay, all double mutants were activated, and the responses were concentration-dependent (Figure 51A). All in all, the double mutants DGαq VA IW and VS IW behaved very similarly. They displayed amplitudes of activation comparable to wild type and slightly higher potencies evident from the left-shift in the concentration-response curves (Figure 51B). In this regard, the mutants are similar to DGαq IW and the same explanation might apply. The changes in amplitude for DGαq VS IW in the kinetic assays were not reproduced in the concentration-response endpoint assay.

DGαq VM IW, however, showed a reduced signaling amplitude with maximum signals reaching about 85% of wild type (Figure 51A and B). This is striking, as the mutant shares not only the VM mutation, but also the rightward shift in potency and the insensitivity towards RGS19 with FIVE which did not show a reduction in efficacy. Even though this behavior can already be classified as non-wild type-like and justifies the exclusion of the mutant from further analysis, we still included it in FR sensitivity investigations in this assay to investigate if the introduction of the

corresponding Gα16 residue in this position is in any way beneficial over the rationally introduced mutations to alanine and serine.

Before continuing the investigation in second messenger assays, we investigated FR sensitivity in the βγ/GRK BRET assay setup. This way, we made sure to only continue if there was a further reduction in FR sensitivity over the DGαq IW mutant or to proceed differently if the introduction of other mutations was required to assure sufficient insensitivity.

All three double mutants were close to completely resistant to FR in the BRET assays performed (Figure 51C). When incubating with 100 µM FR at least 80 % activity remained compared to the wild-type protein. This virtually complete resistance prevents the fit of a concentration-response curve. No pIC_{50} values or fold changes could be calculated for DGαq VA IW, VS IW, and VM IW.

These data unequivocally revealed that the double mutations introduced into DGαq are sufficient to abrogate inhibitor function. The introduction of other mutations is not necessary, and the VA IW and VS IW double mutants will be investigated in the remaining functional assays to ascertain their wild type-like behavior and reduced FR sensitivity. As there is no benefit of using DGαq VM IW over the other double mutants, i.e. the mutant is not visibly superior regarding FR resistance, and we observed a reduced amplitude in the carbachol concentration-response curves as well as in the kinetics, combined with obviously altered RGS sensitivity, this mutant will not be included in further analyses.

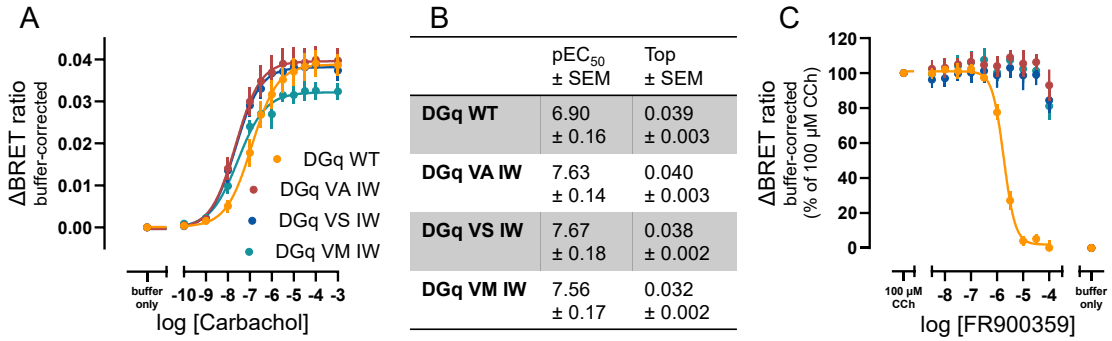

	pEC_{50} ± SEM	Top ± SEM
DGq WT	6.90 ± 0.16	0.039 ± 0.003
DGq VA IW	7.63 ± 0.14	0.040 ± 0.003
DGq VS IW	7.67 ± 0.18	0.038 ± 0.002
DGq VM IW	7.56 ± 0.17	0.032 ± 0.002

Figure 51: DGαq VA IW and VS IW mimic wild-type DGαq in the efficacy and potency of activation, while DGαq VM IW shows slightly reduced efficacy. All double mutants are resistant to FR900359 (FR).
A. *Carbachol (CCh) concentration-response curves measured as buffer-corrected BRET ratio after stimulation with CCh or buffer in HEK293T cells transiently transfected with constructs coding for M3R, split Venus-tagged Gβγ, masGRK3ct-NLuc, DGαq wild type or mutants, and Ric-8A. Data are the means ± SEM of four to five biologically independent experiments.* ***B.*** *Table summarizing pEC_{50} values ± SEM and Tops ± SEM of the CCh concentration-response curves shown in A.* ***C.*** *FR concentration-response curves measured as buffer-corrected BRET ratio after preincubation with FR or buffer and stimulation with CCh or buffer in cells transfected as in A. Data are the means ± SEM of four to five biologically independent experiments. Data for DGαq WT were copied from Figure 22 for clarity.*

With these promising results, we continued the investigation in the second messenger assay. Basal IP_1 accumulation in unstimulated cells was similar to wild type for both double mutants (Figure 52A) demonstrating comparable intrinsic

activities of the G protein variants. Furthermore, while the intrinsic activity of DGq wild type was sensitive to a high concentration of FR as demonstrated earlier (see Figure 42), the double mutants remained unaffected (Figure 52B), suggesting near-complete inhibitor resistance in these variants.

Unfortunately, the carbachol concentration-response curve in the IP_1 accumulation assay was hard to evaluate. This is due to the size of the error bars which might be caused by the lack of exogenous Ric-8A. As also shown in the literature (Himmelreich et al., 2017), expression of this chaperone should be evaluated to aid with expression in future assays with DGαq proteins in non-*Drosophila* cells.

However, the IP_1 accumulation data clearly showed a concentration-dependent reaction of DGq VA IW and VS IW to carbachol (Figure 52C) agreeing with the results from the Gβγ/masGRK3ct assay. Furthermore, the general course of the estimated nonlinear fit of the data suggested similar potencies of signal. While the efficacy seemed to be slightly elevated in the double mutants when considering the nonlinear regression, the response to the highest concentration of carbachol used (1 mM) was quite similar to the wild type. In line with the lack of inhibition of basal IP_1 accumulation, FR did not affect receptor-induced second messenger generation (Figure 52D).

In conclusion, the available data did not indicate any significant difference in the response of the DGαq mutants to carbachol-activated M3R compared to the wild type in second messenger assays but demonstrate the mutants' remarkable resistance to the inhibitor FR.

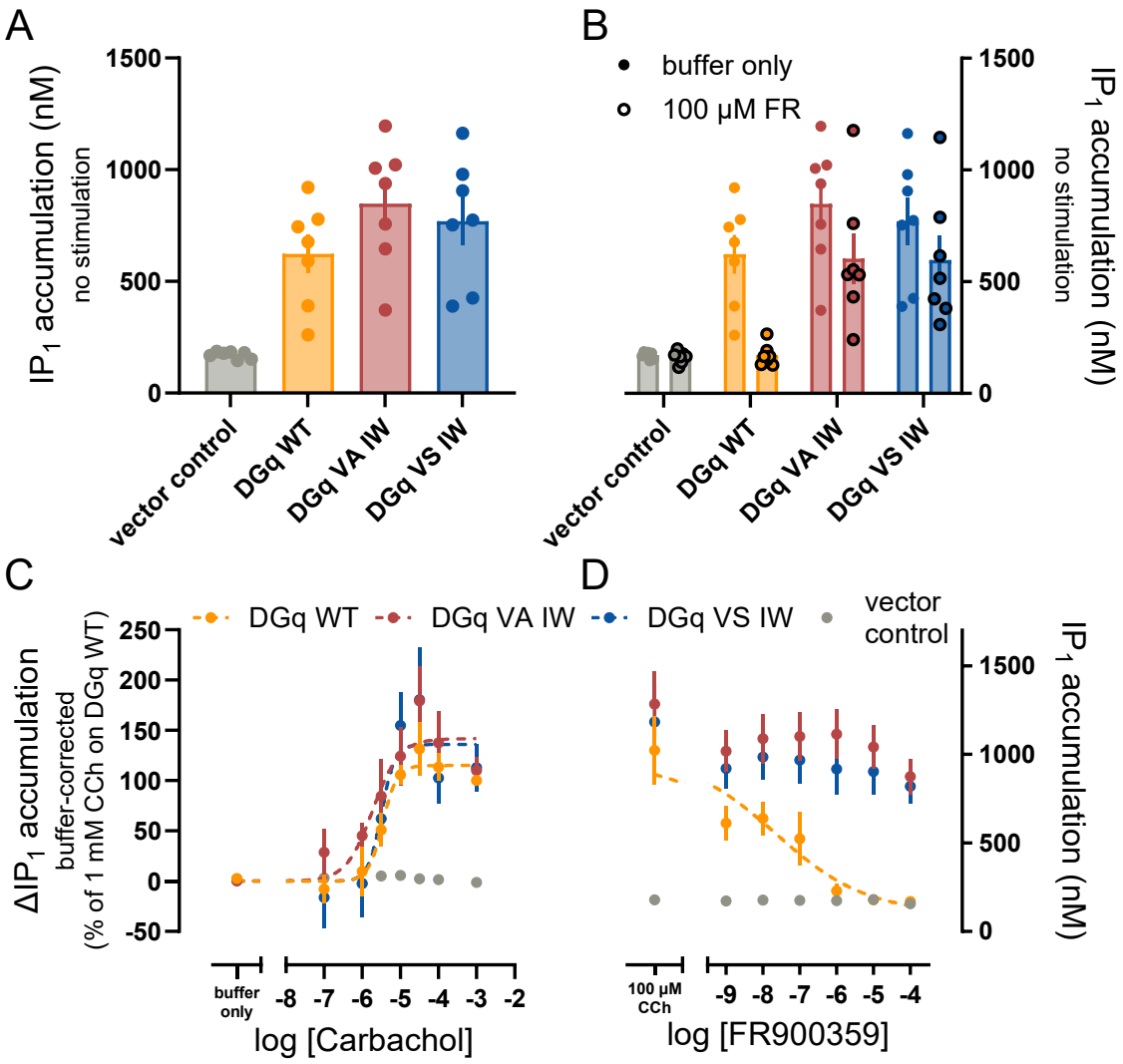

Figure 52: DGq VA IW and VS IW behave wild type-like regarding intrinsic and receptor-stimulated second messenger production but are refractory to inhibitor action as determined in IP₁ accumulation assays.

A. *Intrinsic IP₁ accumulation in HEK293 cells lacking Gαq and Gα11 proteins after CRISPR/Cas9 treatment (HEK293 Gq/11-KO) transiently transfected with constructs coding for DGαq wild type or mutants or empty vector. Bar graphs represent the means ± SEM of seven biologically independent experiments performed by Uli Rick (Kostenis lab, University of Bonn). Data points represent the means of individual experiments.* ***B.*** *Influence of 100 µM FR900359 (FR) on intrinsic IP₁ accumulation in cells transfected as in A. Data are the means ± SEM of seven biologically independent experiments performed by Uli Rick (Kostenis lab, University of Bonn).* ***C.*** *Carbachol (CCh) concentration-response curves measured as buffer-corrected IP₁ accumulation after stimulation with CCh or buffer in cells transfected as in A normalized to the effect of 1 mM CCh on DGq wild type. Data are the means ± SEM of three to seven biologically independent experiments performed by Uli Rick (Kostenis lab, University of Bonn).* ***D.*** *FR concentration-response curves measured as buffer-corrected IP₁ accumulation after preincubation with FR or buffer and stimulation with 100 µM CCh in cells transfected as in A. Data are the means ± SEM of three to seven biologically independent experiments performed by Uli Rick (Kostenis lab, University of Bonn). Data for DGαq WT were copied from Figure 38 and Figure 42 for clarity.*

The deactivation kinetics in the Gβγ/masGRK3ct BRET assay differed between the double mutants and the wild type (see Figure 48). We, therefore, investigated whether this delayed deactivation is also evident at the whole-cell level during the following characterization of the mutants in the DMR setup.

The response to carbachol-activated endogenous M3R was concentration-dependent for both investigated mutants (Figure 53A and B) and matched the wild-type protein's response regarding efficacy and potency (Figure 53B and C). Furthermore, the kinetics of cell shape change in response to carbachol did not differ from wild-type DGq (Figure 53D). The differences in deactivation kinetics on the G protein activation level did evidently not translate into changes in signaling kinetics on the whole-cell level.

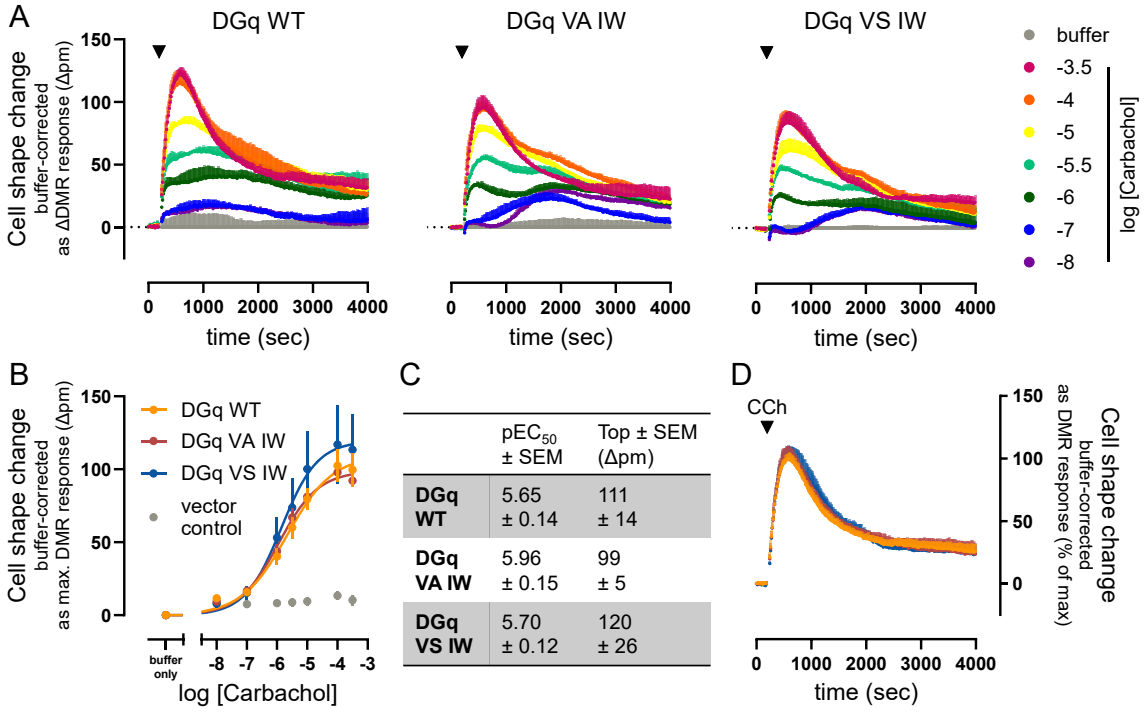

	pEC_{50} ± SEM	Top ± SEM (Δpm)
DGq WT	5.65 ± 0.14	111 ± 14
DGq VA IW	5.96 ± 0.15	99 ± 5
DGq VS IW	5.70 ± 0.12	120 ± 26

Figure 53: DGq VA IW and VS IW behave wild type-like regarding integrated whole-cell response as measured in dynamic mass redistribution (DMR) assays.
A. *Kinetic buffer-corrected DMR traces of HEK293 cells lacking Gαq and Gα11 proteins after CRISPR/Cas9 treatment (HEK293 Gq/11-KO) transiently transfected with constructs coding for Ric-8A and DGαq wild type, mutant or empty vector as indicated. Cells were activated with different concentrations of carbachol (CCh) or buffer after about 3 minutes of baseline measurement. Data are the means + SD of one experiment representative of three to five biologically independent experiments performed by Sergi Bravo (Kostenis lab, University of Bonn).* ***B.*** *CCh concentration-response curves measured as maximal buffer-corrected DMR response after stimulation with CCh or buffer in cells transfected as in A. Data are the means ± SEM of three to five biologically independent experiments performed by Sergi Bravo (Kostenis lab, University of Bonn). The bottom of the nonlinear fit was constrained to 0.* ***C.*** *Table summarizing pEC_{50} values ± SEM and Tops ± SEM of the CCh concentration-response curves shown in B.* ***D.*** *Kinetic buffer-corrected DMR traces of cells transfected as in A normalized to the top of each individual trace. Cells were activated with 100 µM CCh after about 3 minutes of baseline measurement. Data are the means + SD of one experiment representative of three to five biologically independent experiments performed by Sergi Bravo (Kostenis lab, University of Bonn). Data for DGαq WT were copied from Figure 40 for clarity.*

Regarding FR sensitivity, the DMR results confirmed the previous experiments. Even at the whole-cell level – far downstream from the receptor with potential for signal amplification –, DGq VA IW and VS IW were entirely refractory to inhibition by FR (Figure 54A and B). Even the highest concentration used (100 µM) did not impact the signaling response.

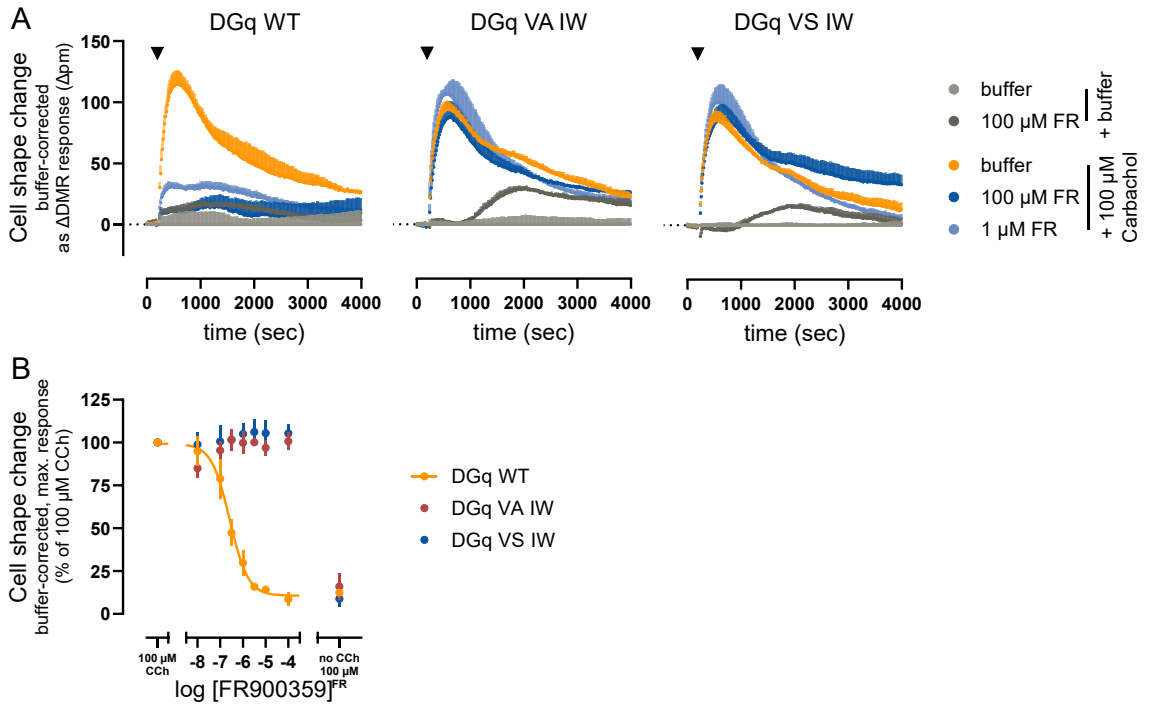

Figure 54: DGq VA IW and VS IW are resistant to FR in dynamic mass redistribution (DMR) assays. ***A.*** *Kinetic buffer-corrected DMR traces of HEK293 cells lacking Gαq and Gα11 proteins after CRISPR/Cas9 treatment (HEK293 Gq/11-KO) transiently transfected with constructs coding for Ric-8A and DGαq wild type, mutant or empty vector as indicated. Cells were preincubated with 1 or 100 µM FR900359 (FR) or buffer and activated with 100 µM carbachol (CCh) or buffer after about 3 minutes of baseline measurement. Data are the means + SD of one experiment representative of three biologically independent experiments performed by Sergi Bravo (Kostenis lab, University of Bonn).* ***B.*** *FR concentration-response curves measured as maximal buffer-corrected DMR response after preincubation with FR or buffer and stimulation with CCh or buffer normalized to the effect of 100 µM CCh without FR in cells transfected as in A. Data are the means ± SEM of three biologically independent experiments performed by Sergi Bravo (Kostenis lab, University of Bonn). Data for DGαq WT were copied from Figure 43 for clarity.*

This extensive characterization of DGαq VA IW and VS IW in HEK293 cells reveals that both mutants possessed wild-type characteristics in all essential readouts tested. Both mutants were expressed at levels similar to wild-type DGαq and localized to the plasma membrane. They were comparable to wild type in their intrinsic signaling activity, as well as ligand-induced activation kinetics, potency, and efficacy. While sensitivity to human RGS proteins might be reduced slightly compared to wild-type DGαq, this did not affect downstream signaling as apparent from IP_1 accumulation and DMR measurements. Moreover, the transferability of this result to *Drosophila* RGS proteins and the functional relevance of this change *in vivo* is hard to predict.

More importantly, both mutants were entirely resistant to inhibition by FR on the G protein, second messenger, and whole-cell response levels. Therefore, we can confidently conclude that the developed *Drosophila* Gαq isoforms meet all requirements for proceeding to *in vivo* work.

5.5. *In vivo* experiments

All *in vivo* assays were performed by our collaborators Dr. Anne-Kristin Dahse and Dr. Nicole Scholz (University of Leipzig).

In this second part of the study, we employed the partially FR-resistant DGαq variant IW, as well as the completely insensitive VA IW and VS IW mutants in live animals to investigate whether FR-induced lethality of *Drosophila melanogaster* is exclusively mediated via inhibition of DGq. If the lethality upon inhibitor-ingestion is indeed mediated by DGq inhibition only, overexpression of FR-resistant mutants should rescue the lethality. This would not only demonstrate the overall suitability of FR in combination with artificial Gα protein subunits as the basis for a chemogenetics-like toolbox but also illustrate the usefulness of the engineered DGαq mutants to investigate causality in Gq protein biology.

5.5.1. Lethality of FR

In preliminary experiments conducted with *Drosophila melanogaster* flies that were fed FR-laced food, the inhibitor exhibited lethality, analogously to the outcomes previously attained in bean bug nymphs (Crüsemann et al., 2018).

To verify these results and to determine an FR concentration that produces a sufficiently low survival rate to allow a comparison of fly lines expressing DGαq mutant proteins without uneconomical use of the compound, we exposed *Drosophila melanogaster* wild-type strain w^{1118} to food supplemented with inhibitor concentrations ranging from 1 µM to 120 µM and recorded their survival over a period of nine days. To control for the effects of the solvent DMSO, four batches of flies were provided with food containing equivalent amounts of DMSO.

It is evident that DMSO was not overly harmful to w^{1118} wild-type flies (Figure 55A). However, higher amounts of DMSO seemed to promote variation between replicates (Figure 55B). While 1 µM of FR did not have a pronounced effect over DMSO, lethality increased with increasing FR concentrations used and over time. The highest concentration (120 µM) killed all flies within six days and, thus, showed lethality comparable to that reported for bean bug nymphs, albeit without the pronounced delay (Crüsemann et al., 2018).

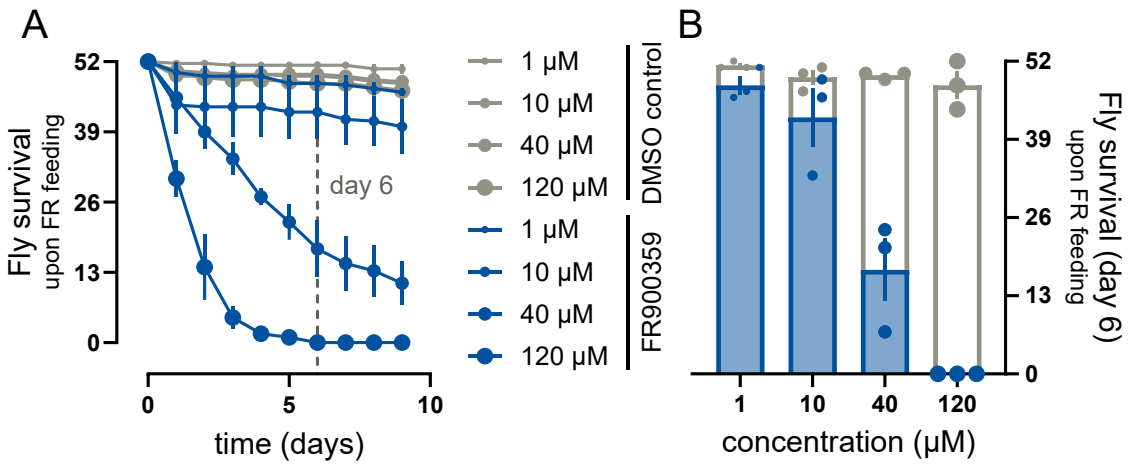

Figure 55: Drosophila melanogaster w^{1118} flies die when ingesting FR.
A. *w^{1118} flies were kept on food containing different FR concentrations or corresponding amounts of DMSO as a control. Survival of flies was recorded for nine days. Day six is indicated with a dashed line. Data are the means ± SEM of three independent biological experiments performed with 52 adult flies (40 female, 12 male).* ***B.*** *Bar graph depiction of fly survival on the sixth day. Bar graphs represent the means ± SEM. Data points represent the means of individual replicates.*

The effect of FR on fly survival is clearly dose-dependent, which prompts an investigation into whether the fate of the flies is also directly related to the amount of inhibitor present in the flies. To explore this, mass spectrometry-coupled high performance liquid chromatography (HPLC/MS) experiments on survivor and victim flies of each condition were performed by Prof. Dr. Max Crüsemann (Goethe University Frankfurt, formerly University of Bonn) and Dr. Wiebke Hanke (formerly University of Bonn) using a protocol previously established for analyzing FR-containing samples.

As expected, both victim and survivor flies in the DMSO conditions were entirely free of FR as measured by FR peak size detected between 13.5 and 16 minutes with a m/z of 1002.54 (Figure 56, for raw traces see Figure 68 in Additional Material). Similarly plausible, the amount of FR present in the victim flies of the FR conditions increased relative to the FR concentration in the food (Figure 56, for raw traces see Figure 68 in Additional Material). However, surviving flies in the FR conditions contained lower levels of FR than their victim counterparts. While there seemed to be differences in FR ingestion among flies kept on the same food, there was an evident correlation between the ingested amount of inhibitor and fly fate.

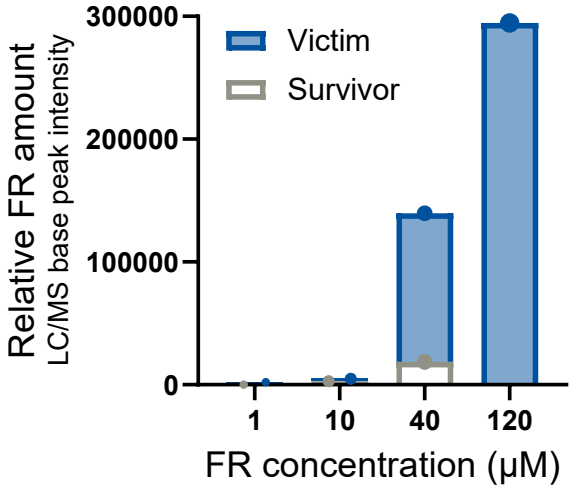

Figure 56: FR amounts are larger in flies that fell victim to FR treatment than in survivors.
Bar graph depiction of the relative FR content in survivor and victim flies of the FR conditions measured after methanol extraction using an HPLC/MS setup for the investigation of FR-containing samples. Bar graphs and data points represent the sum of base peak intensities of signals for unfragmented FR (m/z value of 1002.5400 ± 0.02) between elution times of 13.5 and 16 minutes. Raw HPLC/MS traces are depicted in Figure 68 in Additional Material. Data are values obtained from a single experiment performed on flies of one of the replicates in Figure 55.

5.5.2. Husbandry

To investigate if FR-induced lethality is a direct result of DGq inhibition, we aimed to compare the FR-induced lethality of flies expressing DGαq wild type or engineered mutants side-by-side. To achieve this, one cannot rely on random integration of DGαq cDNA into the genome as this has multiple disadvantages, e.g. the possibility of insertional mutation and unknown position effects, i.e. the influence of enhancers, silencers, and chromatin structure. Most importantly, random integration would place the introduced DGαq isoforms at different positions in the genome, which may result in a differential expression profile for each mutant. This would consequently prohibit direct comparison and complicate data interpretation.

To achieve direct comparability, we utilized the phiC31 integrase system for the site-directed integration of transgenes, thus circumventing the confounding effect of differential expression caused by differential position effects (Groth et al., 2004). Furthermore, phiC31 integrase catalyzes unidirectional integration, which prevents subsequent unwanted excision (Groth et al., 2004). PhiC31 integrase incorporates transgenic DNA plasmids containing a bacterial attachment site (attB) at a phage attachment site (attP) in the *Drosophila* genome creating two hybrid att sites, attL and attR (Groth & Calos, 2004; Markstein et al., 2008) (Figure 57).

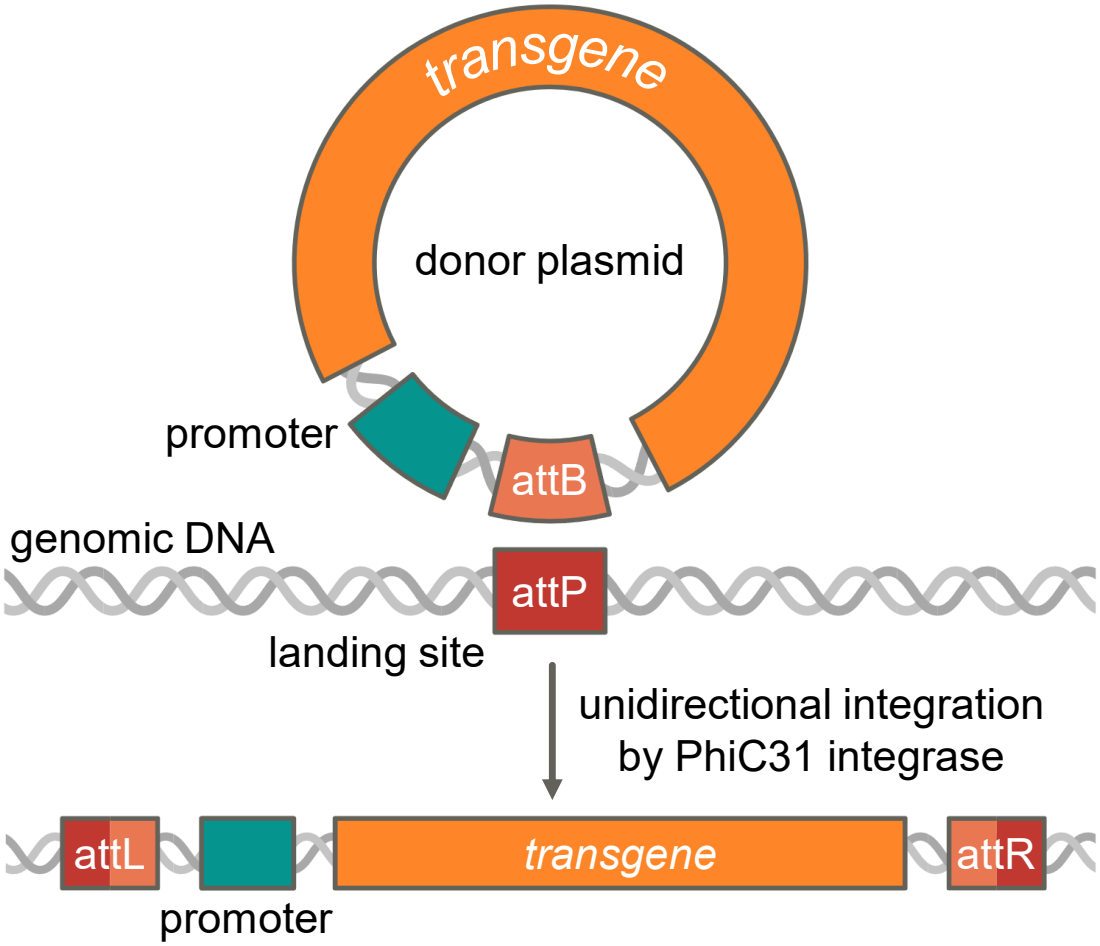

Figure 57: Schematic depiction of PhiC31 integrase action.
A donor plasmid containing the transgene behind a promoter and the bacterial attB site is unidirectionally integrated into genomic DNA containing a phage attP landing site. The integrated transgene and promoter are flanked by the resulting hybrid attL and attR sites. The figure was partially created with BioRender.com.

While there are pseudo attP sites already present in the wild-type *Drosophila* genome (Markstein et al., 2008), we used flies containing the previously introduced attP2 site (RRID:BDSC_8622) (Groth et al., 2004) to place the DGαq isoform DNA on the third (3L) chromosome (681A-B2). This position has been investigated regarding its position effects: transgenes inserted at attP2 show favorably low basal expression and high inducibility compared to other tested attP landing sites (Markstein et al., 2008). Insertion of DGαq wild type at another attP landing site on the second chromosome resulted in leaky expression (Figure 69 in Additional Material). The work with this strain was discontinued.

Induction of transgene expression was realized using the UAS/GAL4 system found in yeast (Brand & Perrimon, 1993) (Figure 58). This system enables the expression of a transgene in a spatiotemporally controlled manner. Briefly, DGαq sequences were cloned behind the upstream regulation sequence (UAS). UAS is recognized by the transcriptional activator GAL4. This way, the expression of the transgene is directly coupled to the expression of GAL4, which can be regulated and restricted

to chosen tissues when put under the control of a specific promoter. Crossing of the “driver” line expressing GAL4 under the control of a selected promoter with the “reporter” line, in which the DGαq transgene is present, will yield a filial generation one (F1) expressing the gene of interest either ubiquitously or in a specific cell population.

Wild-type DGαq isoform G is ubiquitously expressed. To simplify the experimental setup, we, therefore, chose to ubiquitously overexpress the DGαq isoforms of interest using *actin5C-GAL4 (Act5C::GAL4)* driver (Bond & Davidson, 1986; Bond-Matthews & Davidson, 1988). In the F1 progeny, all cells that endogenously express actin express GAL4 and, consequently, the introduced DGαq variant of interest. Even though the *Act5C* promoter is used to produce cytoskeletal actin in all cells (Chung & Keller, 1990) and, thus, causes low levels of ubiquitous expression (Burn et al., 1989), differences in expression levels among tissue types are to be expected. A promoter to control GAL4 expression that allows for equally high expression in all tissues is not known to date (Markstein et al., 2008).

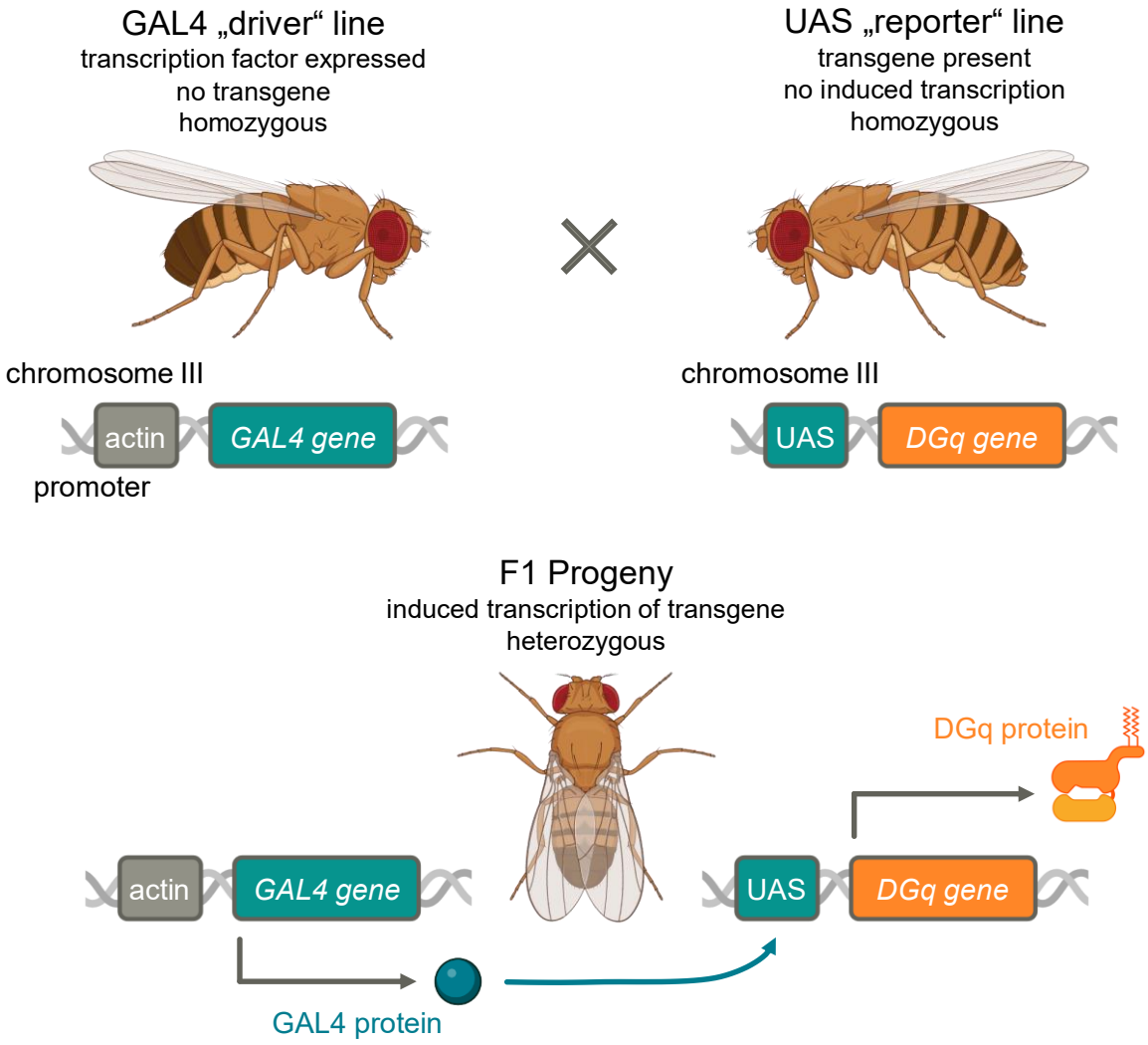

Figure 58: Schematic depiction of the UAS/GAL4 system.
The homozygous GAL4 “driver” fly line expresses the yeast transcription factor GAL4 behind a chosen promoter (in this study: actin5C) but does not contain the transgene. The homozygous UAS “reporter” line encodes the transgene (in this study: DGαq cDNA on the third chromosome) behind a GAL4 binding site (upstream activating sequence, UAS) but does not express GAL4. Crossing the GAL4 “driver” line and the UAS “reporter” line yields heterozygous progeny that produces GAL4 which in turn induces transgene transcription. The figure was partially created with BioRender.com.

Transgenes cloned behind a UAS, in our case 20xUAS, are not entirely silent without induction. However, the attP2 landing site is tightly regulated under basal conditions (Markstein et al., 2008), and the remaining low basal activity is probably not biologically relevant. However, we carried out the necessary controls to account for this. These controls included conducting all experiments with several control fly lines tested side-by-side with the experimental genotypes (*actin5C-GAL4>20xUAS-DGαq isoform*): *actin-GAL4/+* flies express GAL4 under *actin5C* promoter control without a GAL4 binding site or transgene present; *UAS-DGq isoform/+* flies contain the transgenic DNA behind a 20xUAS but do not express GAL4 nor the transgene. These control lines were used to investigate the influence of putative leak expression of sole GAL4 in actin-producing cells and sole DGαq isoform, respectively.

5.5.3. Negative geotaxis assay

Flies ubiquitously overexpressing wild-type and mutant DGαq behind an *actin5C-GAL4* promotor were viable and appeared healthy by visual inspection. No obvious defects or anatomical aberrations were visible. To verify that the transgenic flies did not suffer from visually undetectable defects caused by DGαq overexpression, we performed a simple and robust behavioral assay that investigates a complex instinctual escape response reliant on proper proprioception, locomotion, and complex neurophysiological functions including gravitation-sensing (Ali et al., 2011; Beckingham et al., 2005; Gargano et al., 2005; Inagaki et al., 2010).

In the negative geotaxis assay, flies were shaken to the bottom of the flask and started climbing the walls driven by negative geotaxis instinct. The climbing pass rate, i.e. the percentage of flies climbing a given distance in a given amount of time, can be used as a measure of behavioral health and locomotor capabilities (Ali et al., 2011). This assay is particularly well-suited for investigating flies that overexpress DGαq variants, given the established involvement of Gq in locomotion in mice (S. Offermanns, Hashimoto, et al., 1997) and *C. elegans* (Hanke et al., 2023).

Wild-type w^{1118} flies achieved a 98% climbing pass rate (Dahse, 2024). Flies with known defective locomotion and proprioception served as controls (Figure 59). These controls illustrate how impaired proprioception affects the flies' performance in the negative geotaxis assay. Genotypes of the controls are intentionally not disclosed in order to maintain confidentiality.

"Driver" and "reporter" control fly lines did not show any deviation from the expected climbing pass rate (Figure 59A), indicating that the presence of GAL4 or transgene alone does not influence the performance of flies in the negative geotaxis assay. Similarly, flies overexpressing DGαq wild type or mutants displayed regular climbing behavior (Figure 59B) demonstrating the flies' health. Thus, ubiquitous overexpression of supra-physiological Gq protein levels left all major physiological functions intact.

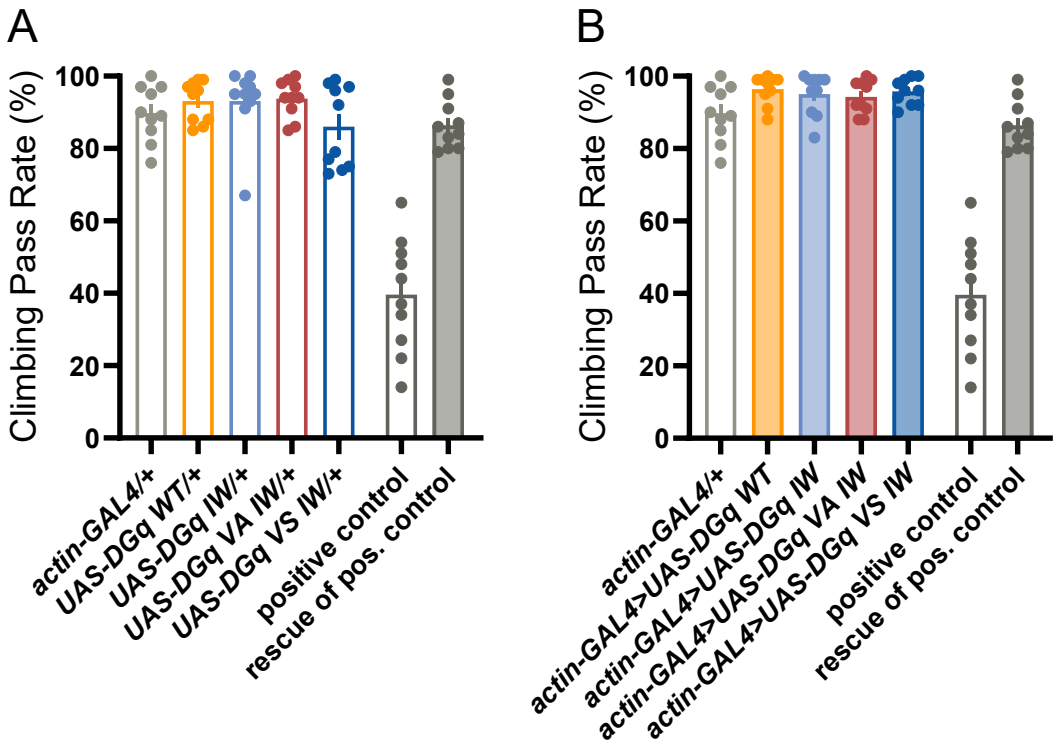

Figure 59: Flies overexpressing DGαq wild-type or mutant proteins are healthy and display regular movement.
A. *The negative geotaxis assay was performed with the control "driver" and "reporter" lines. Flies climbing above the 8 cm mark in 10 seconds were counted towards the pass rate.* ***B.*** *The negative geotaxis assay was performed with flies overexpressing DGαq isoforms as described in A. A strain with defective locomotion and a rescue thereof (genotypes not disclosed due to confidentiality reasons) were used as assay controls. Bar graphs represent the means ± SEM of ten independent replicates performed with 10 virgin female flies each. Data points represent the means of individual replicates.*

5.5.4. FR feeding experiments

With these results on the soundness of transgenic fly line, we proceeded with FR feeding experiments to investigate if overexpression of FR-insensitive mutant DGαq rescues inhibitor-induced lethality.

For final FR feeding experiments, the chosen concentration should result in a survival rate low enough to yield a sufficient assay window to unambiguously show possible rescuing effects of DGαq mutant overexpression, yet not too low so that the inhibitors' effect can still be overcome. Furthermore, we considered that high concentrations of FR are not economical and necessitate high DMSO amounts that increase the variability of results between replicates (see Chapter 5.5.1. Lethality of FR). We, therefore, chose to use the previously selected concentrations 40 and 120 µM for initial feeding experiments with flies overexpressing DGαq wild type.

Interestingly, DGq wild type expression from the third chromosome resulted in a rescue effect on 40 µM FR-containing food but not so on food laced with 120 µM FR (Figure 60). This indicates that flies that can fall back on high amounts of DGαq

protein maintain sufficient residual Gq activity at lower FR concentrations, while high inhibitor concentrations are still sufficient to inhibit such high amounts of protein and are consequently lethal. Based on these results, we hypothesized that the amount of Gq present influences the inhibition properties of FR.

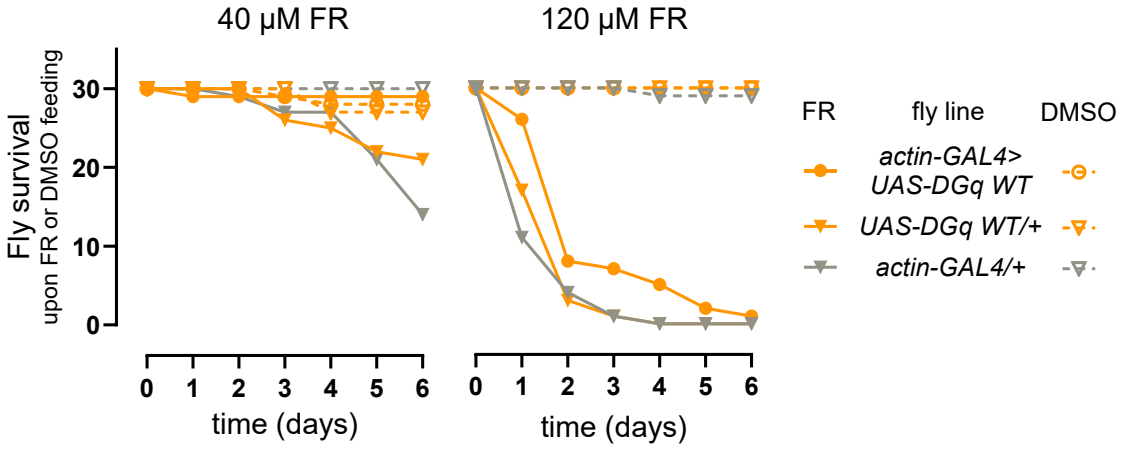

Figure 60: Rescue of FR-induced lethality in Drosophila melanogaster through overexpression of DGαq wild type depends on the inhibitor concentration in the food.
Flies only harboring the gene of (UAS-DGq WT/+) or expressing DGαq wild type (actin-GAL4>UAS-DGq WT) from the third chromosome, as well as the "driver" control line were kept on food laced with 40 (left) or 120 (right) µM FR (filled symbol) or corresponding amounts of DMSO (open symbol). Survival of flies was recorded for six days. Data are absolute numbers of one experiment performed with 30 adult flies (20 female, 10 male).

To test this hypothesis, we made use of the IP_1 accumulation assay described above. Utilizing HEK293 Gq/11-KO cells and transfecting different amounts of mGαq permitted titration and tight control over Gαq amounts present in cells. Total expression levels as determined by enzyme-linked immunosorbent assay (ELISA) were saturated at high amounts of transfected DNA (Figure 61A). Intrinsic and agonist-induced IP_1 accumulation correlated with expression levels, as they were highly dependent on the amount of Gq present.

IP_1 accumulation in vector control cells not expressing any Gαq protein were not affected by FR treatment (Figure 61B). However, the carbachol-induced response in all cells transfected with plasmid DNA coding for Gαq was concentration-dependently diminished by the inhibitor. High-resolution inhibition curves revealed that titration of Gαq amounts did not affect the potency of inhibition. Potency does, therefore, not account for the effect observed in the initial FR feeding experiments (Figure 61C).

The hill slope, in contrast, increased gradually with the amount of expressed protein, moving from an already steep curve at 50 ng transfected DNA to a virtual all-or-nothing response at higher expression levels (Figure 61B and C). Even though these experiments have been performed with murine Gq, an extrapolation of the steeper curve could explain the survival of flies with enhanced DGαq expression on food containing lower concentrations of FR.

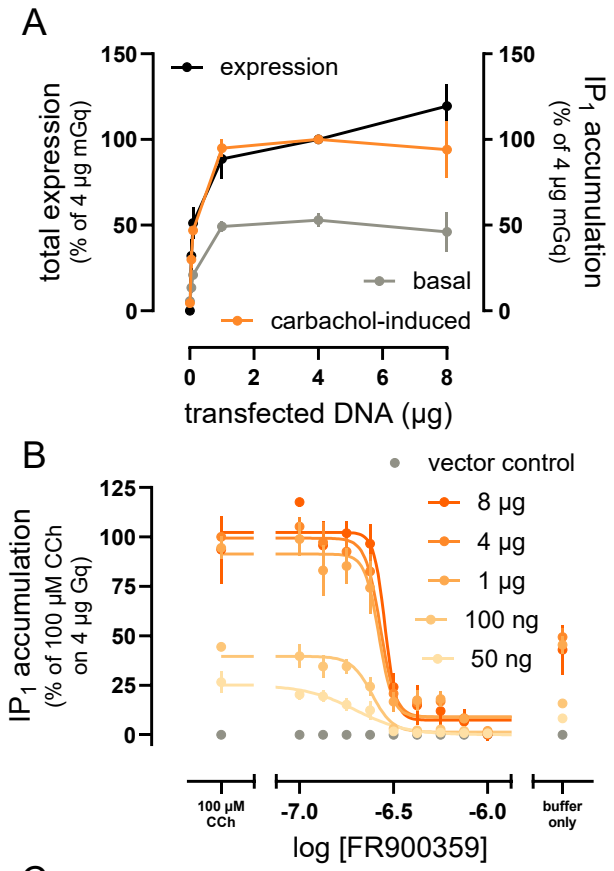

C

	50 ng	100 ng	1 µg	4 µg	8 µg
$logIC_{50}$ ± SEM	6.70 ± 0.05	6.62 ± 0.02	6.58 ± 0.02	6.57 ± 0.01	6.55 ± 0.02
Hill slope ± SEM	-3.22 ± 0.95	-7.92 ± 2.39	-11.70 ± 3.65	-10.91 ± 2.15	-14.57 ± 6.37

Figure 61: Steepness of FR900359 (FR) concentration-inhibition curves is dependent on the amount of mGαq present.
A. *Basal and agonist-induced IP_1 accumulation depends on expression levels of mGαq. Total expression was determined using ELISA in permeabilized HEK293 cells lacking Gαq and Gα11 proteins after CRISPR/Cas9 treatment (HEK293 Gq/11-KO) transiently transfected with increasing amounts of mGαq DNA. IP_1 accumulation was measured after incubation with buffer or 100 µM carbachol (CCh). Data are the means ± SEM normalized to the results with 4 µg transfected mGαq DNA of two to four independent experiments performed in triplicate.* ***B.*** *FR concentration-response curves after pre-incubation with FR and stimulation with 100 µM CCh. Data are the means ± SEM normalized to the effect of 100 µM CCh on cells transfected with 4 µg mGαq DNA of one to four independent experiments performed in triplicate.* ***C.*** *Table summarizing $logIC_{50}$ ± SEM and hill slope values ± SEM of the FR concentration-response curves shown in B.*

This unintentional rescue effect provided a first indication that our hypothesis of solely Gq inhibition-mediated lethality is correct but also underlined the necessity for careful selection of FR concentration in the final FR feeding experiments with DGαq mutant-expressing fly lines. We chose an intermediate concentration of 80 µM which should result in intermediate survival rates and constituted a compromise between a sufficiently lethal effect, and economical and technical considerations.

The survival rates of the control “driver” and all “reporter” fly lines displayed the same susceptibility to FR treatment over the course of six days and tolerated

corresponding amounts of DMSO (Figure 62A). Even though there was no direct intra-assay comparison to wild-type *w*^{1118} flies, the survival of 10 to 20 percent on day six was within the expected range for 80 µM FR treatment.

Actin-GAL4>UAS-DGq WT and *actin-GAL4>UAS-DGq IW* flies showed only a slight rescue to 27 and 36.7 percent survival, respectively, while not being influenced by DMSO (Figure 62B$_{i}$ and B$_{ii}$). In contrast, overexpression of the double mutants VA IW and VS IW led to a strong and obvious rescue to survival rates of 64 and 78 percent, respectively (Figure 62B$_{iii}$ and B$_{iv}$).

These survival rates corresponded well to the gradual introduction of FR resistance in the mutants observed in cellular assays. The less sensitive but not entirely inhibitor-resistant single mutant DGαq IW caused a partial rescue only, whereas the entirely resistant double mutants DGαq VA IW and VS IW strongly increased survival rates over the control line flies.

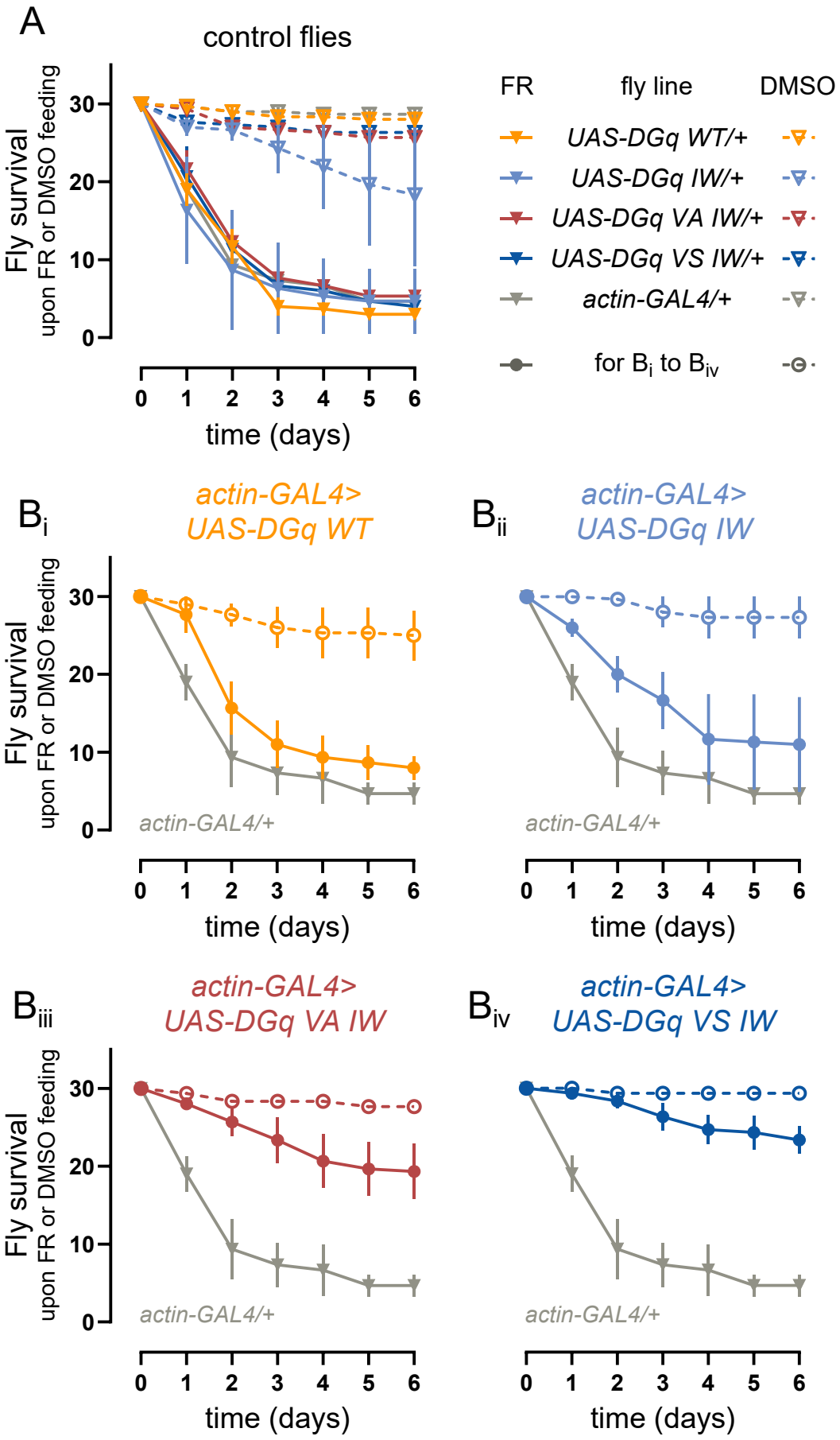
A
control flies
Fly survival
upon FR or DMSO feeding
30
20
10
0
0 1 2 3 4 5 6
time (days)
FR
fly line
DMSO
UAS-DGq WT/+
UAS-DGq IW/+
UAS-DGq VA IW/+
UAS-DGq VS IW/+
actin-GAL4/+
for Bi to Biv
Bi
actin-GAL4>
UAS-DGq WT
actin-GAL4/+
Bii
actin-GAL4>
UAS-DGq IW
actin-GAL4/+
Biii
actin-GAL4>
UAS-DGq VA IW
actin-GAL4/+
Biv
actin-GAL4>
UAS-DGq VS IW
actin-GAL4/+

Figure 62: Overexpression of FR-insensitive DGαq mutants rescues FR-induced lethality in Drosophila melanogaster.
A. *Control "driver" (light grey) and "reporter" (color) fly lines were kept on food laced with 80 µM FR (filled triangle) or the corresponding amount of DMSO (closed triangle). Survival of flies was recorded for six days. Data are the means ± SEM of three independent biological replicates performed with 30 adult flies (20 female, 10 male).* ***B$_{i-iv}$.*** *Fly lines overexpressing DGαq wild type or FR-resistant mutants were kept on food laced with 80 µM FR (filled circle) or the corresponding amount of DMSO (open circle). Survival curves of the "driver" control line on FR-laced food are shown as comparison (light grey). Survival of flies was recorded for six days. Data are the means ± SEM of three independent biological replicates performed with 30 adult flies (20 female, 10 male).*

In conclusion, these data unequivocally demonstrate that the lethality induced by the inhibitor FR in *Drosophila melanogaster* upon ingestion is solely mediated by inhibition of DGq. Rescue of inhibitor-induced lethality by simple overexpression of FR-resistant DGq isoforms established a causal link between DGq inhibition and compound toxicity, strongly suggesting complete specificity and lack of off-target effects.

5.6. Transfer of results to mGαq

The combination of an inhibitor with remarkable specificity *in vitro* and *in vivo* such as FR with mutated resistant target proteins such as the *Drosophila* Gαq mutants presented in this thesis is a valuable tool for establishing causal relationships in cell biology. A similar tool would be of great interest in a murine background, as mice are a more commonly used model organism. Since the mGαq sequence is identical to the human Gαq sequence in all but one residue (Dong et al., 1995), GPCR research with mGq in mice or *in vitro* might be more translatable to human physiology than research in *Drosophila melanogaster*. Therefore, we proceeded with the development of murine FR-resistant Gαq variants.

The sequence of *Drosophila melanogaster* and murine Gαq is 85% identical with the main differences located in helix A and B of the helical domain (Figure 66 in Additional Material). In the FR binding site, there is only a two-residue difference that has little impact on FR sensitivity (see Chapter 1.9. *Drosophila melanogaster* Gαq isoform G in the introduction). Therefore, we deemed transferring the knowledge gained during the generation of *Drosophila* Gαq mutants back to murine Gαq a worthwhile approach (Figure 63A).

We first introduced the successful mutations VA IW and VS IW as individual single mutations into the murine Gαq protein. The original amino acids at these positions are the same as in *Drosophila* Gαq (Figure 63A). Notably, the residue numbering in mGαq, which contains a six-residue N-terminal extension, is shifted by six positions relative to DGαq. The resulting mutants are I190W, V184A, and V184S. We also included the valine-to-methionine mutant V184M. The VM IW mutation has not been used for *Drosophila in vivo* work due to residual FR sensitivity at high concentrations and lower signaling amplitudes. However, we included the mutation in the mouse Gαq mutagenesis as the results could differ. mGαq IW and VM have already been

generated and investigated previously (Malfacini et al., 2019; Patt et al., 2021), allowing us to compare results to already published findings.

We decided to evaluate the mGαq single mutants in comparison to wild-type mGαq in the Gβγ/masGRK3ct BRET assay only, to get a first indication of their signaling behavior and sensitivity to FR. Basal BRET ratios revealed equivalent quenching when plasmid DNA coding for wild type and single mutants was transfected, indicating equal Gβ1γ2 binding when similar expression levels are assumed (Figure 63B). Similarly, the signaling behavior upon activation of the G proteins by ligand-bound receptor was not altered by the introduction of single mutations as evident from the unchanged efficacies and potencies extracted from the recorded carbachol concentration-response curves (Figure 63C and E). Surprisingly, only the isoleucine-to-tryptophan (IW) mutation reduced FR sensitivity approximately 10-fold (Figure 63D and E). The reduction of inhibitor sensitivity of mGαq IW compared to wild type is markedly lower than the effect of the equivalent mutation in the *Drosophila melanogaster* Gαq protein in the same assay setup (> 50-fold reduction, see Chapter 5.3. FR sensitivity).

The initial FR sensitivity of wild-type *Drosophila melanogaster* Gαq, in contrast, was two- to three-fold lower compared to murine Gαq. This shift was reliably recapitulated when the two residues that differ between the FR binding sites of the two proteins were transferred from DGαq to mGαq (Alenfelder, 2019) (see Figure 10). Considering this, the discrepancy in the effect of the IW mutation on both proteins highlights that inhibition by FR is influenced by more residues than just those that have been implicated in inhibitor binding. The entire G protein architecture including the conformation of secondary structure elements may influence the inhibitor properties of FR.

In contrast to IW, mutating valine-184 to alanine, serine, and methionine did not alter the potency of FR inhibition (Figure 63D and E). Since single mutations of valine$^{GhfS2.3}$ have not been characterized in DGαq, these findings could not readily be compared. Nonetheless, we could compare the sensitivity data with published results on mGαq IW and VM (Malfacini et al., 2019; Patt et al., 2021). In these publications, reduction in inhibitor sensitivity is measured in DMR assays and produces higher rightward shifts for both mutants compared to our results (16- and 2-fold, respectively). This does not represent a discrepancy but underlines once again that signaling amplification in the assay of choice influences both pIC_{50} values and apparent potency shifts caused by mutations (see Chapter 5.3. FR sensitivity).

In *Drosophila* Gαq, the combination of the IW mutant with mutations of valine$^{GhfS2.3}$ markedly increased resistance to FR over IW alone (see Chapter 5.4. Second generation of DGq mutants). We were interested in investigating if the combination of a mutation that reduces FR sensitivity about 10-fold (mGαq IW) with mutations

that do not influence inhibitor sensitivity at all (mGαq VA, VS, and VM) would lead to a synergistic effect as has been observed before (Malfacini et al., 2019; Patt et al., 2021) and if such a synergistic effect would be large enough to recapitulate the full FR resistance introduced into DGαq in this way.

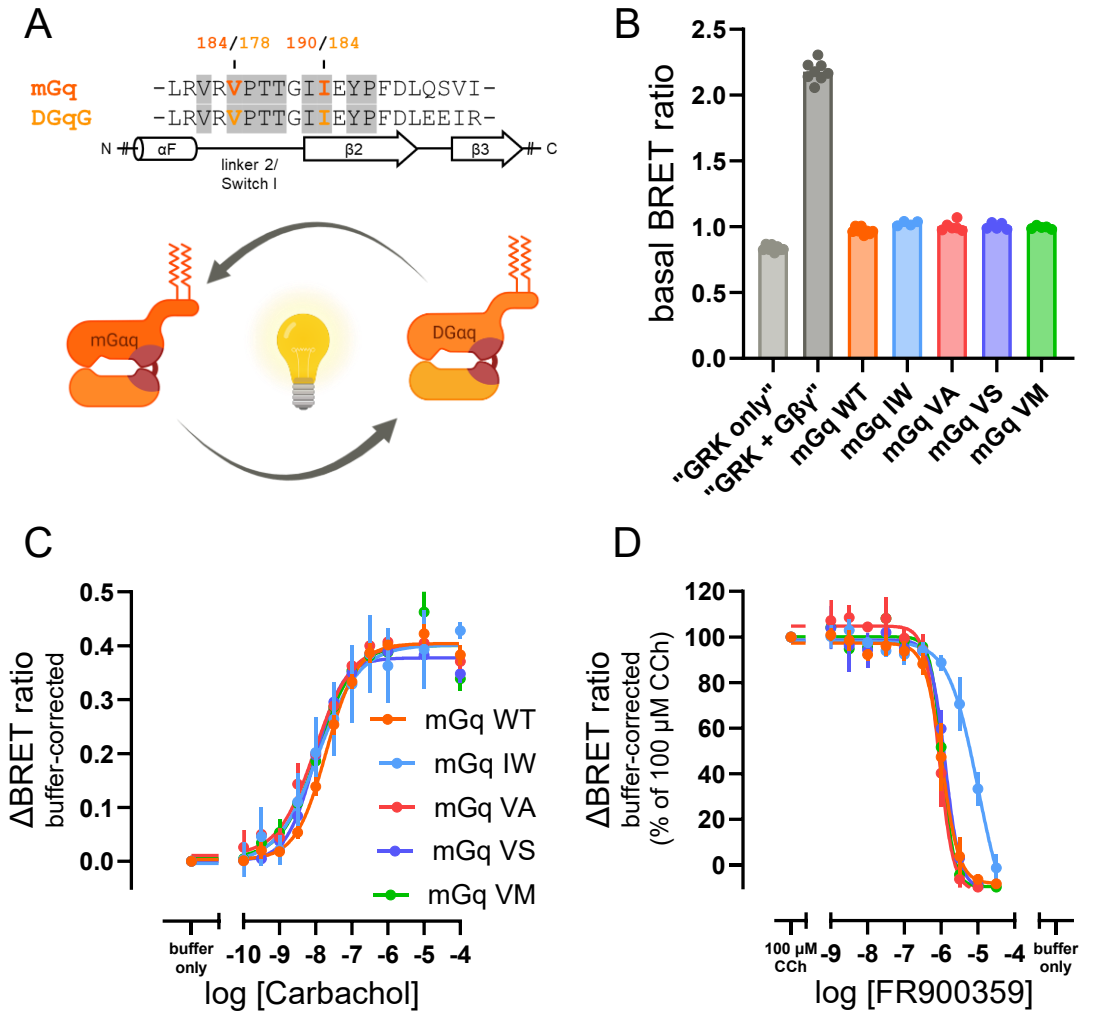

E	mGq WT	mGq IW	mGq VA	mGq VS	mGq VM
Carbachol $logEC_{50}$ ± SEM	7.71 ± 0.07	8.09 ± 0.16	8.01 ± 0.13	8.01 ± 0.07	8.03 ± 0.13
FR $logIC_{50}$ ± SEM	5.95 ± 0.12	5.11 ± 0.12	6.05 ± 0.08	5.89 ± 0.04	5.97 ± 0.06

Figure 63: Mouse Gαq single mutants show wild-type properties and are predominantly FR900359 (FR)-sensitive.
A. *Insights gathered with Drosophila Gαq are used to develop FR-resistant murine Gαq mutants. Partial alignment of the FR binding site of murine and Drosophila Gαq. Mutated residues are highlighted and numbered in orange (mouse) and light orange (Drosophila). Residues involved in FR binding are highlighted in grey (Nishimura et al., 2010). Secondary structural elements are depicted below the sequence with cylinders (α-helices) and arrows (β-sheets). The panel was partially created with BioRender.com.* ***B.*** *Basal BRET ratio measured in HEK293T cells transiently transfected with constructs coding for M3R, and split Venus-tagged Gβγ, masGRK3ct-NLuc, mGαq isoforms as indicated, and Ric-8A. Bar graphs represent the means ± SEM of four to eight biologically independent experiments performed with Dr. Sophie Steinmüller (formerly Kostenis lab, University of Bonn). Data points represent individual replicates.* ***C.*** *Carbachol (CCh) concentration-response curves measured as buffer-corrected BRET ratio after stimulation with CCh in cells transfected as in A. Data*

are the means ± SEM of four to seven biologically independent experiments performed with Dr. Sophie Steinmüller (formerly Kostenis lab, University of Bonn). ***D.*** *FR concentration-response curves measured as buffer-corrected BRET ratio after preincubation with FR and stimulation with CCh in cells transfected as in A normalized to the effect of 100 µM CCh. Data are the means ± SEM of three to seven biologically independent experiments performed with Dr. Sophie Steinmüller (formerly Kostenis lab, University of Bonn).* ***E.*** *Table summarizing pEC_{50} values ± SEM of the CCh concentration-response curves shown in C and pIC_{50} values ± SEM of the FR concentration-response curves shown in D.*

Therefore, we generated double mutants of I190W and each of the valine-184 mutations resulting in mGαq VA IW, VS IW, and VM IW. We similarly characterized these new mGαq double mutants in the Gβγ/masGRK3ct BRET assay investigating mGαq FIVE in parallel. This mutant has already been characterized in the DMR assay (Malfacini et al., 2019) and shows residual FR sensitivity at high concentrations. In addition, we were interested in evaluating the performance of the FIVE mutant in this BRET assay setup compared to double mutants generated based on the DGαq findings.

Analysis of basal BRET ratios demonstrated wild type-equivalent Gβγ binding of all double mutants and mGαq FIVE (Figure 64A) under the assumption of wild type-equivalent expression. Carbachol concentration-response curves were shifted to slightly higher potencies (Figure 64B and D) similar to but less pronounced than in the corresponding DGαq mutants (3- to 3.5-fold vs. 4- to 5-fold). This smaller shift might translate to a smaller impact of the mutations on RGS protein modulation. However, the murine protein has almost the same sequence as human Gαq (Dong et al., 1995) and altered interaction with human modulator proteins could, therefore, be of more consequence. This informed speculation needs to be corroborated with kinetic experiments in the future.

More importantly, FR sensitivity of all mGαq isoforms was highly compromised by the introduction of the selected mutations (Figure 64C and D). As expected from published experiments (Malfacini et al., 2019), mGαq FIVE retained low residual inhibition by FR at high concentrations. Interestingly, the combination of I190W and the valine mutations led to astonishing synergistic effects, entirely abolishing any response to the inhibitor for VS IW. Similarly to the findings in DGαq, FR sensitivity of VM IW was most retained among the double mutants but still limited to the highest concentration of FR used. The magnitude of VM IW's shift is remarkable, as the combination of VM with another mutation at the same position, I190N, only causes a 9-fold shift (Malfacini et al., 2019) in the more sensitive DMR assay in which fold-changes are usually higher. In line with this, comparing the single I190W and I190N in the DMR assay already reveals different effect on FR sensitivity with a 16- and 3-fold change, respectively (Malfacini et al., 2019; Patt et al., 2021). This, in combination with the differential effect of VM, VS, and VA, highlights that not only the chosen position but also the introduced residue tremendously impacts FR sensitivity.

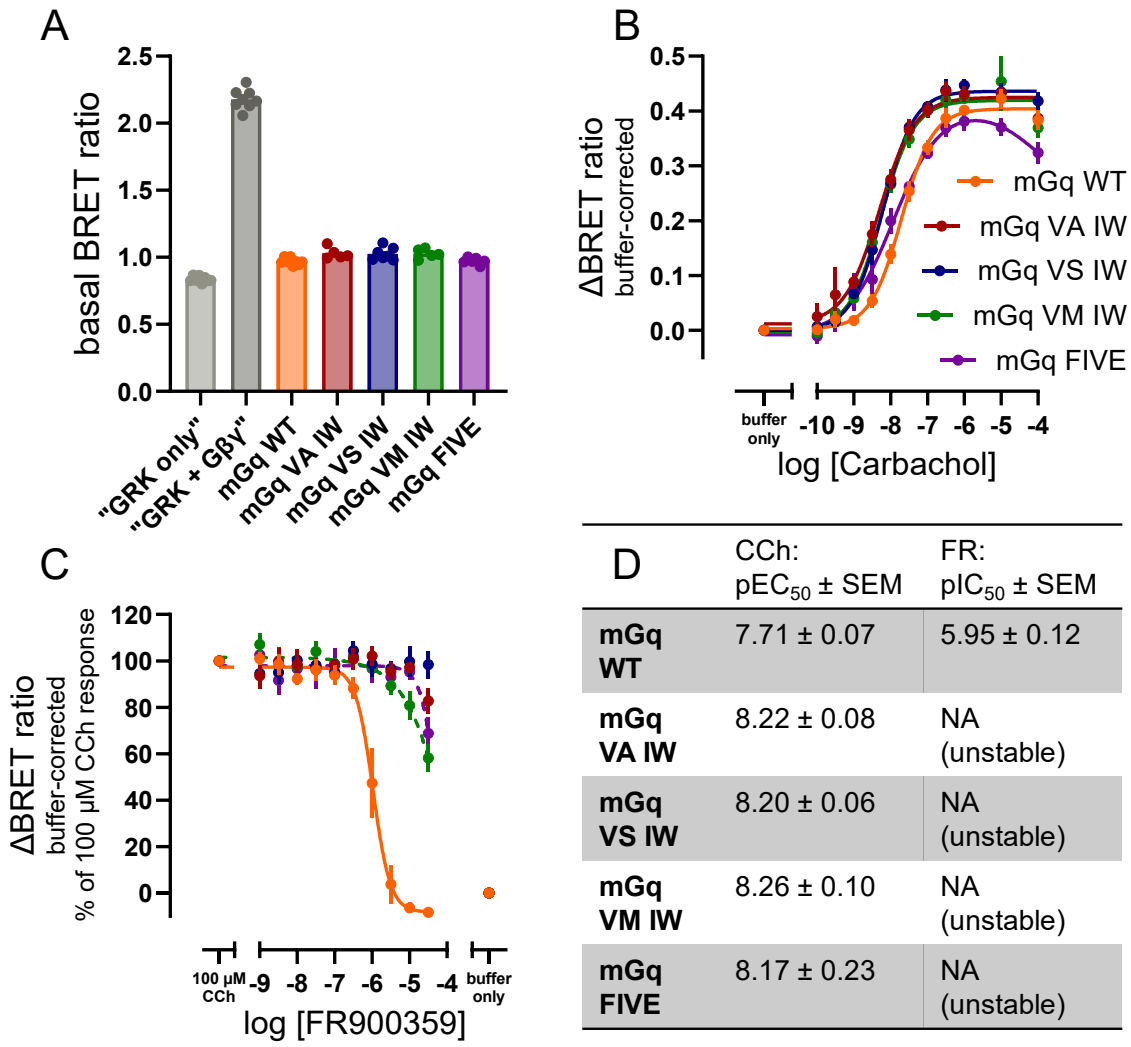

D	CCh: pEC_{50} ± SEM	FR: pIC_{50} ± SEM
mGq WT	7.71 ± 0.07	5.95 ± 0.12
mGq VA IW	8.22 ± 0.08	NA (unstable)
mGq VS IW	8.20 ± 0.06	NA (unstable)
mGq VM IW	8.26 ± 0.10	NA (unstable)
mGq FIVE	8.17 ± 0.23	NA (unstable)

Figure 64: Mouse Gαq double mutants and mGαq FIVE show wild-type properties and are FR900359 (FR)-resistant.
A. *Basal BRET ratio measured in HEK293T cells transiently transfected with constructs coding for M3R, and split Venus-tagged Gβγ, masGRK3ct-NLuc, mGαq isoforms as indicated, and Ric-8A. Bar graphs represent the means ± SEM of five to eight biologically independent experiments performed with Dr. Sophie Steinmüller (formerly Kostenis lab, University of Bonn). Data points represent individual replicates.* ***B.*** *Carbachol (CCh) concentration-response curves measured as buffer-corrected BRET ratio after stimulation with CCh in cells transfected as in A. Data are the means ± SEM of three to seven biologically independent experiments performed with Dr. Sophie Steinmüller (formerly Kostenis lab, University of Bonn).* ***C.*** *FR concentration-response curves measured as buffer-corrected BRET ratio after preincubation with FR and stimulation with CCh in cells transfected as in A normalized to the effect of 100 µM CCh. Data are the means ± SEM of three to seven biologically independent experiments performed with Dr. Sophie Steinmüller (formerly Kostenis lab, University of Bonn).* ***D.*** *Table summarizing pEC_{50} values ± SEM of the CCh concentration-response curves shown in B and pIC_{50} values ± SEM of the FR concentration-response curves shown in C. Data for "GRK only", "GRK + Gβγ", and mGαq WT were copied from Figure 63 for clarity.*

The transfer of the two mutation combinations that rendered DGαq FR-resistant yielded equally FR-resistant mGαq mutants that can be employed *in vitro*. Although a comprehensive functional characterization of the mGαq mutants is still pending, the improvement over the already published inhibitor-insensitive mGαq mutant FK IW (Patt et al., 2021) is already clear: mGαq VS IW and VA IW seemed to retain wild-type functionality. This provides a significant advantage over FK IW which displayed reduced signaling capabilities due to compromised expression and

localization. This also disqualifies mGαq FK IW from usage *in vivo*. In contrast, mGαq VS IW and VA IW might well be used for the generation of transgenic animals if a comprehensive analysis confirms wild-type functionality. Possibly, a reselection of mutations will be necessary to retain proper acceleration of deactivation by RGS proteins. *In vivo* experiments in mice using FR-insensitive mGαq mutants pose an additional challenge compared to *Drosophila melanogaster*. As FR inhibits Gq, G11, and G14 proteins, engineered inhibitor-resistant Gα11 and Gα14 mutants are required for unambiguous interpretation of experiments.

In conclusion, we developed not only FR-insensitive *Drosophila* Gαq variants but also succeeded in transferring these positive results back to murine Gαq. Both sets of mutants in combination with the specific and selective inhibitor FR are tools for the causal investigation of Gq-mediated or -modulated signaling events *in vitro* and additionally *in vivo* in case of *Drosophila melanogaster*.

6. Discussion

The Gq/11 protein inhibitor FR900359 is a tremendously important pharmacological compound in GPCR research due to its specificity, potency, and ease of use. In this study, we aimed to leverage FR's specificity for the development of a chemogenetics-like tool consisting of the inhibitor and an inhibitor-insensitive Gq protein mutant for the application *in vitro* and in the model organism *Drosophila melanogaster*. We substituted two key inhibitor binding residues by rational design to generate *Drosophila* Gαq V178A I184W and V178S I184W. These two double mutants combine wild-type behavior in all relevant aspects tested with remarkable resistance towards FR. Introduction of the mutants into *Drosophila melanogaster* produced healthy flies and relieved the inhibitor-induced lethality in FR feeding experiments, thereby demonstrating the applicability of the tool for causal investigations *in vivo*. Furthermore, we developed the analogous murine Gαq variants V184A I190W and V184S I190W which likewise constitute wild type-like, FR-resistant Gαq proteins. The application of these murine counterparts *in vivo* can be realized in further studies.

6.1. Characterization of DGαq mutants in HEK293 cells

Before employing the selected mutants *in vivo*, we thoroughly characterized their behavior in a set of cell-based assays ultimately confirming wild type-like signaling behavior and resistance to FR. Successful functional expression of *Drosophila* Gαq isoform G enabled investigations in the human HEK293 cell system. In parallel to the investigations detailed in this work, we set out to establish a *Drosophila* Schneider 2 (S2) cell culture in the lab. S2 cells are a semi-adherent, late-stage embryo-derived cell line developed in 1972 (Schneider, 1972). This cell line impresses with its transfectability and has even been proposed as an alternative to mammalian cell lines to study human GPCR signaling based on their ease of culture and genetic tractability (Salim et al., 2024). Using a *Drosophila*-derived cell line to investigate the signaling of the DGαq mutants generated in this project is obviously advantageous, as these cells better simulate the *Drosophila in vivo* environment and provide *Drosophila* receptor, effector, and other interacting proteins. However, endogenous DGαq proteins might hinder the accurate interpretation of data, and all signaling assays, that are well established and used routinely in our lab for HEK293 cells, would need to be validated and established for *Drosophila* S2 cells first.

Even though S2 cells are known for their ease in handling, we failed in setting up initial experiments with this cell line. Even after thorough optimization, the transfection efficiency with polyethylenimine and lipofectamine was low when transfecting green fluorescent protein (GFP). We finally decided to limit the investigations to the HEK293 cell background. This allowed us not only to use HEK293 Gq/11-KO cells, in which the response could be attributed to exogenous

Gq protein only, but also to draw back on already established assay systems. This way, we assured specific investigation of the *Drosophila* Gq protein in question circumventing background responses from endogenous human Gq protein. Furthermore, our results confirmed the overall suitability of the human HEK293 cell line for investigations of foreign-species G proteins (Alenfelder, 2019; Hanke et al., 2023).

The assays we selected to investigate the DGαq mutants' behavior were chosen with the objective of comprehensively covering the G protein signaling cascade and investigating all main features that define a G protein. However, G proteins are complex in their function and regulation, and multiple additional experiments to investigate further G protein characteristics can be imagined. Without doubt, the most interesting addition would be assays to support the IP_1 accumulation data in this thesis. While the results match the observations from the other readouts, improved data quality could increase our confidence in the interpretation. For instance, the reproducibility of the results between assays might have benefitted from coexpression of the G protein chaperone Ric-8A as has been demonstrated in the Gβγ/masGRK3ct BRET assay. Furthermore, a complementary assay could be used to confirm the results and possibly add kinetic information about second messenger production. One such option is the intramolecular BRET-based IP_3 biosensor (Gulyás et al., 2015) which is well established for the investigation of Gq activation and could even be used in conjunction with M3R to directly correlate results to the IP_1 accumulation experiments.

In addition, downstream results of IP_3 production, such as $calcium^{2+}$ release from the endoplasmic reticulum, or the second leg of the signaling cascade initiated by PLCβ-mediated PIP_2 conversion, i.e. DAG-mediated activation of protein kinase C isozymes, could be investigated more directly than via changes in cell morphology, for example using a fluorescent reporter (Violin et al., 2003). Furthermore, other Gq-initiated pathways apart from PLCβ activation such as the activation of RhoA (Vogt et al., 2003) or the transactivation of epidermal growth factor receptor (EGFR) after activation of metabotropic glutamate receptors (mGluRs) (Daub et al., 1997; Yang et al., 2006) could be investigated.

To support the claims of wild type-like intrinsic activity suggested in this thesis, one could further investigate the DGαq protein mutants regarding basal GDP exchange rates or in GTP binding experiments. These questions can be investigated with a modified version of the Gβγ/masGRK3ct BRET assay setup using permeabilized and nucleotide-controlled cells. In the hopes of adding valuable information that can be used for the publication resulting from this project, a modified assay setup is currently being established by the master's student Lorenzo Volontè in the lab.

During our investigations, we detected subtle differences in the mutants' deactivation kinetics in the Gβγ/masGRK3ct BRET assay. We followed up by directly investigating the mutants' sensitivity to human RGS proteins, albeit qualitatively. The observed slight resistance to the GAP activity of one of the RGS proteins tested is sufficient to explain the reduced rate of inactivation. However, it needs not be the exclusive reason for the generated data. A possible additional reason could be a change in intrinsic GTPase activity. Such an alteration of the G proteins properties would be more relevant to *Drosophila in vivo* work than the sensitivity to human RGS proteins and should be investigated, for example using the GTPase Glo assay (Mondal et al., 2015), before using DGαq mutants more intensely *in vivo*. As this assay requires the purification of DGαq wild type as well as mutant proteins, we consider it to extend beyond the scope of this project.

Interestingly, when comparing the effects of CCh and FR on the same Gαq protein variants between the different assays, shifts in both compounds' potencies became apparent. Similarly, the fold-reduction in inhibitor potency caused by mutations also varied between assays. Noticeably, the potency shifts of the DGαq double mutants cannot be compared between assays, as the pIC_{50} values could not be calculated. Similar differences in potency in different assays have been observed before for FR (Hanke et al., 2023; Patt et al., 2021; Schrage et al., 2015) but also for other compounds (Brands et al., 2024; Krebs et al., 2018). At first, these shifts might seem surprising but can be easily attributed to the spatial and temporal distance from the signal initiation, as well as the extent of signal amplification.

6.2. *In vivo* experiments

Apart from all possible experiments to extent the investigation of the engineered DGαq double mutants, we deemed the generated double mutants of DαGq, VA IW and VS IW, sufficiently wild type-like for their initial employment *in vivo*. To investigate their overall suitability, the FR-resistant DGαq mutants developed in this thesis have been introduced ubiquitously into *Drosophila melanogaster* using the GAL4/UAS system. Expression of mutant constructs rescued inhibitor-induced lethality upon ingestion.

To ensure this effect is based on the insensitivity towards FR and not due to any other changes in fly physiology, we performed negative geotaxis assays that monitor a complex climbing instinct necessitating the regular function of a plethora of different cell types and signaling cascades. We chose to monitor the climbing pass rate, that is the number of flies passing a certain climbing height in a certain amount of time and did not notice any aberrant behavior in flies ubiquitously overexpressing DGαq wild type or FR-resistant mutants. A more sensitive endpoint in this assay to determine more subtle alterations in behavior would be to measure the average climbing height in a set time instead of the pass rate (Nichols et al., 2012).

Naturally, the negative geotaxis assay provides only a very broad and superficial readout for the flies' health and overall intact physiology. We deemed this readout sufficient and fitting for the straightforward genetic approach chosen to introduce the engineered DGαq mutants into *Drosophila melanogaster*. For further experiments, we recommend introducing the mutations into the endogenous gene locus, for example using the CRISPR/Cas9 technique (Bassett et al., 2013; Gratz et al., 2014) to substitute all endogenous splice variants for mutated FR-resistant versions. For this more intricate genetic manipulation, we deem a more thorough investigation of fly health necessary, especially regarding physiological functions that are mediated via DGq such as phototransduction (Gu et al., 2020; Hardie & Juusola, 2015; Y. J. Lee et al., 1994; Scott et al., 1995), axonal pathfinding in the *Drosophila* ventral nerve chord (Ratnaparkhi et al., 2002), energy homeostasis and lipid storage (Baumbach et al., 2014), forgetting (Himmelreich et al., 2017), nociception (Herman et al., 2018), and wing disk development (Brodskiy et al., 2019).

Apart from demonstrating the overall applicability of the chemogenetics-like, engineered DGαq isoforms *in vivo*, a few other observations in the FR feeding experiments are noteworthy and coincide with open questions about the ecological significance of the compound. For one, the mechanism behind FR lethality in *Drosophila melanogaster* has not yet been resolved. The effect the inhibitor has on various physiological functions in mammals has been characterized or can be derived from effects of Gαq knock-out for example in mice. This includes the reduction of blood pressure and heart rate after subcutaneous injection in mice and subsequent death of the animal (Meleka et al., 2019). In contrast, DGq has mainly been implicated in less directly vital processes such as visual perception (Y. J. Lee et al., 1994), forgetting (Himmelreich et al., 2017) or nociception (Herman et al., 2018), and in developmental processes (Brodskiy et al., 2019; Ratnaparkhi et al., 2002). However, published data suggest that DGq might also be involved in *Drosophila* cardiac regulation. Several neurotransmitters influence the heart rate in *Drosophila* (Zornik et al., 1999), among them octopamine, dopamine, and acetylcholine, all of which at least partially signal via Gq (Černe et al., 2025; Hana & Lange, 2017; Himmelreich et al., 2017; Ren et al., 2015). An influence of FR on the cardiac function might be a reason for the inhibitor-induced lethality in *Drosophila melanogaster* that could be investigated in the future.

The exact modulation of vital functions by FR in *Drosophila melanogaster* could conveniently be addressed by employing the chemogenetics-like tool developed in this study, for instance by creating a library of fly lines ubiquitously expressing an FR-insensitive mutant apart from one specific tissue in which DGαq wild type is expressed and assaying these fly lines in FR feeding experiments. This way, the contribution of specific tissue functions to the lethal effect of the inhibitor could be

broken down. These results might also reveal why *Drosophila* flies die with a delay of up to six days upon FR ingestion.

Interestingly, there seems to be a correlation between the complexity of the organism and the necessity of Gq signaling for survival. Individual cells, the simplest unit of human life, such as HEK293 cells, cope well with a knock-out of Gαq proteins (Schrage et al., 2015) and are even viable when all Gα subunits are knocked out (Hisano et al., 2019). Less complex organisms, such as the nematodes *Caenorhabditis elegans* and *Heterodera schachtii*, somewhat tolerate loss-of-function mutation or inhibition of Gq family proteins by FR in their adult stage but show abnormal behavior and impediments to Gq-dependent functions such as egg laying (Brundage et al., 1996; Hanke et al., 2023). A homozygous defect of Gq functionality still allows *C. elegans* to hatch but severely impairs development and is mostly lethal for larvae (Brundage et al., 1996). To *Drosophila melanogaster* and *Riptortus pedestris* the feeding of FR in the adult stage is lethal, albeit with a delay of several days even at high concentrations (Crüsemann et al., 2018).

In contrast, mice die within a few hours after subcutaneous injection of FR (Meleka et al., 2019). While Gαq and Gα11 seem to function mostly interchangeable in adult mice, there are pronounced differences in development. A homozygous knock-out of Gα11 is not phenotypically different from wild type, demonstrating that Gαq is sufficient to compensate for a lack in Gα11. In contrast, a full Gαq knock-out is generally viable but manifests in ataxia and increased bleeding times, which also increases the rate of death of pups shortly after birth (S. Offermanns, Hashimoto, et al., 1997; S. Offermanns, Toombs, et al., 1997). One single allele of either Gαq or Gα11 is sufficient for fetal development but pups die shortly after birth, possibly due to malformation of the heart and abnormal lung function. Malformations of the heart are also the cause of the lethality of homozygous Gαq/11-KO mice *in utero* (S. Offermanns et al., 1998).

In summary, while cells lacking all Gα proteins are viable, *Drosophila melanogaster* needs functional Gαq for long-term survival, and complex organisms like mice fully depend on the presence of Gαq and death upon Gq protein inhibition is imminent. Gq family member proteins appear to be of varying importance to the vitality of different species, both in terms of development and in adulthood, and there seems to be a correlation between complexity and Gq dependence of the organism.

In parallel to the initial FR feeding experiments, we performed HPLC/MS analyses of survivor and victim flies. These experiments revealed a correlation between the amount of FR in the fly food and the amount present in victim flies (Figure 56). Survivor flies, however, contained considerably lower amounts of the inhibitor. These results raise the question of how it is possible that some flies do not contain FR after six days on inhibitor-containing food. Possible answers are that the flies did

not ingest the substance in the first place, or that they metabolized or excreted the substance at an increased rate. However, all these explanations are equally unlikely. Thorough mixing of the food during preparation all but excludes the possibility of non-FR-laced food patches in the vials. Furthermore, flies are unlikely to survive starvation for a period of six days, unless they have been selected for starvation resistance (Chauhan et al., 2021; Chippindale et al., 1996). Furthermore, even though fly larvae and adult flies have been shown to turn cannibalistic upon starvation, they seem to not be outfitted to devour uncut and uninjured *Drosophila* carcasses (Ahmad et al., 2015), ruling out cannibalism as an option for take-up of inhibitor-free nutrition. Similarly, enhanced metabolism or excretion in individual *Drosophila* flies seems somewhat unlikely, as all flies tested die during the six-day assay period when higher concentrations of FR are fed (Figure 55), leaving the question of the compound's absence in surviving flies unresolved.

6.3. Isoforms of the same story: on DGαq isoform D

As detailed in the introduction, there is only one gene coding for the *Drosophila* Gαq homolog but there are multiple splice variants, resulting in the expression of three structurally distinct Gαq isoforms in the fruit fly. As explained in the introduction, the efforts in this thesis concentrated solely on generating an FR-resistant variant for one of the isoforms. The primary reason for this is the difference in expression patterns between the variants and their differential involvement in physiology. Isoform G is ubiquitously expressed, while isoform D's expression is specific to the visual system and isoform C is only expressed in the male gonads. The second and more practical reason is the option to characterize isoform G and its mutants in the xenogeneic HEK293 cell system established in the lab, as this isoform seems to interact with the human versions of all other required signaling proteins.

While isoform D has been successfully expressed and activated in HEK293T/17 cells before (Himmelreich et al., 2017), we did not succeed in this regard (Figure 8). A thematically related project, that we were simultaneously working on, also required the expression of species-foreign Gαq proteins in human cells. During these investigations, we discovered that the coexpression of human M3 receptor and the Gq chaperone Ric-8A enables the functional expression of nematode Gαq proteins in HEK293 cells (Hanke et al., 2023). A foreign protein that does not readily exploit the available human signaling apparatus might require assistance with proper folding combined with elevated amounts of exogenously supplied receptor. It is entirely conceivable that functional expression of *Drosophila* Gαq isoform D could be similarly achieved.

This would enable the investigation of the FR sensitivity of this second *Drosophila* Gq isoform. The putative FR binding site of DGqD differs from murine Gαq in four positions. These include the same two differences that DGqG comprises and

additional changes of valine-182$^{G.hfs2.1}$ to alanine and isoleucine-190$^{G.S2.2}$ to leucine. A transfer of all four residue changes to murine Gαq reduces FR sensitivity by 16-fold in DMR assays (Alenfelder, 2019). This suggests that DGqD might be less sensitive to the inhibitor compared to isoform G.

However, in the *in vivo* experiments performed in this study, we did not replace the DGαq gene but merely overexpressed mutant DGαqG isoforms. We argue that exogenous FR-insensitive DGαq should be able to assume the physiological role of the inhibited endogenous wild-type DGαq in the FR feeding experiments. This hypothesis is somewhat supported by the rescue of inhibitor-induced lethality to about 80 % survival upon the expression of DGαq VS IW (Figure 62). Furthermore, our choice of expression system resulted in ubiquitous expression of the FR-insensitive DGαq mutants similar to the expression pattern of DGαqG. However, we cannot assume that this expression pattern also allows for the substitution of potentially FR-sensitive DGαqD. An assumption of the physiological functions of DGαqD by the exogenous mutants cannot be guaranteed.

DGαqD's expression is restricted to the visual system (Alvarez et al., 1996; Y. J. Lee et al., 1990). Its role in the signal transduction of vision in *Drosophila melanogaster* has been thoroughly investigated (Gu et al., 2020; Hardie & Juusola, 2015; Y. J. Lee et al., 1994; Scott et al., 1995). To determine whether DGαqD can be substituted by ubiquitous overexpression of DGαqG mutants, the relationship between visual perception of *Drosophila melanogaster* flies and oral intake of FR could be investigated, for example by exploiting vision-dependent phototaxis in a countercurrent distribution assay (Benzer, 1967). Regardless of whether visual signal transduction via DGαqD in FR-treated flies is still intact, it is unlikely that inhibited DGαqD has any influence on the survival in the FR feeding experiments, as isoform D's role is confined to the visual system and not vital (Cao et al., 2018).

6.4. Development of a chemogenetics-like toolbox

In this project, we suggest the future development of a chemogenetics-like toolbox to overcome the lack of G protein inhibitors for the causal investigation of cellular biology. Such a toolbox requires the design, genetic engineering, and thorough characterization of artificial isoforms with artificially introduced or abolished inhibitor sensitivity for each Gα protein subtype. In this study, we demonstrated the overall feasibility of such an undertaking by developing the first part of this toolbox, an artificially inhibitor-insensitive but otherwise wild type-like *Drosophila* Gαq protein. This thesis, thus, lays the foundation for the further development and implementation of the envisioned toolbox.

However, as evident from this thesis and previous work performed for the predecessor project (see Figure 70 in Additional Material), the development of G protein mutants is not necessarily as straightforward as one might hope but involves

trial and error. Even though we followed a rational design approach in the generation of DGαq VA IW and VS IW, the choice of residues to alter to remove FR sensitivity while maintaining wild type-like behavior is limited and the consequences of mutation are not easily anticipated. The FR binding site in Gαq, Gα11, and Gα14 is a highly functionalized portion of the protein which is fundamental for the tremendous efficacy of inhibition but also complicates any mutational efforts.

Considering the even greater challenge of introducing inhibitor sensitivity into naturally insensitive Gα proteins, using a rational design approach is almost beyond imagination. Even though G proteins have been studied for the greater part of five decades, it is doubtful if our knowledge is advanced enough to invent a *de novo* binding site for the inhibitors by mutation. The alternate and in this case more promising approach of grafting a Gαq-like FR binding site onto an insensitive protein inevitably runs the risk of simultaneously transferring other properties of the donor Gα subunit, such as domain opening kinetics or RGS sensitivity, or of otherwise altering protein characteristics (Boesgaard et al., 2020; Eryilmaz, 2023); unpublished work in the lab).

Possibly, one could exploit directed evolution approaches to function as an alternative to rational design or the transfer of the FR binding site. This approach has already been fruitfully employed in the budding yeast *Saccharomyces cerevisiae* for the generation of GPCR mutants with improved biochemical stability to increase purification yields for structural biology (Schütz et al., 2016). In *S. cerevisiae*, the baker's or brewer's yeast, a singular G protein is expressed which is responsible for transmitting pheromone signals to initiate mating via its Gβγ subunit (Leberer et al., 1997). This fact could prove useful for the development of a directed evolution approach for the generation of artificially FR-sensitive or -insensitive Gα subunits. This way, mutations are not limited to the known FR binding site but might also appear in different parts of the protein and could even compensate for the functional effects of mutations in the FR binding site via long-range allosteric effects. Using this approach, screening of mutant libraries would still be necessary, but the results could exceed what is possible with human knowledge and creativity.

6.5. Speculations on inhibitor development

Still, the envisioned chemogenetics-like toolbox for the investigation of G protein signaling only constitutes a temporary solution for the lack of inhibitors. With work published during the time of this project, the development or discovery of G protein inhibitors for Gα families apart from Gq seems to be more attainable. It stands to argue that more resources and efforts should be invested in the search for inhibitors rather than in the development of a chemogenetics-like toolbox, not least because this endeavor turned out to be less straightforward than initially anticipated.

Recent work by collaborators and our group published in Mühle et al. (2025) reveals further insight into the mechanism of action of FR and YM. Beyond their nature as GDIs, both inhibitors actively stabilize the heterotrimeric form of G11 by forming direct contacts with the Gβγ complex. These results can also be transferred to Gq. Although this property is not the determining feature distinguishing between “good” G protein inhibitors and those that are ineffective in cellular assays, it draws attention to the truly significant difference and caused us to propose a new classification of G protein inhibitors (Figure 65)

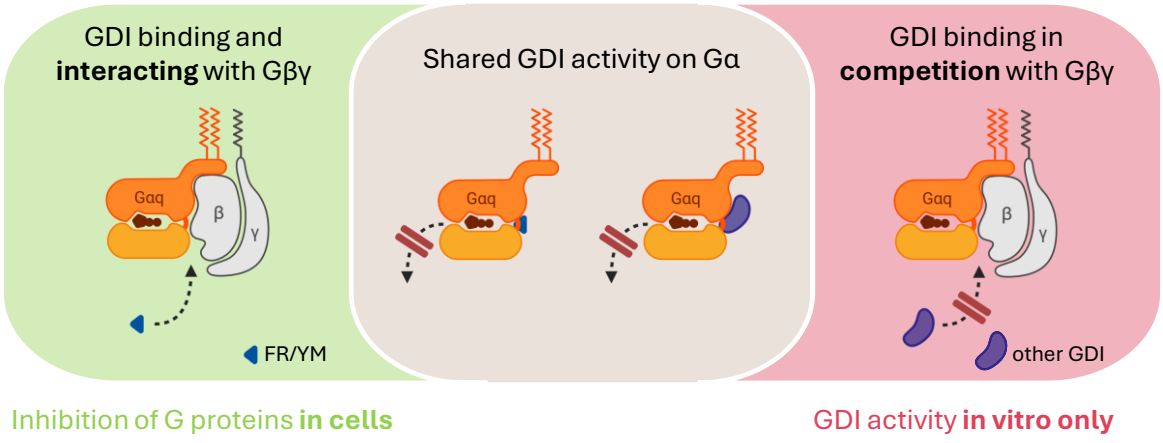

Figure 65: New classification of guanine nucleotide dissociation inhibitors (GDIs) in Mühle et al. (2025). *Functional G protein inhibitors such as FR900359 (FR) and YM-254890 (YM) and nucleotide state-specific binders share their GDI activity. However, only FR/YM-type inhibitors tolerate the simultaneous binding of Gβγ to Gα, allowing them to potently inhibit G protein signaling in cells and even in live animal. Other GDIs might compete with Gβγ which confines their action to the in vitro context. The figure is taken from Mühle et al. (2025) with color changes and was partially created with BioRender.com.*

This new classification draws attention to FR and YM’s ability to bind to functional Gαβγ heterotrimers in living cells. In contrast, nucleotide state-specific inhibitors such as those found in a screening of cyclic peptides binding to Gαs (Dai et al., 2022), while nicely preventing nucleotide exchange on purified proteins, fail to inhibit G protein signaling in cells, probably due to their inability to bind to intact heterotrimer and to displace the Gβγ complex from Gα. These recent developments illustrate that, while screening is more attractive than scaffold-based inhibitor design (Zhang et al., 2018), the method of screening needs to be adjusted. Instead of simply screening for nucleotide state-specific binders of Gα subunits, possible hits should also be able to bind the intact heterotrimer to confer their GDI activity.

Naturally, none of these thoughts take away from the utility of the engineered DGαq mutant/inhibitor pairs design herein as basis for a chemogenetics-like toolbox or, more importantly, as stand-alone tools.

6.6. DGαq mutant/FR pairs as a stand-alone tool

FR and YM are tool compounds that are well-established for the investigation of Gq-mediated or -modulated signaling responses. The chemogenetics-like Gαq isoforms

developed in this thesis will serve to supplement the use of these inhibitors *in vitro* and *in vivo*, as they enable causal investigation of Gq signaling.

Based on its longer commercial availability, YM is more widely used than FR, even though its kinetic properties make it less suitable for some, mostly long-term applications (Mühle et al., 2025; Jan Hendrik Voss, 2023). Although resistance of the Gαq mutants to YM was not directly tested in this thesis, they are most likely equally if not more resistant to YM compared to FR, as mutations in murine Gαq generally confer YM resistance more easily than FR resistance (Malfacini et al., 2019; Patt et al., 2021). Therefore, the DGαq mutants are probably also suited for work with YM.

The fact that the influence of FR and YM on various different signaling pathways, for example Gαs-mediated signaling (Peng et al., 2021) and Gi-Gβγ signaling (Gao & Jacobson, 2016), was readily attributed to unspecific action of the inhibitors rather than to contribution of Gq to the pathway in question clearly shows the need for tools to unambiguously delineate Gq involvement in signaling processes downstream of receptors that are not canonically classified as Gq-coupled.

Gq is involved or implicated in many physiological processes causing disease when dysregulated. Investigations into these processes have benefitted from the employment of FR and YM. Examples include diseases such as asthma in which FR induces airway relaxation (Matthey et al., 2017) or Gq-driven cancer (Annala et al., 2019; Onken et al., 2018). One limitation for the use of FR and YM in live animals is the inhibitor-induced lethality demonstrated in this study for *Drosophila melanogaster* but also for mice by others (Meleka et al., 2019). The combination of FR or YM with inhibitor-resistant murine or *Drosophila* Gq mutants enables the unrestricted use of FR and YM in transgenic live animals. This also circumvents possibly unwanted effects of FR treatment apart from death such as a reduction in blood pressure due to a relaxing effect on vascular smooth muscle cells (Meleka et al., 2019). This method, therefore, allows for simpler investigation but also for tissue-specific research.

Generation of a transgenic animal that expresses an inhibitor-resistant Gαq mutant instead of wild type ubiquitously apart from a single cell population in which the wild-type protein is expressed, enables cell type-specific investigations into Gq protein signaling. The advantage over tissue-specific knock-down or knock-out experiments is evident, as these experiments are strongly influenced by adaptive and compensatory processes such as changes in the expression patterns of other G proteins (Krumins & Gilman, 2006). Furthermore, while only chronic effects can be studied in knock-out experiments, the use of FR, which is expanded by the now available mutants, can capture acute reactions to the loss of Gq. The inhibitor allows the timed inhibition instead of a general lack of signaling in knock-out animals,

offering the possibility of dissecting Gq function in a cell type-specific manner, independent of adaptation or developmental alterations in a knock-out.

Of course, these new tools are also of use in *in vitro* studies. As demonstrated (Patt et al., 2021), inhibitor-resistant Gαq mutants can be used to probe the role of Gq and deconvolve Gq contribution to complex signaling networks. However, they also open an opportunity to investigate open questions about the inhibitors themselves. While FR and YM have generally been characterized as highly specific for Gq, G11, and G14 proteins, YM has also been suggested to mediate part of its anti-hypertensive effect by directly blocking L-type calcium channels (LTCCs) (Meleka et al., 2019). The murine inhibitor-resistant Gαq mutants could be used to directly address this claim. This is especially important, as it might reveal a superiority of FR in selectively investigating Gq-mediated signaling in cardiac physiology and might, therefore, be of direct consequence to the employment of FR and YM in future studies.

These are just a few speculations on how the chemogenetics-like Gαq protein-FR pairs developed in this thesis could be of use in the investigation of Gq-mediated or -modulated signaling. These speculations included the use of the murine FR-resistant Gαq mutants neglecting the fact that the inhibitor also exerts its effect on Gα11 and Gα14, and a direct employment of the mGαq double mutants is not as easily realized as demonstrated for *Drosophila melanogaster* in this thesis. At first glance, the generation of similar inhibitor-insensitive mutants for Gα11 and Gα14 seems necessary. However, it is doubtful if a transfer of the same residue changes from Gαq to Gα11 and Gα14 will yield the desired effect, especially considering that high sequence similarity and apparent functional interchangeability (S. Offermanns et al., 1998) of Gα subunits does not necessitate similar effects of the mutations introduced (see Chapter 6.7. DGαq/mGαq comparison below).

Employment of FR-resistant mGαq mutants in Gα11 knock-out mice might be a viable solution. Knock-out studies in mice show that a lack of Gα11 does not obviously alter mouse physiology (S. Offermanns et al., 1998), suggesting that mGαq is able to functionally replace Gα11 during development and in adult mice. The mGαq double mutants could, therefore, possibly be used in homozygous Gα11 knock-out mice. Even though this method does not allow unequivocal attribution of results to Gq as it most likely takes over the function of the missing Gα11 subunit and the effect of FR on Gα14 remains, at least in tissues in which Gα14 is expressed (Wilkie et al., 1991), but it allows tissue-specific causal investigations into Gq family protein signaling.

6.7. DGαq/mGαq comparison

One interesting observation that was not directly relevant to the progression of the project warrants discussion. The influence of the same mutation in the FR binding site on the FR sensitivities of murine and fly Gαq differs substantially in its extent.

As mentioned before, mouse and *Drosophila* Gαq share 85% of their sequence (see Figure 66 in Additional Material). Their behavior in the Gβγ/masGRK3ct BRET assay is very similar (Figure 71 in Additional Material). Both proteins bind Gβγ to a seemingly similar extent (Figure 71A in Additional Material), though the expression levels cannot be compared directly because the antibody binding affinity for both proteins is not known (Figure 24). Both proteins react very similarly to activation by carbachol-bound M3R regarding kinetics of activation (Figure 71B in Additional Material), as well as efficacy and potency (Figure 71C in Additional Material). The same is true for the proteins' behavior in the DMR assay (Figure 8). In addition to the activation behavior, the inhibitor sensitivity is remarkably similar, as not to say identical in both assays (Figure 71D in Additional Material and Figure 10). The negligible shift in FR potency in the DMR assay is faithfully recapitulated by two amino acid changes in mGαq that essentially introduce the FR binding site of DGαq, and can, therefore, be attributed to this two-residue difference only.

However, despite their strong similarities, the introduction of mutations unfavorable to FR binding has substantially different effects on the sensitivity towards FR. In murine Gαq the single IW mutant shifts the potency 7-fold in the Gβγ/masGRK3ct BRET assay (Figure 63) and 16-fold in the DMR assay (Patt, 2021). In contrast, when introduced into the DGαq protein, this mutation results in a 75-fold and 320-fold potency shift in these two assays, respectively. Unfortunately, the effect cannot be evaluated for the double mutants, as all of them are strongly FR-resistant precluding the calculation and comparison of pIC_{50} values. However, the data collected on the IW single mutant strongly suggests that differences in the protein beyond the FR binding pocket alone contribute to the affinity and/or the inhibitory effect.

This is further corroborated by already published findings on Gα13 (Todd et al., 2024). The constitutively active, chimeric Gα13/q Q226L mutant harbors a transplanted Gαq-like FR binding site in the Gα13 Q226L background. This is achieved through the exchange of eleven amino acids in Gα13 for their Gαq counterparts that directly or indirectly interact with the inhibitor. Interestingly, the chimeric G protein's influence on transcription is only partially susceptible to inhibition by FR. In contrast, FR fully and more potently inhibits Gα13/qSwap Q226L, in which the entire Gαq region accommodating the inhibitor is grafted onto Gα13 by transferring all secondary structure elements lining the FR binding site, i.e. helix 1, linker 1, helix A, helix F, linker2, β-sheet 2, and β-sheet 3. Still, FR is less potent on

Gα13/qSwap Q226L than on Gαq Q209L. This supports the findings on murine and *Drosophila* Gαq from this study and strongly suggests that not only the interacting residues but additionally the overall structural environment of the inhibitor matters for inhibition.

These findings also underline a point made earlier in this discussion: Directing FR sensitivity is more complex than the mere transfer of inhibitor-contacting residues. Since other parts of the G protein might be more involved in inhibitor action than currently imagined, even extensive knowledge of the residues directly involved in FR binding in Gαq, Gα11, and Gα14 might not be sufficient to rationally design mutants of other Gα subunits with satisfactory response to the inhibitor.

With regards to the project at hand, these findings could suggest that the development of an FR-insensitive Gα11 mutants might not benefit from the experience with murine and *Drosophila* Gαq as much as one might hope. Gαq and Gα11 are very similar in sequence, expression, and signaling, and can functionally compensate for each other (S. Offermanns, Hashimoto, et al., 1997; S. Offermanns, Toombs, et al., 1997; S. Offermanns et al., 1998; Simon et al., 1991; Strathmann & Simon, 1990; Wilkie et al., 1991). However, they should not be treated as the same protein. The results of a direct transfer of FR-resistant mutations in Gαq are impossible to predict.

7. Summary

“The depsipeptide natural product FR900359 […] has gained much attention as valuable pharmacological tool and promising therapeutic agent during the last years, because of its unique mechanism of action, the strong and selective inhibition of Gαq proteins.” (Hermes, 2021), as written by a former colleague at the Institute of Pharmaceutical Biology at the University of Bonn, Cornelia Hermes, four years ago. The direction of this trend has not changed in recent years. On the contrary, it has been reinforced by the increasing popularity of FR’s structurally near-identical sister compound YM. The relevance of both Gq inhibitors to fundamental research but also applied sciences in the GPCR research field can hardly be overstated.

It is of no surprise that similar inhibitors for the other G protein families are sought after both by derivatizing FR and YM and using compound library screening. Similarly, in an effort to better understand the mechanism of inhibitor binding and unlock pharmacologic inhibition of the other G proteins families, several projects to generate G proteins with artificial FR binding sites were launched (Eryilmaz, 2023; Malfacini et al., 2019; Onken et al., 2018; Patt et al., 2021; Todd et al., 2024).

These projects and their results lend themselves perfectly to the overarching idea of a chemogenetics-like toolbox consisting of inhibitor-compliant engineered G proteins with artificial FR binding sites. Such tools would perfectly compensate for the current lack of specific pharmacological inhibitors for the other G protein families. Furthermore, this approach would allow for conducting causal experiments *in vitro* and *in vivo*.

In this thesis, we aimed to establish the first complementary building block of this toolbox: FR-resistant Gαq variants that maintain wild type-like signaling properties. These mutants are necessary to restrict the results of any employment of FR in conjunction with FR-sensitive members of other G protein families to the chosen G protein only. In this respect, an FR-insensitive Gαq isoform acts as integral part of the proposed chemogenetic toolbox. Additionally, FR-insensitive Gαq could be employed in conjunction with FR as a stand-alone tool. This would allow for the cell type-specific employment of the inhibitor FR to causally investigate Gq protein-mediated and -modulated signaling events *in vivo*.

We selected *Drosophila melanogaster* as model organism for its genetic tractability that unlocks easy investigation of signaling cascades and approached this project with two complementary strategies known from previous mutational studies on murine Gαq (Malfacini et al., 2019; Patt et al., 2021). Firstly, we transferred the five differing residues of the putative FR binding site from Gα16 to *Drosophila* Gαq to simultaneously transfer its inhibitor resistance. Secondly, we generated two single DGαq mutants by rationally exchanging residues interacting with FR for unfavorable

amino acids. The three resulting DGαq mutants, FIVE, Y69K, and I184W, were subjected to a battery of functional assays to investigate their signaling behavior and FR sensitivity.

DGαq YK displayed a reduction in expression, an altered subcellular localization, and presumably resulting from this, a reduced response to carbachol in the Gβγ/masGRK3ct BRET assay. These results were not entirely surprising but mimicked previous findings for the analogous mutation in murine Gαq. DGαq FIVE demonstrated equivocal subcellular distribution in immunofluorescence microscopy. Furthermore, its deactivation kinetics were decelerated in HEK293T cells probably due to a partial insensitivity to human RGS proteins. As the objective of this project was the generation of wild type-like and inhibitor-resistant DGαq isoforms for employment *in vivo*, we excluded YK and FIVE from further investigations.

In contrast, DGαq IW behaved comparably to DGαq wild type regarding its expression and localization. Additionally, the potency, efficacy, and kinetics of activation were virtually identical to those of the wild-type protein on the levels of G protein dissociation, second messenger accumulation, and whole-cell response. Furthermore, DGαq IW displayed at least a 75-fold reduction in sensitivity to the inhibitor in all three assays tested and, therefore, met all requirements previously set.

We proceeded by introducing a set of secondary complementary mutations into DGαq IW and generated the double mutants DGαq V178A I184W, V178S I184W, and V178M I184W. The first experiments using the Gβγ/masGRK3ct BRET assay revealed a slightly reduced amplitude for the DGαq VM IW mutant in the carbachol concentration-response curves as well as in the kinetics, and no benefits over the other two double mutants. In contrast, extensive characterization unequivocally revealed that DGαq VA IW and VS IW retain wild type-like behavior in all assays employed. Remarkably, both mutants were entirely resistant to the inhibitory action of FR. Therefore, we concluded that the developed *Drosophila* Gαq isoforms met all requirements and proceeded to use them in proof-of-principle experiments *in vivo*.

Ubiquitous overexpression of the mutants in *Drosophila melanogaster* did not cause any obvious defects or anatomical aberrations and did not affect locomotion in negative geotaxis assays. However, introduction of inhibitor-resistant DGαq proteins increased survival under FR feeding from 20% to about 80%. This not only demonstrates the Gq-dependency of FR's lethality in *Drosophila melanogaster* and possibly by extension other FR-sensitive insect species. The results also suggest specificity and lack of off-target effects of the compound and establish the engineered FR-resistant DGαq mutants as chemogenetic tools employable for deconvolution of signaling processes with Gq contribution in live animals.

In a last step, we generated similar tools for the investigation of causal biology in mice. To this end, we transferred the successful combination of mutations to mGαq and generated V184A I190W and V184S I190W double mutants. In a set of initial experiments, the mGαq mutants proved to be wild type-like, FR-resistant Gαq proteins. A broader characterization and application of these tools *in vivo* exceeded the scope of this project and will be done in future.

In summary, the engineered FR-resistant *Drosophila* and mouse Gαq variants constitute the basis of a more extensive toolbox to put all G proteins under pharmacological control of FR. In the course of the development of the engineered G protein variants presented in this thesis and simultaneous, as yet unpublished work on projects by others in the lab, it became increasingly evident that the rational design of artificial FR binding sites, be it to generate or abolish FR sensitivity, while maintaining wild-type (signaling) behavior is not as straightforward as anticipated. At the same time, increased insight into the FR inhibition modalities, i.e. binding in the presence of and interaction with the Gβγ subunit instead of in competition with Gβγ, uncovered a new path towards G protein family-specific inhibitors by refining screening approaches including the Gβγ subunit. Even though this makes success seem increasingly likely, the alternative approach of a chemogenetics-like G protein toolbox presented in this thesis is a valuable relief strategy for the lack of effective, G protein family-specific inhibitors and the chemogenetic G protein-ligand pairs designed in this thesis permit causal investigation of cellular biology *in vitro* and *in vivo*.

Acknowledgements

I want to thank everyone who was involved in the journey that finally led to the submission of this thesis. Please be aware that this expression of thanks and the explicit instances I mention are in no way a complete list of all I am thankful for. For this, I'd need another 150 pages.

A short clarification on what I am thankful for: There is so much more to "doing your PhD" than just lab work and juggling some data. Of course, I want to extend my sincere thanks to everyone who was involved in this project scientifically but even more so, I am incredibly grateful for the advice, discussions, and helping hands in my development as a person. Over the past years, I grew not only as a scientist but also as an individual. I did grow and I could not have done so without the nurturing encounters along the way. Sometimes, I needed watering or fertilization or a trellis to lean on. Sometimes, I needed to be pruned. With the amazing social network that I am truly fortunate to have and the additional short but meaningful encounters, I always had someone to rely on, whatever I needed. Finally, I leave it up to you to decide whether I have grown into a pretty flower, a prickly cactus or something in between.

My deepest gratitude goes to my supervisor Prof. Dr. Evi Kostenis. Thank you for giving me the space to grow. Thank you for telling me, during a social event when I was about to hand in my Master's thesis: "Du MUSST einen Doktor machen!". Even though it might seem to you as if I am not carefully listening sometimes, I usually do, and there are a lot of things you have said that will stay with me for a long time. Working with you has brought a lot of joy. I am proud to say in the past years, I have found my passion and my calling in your lab and under your tutelage. I hope to continue the deep conversations about science and life in general and profit from your knowledge. See you soon at Meyer's!

Heartfelt thanks go to Prof. Dr. Bernd Fleischmann for second supervision as part of the Research Training Group. Even though our meetings were virtual for the most part, I profited from your scientific input. I would also like to thank Prof. Dr. Ilona Grunwald Kadow and Prof. Dr. Martin Baunach for their willingness to be part of my examination committee. Thank you for your time and effort.

I gratefully acknowledge the Deutsche Forschungsgemeinschaft (DFG) for funding this project and supporting my membership in the Research Training Group 1873. Apart from the retreats and symposia which were scientifically top notch, the RTG1873 enabled me to go to my first international conference and do a three-month research stay in Boston.

Deepest gratitude goes to everyone who was scientifically involved in this project. First and foremost, I want to thank Dr. Nicole Scholz and Dr. Anne-Kristin Dahse.

Thank you for performing the *in vivo* experiments and engaging scientific discussions. You were extraordinarily friendly during our visits, and it was an honor working with you. Finally, thank you for your patience. I look forward to the joint publication that this project will cumulate in (very soon!).

Thank you to Dr. Julian Patt and Dr. Nicole Merten for the many hours you spent introducing me to and supporting me with lab work and getting me started on this project. Thank you to everyone else who contributed to this thesis by performing experiments: Sergi Bravo, Prof. Dr. Max Crüsemann, Dr. Wiebke Hanke, Lars Jürgenliemke, Aram Kamalizade, Uli Rick, Dr. Sophie Steinmüller, and Lorenzo Volonté. Thank you to Chris Ulbricht for his help and patience with my seemingly endless questions about LC/MS specifics. Thank you to Dr. Stefan Kehraus, Dr. Wiebke Hanke, and Prof. Dr. Gabriele König for their bottomless supply of FR in copious quantities.

A particularly warm thanks goes to Prof. Dr. Mikel Garcia-Marcos for welcoming me to his lab and supporting me in collecting the neatest data I have ever generated. I am very grateful for the unique experience of staying in the US for three months but also getting to know a different lab with its exceptional lab culture. I learned the ins and outs of BRET assays from you, but you also offered a perspective on what makes a fully formed scientist and how to improve further. I am thankful for your mentorship that, I feel, has extended beyond my stay in your lab. I will always look forward to meeting you at conferences or on visits to Boston. Thank you also to every single person in Mikel's lab, especially Dr. Alex Luebbers, and to the few people from the Harris' lab that I met for making my stay as fun and exciting as it was.

Thank you to everyone who was otherwise involved in this work or supported me. Tania, thank you for the countless conversations about all the small, hard things in life and for being such an incredibly warm-hearted person. Jesus, thank you for the open door, the critical thinking, and being a second mentor. Katja, thank you for putting up with every little administrative question and for your amazing competence. Thomas, thank you for all the little things you made possible when I had another one of my oh-so-precious and urgent ideas and the friendly chats in the hallway. Ralf, thank you for your help in keeping me employed for as long as possible and for the few minutes we often shared at the coffee machine before the lab meeting.

Apart from working on this project with your hands, thank you to everybody who granted this a part of their minds. I am thankful for your scientific input into this project and value your time and efforts.

Thank you to the entire (including former) AG Kostenlos squad. Over the years, you have become more than coworkers. I consider you friends if not even part of the

extended family with all the ups and downs that come with this. You are an enormous enrichment to my life (not only when helping me move for the umpteenth time in as many months). I am truly spoiled by the experience of working and spending free time with you. Thank you for the time spent on the couch in the social room, in the Mensa, during one of the many celebrations in the seminar room or the library, vorm Schloss, and everywhere else. And thank you for all the support, constructive criticism, advice, encouragement, and understanding, all the small things that happened in this time.

Thank you to everyone who completed and complemented the “work friends” in my life: Freddy, Lukas, René, Sophie, Sophie, Susi, Steffi, Irene, Thomas, Nina, Chrissy, and all the other line dancers, Norman, Katha, Basti, Michael, Flo, and the remaining BOTC enthusiasts. Thank you for being the friends that you are. There are not enough words in any dictionary to express how much all of you mean to me and how grateful I am to know you.

Thank you to Jürgen und Lina for keeping me on my feet. Without your support I might not have made it. You are undoubtedly the best physiotherapists in the world. Thank you to Charlotte and my other workout buddies for the break time we spent talking about Gott und die Welt and for the encouragement (and sometime blatant expectations) to motivate me.

Thank you to my family: Mama, Papa, Lydia, Dirk, Beate, Horst, Heinz, Christiane. Thank you for the hours of conversation in person or on the phone, for listening to my complaints but also to enthusiastic lab bench tales. Thank you for your advice and keeping me occupied on weekends. Thank you for the postcards that always make my day. Thank you for putting up with me and for the vast amounts of love that you have shown me. Sometimes, I can’t believe how fortunate I am to have all of you in my life. All I can hope for is to live up to being the person you see in me.

Thanks also to the fellow minds I met at the various conferences I’ve been privileged to attend over the past few years. Gabriele, I think there is no one I got along with this well from the first minute we met. You’re one of my favorite people. Drew, you are so sincere and thoughtful that it is always a pleasure spending time with you. Thank you for everyone who became a mentor to me over time: Hannes and Martha, and so many more who I could not possibly list here.

Special thanks go to Freddy and Coco who voluntarily (!) shared their space with me. You kept me sane (I think?) through this time. I love you both <3

Additional material

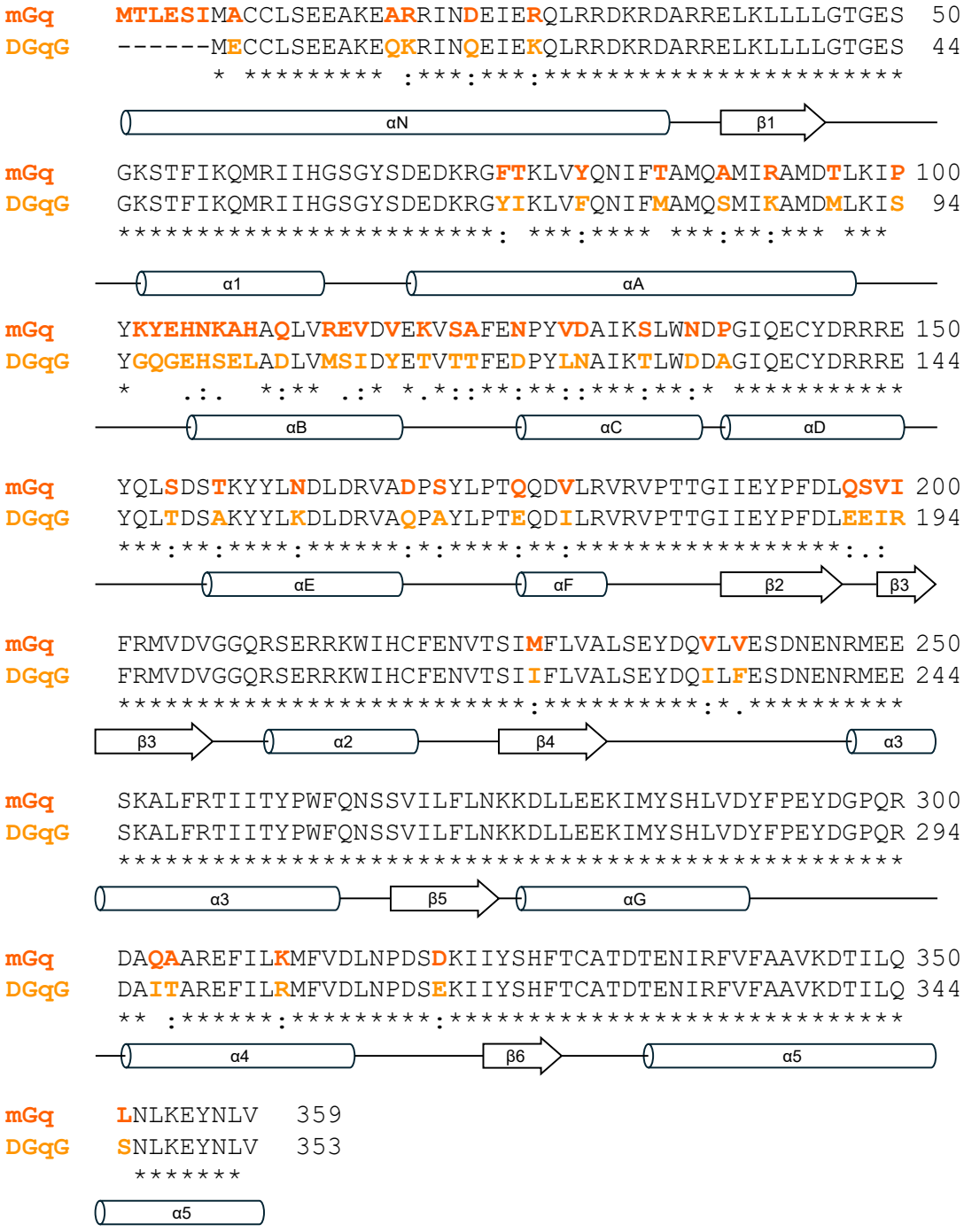

Figure 66: Full alignment of mGαq and DGqαG sequences.
Differing residues are marked in dark orange in the mGαq sequence and in light orange in the DGαqG sequence. Secondary structural elements are depicted below the sequence with cylinders (α-helices) and arrows (β-sheets). Asterisks (*) signify identical amino acids. Colons (:) and periods (.) signify strongly and weakly similar properties of the compared amino acids with a scoring of >0.5 and ≤0.5 in the Gonnet PAM 250 matrix, respectively.

Table 28: Comparison of relevant position numbering in murine Gαq, Drosophila Gαq, and the Common Gα Numbering System (CGN) *(Flock et al., 2015)*.

Residue and Position in murine Gαq	Residue and Position in *Drosophila* Gαq	Residue Number according to the CGN
Serine-53	Serine-47	G.H1.2
Isoleucine-56	Isoleucine-50	G.H1.5
Lysine-57	Lysine-51	G.H1.6
Arginine-60	Arginine-54	G.H1.9
Tyrosine-67	Tyrosine-61	G.h1ha.4
Asparagine-71	Asparagine-65	H.HA.3
Phenylalanine-75	Tyrosine-69	H.HA.7
Leucine-78	Leucine-72	H.HA.10
Valine-184	Valine-178	G.hfs2.3
Threonine-187	Threonine-181	G.hfs2.7
Isoleucine-190	Isoleucine-184	G.S2.2

Table 29: Mutations introduced into Drosophila melanogaster DGαq isoform G including reasoning.
a Based on the Common Gα Numbering System (CGN) (Flock et al., 2015)

Mutation (Nomenclature)	Position[a]	Wild-type Residue	Introduced Residue	Reason for Mutation
D65E	H.HA.3	Aspartic acid	Glutamic acid	transfer of Gα16 FR binding site
Y69K	H.HA.7	Tyrosine	Lysine	introduction of polar residue, removal of nonpolar interactions, electrostatic repulsion
V176S	G.hfs2.1	Valine	Serine	transfer of Gα16 FR binding site
V178A	G.hfs2.3	Valine	Alanine	introduction of bulky residue, steric hindrance
V178M	G.hfs2.3	Valine	Methionine	introduction of bulky residue, steric hindrance, transfer of Gα16 FR binding site
V178S	G.hfs2.3	Valine	Serine	introduction of polar residue, removal of nonpolar interactions, electrostatic repulsion
I184N	G.S2.2	Isoleucine	Asparagine	transfer of Gα16 FR binding site
I184W	G.S2.2	Isoleucine	Tryptophan	introduction of bulky residue, steric hindrance
P187C	G.S2.5	Proline	Cysteine	transfer of Gα16 FR binding site
FIVE	Combination of D65E, V176S, V178M, I184N, and P187C			transfer of Gα16 FR binding site

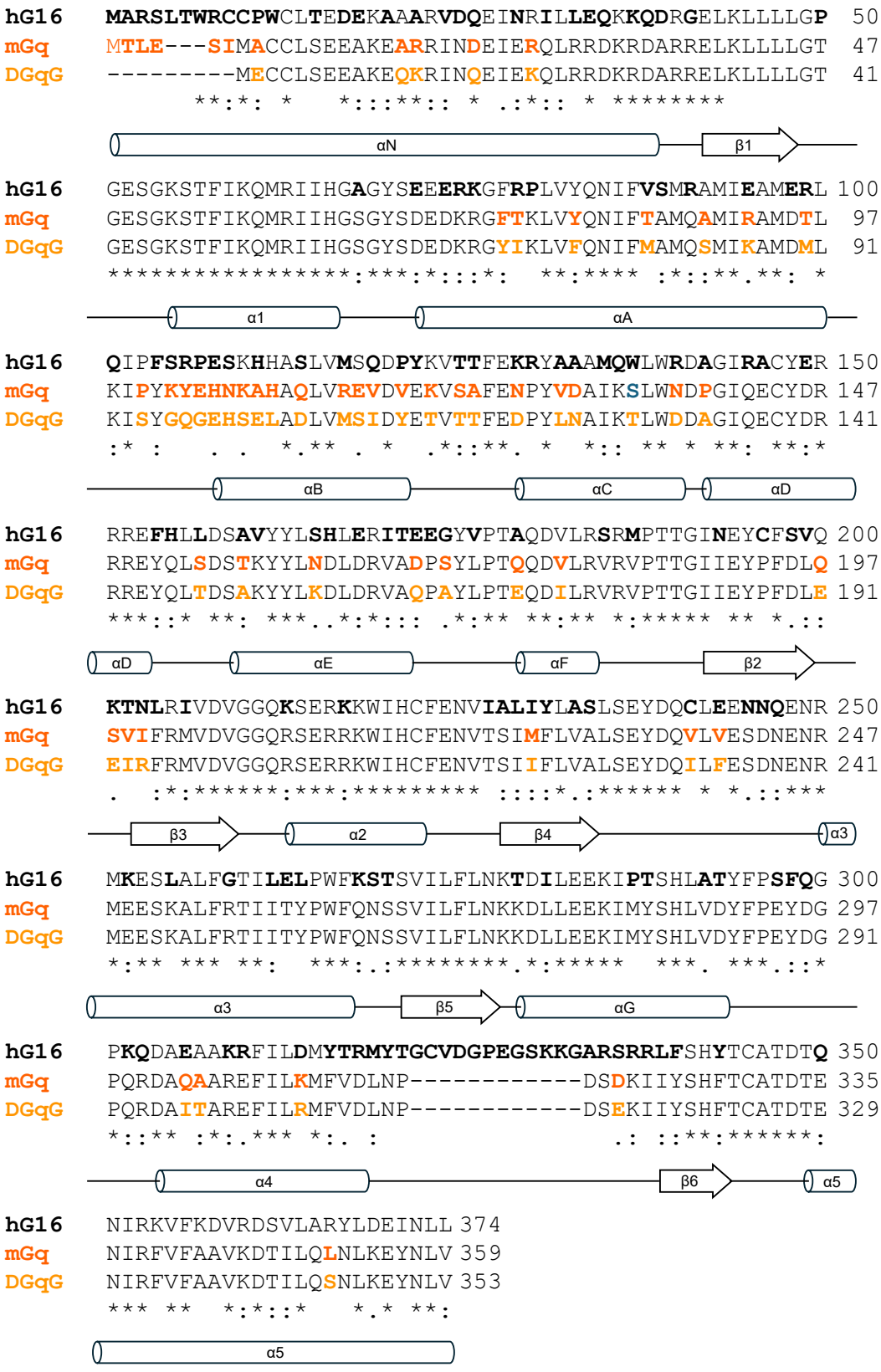

Figure 67: Full alignment of hGα16, mGαq, and DGαqG sequences.
Residues differing between mGαq and DGαqG are marked bold and dark orange in the mGαq sequence and in bold and light orange in the DGαqG sequence. Residues differing between hGα16 and mGαq are marked bold and black in the hGα16 sequence. Secondary structural elements are depicted below the sequence with cylinders (α-helices) and arrows (β-sheets). Asterisks (*) signify identical amino acids. Colons (:) and periods (.) signify strongly and weakly similar properties of the compared amino acids with a scoring of >0.5 and ≤0.5 in the Gonnet PAM 250 matrix, respectively.

Table 30: Mutations introduced into murine Gαq including reasoning.
a Based on the Common Gα Numbering System (CGN) (Flock et al., 2015)

Mutation (Nomenclature)	Position[a]	Wild-type Residue	Introduced Residue	Reason for Mutation
D71E	H.HA.3	Aspartic acid	Glutamic acid	transfer of Gα16 FR binding site
V182S	G.hfs2.1	Valine	Serine	transfer of Gα16 FR binding site
V184A	G.hfs2.3	Valine	Alanine	introduction of bulky residue, steric hindrance
V184M	G.hfs2.3	Valine	Methionine	introduction of bulky residue, steric hindrance, transfer of Gα16 FR binding site
V184S	G.hfs2.3	Valine	Serine	introduction of polar residue, removal of nonpolar interactions, electrostatic repulsion
I190N	G.S2.2	Isoleucine	Asparagine	transfer of Gα16 FR binding site
I190W	G.S2.2	Isoleucine	Tryptophan	introduction of bulky residue, steric hindrance
P193C	G.S2.5	Proline	Cysteine	transfer of Gα16 FR binding site
FIVE	Combination of D71E, V182S, V184M, I190N, and P193C			transfer of Gα16 FR binding site

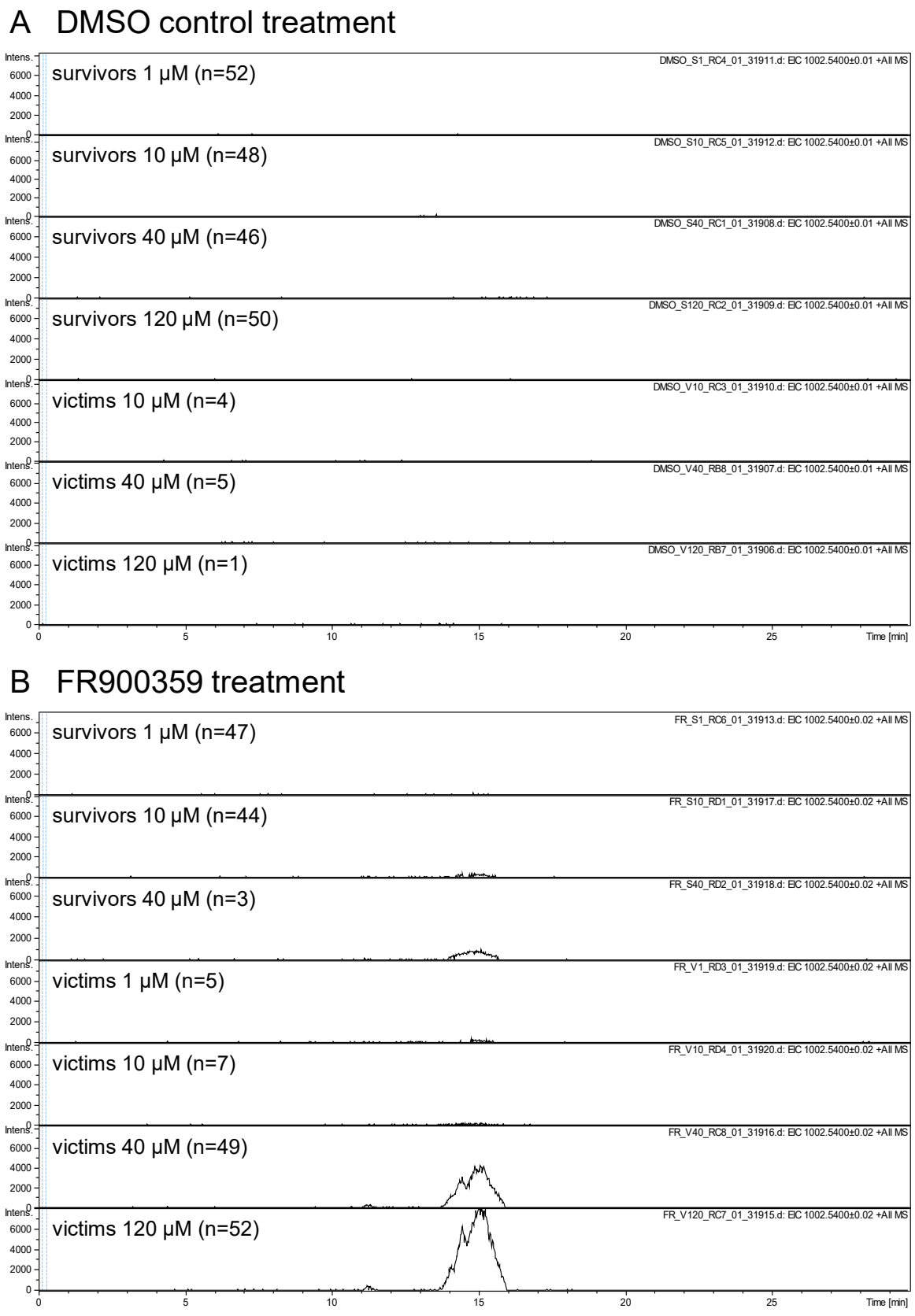

Figure 68: Raw HPLC/MS traces used to calculate relative FR amounts in victim and survivor flies from FR feeding experiments.

A. *FR content in survivor and victim flies of DMSO conditions was measured after methanol extraction using an HPLC/MS setup for the investigation of FR-containing samples. Shown chromatograms depict signal intensities for unfragmented FR (m/z value of 1002.5400 ± 0.02) over elution time. Data are traces obtained from a single*

experiment performed on flies of one of the replicates in Figure 55. ***B.*** *FR content in survivor and victim flies of the FR conditions. Data are depicted analogous to A.*

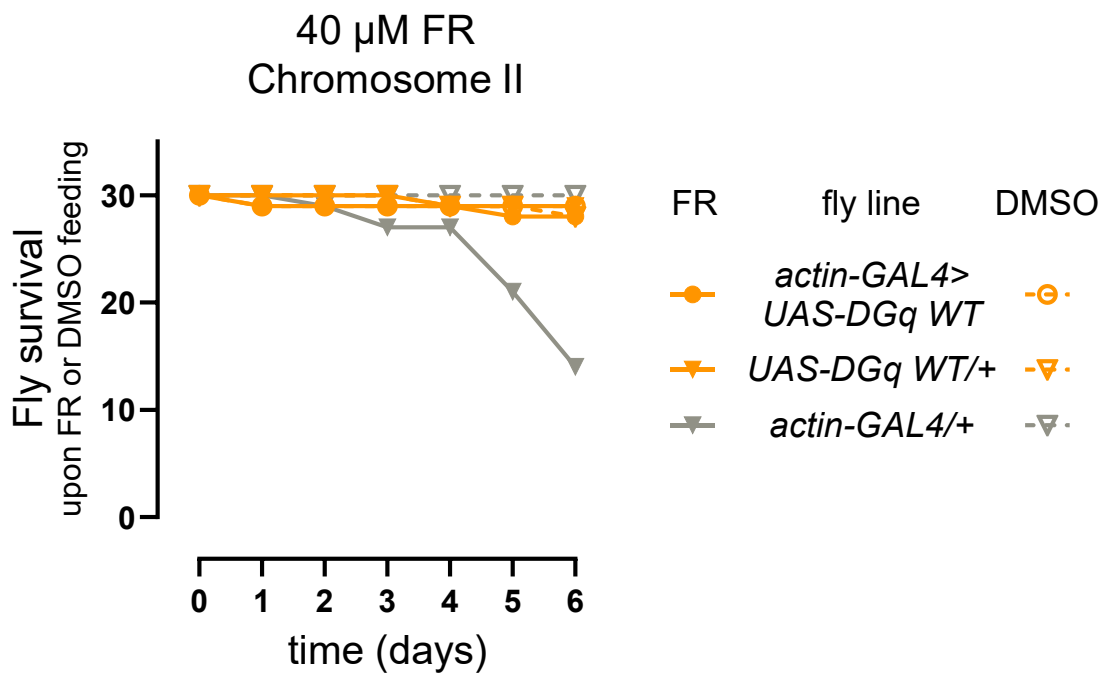

Figure 69: Leaky expression of DGαq wild type from an insertion site on chromosome II results in rescue of FR-induced lethality in Drosophila melanogaster.
Flies only harboring the gene of (UAS-DGq WT/+) or expressing DGαq wild type (actin-GAL4>UAS-DGq WT) from the second chromosome, as well as the "driver" control line were kept on food laced with 40 µM FR (filled symbol) or the corresponding amount of DMSO (open symbol). Survival of flies was recorded for six days. Data are absolute numbers of one experiment performed with 30 adult flies (20 female, 10 male).

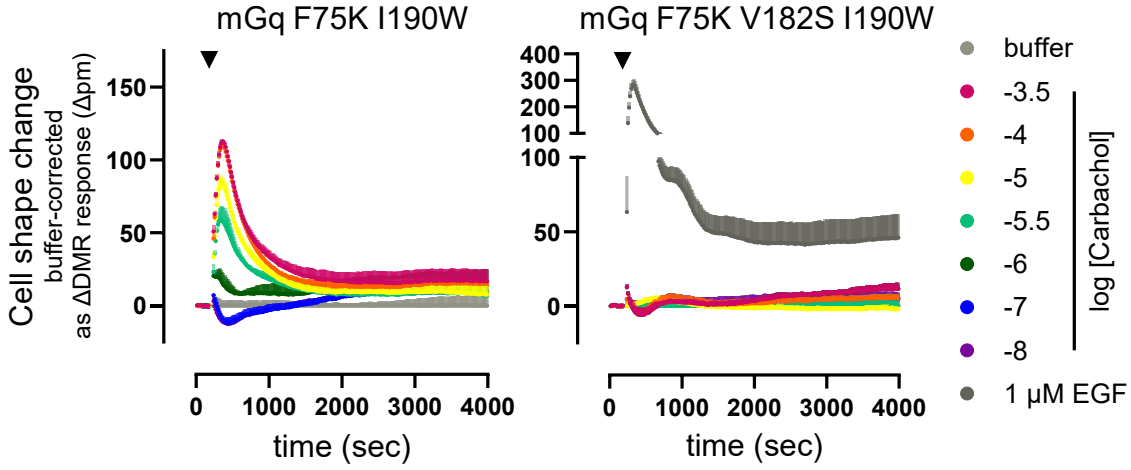

Figure 70: In the background of mGq F75K I190W, the additional mutation V182S is detrimental to G protein function as measured in dynamic mass redistribution (DMR) assays, even though it is tolerated in mGq FIVE.
Kinetic buffer-corrected DMR traces of HEK293 cells lacking Gαq and Gα11 proteins after CRISPR/Cas9 treatment (HEK293 Gq/11-KO) transiently transfected with constructs coding for mGαq F75K I190W (left) or mGαq F75K V182S I190W (right). Cells are activated with different concentrations of carbachol (CCh) or buffer after about 3 minutes of baseline measurement. Data are the means + SD of one experiment representative of three biologically independent experiments. Data presented in this figure have been recorded for Alenfelder (2019) and Patt (2021) but have not been included in these publications.

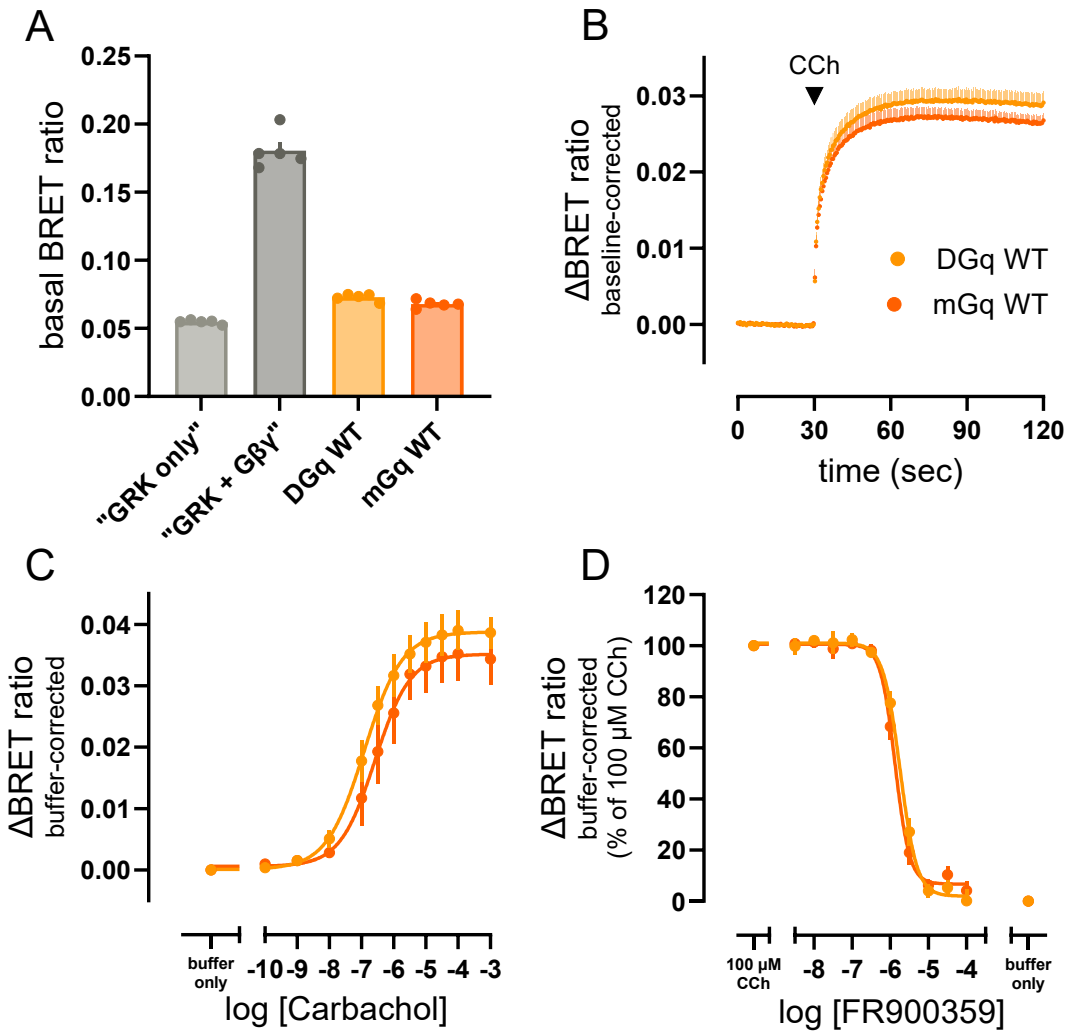

Figure 71: Drosophila and murine DGαq behave very similarly regarding Gβγ binding, activation kinetics, potency and efficacy of carbachol (CCh) response and FR900359 (FR) sensitivity in the Gβγ/masGRK3ct BRET assay.

A. *Basal BRET ratio measured in HEK293T cells transiently transfected with constructs coding for M3R, masGRK3ct-NLuc, split Venus-tagged Gβγ, Ric-8A, DGαq or mGαq wild type as indicated, and Ric-8A. Bar graphs represent the means ± SEM of five biologically independent experiments. Data points represent individual replicates.* ***B.*** *Kinetic baseline-corrected BRET traces of cells transfected as in A. Cells were activated with 100 µM CCh after 30 seconds of baseline measurement. Data are the means + SEM of four to five biologically independent experiments.* ***C.*** *CCh concentration-response curves measured as buffer-corrected BRET ratio after stimulation with CCh or buffer in cells transfected as in A. Data are the means ± SEM of four to five biologically independent experiments.* ***D.*** *FR concentration-response curves measured as buffer-corrected BRET ratio after preincubation with FR or buffer and stimulation with CCh or buffer in cells transfected as in A normalized to the effect of 100 µM CCh. Data are the means ± SEM of five biologically independent experiments. Data for "GRK only", "GRK + Gβγ", and DGαq WT were copied from Figure 23, Figure 27, and Figure 22 for clarity.*

Publications

Peer-reviewed journal articles

1. Steinmüller SAM, Thompson K, **Alenfelder J**, Drube J, Hoffmann C, Kostenis E, Thompson D, Hislop JN. Identification of a regulatory sequence within the third intracellular loop that governs β-arrestin binding to the muscarinic M5 receptor. Cell Signal. 2025 Jul 17:112004. doi: 10.1016/j.cellsig.2025.112004. Epub ahead of print. PMID: 40683329.

2. **Alenfelder J**[#], Chronis IB[#], Nemec K[#], Shahraki A[#]. Commentary on the fourth Transatlantic G Protein-Coupled Receptor Symposium for early-career investigators. Mol Pharmacol. 2025 Jun 28;107(7):100052. doi: 10.1016/j.molpha.2025.100052. Epub ahead of print. PMID: 40582039.
   [#] Contributed equally.

3. Mühle J[#], **Alenfelder J**[#], Rodrigues MJ[#], Jürgenliemke L[#], Guixà-González R, Grätz L, Andres F, Bacchin A, Hennig M, Schihada H, Crüsemann M, König GM, Schertler G, Kostenis E, Deupi X. Cyclic peptide inhibitors function as molecular glues to stabilize Gq/11 heterotrimers. Proc Natl Acad Sci U S A. 2025 May 13;122(19):e2418398122. doi: 10.1073/pnas.2418398122. Epub 2025 May 7. PMID: 40333756.
   [#] Contributed equally.

4. Bormann A, Körner MB, Dahse AK, Gläser MS, Irmer J, Lede V, **Alenfelder J**, Lehmann J, Hall DCN, Thane M, Schleyer M, Kostenis E, Schöneberg T, Bigl M, Langenhan T, Ljaschenko D, Scholz N. Intron retention of an adhesion GPCR generates 1TM isoforms required for 7TM-GPCR function. Cell Rep. 2025 Jan 28;44(1):115078. doi: 10.1016/j.celrep.2024.115078. Epub 2024 Dec 19. PMID: 39705141.

5. Brands J, Bravo S, Jürgenliemke L, Grätz L, Schihada H, Frechen F, **Alenfelder J**, Pfeil C, Ohse PG, Hiratsuka S, Kawakami K, Schmacke LC, Heycke N, Inoue A, König G, Pfeifer A, Wachten D, Schulte G, Steinmetzer T, Watts VJ, Gomeza J, Simon K, Kostenis E. A molecular mechanism to diversify Ca2+ signaling downstream of Gs protein-coupled receptors. Nat Commun. 2024 Sep 3;15(1):7684. doi: 10.1038/s41467-024-51991-6. PMID: 39227390; PMCID: PMC11372221.

6. Kostenis E, Jürgenliemke L, **Alenfelder J**. G protein-mediated signal transduction: a molecular choreography of G protein activation after GTP binding. Signal Transduct Target Ther. 2024 Jul 16;9(1):188. doi: 10.1038/s41392-024-01903-3.

7. Seidinger A, Roberts R, Bai Y, Müller M, Pfeil E, Matthey M, Rieck S, **Alenfelder J**, König GM, Pfeifer A, Kostenis E, Klinke A, Fleischmann BK, Wenzel D. Pharmacological Gq inhibition induces strong pulmonary vasorelaxation and reverses pulmonary hypertension. EMBO Mol Med. 2024 Aug;16(8):1930-1956. doi: 10.1038/s44321-024-00096-0. Epub 2024 Jul 8.

8. Berger T, **Alenfelder J**, Steinmüller S, Heimann D, Gohain N, Petras D, Wang M, Berger R, Kostenis E, Reher R. A MassQL-Integrated Molecular Networking Approach for the Discovery and Substructure Annotation of Bioactive Cyclic Peptides. J Nat Prod. 2024 Apr 26;87(4):692-704. doi: 10.1021/acs.jnatprod.3c00750. Epub 2024 Feb 22.

9. Hanke W[#], **Alenfelder J[#]**, Liu J, Gutbrod P, Kehraus S, Crüsemann M, Dörmann P, Kostenis E, Scholz M, König GM. The Bacterial G_q Signal Transduction Inhibitor FR900359 Impairs Soil-Associated Nematodes. J Chem Ecol. 2023 Oct;49(9-10):549-569. doi: 10.1007/s10886-023-01442-1. Epub 2023 Jul 15.
   [#] Contributed equally.

10. Hanke W, Patt J, **Alenfelder J**, Voss JH, Zdouc MM, Kehraus S, Kim JB, Grujičić GV, Namasivayam V, Reher R, Müller CE, Kostenis E, Crüsemann M, König GM. Feature-Based Molecular Networking for the Targeted Identification of G_q-Inhibiting FR900359 Derivatives. J Nat Prod. 2021 Jul 23;84(7):1941-1953. doi: 10.1021/acs.jnatprod.1c00194. Epub 2021 Jul 1.

11. Patt J, **Alenfelder J**, Pfeil EM, Voss JH, Merten N, Eryilmaz F, Heycke N, Rick U, Inoue A, Kehraus S, Deupi X, Müller CE, König GM, Crüsemann M, Kostenis E. An experimental strategy to probe Gq contribution to signal transduction in living cells. J Biol Chem. 2021 Jan-Jun;296:100472. doi: 10.1016/j.jbc.2021.100472. Epub 2021 Feb 25.

12. Hermes C, Richarz R, Wirtz DA, Patt J, Hanke W, Kehraus S, Voß JH, Küppers J, Ohbayashi T, Namasivayam V, **Alenfelder J**, Inoue A, Mergaert P, Gütschow M, Müller CE, Kostenis E, König GM, Crüsemann M. Thioesterase-mediated side chain transesterification generates potent Gq signaling inhibitor FR900359. Nat Commun. 2021 Jan 8;12(1):144. doi: 10.1038/s41467-020-20418-3.

In preparation

One first authored paper in preparation for submission.

List of Figures

List of Tables

Abbreviations

Table 31: Abbreviations.

Abbreviation	Definition
Act5C	*actin5C* promotor
add	addition
AHD	α-helical domain
as	antisense
Atrp	atropine
attB	bacterial attachment site, used for the PhiC31 integrase system
attL	hybrid site, results from integration via PhiC31 integrase
attP	phage attachment site, used for the PhiC31 integrase system
attR	hybrid site, results from integration via PhiC31 integrase
BamHI	first (I) restriction enzyme isolated from *Bacillus amyloliquefaciens* (Bam) in Hindustan (H)
bp(s)	base pair(s)
BRET	bioluminescence resonance energy transfer
BSA	bovine serum albumin
C. elegans	*Caenorhabditis elegans*
Ca^{2+}	calcium ion
$Ca_3(PO_4)_2$	calcium phosphate
CAAX	plasmamembrane-targeting motif consisting of a cysteine, two aliphatic amino acids, and one additional amino acid
CCh	carbachol, carbamoylcholine
cDNA	complementary DNA
cEK	internal identifier for cell lines
CGN	Common Gα Numbering
CHO cells	chinese hamster ovary cell line
CRISPR/Cas9	clustered regularly interspaced short palindromic repeats/CRISPR associated protein 9
Cy3	cyanine 3
D. melanogaster	*Drosophila melanogaster*
DAG	diacylglycerol
DAPI	4′,6-diamidino-2-phenylindole
DFG	Deutsche Forschungsgemeinschaft

Table 28 continued.

Abbreviation	Definition
DGq	*Drosophila melanogaster* Gq
DG_{q1}	alternative nomenclature for *Drosophila melanogaster* Gαq isoform D
DG_{q2}	alternative nomenclature for *Drosophila melanogaster* Gαq isoform G
DGqA	alternative nomenclature for *Drosophila melanogaster* Gαq isoform D
DGqB	alternative nomenclature for *Drosophila melanogaster* Gαq isoform G
dGqα-1	alternative nomenclature for *Drosophila melanogaster* Gαq isoform D
dGqα-2	alternative nomenclature for *Drosophila melanogaster* Gαq isoform G
DGαq	*Drosophila melanogaster* Gαq
DGαqC	*Drosophila melanogaster* Gαq isoform C
DGαqD	*Drosophila melanogaster* Gαq isoform D
DGαqG	*Drosophila melanogaster* Gαq isoform G
DGαq-PA	alternative nomenclature for *Drosophila melanogaster* Gαq isoform D
DGαq-PG	alternative nomenclature for *Drosophila melanogaster* Gαq isoform G
DMEM	Dulbecco's modified Eagle's Medium
DMR	dynamic mass redistribution
DMSO	dimethyl sulfoxide
DNA	deoxyribonucleic acid
dNTPs	nucleoside triphosphates containing deoxyribose
DpnI	first (I) restriction enzyme isolated from *Streptococcus* (formerly *Diplococcus*) *pneumoniae*
DTT	dithiothreitol
E. coli	*Escherichia coli*
EcoRI	first (I) restriction enzyme isolated from *Escherichia coli* strain RY13
EDTA	ethylenediaminetetraacetic acid
EGF	epidermal growth factor
EGFR	epidermal growth factor receptor
ELISA	enzyme-linked immunosorbent assay
EMBL-EBI	European Molecular Biology Laboratory-European Bioinformatics Institute
ERK	extracellular signal-regulated kinases
F1	filial generation one
FBS	filtrated bovine serum
Fig.	figure

Table 28 continued.

Abbreviation	Definition
FITC	fluorescein-5-isothiocyanat
FR	FR900359
FRET	Förster resonance energy transfer
frs gene cluster	FR nonribosomal peptide synthetase gene cluster
fwd	forward
G protein	guanine nucleotide-binding protein
GAIP	G-alpha-interacting protein, also known as RGS19
GAP	GTPase-accelerating protein
GDI	guanine nucleotide dissociation inhibitor
GDP	guanosine diphosphate
GEF	guanine nucleotide exchange factor
GFP	green fluorescent protein
GPCR	G protein-coupled receptor
Gq	Gq protein
GRK3	G protein-coupled receptor kinase 3
GSBB	goat serum blocking buffer
GTP	guanosine triphosphate
H. schachtii	*Heteroder schachtii*
HA(-tag)	human influenza hemagglutinin(-tag)
HBS	HEPES-buffered saline
HBSS	Hanks' Balanced Salt Solution
HEK293 cells	human embryonal kidney 293 cells
HEK293 Gq/11/12/13-KO	HEK293 cells lacking Gαq, Gα11, Gα12, and Gα13 proteins after CRISPR/Cas9 treatment
HEK293 Gq/11-KO	HEK293 cells lacking Gαq, and Gα11 proteins after CRISPR/Cas9 treatment
HEK293 Gs/olf/q/11/12/13/z-KO (HEK293 Δ7)	HEK293 cells lacking Gαs, Gαolf, Gαq, Gα11, Gα12, Gα13, and Gαz proteins after CRISPR/Cas9 treatment
HEPES	4-(2-hydroxyethyl)-1-piperazineethanesulfonic acid
hGαq	human Gαq
hGβ1	human G protein β1 subunit
hGγ2	human G protein γ2 subunit
HPLC/MS	high performance liquid chromatography/ mass spectrometry
HRP	horseradish peroxidase
HTRF	homogeneous time-resolved fluorescence
Hz	Hertz
IB	immunoblotted
Int. ID	internal identifier, e.g. pEK or cEK number

Table 28 continued.

Abbreviation	Definition
$IP_{(1)}$	inositol monophosphate
IP_3	inositol 1,4,5-trisphosphate
IP_3R	IP_3 receptor calcium channels
KCH_3COO	potassium acetate
kDa	kiloDalton
keV	kiloelectronvolt
KO	knock-out
KpnI	first (I) restriction enzyme isolated from *Klebsiella pneumoniae*
LB	lysogeny broth
LiCl	lithium chloride
M	million or molar
m/z	mass-to-charge ratio
M3R/M3 receptor	M3 muscarinic acetylcholine receptor
MAP	mitogen-activated protein
MAPK	mitogen-activated protein kinase
mas	myristic acid attachment peptide
masGRK3ct	myristic acid attachment peptide (mas)-tagged c-terminal fragment (ct) of G protein-coupled receptor kinase 3 (GRK3)
$Mg(CH_3COO)_2$	magnesium acetate
mGluR	metabotropic glutamate receptors
mGq	murine Gq
mGαq	murine Gαq
MS/MS	tandem mass spectrometry
Na_2HPO_4	disodium phosphate
NaCl	sodium chloride
NaOH	sodium hydroxide
NG	NeonGreen
NG-CAAX	NeonGreen with a plasmamembrane-targeting motif
NheI	first (I) restriction enzyme isolated from *Nocardia haematophila*
NLuc	NanoLuc® luciferase
OptiMEM™	optimized minimal essential medium
PAM matrix	point accepted mutation matrix
PBS	phosphate-buffered saline
PCR	polymerase chain reaction
PDB	Protein Data Bank
PDL	poly-D-lysine
pEC_{50}	negative decadic logarithm of the half-maximal effective concentration

Table 28 continued.

Abbreviation	Definition
PEI	polyethylenimine
pEK	internal identifier for plasmids
PFA	paraformaldehyde
Pfu	*Pyrococcus furiosus*
PhD	Philosophiae Doctor
pIC_{10}	negative decadic logarithm of the10% inhibitory concentration
pIC_{50}	negative decadic logarithm of the half-maximal inhibitory concentration
pIC_{90}	negative decadic logarithm of the 90% inhibitory concentration
PIP_2	phosphatidylinositol 4,5-bisphosphate
PLCβ	phospholipase C β
PTX	pertussis toxin
PVDF	polyvinylidene difluoride
R^2	coefficient of determination
rcf	relative centrifugal force
RET	resonance energy transfer
rev	reverse
RGS	regulator of G protein signaling
RHD	Ras-homology domain
Ric-8A	resistance to inhibitors of cholinesterase-8A
RP	reversed-phase
rpm	revolutions per minute
RTG1873	Research Training Group 1873
s	sense
S. cerevisiae	*Saccharomyces cerevisiae*
S2 cells	*Drosophila melanogaster* Schneider 2 cells
SD	standard deviation
SDS-PAGE	sodium dodecyl sulfate–polyacrylamide gel electrophoresis
SEM	standard errer of the means
Sf9 cells	*Spodoptera frugiperda* cell line
$t_{1/2}$	time required for the signal to return to 50% of its peak value
$t_{1/4}$	time required for the signal to return to 25% of its peak value
TAE	tris acetate EDTA buffer
TBS	tris-buffered saline
TBST	tris-buffered saline supplemented with 0.1% Tween20
Temp.	temperature
TMB	3,3',5,5' tetramethylbenzidine

Table 28 continued.

Abbreviation	Definition
tris	tris(hydroxymethyl)aminomethane
UAS	upstream activation sequence
UF	University of Florida
US	United States
V	Volt
w/o	without
WB	western blot(ting)
WT	wild type pr wild-type
YM	YM-254890

References

Ahmad, M., Chaudhary, S. U., Afzal, A. J., & Tariq, M. (2015). Starvation-Induced Dietary Behaviour in Drosophila melanogaster Larvae and Adults. *Scientific Reports*, *5*(1), 14285. https://doi.org/10.1038/srep14285

Alenfelder, J. (2019). *Etablierung eines experimentellen Ansatzes zur Bestimmung der FR-Empfindlichkeit natürlich auftretender Gq-Isoformen* [Masterarbeit]. Rheinische Friedrich-Wilhelms-Universität Bonn, Bonn.

Ali, Y. O., Escala, W., Ruan, K., & Zhai, R. G. (2011). Assaying locomotor, learning, and memory deficits in Drosophila models of neurodegeneration. *Journal of Visualized Experiments : JoVE.* Advance online publication. https://doi.org/10.3791/2504

Alvarez, C. E., Robison, K., & Gilbert, W. (1996). Novel Gq alpha isoform is a candidate transducer of rhodopsin signaling in a Drosophila testes-autonomous pacemaker. *Proceedings of the National Academy of Sciences*, *93*(22), 12278–12282. https://doi.org/10.1073/pnas.93.22.12278

Annala, S., Feng, X., Shridhar, N., Eryilmaz, F., Patt, J., Yang, J., Pfeil, E. M [Eva M.], Cervantes-Villagrana, R. D., Inoue, A., Häberlein, F., Slodczyk, T., Reher, R., Kehraus, S., Monteleone, S., Schrage, R., Heycke, N., Rick, U [Ulrike], Engel, S., Pfeifer, A., . . . Kostenis, E. (2019). Direct targeting of Gαq and Gα11 oncoproteins in cancer cells. *Science Signaling*, *12*(573). https://doi.org/10.1126/scisignal.aau5948

Ashkenazi, A., Peralta, E. G., Winslow, J. W., Ramachandran, J., & Capon, D. J. (1989). Functional diversity of muscarinic receptor subtypes in cellular signal transduction and growth. *Trends in Pharmacological Sciences*, *Suppl*, 16–22.

Atwood, B. K., Lopez, J., Wager-Miller, J., Mackie, K., & Straiker, A. (2011). Expression of G protein-coupled receptors and related proteins in HEK293, AtT20, BV2, and N18 cell lines as revealed by microarray analysis. *BMC Genomics*, *12*(1), 14. https://doi.org/10.1186/1471-2164-12-14

Ayoub, M. A. (2018). Small molecules targeting heterotrimeric G proteins. *European Journal of Pharmacology*, *826*, 169–178. https://doi.org/10.1016/j.ejphar.2018.03.003

Baker, J. G., Hill, S. J., & Summers, R. J. (2011). Evolution of β-blockers: From anti-anginal drugs to ligand-directed signalling. *Trends in Pharmacological Sciences*, *32*(4), 227–234. https://doi.org/10.1016/j.tips.2011.02.010

Ban, T. A. (2006). The role of serendipity in drug discovery. *Dialogues in Clinical Neuroscience*, *8*(3), 335–344. https://doi.org/10.31887/DCNS.2006.8.3/tban

Bassett, A. R., Tibbit, C., Ponting, C. P., & Liu, J.-L. (2013). Highly efficient targeted mutagenesis of Drosophila with the CRISPR/Cas9 system. *Cell Reports*, *4*(1), 220–228. https://doi.org/10.1016/j.celrep.2013.06.020

Baumbach, J., Hummel, P., Bickmeyer, I., Kowalczyk, K. M., Frank, M., Knorr, K., Hildebrandt, A., Riedel, D., Jäckle, H., & Kühnlein, R. P. (2014). A Drosophila in vivo screen identifies store-operated calcium entry as a key regulator of adiposity. *Cell Metabolism*, *19*(2), 331–343. https://doi.org/10.1016/j.cmet.2013.12.004

Beckingham, K. M., Texada, M. J., Baker, D. A., Munjaal, R., & Armstrong, J. D. (2005). Genetics of graviperception in animals. *Advances in Genetics*, *55*, 105–145. https://doi.org/10.1016/S0065-2660(05)55004-1

Benzer, S. (1967). Behavioral Mutants of Drosophila Isolated by Countercurrent Distribution. *Proceedings of the National Academy of Sciences*, *58*(3), 1112–1119. https://doi.org/10.1073/pnas.58.3.1112

Berman, D. M., Wilkie, T. M., & Gilman, A. G [A. G.] (1996). Gaip and RGS4 are GTPase-activating proteins for the Gi subfamily of G protein alpha subunits. *Cell*, *86*(3), 445–452. https://doi.org/10.1016/s0092-8674(00)80117-8

Bernard, P., Fleming, A., Lacombe, A., Harley, V. R., & Vilain, E. (2008). Wnt4 inhibits beta-catenin/TCF signalling by redirecting beta-catenin to the cell membrane. *Biology of the Cell*, *100*(3), 167–177. https://doi.org/10.1042/BC20070072

Berridge, M. J., Bootman, M. D., & Roderick, H. L. (2003). Calcium signalling: Dynamics, homeostasis and remodelling. *Nature Reviews. Molecular Cell Biology*, *4*(7), 517–529. https://doi.org/10.1038/nrm1155

Berstein, G., Blank, J. L., Jhon, D. Y., Exton, J. H., Rhee, S. G., & Ross, E. M [E. M.] (1992). Phospholipase C-beta 1 is a GTPase-activating protein for Gq/11, its physiologic regulator. *Cell*, *70*(3), 411–418. https://doi.org/10.1016/0092-8674(92)90165-9

Biddlecome, G. H., Berstein, G., & Ross, E. M [E. M.] (1996). Regulation of phospholipase C-beta1 by Gq and m1 muscarinic cholinergic receptor. Steady-state balance of receptor-mediated activation and GTPase-activating protein-promoted deactivation. *Journal of Biological Chemistry*, *271*(14), 7999–8007. https://doi.org/10.1074/jbc.271.14.7999

Bockaert, J., & Pin, J. P. (1998). Utiliser un recepteur couplé aux protéines G pour communiquer. Un succès évolutif [Use of a G-protein-coupled receptor to communicate. An evolutionary success]. *Comptes rendus de l'Academie des sciences. Serie III, Sciences de la vie*, *321*(7), 529–551. https://doi.org/10.1016/s0764-4469(98)80455-1

Bockaert, J., & Pin, J. P. (1999). Molecular tinkering of G protein-coupled receptors: An evolutionary success. *The EMBO Journal*, *18*(7), 1723–1729. https://doi.org/10.1093/emboj/18.7.1723

Boesgaard, M. W., Harpsøe, K., Malmberg, M., Underwood, C. R., Inoue, A., Mathiesen, J. M., König, G. M., Kostenis, E., Gloriam, D. E., & Bräuner-Osborne, H. (2020). Delineation of molecular determinants for FR900359 inhibition

of Gq/11 unlocks inhibition of Gαs. *The Journal of Biological Chemistry*, *295*(40), 13850–13861. https://doi.org/10.1074/jbc.RA120.013002

Böhme, I., & Beck-Sickinger, A. G. (2009). Illuminating the life of GPCRs. *Cell Communication and Signaling : CCS*, *7*, 16. https://doi.org/10.1186/1478-811X-7-16

Bond, B. J., & Davidson, N. (1986). The Drosophila melanogaster actin 5C gene uses two transcription initiation sites and three polyadenylation sites to express multiple mRNA species. *Molecular and Cellular Biology*, *6*(6), 2080–2088. https://doi.org/10.1128/mcb.6.6.2080-2088.1986

Bond-Matthews, B., & Davidson, N. (1988). Transcription from each of the Drosophila act5C leader exons is driven by a separate functional promoter. *Gene*, *62*(2), 289–300. https://doi.org/10.1016/0378-1119(88)90566-5

Bonifer, C., Hanke, W., Mühle, J., Löhr, F., Becker-Baldus, J., Nagel, J., Schertler, G. F. X., Müller, C. E., König, G. M., Hilger, D., & Glaubitz, C. (2024). Structural response of G protein binding to the cyclodepsipeptide inhibitor FR900359 probed by NMR spectroscopy. *Chemical Science*, *15*(32), 12939–12956. https://doi.org/10.1039/D4SC01950D

Bootman, M. D., & Bultynck, G. (2020). Fundamentals of Cellular Calcium Signaling: A Primer. *Cold Spring Harbor Perspectives in Biology*, *12*(1). https://doi.org/10.1101/cshperspect.a038802

Brand, A. H., & Perrimon, N [N.] (1993). Targeted gene expression as a means of altering cell fates and generating dominant phenotypes. *Development (Cambridge, England)*, *118*(2), 401–415. https://doi.org/10.1242/dev.118.2.401

Brands, J., Bravo, S., Jürgenliemke, L., Grätz, L., Schihada, H., Frechen, F., Alenfelder, J., Pfeil, C., Ohse, P. G., Hiratsuka, S., Kawakami, K., Schmacke, L. C., Heycke, N., Inoue, A., König, G., Pfeifer, A., Wachten, D., Schulte, G., Steinmetzer, T., . . . Kostenis, E. (2024). A molecular mechanism to diversify Ca2+ signaling downstream of Gs protein-coupled receptors. *Nature Communications*, *15*(1), 7684. https://doi.org/10.1038/s41467-024-51991-6

Brodskiy, P. A., Wu, Q., Soundarrajan, D. K., Huizar, F. J., Chen, J., Liang, P., Narciso, C., Levis, M. K., Arredondo-Walsh, N., Chen, D. Z., & Zartman, J. J. (2019). Decoding Calcium Signaling Dynamics during Drosophila Wing Disc Development. *Biophysical Journal*, *116*(4), 725–740. https://doi.org/10.1016/j.bpj.2019.01.007

Brundage, L., Avery, L., Katz, A., Kim, U. J., Mendel, J. E., Sternberg, P. W., & Simon, M. I. (1996). Mutations in a C. Elegans Gqalpha gene disrupt movement, egg laying, and viability. *Neuron*, *16*(5), 999–1009. https://doi.org/10.1016/S0896-6273(00)80123-3

Burkhard, K., & Shapiro, P. (2010). Use of inhibitors in the study of MAP kinases. *Methods in Molecular Biology (Clifton, N.J.)*, *661*, 107–122. https://doi.org/10.1007/978-1-60761-795-2_6

Burn, T. C., Vigoreaux, J. O., & Tobin, S. L. (1989). Alternative 5C actin transcripts are localized in different patterns during Drosophila embryogenesis. *Developmental Biology*, *131*(2), 345–355. https://doi.org/10.1016/s0012-1606(89)80008-9

Cabrera-Vera, T. M., Vanhauwe, J., Thomas, T. O., Medkova, M., Preininger, A., Mazzoni, M. R., & Hamm, H. E [Heidi E.] (2003). Insights into G protein structure, function, and regulation. *Endocrine Reviews*, *24*(6), 765–781. https://doi.org/10.1210/er.2000-0026

Campbell, A. P., & Smrcka, A. V [Alan V.] (2018). Targeting G protein-coupled receptor signalling by blocking G proteins. *Nature Reviews. Drug Discovery*, *17*(11), 789–803. https://doi.org/10.1038/nrd.2018.135

Cao, J., Bollepalli, M. K., Hu, Y., Zhang, J., Li, Q., Li, H., Chang, H., Xiao, F., Hardie, R. C., Rong, Y. S., & Hu, W. (2018). A Single Residue Mutation in the Gαq Subunit of the G Protein Complex Causes Blindness in Drosophila. *G3 (Bethesda, Md.)*, *8*(1), 363–371. https://doi.org/10.1534/g3.117.300340

Carlier, A [Aurelien], Fehr, L., Pinto-Carbó, M., Schäberle, T., Reher, R., Dessein, S., König, G., & Eberl, L. (2016). The genome analysis of Candidatus Burkholderia crenata reveals that secondary metabolism may be a key function of the Ardisia crenata leaf nodule symbiosis. *Environmental Microbiology*, *18*(8), 2507–2522. https://doi.org/10.1111/1462-2920.13184

Černe, U., Horvat, A., Sanjković, E., Kozoderc, N., Kreft, M., Zorec, R., Scholz, N., & Vardjan, N. (2025). Ca2+ excitability of glia to neuromodulator octopamine in Drosophila living brain is greater than that of neurons. *Acta Physiologica (Oxford, England)*, *241*(2), e14270. https://doi.org/10.1111/apha.14270

Chan, P., Thomas, C. J., Sprang, S. R [Stephen R.], & Tall, G. G. (2013). Molecular chaperoning function of Ric-8 is to fold nascent heterotrimeric G protein α subunits. *Proceedings of the National Academy of Sciences of the United States of America*, *110*(10), 3794–3799. https://doi.org/10.1073/pnas.1220943110

Chauhan, V., Anis, A., & Chauhan, A. (2021). Effects of Starvation on the Levels of Triglycerides, Diacylglycerol, and Activity of Lipase in Male and Female Drosophila Melanogaster. *Journal of Lipids*, *2021*, 5583114. https://doi.org/10.1155/2021/5583114

Chippindale, A. K., Chu, T. J. F., & Rose, M. R. (1996). Complex TRADE-OFFS AND THE EVOLUTION OF STARVATION RESISTANCE IN DROSOPHILA MELANOGASTER. *Evolution; International Journal of Organic Evolution*, *50*(2), 753–766. https://doi.org/10.1111/j.1558-5646.1996.tb03885.x

Chua, V., Lapadula, D., Randolph, C., Benovic, J. L., Wedegaertner, P. B [Philip B.], & Aplin, A. E. (2017). Dysregulated GPCR Signaling and Therapeutic Options in Uveal Melanoma. *Molecular Cancer Research : MCR*, *15*(5), 501–506. https://doi.org/10.1158/1541-7786.MCR-17-0007

Chung, Y. T., & Keller, E. B. (1990). Regulatory elements mediating transcription from the Drosophila melanogaster actin 5C proximal promoter. *Molecular and Cellular Biology*, *10*(1), 206–216. https://doi.org/10.1128/mcb.10.1.206-216.1990

Clapham, D. E [D. E.], & Neer, E. J. (1997). G protein beta gamma subunits. *Annual Review of Pharmacology and Toxicology*, *37*, 167–203. https://doi.org/10.1146/annurev.pharmtox.37.1.167

Clapham, D. E [David E.] (2007). Calcium signaling. *Cell*, *131*(6), 1047–1058. https://doi.org/10.1016/j.cell.2007.11.028

Coleman, A. W., Maguire, M. J., & Coleman, J. R. (1981). Mithramycin- and 4'-6-diamidino-2-phenylindole (DAPI)-DNA staining for fluorescence microspectrophotometric measurement of DNA in nuclei, plastids, and virus particles. *The Journal of Histochemistry and Cytochemistry : Official Journal of the Histochemistry Society*, *29*(8), 959–968. https://doi.org/10.1177/29.8.6168681

Coleman, D. E., Berghuis, A. M., Lee, E., Linder, M. E., Gilman, A. G [A. G.], & Sprang, S. R [S. R.] (1994). Structures of active conformations of Gi alpha 1 and the mechanism of GTP hydrolysis. *Science (New York, N.Y.)*, *265*(5177), 1405–1412. https://doi.org/10.1126/science.8073283

Coleman, D. E., & Sprang, S. R [S. R.] (1998). Crystal structures of the G protein Gi alpha 1 complexed with GDP and Mg2+: A crystallographic titration experiment. *Biochemistry*, *37*(41), 14376–14385. https://doi.org/10.1021/bi9810306

Conklin, B. R., Brann, M. R., Buckley, N. J., Ma, A. L., Bonner, T. I., & Axelrod, J. (1988). Stimulation of arachidonic acid release and inhibition of mitogenesis by cloned genes for muscarinic receptor subtypes stably expressed in A9 L cells. *Proceedings of the National Academy of Sciences*, *85*(22), 8698–8702. https://doi.org/10.1073/pnas.85.22.8698

Crüsemann, M., Reher, R., Schamari, I., Brachmann, A. O., Ohbayashi, T., Kuschak, M., Malfacini, D., Seidinger, A., Pinto-Carbó, M., Richarz, R., Reuter, T., Kehraus, S., Hallab, A., Attwood, M., Schiöth, H. B., Mergaert, P., Kikuchi, Y., Schäberle, T. F., Kostenis, E., . . . König, G. M. (2018). Heterologous Expression, Biosynthetic Studies, and Ecological Function of the Selective Gq-Signaling Inhibitor FR900359. *Angewandte Chemie (International Ed. In English)*, *57*(3), 836–840.

Dahse, A.-K. (2024). *The versatile model organism Drosophila melanogaster – Insight into ADGRL/Cirl biology, Gq-dependent effects of a plant-derived toxin, and aspects of neuronal biomechanics* [Dissertation]. University Leipzig, Leipzig.

Dai, S. A., Hu, Q., Gao, R., Blythe, E. E., Touhara, K. K., Peacock, H., Zhang, Z., Zastrow, M. von, Suga, H., & Shokat, K. M. (2022). State-selective modulation of heterotrimeric Gαs signaling with macrocyclic peptides. *Cell*, *185*(21), 3950-3965.e25. https://doi.org/10.1016/j.cell.2022.09.019

Daub, H., Wallasch, C., Lankenau, A., Herrlich, A., & Ullrich, A. (1997). Signal characteristics of G protein-transactivated EGF receptor. *The EMBO Journal*, *16*(23), 7032–7044. https://doi.org/10.1093/emboj/16.23.7032

Day, P. W., Tesmer, J. J. G., Sterne-Marr, R., Freeman, L. C., Benovic, J. L., & Wedegaertner, P. B [Philip B.] (2004). Characterization of the GRK2 binding site of Galphaq. *Journal of Biological Chemistry*, *279*(51), 53643–53652. https://doi.org/10.1074/jbc.M401438200

Dayhoff, M. O. (Ed.). (1979). *Atlas of protein sequence and structure* (Vol. 5). National Biomedical Research Foundation.

Devost, D., Sleno, R., Pétrin, D., Zhang, A., Shinjo, Y., Okde, R., Aoki, J., Inoue, A., & Hébert, T. E. (2017). Conformational Profiling of the AT1 Angiotensin II Receptor Reflects Biased Agonism, G Protein Coupling, and Cellular Context. *The Journal of Biological Chemistry*, *292*(13), 5443–5456. https://doi.org/10.1074/jbc.M116.763854

DiGiacomo, V., Maziarz, M., Luebbers, A., Norris, J. M., Laksono, P., & Garcia-Marcos, M. (2020). Probing the mutational landscape of regulators of G protein signaling proteins in cancer. *Science Signaling*, *13*(617). https://doi.org/10.1126/scisignal.aax8620

Dong, Q., Shenker, A., Way, J., Haddad, B. R., Lin, K., Hughes, M. R., McBride, O. W., Spiegel, A. M., & Battey, J. (1995). Molecular cloning of human G alpha q cDNA and chromosomal localization of the G alpha q gene (GNAQ) and a processed pseudogene. *Genomics*, *30*(3), 470–475. https://doi.org/10.1006/geno.1995.1267

Doytchinova, I. (2022). Drug Design-Past, Present, Future. *Molecules (Basel, Switzerland)*, *27*(5). https://doi.org/10.3390/molecules27051496

DuBridge, R. B., Tang, P., Hsia, H. C., Leong, P. M., Miller, J. H., & Calos, M. P [M. P.] (1987). Analysis of mutation in human cells by using an Epstein-Barr virus shuttle system. *Molecular and Cellular Biology*, *7*(1), 379–387. https://doi.org/10.1128/MCB.7.1.379

Eglen, R. M., Gilchrist, A., & Reisine, T. (2008). The use of immortalized cell lines in GPCR screening: The good, bad and ugly. *Combinatorial Chemistry & High Throughput Screening*, *11*(7), 560–565. https://doi.org/10.2174/138620708785204144

Eryilmaz, F. (2023). *Inhibition of heterotrimeric Gs proteins by FR900359 - more than a simple transfer of the inhibitor binding site* [Dissertation, Rheinischen Friedrich-Wilhelms-Universität Bonn, Bonn]. bonndoc.ulb.uni-bonn.de. https://bonndoc.ulb.uni-bonn.de/xmlui/handle/20.500.11811/10671

Evanko, D. S., Thiyagarajan, M. M., & Wedegaertner, P. B [P. B.] (2000). Interaction with Gbetagamma is required for membrane targeting and palmitoylation of Galpha(s) and Galpha(q). *Journal of Biological Chemistry*, *275*(2), 1327–1336. https://doi.org/10.1074/jbc.275.2.1327

Flock, T., Ravarani, C. N. J., Sun, D., Venkatakrishnan, A. J., Kayikci, M., Tate, C. G., Veprintsev, D. B., & Babu, M. M. (2015). Universal allosteric mechanism for Gα activation by GPCRs. *Nature*, *524*(7564), 173–179. https://doi.org/10.1038/nature14663.

Fogel, D. B. (2018). Factors associated with clinical trials that fail and opportunities for improving the likelihood of success: A review. *Contemporary Clinical Trials Communications*, *11*, 156–164. https://doi.org/10.1016/j.conctc.2018.08.001

Fredriksson, R., Lagerström, M. C., Lundin, L.-G., & Schiöth, H. B. (2003). The G-protein-coupled receptors in the human genome form five main families. Phylogenetic analysis, paralogon groups, and fingerprints. *Molecular Pharmacology*, *63*(6), 1256–1272. https://doi.org/10.1124/mol.63.6.1256

Fredriksson, R., & Schiöth, H. B. (2005). The repertoire of G-protein-coupled receptors in fully sequenced genomes. *Molecular Pharmacology*, *67*(5), 1414–1425. https://doi.org/10.1124/mol.104.009001

Freissmuth, M., Boehm, S., Beindl, W., Nickel, P., Ijzerman, A. P., Hohenegger, M., & Nanoff, C. (1996). Suramin analogues as subtype-selective G protein inhibitors. *Molecular Pharmacology*, *49*(4), 602–611.

Fujioka, M., Koda, S., Morimoto, Y., & Biemann, K. (1988). Structure of FR900359, a cyclic depsipeptide from Ardisia crenata sims. *The Journal of Organic Chemistry*, *53*(12), 2820–2825. https://doi.org/10.1021/jo00247a030

Fukuda, K., Higashida, H., Kubo, T., Maeda, A., Akiba, I., Bujo, H., Mishina, M., & Numa, S. (1988). Selective coupling with K+ currents of muscarinic acetylcholine receptor subtypes in NG108-15 cells. *Nature*, *335*(6188), 355–358. https://doi.org/10.1038/335355a0

Gabay, M., Pinter, M. E., Wright, F. A., Chan, P., Murphy, A. J., Valenzuela, D. M., Yancopoulos, G. D., & Tall, G. G. (2011). Ric-8 proteins are molecular chaperones that direct nascent G protein α subunit membrane association. *Science Signaling*, *4*(200), ra79. https://doi.org/10.1126/scisignal.2002223

Gao, Z.-G., & Jacobson, K. A. (2016). On the selectivity of the Gαq inhibitor UBO-QIC: A comparison with the Gαi inhibitor pertussis toxin. *Biochemical Pharmacology*, *107*, 59–66. https://doi.org/10.1016/j.bcp.2016.03.003

Gargano, J. W., Martin, I., Bhandari, P., & Grotewiel, M. S. (2005). Rapid iterative negative geotaxis (RING): A new method for assessing age-related locomotor decline in Drosophila. *Experimental Gerontology*, *40*(5), 386–395. https://doi.org/10.1016/j.exger.2005.02.005

Gilman, A. G [Alfred G.] (1987). G Proteins: Transducers of receptor-generated signals. *Annual Review of Biochemistry*, *56*(Volume 56, 1987), 615–649. https://doi.org/10.1146/annurev.bi.56.070187.003151

Goldman, D. W., Chang, F. H., Gifford, L. A., Goetzl, E. J., & Bourne, H. R. (1985). Pertussis toxin inhibition of chemotactic factor-induced calcium mobilization and

function in human polymorphonuclear leukocytes. *The Journal of Experimental Medicine*, *162*(1), 145–156. https://doi.org/10.1084/jem.162.1.145

Gonnet, G. H., Cohen, M. A., & Benner, S. A. (1992). Exhaustive matching of the entire protein sequence database. *Science (New York, N.Y.)*, *256*(5062), 1443–1445. https://doi.org/10.1126/science.1604319

Goujon, M., McWilliam, H., Li, W., Valentin, F., Squizzato, S., Paern, J., & Lopez, R. (2010). A new bioinformatics analysis tools framework at EMBL-EBI. *Nucleic Acids Research*, *38*(Web Server issue), W695-9. https://doi.org/10.1093/nar/gkq313

Gratz, S. J., Ukken, F. P., Rubinstein, C. D., Thiede, G., Donohue, L. K., Cummings, A. M., & O'Connor-Giles, K. M. (2014). Highly specific and efficient CRISPR/Cas9-catalyzed homology-directed repair in Drosophila. *Genetics*, *196*(4), 961–971. https://doi.org/10.1534/genetics.113.160713

Groth, A. C., & Calos, M. P [Michele P.] (2004). Phage integrases: Biology and applications. *Journal of Molecular Biology*, *335*(3), 667–678. https://doi.org/10.1016/j.jmb.2003.09.082

Groth, A. C., Fish, M., Nusse, R., & Calos, M. P [Michele P.] (2004). Construction of transgenic Drosophila by using the site-specific integrase from phage phiC31. *Genetics*, *166*(4), 1775–1782. https://doi.org/10.1093/genetics/166.4.1775

Gu, Q., Wu, J., Tian, Y., Cheng, S., Zhang, Z. C., & Han, J. (2020). Gαq splice variants mediate phototransduction, rhodopsin synthesis, and retinal integrity in Drosophila. *The Journal of Biological Chemistry*, *295*(17), 5554–5563. https://doi.org/10.1074/jbc.RA120.012764

Gulyás, G., Tóth, J. T., Tóth, D. J., Kurucz, I., Hunyady, L., Balla, T., & Várnai, P. (2015). Measurement of inositol 1,4,5-trisphosphate in living cells using an improved set of resonance energy transfer-based biosensors. *PloS One*, *10*(5), e0125601. https://doi.org/10.1371/journal.pone.0125601

Hana, S., & Lange, A. B. (2017). Cloning and Functional Characterization of Octβ2-Receptor and Tyr1-Receptor in the Chagas Disease Vector, Rhodnius prolixus. *Frontiers in Physiology*, *8*, 744. https://doi.org/10.3389/fphys.2017.00744

Hanke, W., Alenfelder, J., Liu, J., Gutbrod, P., Kehraus, S., Crüsemann, M., Dörmann, P., Kostenis, E., Scholz, M., & König, G. M. (2023). The Bacterial Gq Signal Transduction Inhibitor FR900359 Impairs Soil-Associated Nematodes. *Journal of Chemical Ecology*, *49*(9-10), 549–569. https://doi.org/10.1007/s10886-023-01442-1

Hardie, R. C., & Juusola, M. (2015). Phototransduction in Drosophila. *Current Opinion in Neurobiology*, *34*, 37–45. https://doi.org/10.1016/j.conb.2015.01.008

Hargrave, P. A., Hamm, H. E [H. E.], & Hofmann, K. P. (1993). Interaction of rhodopsin with the G-protein, transducin. *BioEssays : News and Reviews in*

Molecular, Cellular and Developmental Biology, *15*(1), 43–50. https://doi.org/10.1002/bies.950150107

Hepler, J. R., Berman, D. M., Gilman, A. G [A. G.], & Kozasa, T [T.] (1997). Rgs4 and GAIP are GTPase-activating proteins for Gq alpha and block activation of phospholipase C beta by gamma-thio-GTP-Gq alpha. *Proceedings of the National Academy of Sciences of the United States of America*, *94*(2), 428–432. https://doi.org/10.1073/pnas.94.2.428

Herman, J. A., Willits, A. B., & Bellemer, A. (2018). Gαq and Phospholipase Cβ signaling regulate nociceptor sensitivity in Drosophila melanogaster larvae. *PeerJ*, *6*, e5632. https://doi.org/10.7717/peerj.5632

Hermes, C. (2021). *Investigations into side chain assembly and attachment during biosynthesis of the G protein inhibitor FR900359* [Dissertation, Rheinischen Friedrich-Wilhelms-Universität Bonn, Bonn]. bonndoc.ulb.uni-bonn.de. https://bonndoc.ulb.uni-bonn.de/xmlui/handle/20.500.11811/9126

Hermes, C., Richarz, R., Wirtz, D. A., Patt, J., Hanke, W., Kehraus, S., Voß, J. H., Küppers, J., Ohbayashi, T., Namasivayam, V., Alenfelder, J., Inoue, A., Mergaert, P., Gütschow, M., Müller, C. E., Kostenis, E., König, G. M., & Crüsemann, M. (2021). Thioesterase-mediated side chain transesterification generates potent Gq signaling inhibitor FR900359. *Nature Communications*, *12*(1), 144. https://doi.org/10.1038/s41467-020-20418-3

Himmelreich, S., Masuho, I., Berry, J. A., MacMullen, C., Skamangas, N. K., Martemyanov, K. A., & Davis, R. L. (2017). Dopamine Receptor DAMB Signals via Gq to Mediate Forgetting in Drosophila. *Cell Reports*, *21*(8), 2074–2081. https://doi.org/10.1016/j.celrep.2017.10.108

Hisano, Y., Kono, M., Cartier, A., Engelbrecht, E., Kano, K., Kawakami, K., Xiong, Y., Piao, W., Galvani, S., Yanagida, K., Kuo, A., Ono, Y., Ishida, S., Aoki, J., Proia, R. L., Bromberg, J. S., Inoue, A., & Hla, T. (2019). Lysolipid receptor cross-talk regulates lymphatic endothelial junctions in lymph nodes. *The Journal of Experimental Medicine*, *216*(7), 1582–1598. https://doi.org/10.1084/jem.20181895

Hollins, B., Kuravi, S., Digby, G. J., & Lambert, N. A. (2009). The c-terminus of GRK3 indicates rapid dissociation of G protein heterotrimers. *Cellular Signalling*, *21*(6), 1015–1021. https://doi.org/10.1016/j.cellsig.2009.02.017

Hulme, E. C., Birdsall, N. J., & Buckley, N. J. (1990). Muscarinic receptor subtypes. *Annual Review of Pharmacology and Toxicology*, *30*(Volume 30, 1990), 633–673. https://doi.org/10.1146/annurev.pa.30.040190.003221

Inagaki, H. K., Kamikouchi, A., & Ito, K. (2010). Methods for quantifying simple gravity sensing in Drosophila melanogaster. *Nature Protocols*, *5*(1), 20–25. https://doi.org/10.1038/nprot.2009.196

Katanayeva, N., Kopein, D., Portmann, R., Hess, D., & Katanaev, V. L. (2010). Competing activities of heterotrimeric G proteins in Drosophila wing maturation. *PloS One*, *5*(8), e12331. https://doi.org/10.1371/journal.pone.0012331

Keen, A. C., Pedersen, M. H., Lemel, L., Scott, D. J., Canals, M., Littler, D. R., Beddoe, T., Ono, Y., Shi, L., Inoue, A., Javitch, J. A., & Lane, J. R. (2022). Ozitx, a pertussis toxin-like protein for occluding inhibitory G protein signalling including Gαz. *Communications Biology*, *5*(1), 256. https://doi.org/10.1038/s42003-022-03191-5

Kolakowski, L. F. (1994). Gcrdb: A G-protein-coupled receptor database. *Receptors & Channels*, *2*(1), 1–7.

Krebs, K. M., Pfeil, E. M [Eva M.], Simon, K., Grundmann, M., Häberlein, F., Bautista-Aguilera, O. M., Gütschow, M., Weaver, C. D., Fleischmann, B. K., & Kostenis, E. (2018). Label-Free Whole Cell Biosensing for High-Throughput Discovery of Activators and Inhibitors Targeting G Protein-Activated Inwardly Rectifying Potassium Channels. *ACS Omega*, *3*(11), 14814–14823. https://doi.org/10.1021/acsomega.8b02254

Krumins, A. M., & Gilman, A. G [Alfred G.] (2006). Targeted knockdown of G protein subunits selectively prevents receptor-mediated modulation of effectors and reveals complex changes in non-targeted signaling proteins. *Journal of Biological Chemistry*, *281*(15), 10250–10262. https://doi.org/10.1074/jbc.M511551200

Kwok-Keung Fung, B., & Stryer, L. (1980). Photolyzed rhodopsin catalyzes the exchange of GTP for bound GDP in retinal rod outer segments. *Proceedings of the National Academy of Sciences of the United States of America*, *77*(5), 2500–2504. https://doi.org/10.1073/pnas.77.5.2500

Lambert, N. A., Johnston, C. A., Cappell, S. D., Kuravi, S., Kimple, A. J., Willard, F. S., & Siderovski, D. P. (2010). Regulators of G-protein signaling accelerate GPCR signaling kinetics and govern sensitivity solely by accelerating GTPase activity. *Proceedings of the National Academy of Sciences of the United States of America*, *107*(15), 7066–7071. https://doi.org/10.1073/pnas.0912934107

Lambright, D. G., Noel, J. P., Hamm, H. E [H. E.], & Sigler, P. B. (1994). Structural determinants for activation of the alpha-subunit of a heterotrimeric G protein. *Nature*, *369*(6482), 621–628. https://doi.org/10.1038/369621a0

Lambright, D. G., Sondek, J [J.], Bohm, A., Skiba, N. P., Hamm, H. E [H. E.], & Sigler, P. B. (1996). The 2.0 A crystal structure of a heterotrimeric G protein. *Nature*, *379*(6563), 311–319. https://doi.org/10.1038/379311a0

Landis, C. A., Masters, S. B., Spada, A., Pace, A. M., Bourne, H. R., & Vallar, L. (1989). Gtpase inhibiting mutations activate the alpha chain of Gs and stimulate adenylyl cyclase in human pituitary tumours. *Nature*, *340*(6236), 692–696. https://doi.org/10.1038/340692a0

Leberer, E., Thomas, D. Y., & Whiteway, M. (1997). Pheromone signalling and polarized morphogenesis in yeast. *Current Opinion in Genetics & Development*, *7*(1), 59–66. https://doi.org/10.1016/S0959-437X(97)80110-4

Lee, S. B., Shin, S. H., Hepler, J. R., Gilman, A. G [A. G.], & Rhee, S. G. (1993). Activation of phospholipase C-beta 2 mutants by G protein alpha q and beta gamma subunits. *Journal of Biological Chemistry*, *268*(34), 25952–25957. https://doi.org/10.1016/S0021-9258(19)74479-2

Lee, Y. J., Dobbs, M. B., Verardi, M. L., & Hyde, D. R. (1990). Dgq: A drosophila gene encoding a visual system-specific G alpha molecule. *Neuron*, *5*(6), 889–898. https://doi.org/10.1016/0896-6273(90)90349-k

Lee, Y. J., Shah, S., Suzuki, E., Zars, T., O'Day, P. M., & Hyde, D. R. (1994). The Drosophila dgq gene encodes a G alpha protein that mediates phototransduction. *Neuron*, *13*(5), 1143–1157. https://doi.org/10.1016/0896-6273(94)90052-3

Lim, Y. H., Bacchiocchi, A., Qiu, J., Straub, R., Bruckner, A., Bercovitch, L., Narayan, D., McNiff, J., Ko, C., Robinson-Bostom, L., Antaya, R., Halaban, R., & Choate, K. A. (2016). Gna14 Somatic Mutation Causes Congenital and Sporadic Vascular Tumors by MAPK Activation. *American Journal of Human Genetics*, *99*(2), 443–450. https://doi.org/10.1016/j.ajhg.2016.06.010

Logothetis, D. E., Kurachi, Y., Galper, J., Neer, E. J., & Clapham, D. E [D. E.] (1987). The beta gamma subunits of GTP-binding proteins activate the muscarinic K+ channel in heart. *Nature*, *325*(6102), 321–326. https://doi.org/10.1038/325321a0

Lyon, A. M., Dutta, S., Boguth, C. A., Skiniotis, G., & Tesmer, J. J. G. (2013). Full-length Gα(q)-phospholipase C-β3 structure reveals interfaces of the C-terminal coiled-coil domain. *Nature Structural & Molecular Biology*, *20*(3), 355–362. https://doi.org/10.1038/nsmb.2497

Madeira, F., Madhusoodanan, N., Lee, J., Eusebi, A., Niewielska, A., Tivey, A. R. N., Lopez, R., & Butcher, S. (2024). The EMBL-EBI Job Dispatcher sequence analysis tools framework in 2024. *Nucleic Acids Research*, *52*(W1), W521-W525. https://doi.org/10.1093/nar/gkae241

Malfacini, D., Patt, J., Annala, S., Harpsøe, K., Eryilmaz, F., Reher, R., Crüsemann, M., Hanke, W., Zhang, H., Tietze, D., Gloriam, D. E., Bräuner-Osborne, H., Strømgaard, K., König, G. M., Inoue, A., Gomeza, J [Jesus], & Kostenis, E. (2019). Rational design of a heterotrimeric G protein α subunit with artificial inhibitor sensitivity. *The Journal of Biological Chemistry*, *294*(15), 5747–5758. https://doi.org/10.1074/jbc.RA118.007250

Markstein, M., Pitsouli, C., Villalta, C., Celniker, S. E., & Perrimon, N [Norbert] (2008). Exploiting position effects and the gypsy retrovirus insulator to engineer precisely expressed transgenes. *Nature Genetics*, *40*(4), 476–483. https://doi.org/10.1038/ng.101

Masuho, I., Balaji, S., Muntean, B. S., Skamangas, N. K., Chavali, S., Tesmer, J. J. G., Babu, M. M., & Martemyanov, K. A. (2020). A Global Map of G Protein Signaling Regulation by RGS Proteins. *Cell*, *183*(2), 503-521.e19. https://doi.org/10.1016/j.cell.2020.08.052

Masuho, I., Ostrovskaya, O., Kramer, G. M., Jones, C. D., Xie, K., & Martemyanov, K. A. (2015). Distinct profiles of functional discrimination among G proteins determine the actions of G protein-coupled receptors. *Science Signaling*, *8*(405), ra123. https://doi.org/10.1126/scisignal.aab4068

Matthey, M., Roberts, R., Seidinger, A., Simon, A., Schröder, R., Kuschak, M., Annala, S., König, G. M., Müller, C. E., Hall, I. P., Kostenis, E., Fleischmann, B. K., & Wenzel, D. (2017). Targeted inhibition of Gq signaling induces airway relaxation in mouse models of asthma. *Science Translational Medicine*, *9*(407). https://doi.org/10.1126/scitranslmed.aag2288

Maziarz, M., Park, J.-C., Leyme, A., Marivin, A., Garcia-Lopez, A., Patel, P. P., & Garcia-Marcos, M. (2020). Revealing the Activity of Trimeric G-proteins in Live Cells with a Versatile Biosensor Design. *Cell*, *182*(3), 770-785.e16. https://doi.org/10.1016/j.cell.2020.06.020

McNeely, P. M., Naranjo, A. N., & Robinson, A. S. (2012). Structure-function studies with G protein-coupled receptors as a paradigm for improving drug discovery and development of therapeutics. *Biotechnology Journal*, *7*(12), 1451–1461. https://doi.org/10.1002/biot.201200076

Meleka, M. M., Edwards, A. J., Xia, J., Dahlen, S. A., Mohanty, I., Medcalf, M., Aggarwal, S., Moeller, K. D., Mortensen, O. V., & Osei-Owusu, P. (2019). Anti-hypertensive mechanisms of cyclic depsipeptide inhibitor ligands for Gq/11 class G proteins. *Pharmacological Research*, *141*, 264–275. https://doi.org/10.1016/j.phrs.2019.01.012

Mondal, S., Hsiao, K., & Goueli, S. A. (2015). A Homogenous Bioluminescent System for Measuring GTPase, GTPase Activating Protein, and Guanine Nucleotide Exchange Factor Activities. *Assay and Drug Development Technologies*, *13*(8), 444–455. https://doi.org/10.1089/adt.2015.643

Mühle, J., Alenfelder, J., Rodrigues, M. J., Jürgenliemke, L., Guixà-González, R., Grätz, L., Andres, F., Bacchin, A., Hennig, M., Schihada, H., Crüsemann, M., König, G. M., Schertler, G., Kostenis, E., & Deupi, X. (2025). Cyclic peptide inhibitors function as molecular glues to stabilize Gq/11 heterotrimers. *Proceedings of the National Academy of Sciences of the United States of America*, *122*(19), e2418398122. https://doi.org/10.1073/pnas.2418398122

Nance, M. R., Kreutz, B., Tesmer, V. M., Sterne-Marr, R., Kozasa, T [Tohru], & Tesmer, J. J. G. (2013). Structural and functional analysis of the regulator of G protein signaling 2-gαq complex. *Structure (London, England : 1993)*, *21*(3), 438–448. https://doi.org/10.1016/j.str.2012.12.016

Narayanan, A. S., & Rothenfluh, A. (2016). I Believe I Can Fly! Use of Drosophila as a Model Organism in Neuropsychopharmacology Research. *Neuropsychopharmacology : Official Publication of the American College of Neuropsychopharmacology*, *41*(6), 1439–1446. https://doi.org/10.1038/npp.2015.322

Navot, S., & Kosloff, M. (2019). Structural design principles that underlie the multi-specific interactions of Gαq with dissimilar partners. *Scientific Reports*, *9*(1), 6898. https://doi.org/10.1038/s41598-019-43395-0

Neuwald, A. F. (2007). Galpha Gbetagamma dissociation may be due to retraction of a buried lysine and disruption of an aromatic cluster by a GTP-sensing Arg Trp pair. *Protein Science : A Publication of the Protein Society*, *16*(11), 2570–2577. https://doi.org/10.1110/ps.073098107

Neves, S. R., Ram, P. T., & Iyengar, R. (2002). G protein pathways. *Science (New York, N.Y.)*, *296*(5573), 1636–1639. https://doi.org/10.1126/science.1071550

Nichols, C. D., Becnel, J., & Pandey, U. B. (2012). Methods to assay Drosophila behavior. *Journal of Visualized Experiments : JoVE.* Advance online publication. https://doi.org/10.3791/3795

Nishimura, A., Kitano, K., Takasaki, J., Taniguchi, M., Mizuno, N., Tago, K., Hakoshima, T., & Itoh, H. (2010). Structural basis for the specific inhibition of heterotrimeric Gq protein by a small molecule. *Proceedings of the National Academy of Sciences of the United States of America*, *107*(31), 13666–13671. https://doi.org/10.1073/pnas.1003553107

Noel, J. P., Hamm, H. E [H. E.], & Sigler, P. B. (1993). The 2.2 A crystal structure of transducin-alpha complexed with GTP gamma S. *Nature*, *366*(6456), 654–663. https://doi.org/10.1038/366654a0

Offermanns, S [S.], Hashimoto, K., Watanabe, M., Sun, W., Kurihara, H., Thompson, R. F., Inoue, Y., Kano, M., & Simon, M. I. (1997). Impaired motor coordination and persistent multiple climbing fiber innervation of cerebellar Purkinje cells in mice lacking Galphaq. *Proceedings of the National Academy of Sciences*, *94*(25), 14089–14094. https://doi.org/10.1073/pnas.94.25.14089

Offermanns, S [S.], Toombs, C. F., Hu, Y. H., & Simon, M. I. (1997). Defective platelet activation in G alpha(q)-deficient mice. *Nature*, *389*(6647), 183–186. https://doi.org/10.1038/38284

Offermanns, S [S.], Zhao, L. P., Gohla, A., Sarosi, I., Simon, M. I., & Wilkie, T. M. (1998). Embryonic cardiomyocyte hypoplasia and craniofacial defects in G alpha q/G alpha 11-mutant mice. *The EMBO Journal*, *17*(15), 4304–4312. https://doi.org/10.1093/emboj/17.15.4304

Offermanns, S [Stefan] (2003). G-proteins as transducers in transmembrane signalling. *Progress in Biophysics and Molecular Biology*, *83*(2), 101–130. https://doi.org/10.1016/s0079-6107(03)00052-x

Oldham, W. M., & Hamm, H. E [Heidi E.] (2008). Heterotrimeric G protein activation by G-protein-coupled receptors. *Nature Reviews. Molecular Cell Biology*, *9*(1), 60–71. https://doi.org/10.1038/nrm2299

Onken, M. D., Makepeace, C. M., Kaltenbronn, K. M., Kanai, S. M., Todd, T. D., Wang, S., Broekelmann, T. J., Rao, P. K., Cooper, J. A., & Blumer, K. J. (2018).

Targeting nucleotide exchange to inhibit constitutively active G protein α subunits in cancer cells. *Science Signaling*, *11*(546). https://doi.org/10.1126/scisignal.aao6852

Onken, M. D., Worley, L. A., Long, M. D., Duan, S., Council, M. L., Bowcock, A. M., & Harbour, J. W. (2008). Oncogenic mutations in GNAQ occur early in uveal melanoma. *Investigative Ophthalmology & Visual Science*, *49*(12), 5230–5234. https://doi.org/10.1167/iovs.08-2145

Orsulic, S., Huber, O., Aberle, H., Arnold, S., & Kemler, R. (1999). E-cadherin binding prevents beta-catenin nuclear localization and beta-catenin/LEF-1-mediated transactivation. *Journal of Cell Science*, *112 (Pt 8)*, 1237–1245. https://doi.org/10.1242/jcs.112.8.1237

Papasergi-Scott, M. M., Pérez-Hernández, G., Batebi, H., Gao, Y., Eskici, G., Seven, A. B., Panova, O., Hilger, D., Casiraghi, M., He, F., Maul, L., Gmeiner, P., Kobilka, B. K., Hildebrand, P. W., & Skiniotis, G. (2024). Time-resolved cryo-EM of G-protein activation by a GPCR. *Nature*, *629*(8014), 1182–1191. https://doi.org/10.1038/s41586-024-07153-1

Parenti, M., Viganó, M. A., Newman, C. M., Milligan, G [G.], & Magee, A. I. (1993). A novel N-terminal motif for palmitoylation of G-protein alpha subunits. *The Biochemical Journal*, *291 (Pt 2)*(Pt 2), 349–353. https://doi.org/10.1042/bj2910349

Patt, J. (2021). *In-vitro Studies on the Selective Gq Proteins Inhibitors FR900359 and YM-254890; Mechanisms of Action and Pharmacological Applications* [Dissertation, Rheinischen Friedrich-Wilhelms-Universität Bonn, Bonn]. Original source.

Patt, J., Alenfelder, J., Pfeil, E. M [Eva Marie], Voss, J. H [Jan Hendrik], Merten, N., Eryilmaz, F., Heycke, N., Rick, U [Uli], Inoue, A., Kehraus, S., Deupi, X., Müller, C. E., König, G. M., Crüsemann, M., & Kostenis, E. (2021). An experimental strategy to probe Gq contribution to signal transduction in living cells. *The Journal of Biological Chemistry*, *296*, 100472. https://doi.org/10.1016/j.jbc.2021.100472

Peng, Q., Alqahtani, S., Nasrullah, M. Z. A., & Shen, J. (2021). Functional evidence for biased inhibition of G protein signaling by YM-254890 in human coronary artery endothelial cells. *European Journal of Pharmacology*, *891*, 173706. https://doi.org/10.1016/j.ejphar.2020.173706

Pierce, K. L., Premont, R. T., & Lefkowitz, R. J. (2002). Seven-transmembrane receptors. *Nature Reviews. Molecular Cell Biology*, *3*(9), 639–650. https://doi.org/10.1038/nrm908

Pistorius, D., Buntin, K., Weber, E., Richard, E., Bouquet, C., Wollbrett, S., Regenass, H., Peón, V., Böhm, M., Kessler, R., Gempeler, T., Haberkorn, A., Wimmer, L., Lanshoeft, C., Davis, J., Hainzl, D., D'Alessio, J. A., Manchado, E., & Petersen, F. (2022). Promoter-Driven Overexpression in Chromobacterium vaccinii Facilitates Access to FR900359 and Yields Novel Low Abundance Analogs.

Chemistry (Weinheim an Der Bergstrasse, Germany), *28*(8), e202103888. https://doi.org/10.1002/chem.202103888

Polyanovsky, V., Lifanov, A., Esipova, N., & Tumanyan, V. (2020). The ranging of amino acids substitution matrices of various types in accordance with the alignment accuracy criterion. *BMC Bioinformatics*, *21*(Suppl 11), 294. https://doi.org/10.1186/s12859-020-03616-0

Ratnaparkhi, A., Banerjee, S., & Hasan, G. (2002). Altered levels of Gq activity modulate axonal pathfinding in Drosophila. *The Journal of Neuroscience : The Official Journal of the Society for Neuroscience*, *22*(11), 4499–4508. https://doi.org/10.1523/JNEUROSCI.22-11-04499.2002

Reher, R., Kühl, T., Annala, S., Benkel, T., Kaufmann, D., Nubbemeyer, B., Odhiambo, J. P., Heimer, P., Bäuml, C. A., Kehraus, S., Crüsemann, M., Kostenis, E., Tietze, D., König, G. M., & Imhof, D. (2018). Deciphering Specificity Determinants for FR900359-Derived Gq α Inhibitors Based on Computational and Structure-Activity Studies. *ChemMedChem*, *13*(16), 1634–1643. https://doi.org/10.1002/cmdc.201800304

Reher, R., Kuschak, M., Heycke, N., Annala, S., Kehraus, S., Dai, H.-F., Müller, C. E., Kostenis, E., König, G. M., & Crüsemann, M. (2018). Applying Molecular Networking for the Detection of Natural Sources and Analogues of the Selective Gq Protein Inhibitor FR900359. *Journal of Natural Products*, *81*(7), 1628–1635. https://doi.org/10.1021/acs.jnatprod.8b00222

Ren, G. R., Folke, J., Hauser, F., Li, S., & Grimmelikhuijzen, C. J. P. (2015). The A- and B-type muscarinic acetylcholine receptors from Drosophila melanogaster couple to different second messenger pathways. *Biochemical and Biophysical Research Communications*, *462*(4), 358–364. https://doi.org/10.1016/j.bbrc.2015.04.141

Richardson, J. S. (1981). The anatomy and taxonomy of protein structure. *Advances in Protein Chemistry*, *34*, 167–339. https://doi.org/10.1016/s0065-3233(08)60520-3

Robishaw, J. D., & Berlot, C. H. (2004). Translating G protein subunit diversity into functional specificity. *Current Opinion in Cell Biology*, *16*(2), 206–209. https://doi.org/10.1016/j.ceb.2004.02.007

Ross, E. M [E. M.] (1995). G protein GTPase-activating proteins: Regulation of speed, amplitude, and signaling selectivity. *Recent Progress in Hormone Research*, *50*, 207–221. https://doi.org/10.1016/b978-0-12-571150-0.50013-5

Ross, E. M [E. M.], & Wilkie, T. M. (2000). Gtpase-activating proteins for heterotrimeric G proteins: Regulators of G protein signaling (RGS) and RGS-like proteins. *Annual Review of Biochemistry*, *69*, 795–827. https://doi.org/10.1146/annurev.biochem.69.1.795

Ross, E. M [Elliott M.] (2008). Coordinating speed and amplitude in G-protein signaling. *Current Biology : CB*, *18*(17), R777-R783. https://doi.org/10.1016/j.cub.2008.07.035

Saitoh, O [O.], Kubo, Y [Y.], Miyatani, Y., Asano, T., & Nakata, H. (1997). Rgs8 accelerates G-protein-mediated modulation of K+ currents. *Nature*, *390*(6659), 525–529. https://doi.org/10.1038/37385

Saitoh, O [Osamu], Murata, Y., Odagiri, M., Itoh, M., Itoh, H., Misaka, T., & Kubo, Y [Yoshihiro] (2002). Alternative splicing of RGS8 gene determines inhibitory function of receptor type-specific Gq signaling. *Proceedings of the National Academy of Sciences of the United States of America*, *99*(15), 10138–10143. https://doi.org/10.1073/pnas.152085999

Salim, E., Hori, A., Matsubara, K., Takano-Shimizu, T., Pratomo, A. R., Marianne, M., Syahputra, A., Husori, D. I., Inoue, A., Abdullah, M. A., Shamsudin, N. F., Rullah, K., & Kuraishi, T. (2024). Detection of Human GPCR Activity in Drosophila S2 Cells Using the Tango System. *International Journal of Molecular Sciences*, *26*(1), 202. https://doi.org/10.3390/ijms26010202

Scharf, M. M., Humphrys, L. J., Berndt, S., Di Pizio, A., Lehmann, J., Liebscher, I., Nicoli, A., Niv, M. Y., Peri, L., Schihada, H., & Schulte, G. (2025). The dark sides of the GPCR tree - research progress on understudied GPCRs. *British Journal of Pharmacology*, *182*(14), 3109–3134. https://doi.org/10.1111/bph.16325

Schindelin, J., Arganda-Carreras, I., Frise, E., Kaynig, V., Longair, M., Pietzsch, T., Preibisch, S., Rueden, C., Saalfeld, S., Schmid, B., Tinevez, J.-Y., White, D. J., Hartenstein, V., Eliceiri, K., Tomancak, P., & Cardona, A. (2012). Fiji: An open-source platform for biological-image analysis. *Nature Methods*, *9*(7), 676–682. https://doi.org/10.1038/nmeth.2019

Schmitz, E. A., Takahashi, H., & Karakas, E. (2022). Structural basis for activation and gating of IP3 receptors. *Nature Communications*, *13*(1), 1408. https://doi.org/10.1038/s41467-022-29073-2

Schneider, I. (1972). Cell lines derived from late embryonic stages of Drosophila melanogaster. *Development (Cambridge, England)*, *27*(2), 353–365. https://doi.org/10.1242/dev.27.2.353

Schrage, R., Schmitz, A.-L., Gaffal, E., Annala, S., Kehraus, S., Wenzel, D., Büllesbach, K. M., Bald, T., Inoue, A., Shinjo, Y., Galandrin, S., Shridhar, N., Hesse, M., Grundmann, M., Merten, N., Charpentier, T. H., Martz, M., Butcher, A. J., Slodczyk, T., . . . Kostenis, E. (2015). The experimental power of FR900359 to study Gq-regulated biological processes. *Nature Communications*, *6*, 10156. https://doi.org/10.1038/ncomms10156

Schröder, R., Janssen, N., Schmidt, J., Kebig, A., Merten, N., Hennen, S., Müller, A., Blättermann, S., Mohr-Andrä, M., Zahn, S., Wenzel, J., Smith, N. J., Gomeza, J [Jesús], Drewke, C., Milligan, G [Graeme], Mohr, K., & Kostenis, E. (2010). Deconvolution of complex G protein-coupled receptor signaling in live cells

using dynamic mass redistribution measurements. *Nature Biotechnology*, *28*(9), 943–949. https://doi.org/10.1038/nbt.1671

Schröder, R., Schmidt, J., Blättermann, S., Peters, L., Janssen, N., Grundmann, M., Seemann, W., Kaufel, D., Merten, N., Drewke, C., Gomeza, J [Jesus], Milligan, G [Graeme], Mohr, K., & Kostenis, E. (2011). Applying label-free dynamic mass redistribution technology to frame signaling of G protein-coupled receptors noninvasively in living cells. *Nature Protocols*, *6*(11), 1748–1760. https://doi.org/10.1038/nprot.2011.386

Schütz, M., Schöppe, J., Sedlák, E., Hillenbrand, M., Nagy-Davidescu, G., Ehrenmann, J., Klenk, C., Egloff, P., Kummer, L., & Plückthun, A. (2016). Directed evolution of G protein-coupled receptors in yeast for higher functional production in eukaryotic expression hosts. *Scientific Reports*, *6*(1), 21508. https://doi.org/10.1038/srep21508

Scott, K., Becker, A., Sun, Y., Hardy, R., & Zuker, C. (1995). Gq alpha protein function in vivo: Genetic dissection of its role in photoreceptor cell physiology. *Neuron*, *15*(4), 919–927. https://doi.org/10.1016/0896-6273(95)90182-5

Sievers, F., Wilm, A., Dineen, D., Gibson, T. J., Karplus, K., Li, W., Lopez, R., McWilliam, H., Remmert, M., Söding, J., Thompson, J. D., & Higgins, D. G. (2011). Fast, scalable generation of high-quality protein multiple sequence alignments using Clustal Omega. *Molecular Systems Biology*, *7*, 539. https://doi.org/10.1038/msb.2011.75

Simon, M. I., Strathmann, M. P., & Gautam, N. (1991). Diversity of G proteins in signal transduction. *Science (New York, N.Y.)*, *252*(5007), 802–808. https://doi.org/10.1126/science.1902986

Smith, H. A., Thillaiappan, N. B., & Rossi, A. M. (2023). Ip3 receptors: An "elementary" journey from structure to signals. *Cell Calcium*, *113*, 102761. https://doi.org/10.1016/j.ceca.2023.102761

Smrcka, A. V [A. V.] (2008). G protein βγ subunits: Central mediators of G protein-coupled receptor signaling. *Cellular and Molecular Life Sciences : CMLS*, *65*(14), 2191–2214. https://doi.org/10.1007/s00018-008-8006-5

Smrcka, A. V [A. V.], & Sternweis, P. C. (1993). Regulation of purified subtypes of phosphatidylinositol-specific phospholipase C beta by G protein alpha and beta gamma subunits. *Journal of Biological Chemistry*, *268*(13), 9667–9674. https://doi.org/10.1016/S0021-9258(18)98401-2

Sondek, J [J.], Lambright, D. G., Noel, J. P., Hamm, H. E [H. E.], & Sigler, P. B. (1994). Gtpase mechanism of Gproteins from the 1.7-A crystal structure of transducin alpha-GDP-AIF-4. *Nature*, *372*(6503), 276–279. https://doi.org/10.1038/372276a0

Soundararajan, M., Willard, F. S., Kimple, A. J., Turnbull, A. P., Ball, L. J., Schoch, G. A., Gileadi, C., Fedorov, O. Y., Dowler, E. F., Higman, V. A., Hutsell, S. Q., Sundström, M., Doyle, D. A., & Siderovski, D. P. (2008). Structural

diversity in the RGS domain and its interaction with heterotrimeric G protein alpha-subunits. *Proceedings of the National Academy of Sciences of the United States of America*, *105*(17), 6457–6462. https://doi.org/10.1073/pnas.0801508105

Spangrude, G. J., Braaten, B. A., & Daynes, R. A. (1984). Molecular mechanisms of lymphocyte extravasation. I. Studies of two selective inhibitors of lymphocyte recirculation. *Journal of Immunology (Baltimore, Md. : 1950)*, *132*(1), 354–362.

Spindler, S. R., & Hartenstein, V. (2010). The Drosophila neural lineages: A model system to study brain development and circuitry. *Development Genes and Evolution*, *220*(1-2), 1–10. https://doi.org/10.1007/s00427-010-0323-7

Sprang, S. R [Stephen R.] (2016). Invited review: Activation of G proteins by GTP and the mechanism of Gα-catalyzed GTP hydrolysis. *Biopolymers*, *105*(8), 449–462. https://doi.org/10.1002/bip.22836

Sternweis, P. C., & Smrcka, A. V [A. V.] (1992). Regulation of phospholipase C by G proteins. *Trends in Biochemical Sciences*, *17*(12), 502–506. https://doi.org/10.1016/0968-0004(92)90340-F

Stothard, P. (2000). The sequence manipulation suite: Javascript programs for analyzing and formatting protein and DNA sequences. *BioTechniques*, *28*(6), 1102, 1104. https://doi.org/10.2144/00286ir01

Strathmann, M., & Simon, M. I. (1990). G protein diversity: A distinct class of alpha subunits is present in vertebrates and invertebrates. *Proceedings of the National Academy of Sciences*, *87*(23), 9113–9117. https://doi.org/10.1073/pnas.87.23.9113

Syrovatkina, V., Alegre, K. O., Dey, R., & Huang, X.-Y. (2016). Regulation, Signaling, and Physiological Functions of G-Proteins. *Journal of Molecular Biology*, *428*(19), 3850–3868. https://doi.org/10.1016/j.jmb.2016.08.002

Takasaki, J., Saito, T., Taniguchi, M., Kawasaki, T., Moritani, Y., Hayashi, K., & Kobori, M. (2004). A novel Galphaq/11-selective inhibitor. *The Journal of Biological Chemistry*, *279*(46), 47438–47445. https://doi.org/10.1074/jbc.M408846200

Talluri, S., Bhatt, A., & Smith, D. P. (1995). Identification of a Drosophila G protein alpha subunit (dGq alpha-3) expressed in chemosensory cells and central neurons. *Proceedings of the National Academy of Sciences of the United States of America*, *92*(25), 11475–11479. https://doi.org/10.1073/pnas.92.25.11475

Taniguchi, M., Nagai, K., Arao, N., Kawasaki, T., Saito, T., Moritani, Y., Takasaki, J., Hayashi, K., Fujita, S., Suzuki, K., & Tsukamoto, S. (2003). Ym-254890, a novel platelet aggregation inhibitor produced by Chromobacterium sp. Qs3666. *The Journal of Antibiotics*, *56*(4), 358–363. https://doi.org/10.7164/antibiotics.56.358

Taylor, V. G., Bommarito, P. A., & Tesmer, J. J. G. (2016). Structure of the Regulator of G Protein Signaling 8 (RGS8)-Gαq Complex: Molecular BASIS FOR Gα SELECTIVITY. *The Journal of Biological Chemistry*, *291*(10), 5138–5145. https://doi.org/10.1074/jbc.M115.712075

Tesmer, J. J., Berman, D. M., Gilman, A. G [A. G.], & Sprang, S. R [S. R.] (1997). Structure of RGS4 bound to AlF4--activated G(i alpha1): Stabilization of the transition state for GTP hydrolysis. *Cell*, *89*(2), 251–261. https://doi.org/10.1016/s0092-8674(00)80204-4

Todd, T. D., Vithani, N., Singh, S., Bowman, G. R., Blumer, K. J., & Soranno, A. (2024). Stabilization of interdomain closure by a G protein inhibitor. *Proceedings of the National Academy of Sciences of the United States of America*, *121*(36), e2311711121. https://doi.org/10.1073/pnas.2311711121

Traut, T. W. (1994). Physiological concentrations of purines and pyrimidines. *Molecular and Cellular Biochemistry*, *140*(1), 1–22. https://doi.org/10.1007/BF00928361

Trent, T., Miller, J. J., Blumer, K. J., & Bowman, G. R. (2025). The G Protein Inhibitor YM-254890 is an Allosteric Glue. *Journal of Molecular Biology*, 169084. https://doi.org/10.1016/j.jmb.2025.169084

Ugur, B., Chen, K., & Bellen, H. J. (2016). Drosophila tools and assays for the study of human diseases. *Disease Models & Mechanisms*, *9*(3), 235–244. https://doi.org/10.1242/dmm.023762

Vallar, L., Spada, A., & Giannattasio, G. (1987). Altered Gs and adenylate cyclase activity in human GH-secreting pituitary adenomas. *Nature*, *330*(6148), 566–568. https://doi.org/10.1038/330566a0

van Raamsdonk, C. D., Bezrookove, V., Green, G., Bauer, J., Gaugler, L., O'Brien, J. M., Simpson, E. M., Barsh, G. S., & Bastian, B. C. (2009). Frequent somatic mutations of GNAQ in uveal melanoma and blue naevi. *Nature*, *457*(7229), 599–602. https://doi.org/10.1038/nature07586

Venken, K. J. T., Sarrion-Perdigones, A., Vandeventer, P. J., Abel, N. S., Christiansen, A. E., & Hoffman, K. L. (2016). Genome engineering: Drosophila melanogaster and beyond. *Wiley Interdisciplinary Reviews. Developmental Biology*, *5*(2), 233–267. https://doi.org/10.1002/wdev.214

Violin, J. D., Zhang, J., Tsien, R. Y., & Newton, A. C. (2003). A genetically encoded fluorescent reporter reveals oscillatory phosphorylation by protein kinase C. *The Journal of Cell Biology*, *161*(5), 899–909. https://doi.org/10.1083/jcb.200302125

Vogt, S., Grosse, R., Schultz, G., & Offermanns, S [Stefan] (2003). Receptor-dependent RhoA activation in G12/G13-deficient cells: Genetic evidence for an involvement of Gq/G11. *Journal of Biological Chemistry*, *278*(31), 28743–28749. https://doi.org/10.1074/jbc.M304570200

Voss, J. H [Jan H.], Nagel, J., Rafehi, M., Guixà-González, R., Malfacini, D., Patt, J., Kehraus, S., Inoue, A., König, G. M., Kostenis, E., Deupi, X., Namasivayam, V., & Müller, C. E. (2021). Unraveling binding mechanism and kinetics of macrocyclic Gαq protein inhibitors. *Pharmacological Research*, *173*, 105880. https://doi.org/10.1016/j.phrs.2021.105880

Voss, J. H [Jan Hendrik] (2023). Recommended Tool Compounds: Application of YM-254890 and FR900359 to Interrogate Gαq/11-Mediated Signaling Pathways. *ACS Pharmacology & Translational Science*, *6*(12), 1790–1800. https://doi.org/10.1021/acsptsci.3c00214

Vries, L. de, Mousli, M., Wurmser, A., & Farquhar, M. G. (1995). Gaip, a protein that specifically interacts with the trimeric G protein G alpha i3, is a member of a protein family with a highly conserved core domain. *Proceedings of the National Academy of Sciences of the United States of America*, *92*(25), 11916–11920. https://doi.org/10.1073/pnas.92.25.11916

Vries, L. de, Zheng, B., Fischer, T., Elenko, E., & Farquhar, M. G. (2000). The regulator of G protein signaling family. *Annual Review of Pharmacology and Toxicology*, *40*, 235–271. https://doi.org/10.1146/annurev.pharmtox.40.1.235

Wagner, N., Laugks, U., Heckmann, M., Asan, E., & Neuser, K. (2015). Aging Drosophila melanogaster display altered pre- and postsynaptic ultrastructure at adult neuromuscular junctions. *The Journal of Comparative Neurology*, *523*(16), 2457–2475. https://doi.org/10.1002/cne.23798

Waldo, G. L., Ricks, T. K., Hicks, S. N., Cheever, M. L., Kawano, T., Tsuboi, K., Wang, X., Montell, C., Kozasa, T [Tohru], Sondek, J [John], & Harden, T. K. (2010). Kinetic scaffolding mediated by a phospholipase C-beta and Gq signaling complex. *Science (New York, N.Y.)*, *330*(6006), 974–980. https://doi.org/10.1126/science.1193438

Wall, M. A., Coleman, D. E., Lee, E., Iñiguez-Lluhi, J. A., Posner, B. A., Gilman, A. G [A. G.], & Sprang, S. R [S. R.] (1995). The structure of the G protein heterotrimer Gi alpha 1 beta 1 gamma 2. *Cell*, *83*(6), 1047–1058. https://doi.org/10.1016/0092-8674(95)90220-1

Wedegaertner, P. B [P. B.], Chu, D. H., Wilson, P. T., Levis, M. J., & Bourne, H. R. (1993). Palmitoylation is required for signaling functions and membrane attachment of Gq alpha and Gs alpha. *Journal of Biological Chemistry*, *268*(33), 25001–25008.

Wedegaertner, P. B [P. B.], Wilson, P. T., & Bourne, H. R. (1995). Lipid modifications of trimeric G proteins. *Journal of Biological Chemistry*, *270*(2), 503–506. https://doi.org/10.1074/jbc.270.2.503

Wettschureck, N., & Offermanns, S [Stefan] (2005). Mammalian G proteins and their cell type specific functions. *Physiological Reviews*, *85*(4), 1159–1204. https://doi.org/10.1152/physrev.00003.2005

Wilkie, T. M., Gilbert, D. J., Olsen, A. S., Chen, X. N., Amatruda, T. T., Korenberg, J. R., Trask, B. J., Jong, P. de, Reed, R. R., & Simon, M. I. (1992). Evolution of the mammalian G protein alpha subunit multigene family. *Nature Genetics*, *1*(2), 85–91. https://doi.org/10.1038/ng0592-85

Wilkie, T. M., Scherle, P. A., Strathmann, M. P., Slepak, V. Z., & Simon, M. I. (1991). Characterization of G-protein alpha subunits in the Gq class: Expression in

murine tissues and in stromal and hematopoietic cell lines. *Proceedings of the National Academy of Sciences*, *88*(22), 10049–10053. https://doi.org/10.1073/pnas.88.22.10049

Wilson, P. T., & Bourne, H. R. (1995). Fatty acylation of alpha z. Effects of palmitoylation and myristoylation on alpha z signaling. *Journal of Biological Chemistry*, *270*(16), 9667–9675. https://doi.org/10.1074/jbc.270.16.9667

Wright, S. C., Avet, C., Gaitonde, S. A., Muneta-Arrate, I., Le Gouill, C., Hogue, M., Breton, B., Koutsilieri, S., Diez-Alarcia, R., Héroux, M., Lauschke, V. M., & Bouvier, M. (2024). Conformation- and activation-based BRET sensors differentially report on GPCR-G protein coupling. *Science Signaling*, *17*(841), eadi4747. https://doi.org/10.1126/scisignal.adi4747

Wynne, B. M., Chiao, C.-W., & Webb, R. C. (2009). Vascular Smooth Muscle Cell Signaling Mechanisms for Contraction to Angiotensin II and Endothelin-1. *Journal of the American Society of Hypertension*, *3*(2), 84–95. https://doi.org/10.1016/j.jash.2008.09.002

Xiong, X.-F., Zhang, H., Boesgaard, M. W., Underwood, C. R., Bräuner-Osborne, H., & Strømgaard, K. (2019). Structure-Activity Relationship Studies of the Natural Product Gq/11 Protein Inhibitor YM-254890. *ChemMedChem*, *14*(8), 865–870. https://doi.org/10.1002/cmdc.201900018

Xiong, X.-F., Zhang, H., Underwood, C. R., Harpsøe, K., Gardella, T. J., Wöldike, M. F., Mannstadt, M., Gloriam, D. E., Bräuner-Osborne, H., & Strømgaard, K. (2016). Total synthesis and structure-activity relationship studies of a series of selective G protein inhibitors. *Nature Chemistry*, *8*(11), 1035–1041. https://doi.org/10.1038/nchem.2577

Xu, N., Bradley, L., Ambdukar, I., & Gutkind, J. S [J. S.] (1993). A mutant alpha subunit of G12 potentiates the eicosanoid pathway and is highly oncogenic in NIH 3T3 cells. *Proceedings of the National Academy of Sciences of the United States of America*, *90*(14), 6741–6745. https://doi.org/10.1073/pnas.90.14.6741

Yang, L., Mao, L., Chen, H., Catavsan, M., Kozinn, J., Arora, A., Liu, X., & Wang, J. Q. (2006). A signaling mechanism from G alpha q-protein-coupled metabotropic glutamate receptors to gene expression: Role of the c-Jun N-terminal kinase pathway. *The Journal of Neuroscience : The Official Journal of the Society for Neuroscience*, *26*(3), 971–980. https://doi.org/10.1523/JNEUROSCI.4423-05.2006

Zhang, H., Nielsen, A. L., Boesgaard, M. W., Harpsøe, K., Daly, N. L., Xiong, X.-F., Underwood, C. R., Haugaard-Kedström, L. M., Bräuner-Osborne, H., Gloriam, D. E., & Strømgaard, K. (2018). Structure-activity relationship and conformational studies of the natural product cyclic depsipeptides YM-254890 and FR900359. *European Journal of Medicinal Chemistry*, *156*, 847–860. https://doi.org/10.1016/j.ejmech.2018.07.023

Zhang, H., Xiong, X.-F., Boesgaard, M. W., Underwood, C. R., Bräuner-Osborne, H., & Strømgaard, K. (2017). Structure-Activity Relationship Studies of the Cyclic Depsipeptide Natural Product YM-254890, Targeting the Gq Protein. *ChemMedChem*, *12*(11), 830–834. https://doi.org/10.1002/cmdc.201700155

Ziehm, M., Piper, M. D., & Thornton, J. M. (2013). Analysing variation in Drosophila aging across independent experimental studies: A meta-analysis of survival data. *Aging Cell*, *12*(5), 917–922. https://doi.org/10.1111/acel.12123

Zornik, E., Paisley, K., & Nichols, R. (1999). Neural transmitters and a peptide modulate Drosophila heart rate. *Peptides*, *20*(1), 45–51. https://doi.org/10.1016/s0196-9781(98)00151-x